STUDIES ON WATER DESALINATION USING OSMOTIC PRESSURE-DRIVEN PROCESSES

A Thesis Submitted

for the Degree of

DOCTOR OF PHILOSOPHY

by

Kudzai Hamish Ruzvidzo
(2K21/PHDCH/03)

Under the Supervision of

Supervisor	**Co-supervisor**
Dr. Manish Jain	**Dr. Raminder Kaur**
Assistant Professor	**Associate Professor**
Department of Applied Chemistry	**Department of Applied Chemistry**
Delhi Technological University	**Delhi Technological University**

To the

Department of Applied Chemistry

DELHI TECHNOLOGICAL UNIVERSITY
(Formerly Delhi College of Engineering)
Shahbad Daulatpur, Main Bawana Road, Delhi-110042, India

July, 2025

ACKNOWLEDGMENTS

DELHI TECHNOLOGICAL UNIVERSITY
(Formerly Delhi College of Engineering)
Shahbad Daulatpur, Main Bawana Road, Delhi-110042, India

<u>CANDIDATE'S DECLARATION</u>

I **Kudzai Hamish Ruzvidzo** hereby certify that the work which is being presented in the thesis entitled **"Studies on water desalination using osmotic pressure-driven processes"** in partial fulfilment for the award of the Degree of Doctor of Philosophy, submitted in the Department of **Applied Chemistry**, Delhi Technological University is an authentic record of my own work carried out during the period from 8/8/2021 to 31/12/2024 under the supervision of **Dr. Manish Jain** and **Dr. Raminder Kaur.**

The matter presented in the thesis has not been submitted by me for the award of any other degree of this or any other Institute.

Candidate's Signature

This is to certify that the student has incorporated all the corrections suggested by the examiners in the thesis and the statement made by the candidate is correct to the best of our knowledge.

Signature of Supervisor (s)   **Signature of External Examiner**

DELHI TECHNOLOGICAL UNIVERSITY

(Formerly Delhi College of Engineering)
Shahbad Daulatpur, Main Bawana Road, Delhi-110042, India

CERTIFICATE BY THE SUPERVISOR(s)

Certified that **Kudzai Hamish Ruzvidzo (2K21/PHDCH/03)** has carried out their search work presented in this thesis entitled **"Studies on water desalination using osmotic pressure-driven processes"** for the award of **Doctor of Philosophy** from Department of Applied Chemistry, Delhi Technological University, Delhi, under our supervision. The thesis embodies results of original work, and studies are carried out by the student himself and the contents of the thesis do not form the basis for the award of any other degree to the candidate or to anybody else from this or any other University/Institution.

Dr. Manish Jain   **Dr. Raminder Kaur**

(Supervisor)   (Co-Supervisor)

Assistant Professor   Associate Professor
Department of Applied Chemistry   Department of Applied Chemistry
Delhi Technological University   Delhi Technological University

Date:

ABSTRACT

The global population growth has intensified the demand on finite freshwater resources. Membrane separation technologies offer economically viable solutions for seawater desalination. Forward osmosis (FO) has emerged as a promising alternative to reverse osmosis (RO) due to its operation without external hydraulic pressure and inherently lower membrane fouling propensity. However, the commercialization of FO remains limited due to the lack of optimal draw solutions and energy-intensive regeneration processes. This thesis investigates the development of novel phase-separating binary and ternary organic draw solutions for brackish and seawater desalination using FO, exploiting their lower critical solution temperature (LCST) behaviours to enable cost-effective draw solution regeneration. The research establishes theoretical foundations through data-driven techniques using Artificial Neural Networks (ANN) to address the limitations of traditional solution-diffusion models, particularly for multi-component and neutral draw solutions. Through systematic experimental procedures, the study evaluates 4 binary and 6 ternary systems incorporating sodium carboxymethyl cellulose (NaCMC) and propylene glycol propyl ether (PGPE). This is followed by sixteen distinct draw solution compositions of hydroxypropyl cellulose (HPC) and PGPE, including single-solute and ternary mixtures with varying HPC (0.25 – 2 wt.%) and PGPE (1.25 - 3.75 M) concentrations. The research employs comprehensive characterization techniques to analyze physico-chemical properties and osmotic performance, including measurements of osmotic pressure, viscosity, concentration, pH, density, cloud point determinations and membrane compatibility. The experiments were conducted using a custom FO setup with a harvested HTI CTA membrane in AL-FS mode. An ANN model incorporating nine input parameters - FO run details, temperatures, concentrations, flow rates and draw solution molecular weights - predicts permeate fluxes, developed using 312 experimental data points collected during 120-minute FO runs with various draw solutions. The work includes a thorough techno-economic assessment evaluating both operating expenditures (OPEX) and capital expenditures (CAPEX) for the FO process and phase separation (PS) draw regeneration,

ultimately providing significant research outcomes and recommendations for advancing the study of phase-separating organic draw solutions in FO desalination.

Dedicated with profound gratitude:

To the unwavering support of
Sekuru and Gogo Ruzvidzo, my
cherished parents;

To **Mitchello**, my little sister;

And to **Kudzai Hamish Ruzvidzo
Jr.**, my beloved son and greatest
inspiration.

You four are the cornerstones of my
world and the driving force behind
this achievement

"Mhofu kufunda handi kudzidza"

LIST OF PUBLICATIONS

1. **Kudzai Hamish Ruzvidzo**, Raminder Kaur and Manish Jain (2024), "Novel polyelectrolyte-glycol ether ternary phase-separating draw solutions for desalination using forward osmosis", *Desalination*, Volume 586, 117897, (SCIE indexed) (Impact Factor – 8.3)

2. **Kudzai Hamish Ruzvidzo**, Raminder Kaur and Manish Jain (2024), "Enhanced forward osmosis desalination of brackish water using phase-separating ternary organic draw solutions of hydroxypropyl cellulose and propylene glycol propyl ether", *Water Environment Research*, 96(8), e11110, (SCIE indexed) (Impact Factor – 2.5)

3. **Kudzai Hamish Ruzvidzo**, Ashwani Kumar Tiwari, Raminder Kaur and Manish Jain, "A critical review on the progress, challenges and future outlook of forward osmosis desalination in the 21st century" – **UNDER REVIEW**

4. **Kudzai Hamish Ruzvidzo**, Ashwani Kumar Tiwari, Raminder Kaur and Manish Jain, "Artificial neural network-based modeling of forward osmosis-phase separation desalination processes with novel ternary organic draw solutions" – **SUBMITTTED**

CONFERENCE PROCEEDINGS

1. **Kudzai Hamish Ruzvidzo**, Raminder Kaur and Manish Jain (2023), **poster presentation** on title: "Overview of osmotic pressure-driven water desalination processes in the Indian context", Conference on Desalination, Brine management and Water recycling (DeSaltM 23), organized by Environmental Science and Engineering Department, Indian Institute of Technology Bombay (IIT-B), Mumbai, India, July 21 – 22, 2023.

2. **Kudzai Hamish Ruzvidzo**, Raminder Kaur and Manish Jain (2023), **oral presentation** on title: "Exploring novel organic draw solutions for forward osmosis desalination of brackish water: A comprehensive study", International Conference on Basic, Analytical and Allied Sciences at the Interface of Carbohydrates and Biomass Valorisation (CARBO XXXVII), jointly organized

by Department of Applied Chemistry, Delhi Technological University (DTU), Delhi, India, and the Association of Carbohydrate Chemists and Technologists (India), Delhi, India, November 30 – December 2, 2023.

3. **Kudzai Hamish Ruzvidzo**, Raminder Kaur and Manish Jain (2023), **oral presentation** on title: "Rheological, Physical, Thermal, Spectroscopical, Chemical and Electrical properties of novel organic draw solutes for forward osmosis desalination of brackish and seawater feed solutions", 2nd International Conference on Recent Trends in Materials Science & Devices 2023 (ICRTMD 2023), jointly organized by Research Plateau Publishers (An academic publisher of scientific and technical journals) & Sat Kabir Institute of Technology & Management Bahadurgarh, Haryana, India (Affiliated to M.D. University, Rohtak, Haryana, India), December 29 – 31, 2023. **Awarded best paper presentation award**

4. **Kudzai Hamish Ruzvidzo**, Raminder Kaur and Manish Jain (2024), **oral presentation** on title: "Exploring novel organic draw solutions for forward osmosis desalination: Performance, regeneration, modeling, and cost analysis", Emerging Techno-Economic Development for Sustainable Environment (ETDSE – 2024), organized by Department of Chemical Engineering Institute of Engineering & Science Indore, Indore, Madhya Pradesh, India, 12 – 13 January, 2024.

TABLE OF CONTENTS

Title	Page No.

LIST OF TABLES

LIST OF FIGURES

LIST OF SYMBOLS, ABBREVIATIONS AND NOMENCLATURE

Symbol	Notations
AB	Ammonium Bicarbonate
AL-FS	Active layer facing feed solution
ANN	Artificial neural network
CAPEX	Capital expenditure
CDI	Capacitive deionization
CP	Concentration polarization
CTA	Cellulose triacetate
DMAEMA	2-(Dimethylamino) ethyl methacrylate
DS	Draw solute
DT	Decision tree
ECP	External concentration polarization
ED	Electrodialysis
EIA	Environmental impact assessment
EMPs	Environmental monitoring plans
FO	Forward osmosis
FO/Cry/RO	Forward osmosis/crystallization/reverse osmosis
FO-AGMD	Forward osmosis-air gap membrane distillation
FO-MD	Hybrid forward osmosis and membrane distillation
FO-NF	Hybrid forward osmosis and nanofiltration
FO-PDMP	Forward osmosis - pressure-driven membrane processes
FO-SE	Forward osmosis-solar evaporation
GFO	Graphene oxide-enhanced forward osmosis
GHGs	Greenhouse gases
HA	Hyaluronic acid
HDH	Humidification-dehumidification
HEC	Hydroxyethyl cellulose
HL	Hidden layer
HPC	Hydroxypropyl cellulose
HPC–PGPE	Hydroxypropyl cellulose–propylene glycol propyl ether
ICP	Internal concentration polarization
IL	Ionic liquid
LCST	Lower critical solution temperature
MD	Membrane distillation
MED	Multiple effect distillation
MF	Microfiltration
MLR	Multiple linear regression
MNPs	Magnetic nanoparticles
MSE	Mean square error

MSF	Multi-stage flash distillation
MVC	Mechanical vapour compression
NaCMC	Sodium carboxymethyl cellulose
NaCMC–PGPE	Sodium carboxymethyl cellulose–propylene glycol propyl ether
NF	Nanofiltration
NPHs	Nanocomposite polymer hydrogels
NR	Not reported
OPEX	Operating expenditure
PAGB	Poly (propylene glycol-ran-ethylene glycol) monobutyl ethers
PAGs	Polyalkylene glycols
PEG	Poly (ethylene glycol)
PEI:rGO	Polyethyleneimine crosslinked reduced graphene oxide
PEO	Pressure enhanced osmosis
PFO	Photocatalysis and forward osmosis
PGPE	Propylene glycol propyl ether
PRO	Pressure retarded osmosis
PS	Phase separation
PSA	Poly (sodium acrylate)
PVA	Poly (vinyl alcohol)
RED-FO	Reverse electrodialysis-forward osmosis
RO	Reverse osmosis
RO-MD	Hybrid reverse osmosis and membrane distillation
RSF	Reverse solute flux
S-D	Solution-Diffusion
SEC	Specific Energy Consumption
SEM	Scanning electron microscopy
S-K	Spiegler-Kedem
SRSF	Specific reverse solute flux
SSA	Sewage sludge ash
SVR	Support vector regression
SWRO	Seawater reverse osmosis
TEA	Techno-economic assessment
TFC	Thin film composite
TFN	Thin film nanocomposite
TMILs	Thermo-responsive magnetic ionic liquids
TPM	Tripropylene glycol methyl ether
TPnB	Tripropylene glycol n-butyl ether
TPU	Thermoplastic polyurethane
TRDS	Thermally responsive draw solutes
TSSE	Temperature swing solvent extraction

TVC	Thermal vapour compression
UF	Ultrafiltration
UV	Ultraviolet

CHAPTER 1

INTRODUCTION AND LITERATURE REVIEW

1.1 Introduction

1.1.1   Global water scarcity

Freshwater scarcity is a global issue being exacerbated by population growth and climate change [1, 2]. Water scarcity occurs when freshwater demand exceeds supply [3]. India, now the world's most populous nation, is projected to face a water crisis by 2030 due to various factors including population growth, industrialization, urbanization, poor water management, pollution and climate change [4]. By 2025, over 1.8 billion people could face serious water shortages, particularly in Southeast Asia and Africa [5], as shown in Figure 1.1.
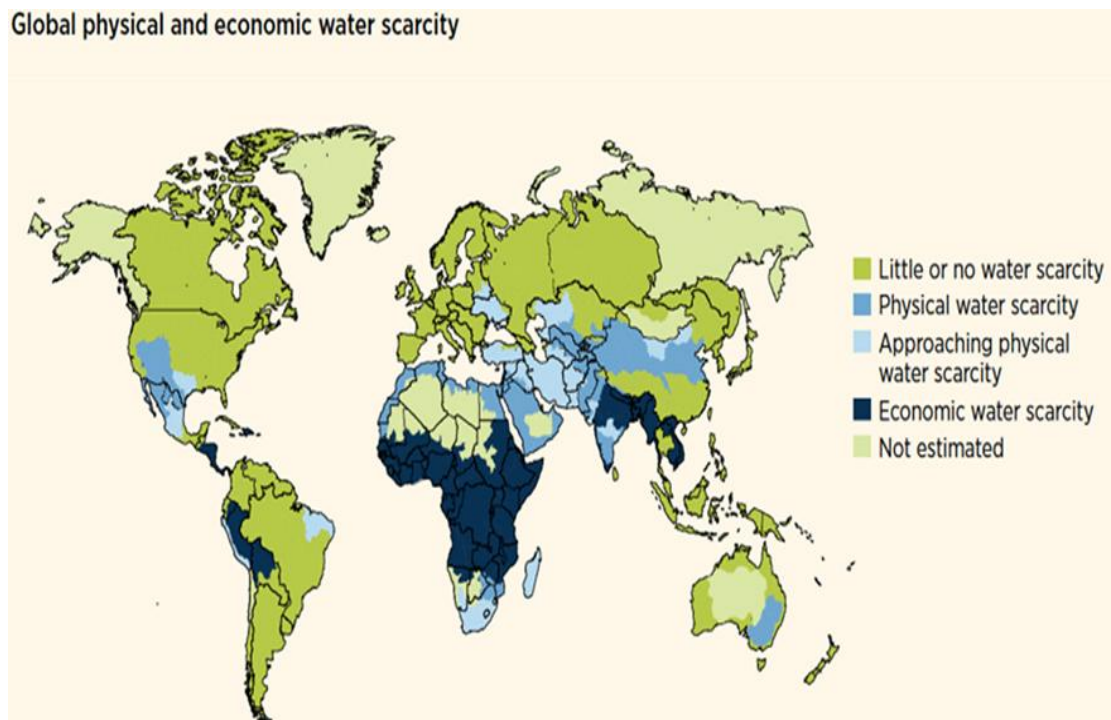
Figure 1.1: Global water scarcity trends by regions (Adapted from World Water Development Report 4. World Water Assessment Programme (WWAP), March 2012)

Despite India's projected improvement by 2040, its vast coastline provides an opportunity for innovative solutions like desalination [6]. Access to clean water is vital to prevent waterborne diseases as demonstrated by the 2023 cholera outbreak in Zimbabwe [7].

1.1.2 Pressure-driven membrane separation processes

Addressing global freshwater scarcity requires a comprehensive strategy that preserves water, improves governance and develops novel technologies to tap into non-traditional water sources [8]. Membrane separation processes use specially engineered membranes to separate freshwater from saltwater [9]. These methods are crucial for desalination, treating wastewater and water reclamation [10]. Membrane processes such as reverse osmosis (RO) offer a more sustainable alternative to conventional, energy-intensive desalination techniques [11]. Spent RO membranes can be recycled for lower rejection applications or repurposed as nanofiltration (NF) or ultrafiltration (UF) membranes [12]. They can also be used in membrane biofilm reactors or as support for regenerated anion-exchange membranes [12]. Membranes allow specific molecules or ions to pass based on size, charge and other physicochemical properties. Membrane separation processes are driven by pressure gradients, concentration differentials, electrical potential and temperature gradients [13]. Microfiltration (MF) uses larger pore sizes to separate particulates like bacteria and fungi [14]. UF and NF use progressively smaller pores to retain larger molecules and separate ions, organic molecules and some viruses [15]. RO, with the smallest pore sizes, effectively removes dissolved salts and impurities thereby generating freshwater from seawater or brine [16]. Figure 1.2 shows these membrane separation processes.
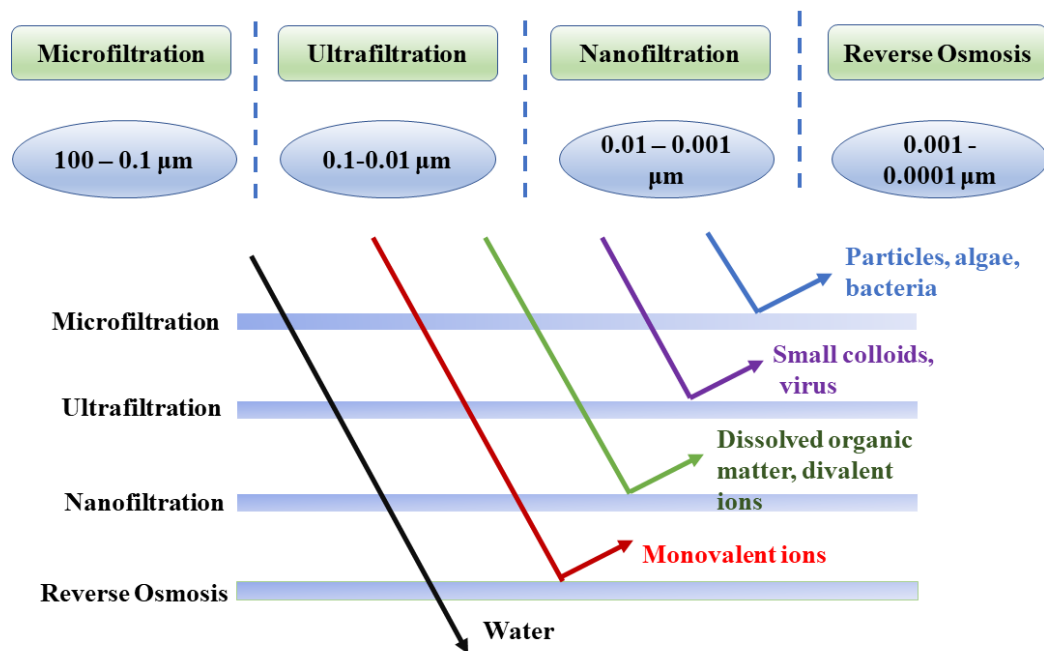
Figure 1.2: Different membrane separation processes

1.1.3 Osmotically driven membrane processes

Osmotically driven processes such as forward osmosis (FO) operate at substantially lower hydraulic pressures than pressure-driven systems by relying on natural osmotic pressure gradients as the driving force [17]. This eliminates the energy-intensive high-pressure pumps required in RO systems thereby reducing membrane fouling associated with elevated operating pressures [17]. Additionally, osmotically driven processes demonstrate greater application versatility, effectively treating feed solutions and contaminants that would rapidly compromise pressure-driven membranes [17]. Operating at low pressures contributes to extended membrane lifespans and reduced equipment costs compared to pressure-driven processes [17 - 20, 134].

In RO, external pressure counteracts osmotic pressure, forcing water from a high to low concentration solution through a semi-permeable membrane [17]. RO is widely adopted for seawater desalination, water purification and solvent separation despite being energy-intensive [18]. FO passively separates water from a feed to a concentrated draw solution driven by the osmotic pressure difference [19]. Operating

at a transmembrane pressure lower than the osmotic pressure, FO eliminates the need for external pressure, making it energy-efficient for wastewater management and concentrating food products [20]. Pressure Retarded Osmosis (PRO) allows controlled water flow from a low to high concentration solution under a pressure less than the osmotic pressure difference [21]. The osmotically driven water flow can be harnessed to drive a turbine or other mechanical device, converting the salinity gradient energy into usable mechanical energy [22]. The differences between RO, FO, PRO and pressure enhanced osmosis (PEO) are shown in Figure 1.3.
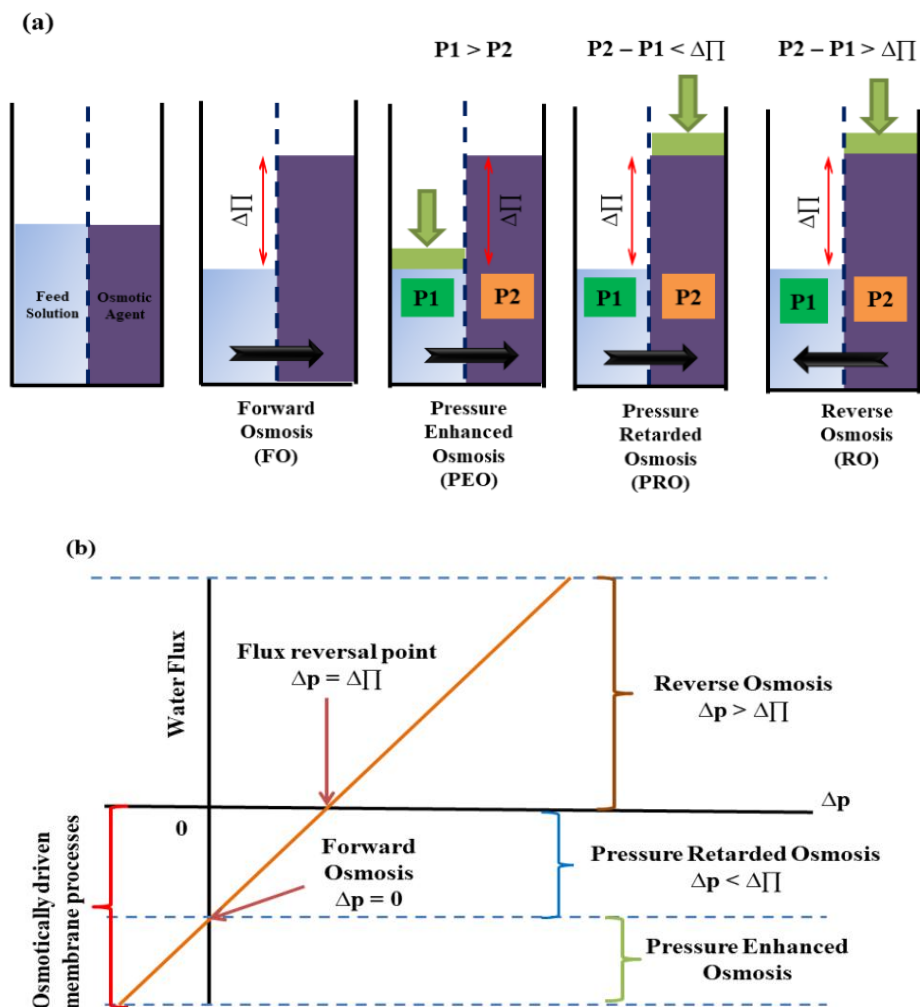
Figure 1.3: (a) Osmotically driven membrane processes (b) Family of osmotically driven membrane process for an ideal semi-permeable membrane (Adapted from Peter G. Nicoll, The International Desalination Association World Congress on Desalination and Water Reuse, Tianjin, China, 2013)

This review focuses on FO desalination, an energy-efficient, low-fouling alternative to conventional desalination methods [19]. FO, depicted in Figure 1.4, uses an osmotic pressure gradient to transport water across a semi-permeable membrane.

The diluted draw solution is then reconcentrated and reused, thereby making FO a potentially efficient cyclic system.
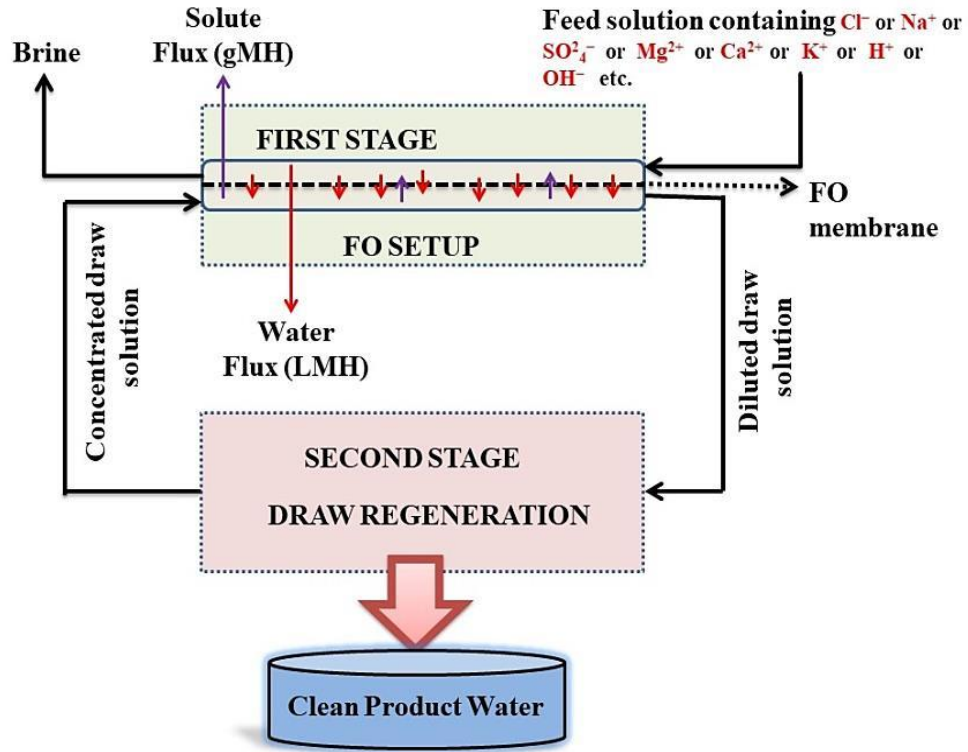
Figure 1.4: FO desalination process

1.2 Literature review

1.2.1   Past reviews on FO processes (2019 – 2024)

The field of FO desalination has seen a surge in comprehensive literature reviews over the past five to six years, with researchers critically analysing various aspects of FO desalination processes [23 – 48]. These reviews have covered a wide range of topics, including the fundamental principles of the FO desalination process, the complex phenomenon of reverse solute flux (RSF), the development and optimization of FO polymeric membranes and their associated flux performance, the exploration of hydrogels as draw solutes, the challenges posed by organic fouling,

the integration of FO with membrane distillation (MD) for wastewater treatment applications, the emergence of novel desalination technologies, the environmental impacts of desalination and brine treatment strategies, as well as the implementation of standalone and hybrid FO systems for water treatment. An analysis of 25 such reviews conducted over the past five years has revealed significant insights and highlighted critical research gaps that still need to be addressed. Table 1.1 summarizes these reviews' main points and research gaps.

Table 1.1: Main points and research gaps from some review publications on FO processes from 2019 to 2024

Reviewer(s)	Main highlights from the review and stated research gaps
Zou et al., [23]	- Optimizing RSF mitigation involves intelligent DS selection, use of novel DS like stimuli-responsive polymers and surfactants. However, limited data, energy-intensive regeneration, potential health risks and the need for improved reporting and analysis are challenges. - RSF control in FO is less studied than anti-fouling research despite their close correlation in operational strategies and membrane development.
Tharayil et al., [24]	- FO desalination, despite its challenges and efficiency issues, can be improved with high-rejection membranes and optimal draw agents. - Utilizing waste heat and renewables could advance FO, but its economic viability and scalability are still uncertain.
Li et al., [25]	- Future FO process research will concentrate on membrane materials, draw solutes, fouling mechanisms and cleaning strategies, with a focus on high water flux, low RSF and material modification. - In-depth research on membrane fouling mechanisms is needed to support the development and cleaning of membrane materials, an area currently lacking sufficient study
Wang et al., [26]	- Various techniques are used to enhance hydrogels as draw solutes in the FO process. Despite their thermal responsiveness, their dewatering efficiency needs improvement. - Integrating a reversible bidirectional shape memory polymer and designing a semi-interpenetrating network of thermo-sensitive and conductive hybrid hydrogels could enhance this efficiency. - Optimal draw solutes are yet to be found, requiring designs that balance low energy use and easy production. - Addressing these issues necessitates interdisciplinary chemistry, materials science and process engineering expertise.
Yadav et al., [27]	- Commercializing FO faces financial hurdles and fouling issues. - Optimal FO membranes need high water flux and low structural parameters. - Real-time tracking of foulants can help mitigate fouling. - Efficient cleaning methods and innovative techniques like UV and ultrasound need exploration.

	- Applying research findings to real-time scenarios and long-term experiments can help commercialize FO.
Abu-Zurayk et al., [28]	- Cellulose acetate's use in membrane filtration is hampered by fouling. - Antifouling strategies include pre-treatment, cleaning, modification and coating. - Future research should focus on the comparative study of antifouling behaviour between cellulose acetate and cellulose triacetate, an area currently underexplored in the literature. - Future studies should investigate how preparation methods like solution casting, electrospinning and spin coating influence the membrane's morphology and structure.
Ibrar et al., [29]	- To make FO-MD competitive in desalination, the cost of FO membranes must be reduced and a low-energy process for DS recovery, possibly using waste heat or solar energy, is needed. - The energy-intensive DS recovery hinders FO's independent commercialization.
Ahmed et al., [30]	- Nanoscience has enhanced desalination technologies by improving membrane performance. - However, full-scale FO desalination requires low-cost recovery methods and more focus on system design and engineering for upscaling, despite the benefits of carbon nanomaterials.
Zhan et al., [31]	- Commercializing FO faces challenges like DS regeneration and energy use. - However, FO without DS regeneration shows promise. - The simultaneous osmotic dilution and concentration (SODC) concept, particularly in wastewater reclamation, suggests potential for future commercialization.
Panagopoulos & Haralambous, [32]	- Desalination's significant environmental impacts, such as brine discharge and high energy use, can be mitigated through strategies like EIA, EMPs and using renewable energy sources. - Green anti-scalants and careful plant location can further reduce its ecological footprint.
Chiao et al., [33]	- Zwitterions in desalination research, used in membranes and draw solutions, present a trade-off between osmotic pressure and product recovery, with potential resolution through temperature and magnetic responsive zwitterionic polymers.
Mohammadifakhr et al., [34]	- FO's low water fluxes, compared to RO, could be improved by optimizing membrane support thickness and enhancing draw solute diffusivity, which reduces ICP. - Accurate methods for ICP estimation are needed for next-generation FO membrane supports
Ibraheem et al., [35]	- Future FO research should prioritize developing efficient, sustainable membranes and draw solutions, transitioning from lab to large-scale implementation and designing a renewable energy-

	powered draw solution regeneration system.
Salamanca et al., [36]	▪ Future FO research should concentrate on system optimization, process integration and commercial scaling, with a focus on academia-industry collaboration for innovation in desalination, wastewater treatment, resource recovery and water reuse.
Park and Lee, [37]	▪ South Korea's desalination research, active since 2006, focuses on energy-efficient and environmentally friendly solutions. ▪ It explores various technologies, caters to municipal and industrial needs and addresses environmental concerns. ▪ Despite advancements, further research and government support are needed for commercialization.
Singh et al., [38]	▪ The FO process, linked to DS and its regeneration, can reduce costs by minimizing storage and pumping. ▪ Future research will focus on process development, membrane fabrication and fouling control strategies. ▪ Its application in various fields could stimulate commercial FO membrane production.
Mahto et al., [39]	▪ FO-based hybrid processes excel in wastewater treatment and sludge dewatering. ▪ Future research should focus on sustainable solutions, economic viability and scaling up novel technologies for commercialization, guiding industries towards the most efficient and sustainable effluent treatment technology.
Xu et al., [40]	▪ Optimizing membrane materials and draw solutes is key for efficient FO water treatment. ▪ Future treatments will use solutes that maximize osmotic pressure and minimize fouling, with a focus on limiting reverse solute migration. ▪ Hybrid systems can enhance sustainability by reducing energy use and operating costs.
Suwaileh et al., [41]	▪ Addressing technical challenges in wastewater treatment, testing with actual wastewater and developing energy-efficient methods for draw solution recycling are crucial. ▪ Integrated hybrid methods, advanced nanomaterials for membranes and real-time assessments of membrane fouling can enhance efficiency. ▪ Further research is needed on permeability-selectivity trade-off.
Wang and Liu, [42]	▪ Future research should focus on improving membrane performance, exploring efficient draw solutions, conducting large-scale experiments, expanding FO technology's industrial applications

	and enhancing recovery efficiency while reducing energy consumption.
Ahmed et al., [43]	▪ High energy use limits desalination technologies, but advancements and process hybridization can reduce costs. ▪ Optimizing draw solutions for hybrid processes like FO-MD is crucial. ▪ More research is needed on the energy usage of hybrid systems and the integration of renewable energy with these technologies.
Skuse et al., [44]	▪ While FO desalinates seawater more efficiently than RO, its high energy need for draw solution recovery limits its efficiency. ▪ Hybrid FO and RO systems can reduce energy use, but require further testing. ▪ As desalination demand grows, integrating new technologies with RO could lessen environmental impacts and costs, warranting further research.
Giagnorio et al., [45]	▪ Complex solutes in FO systems heighten environmental impacts. ▪ Energy supply and solute management are key impacts in large-scale FO plants. ▪ Sodium-based solutes in FO-PDMP systems increase energy demands despite low impacts. ▪ High-impact solutes like $MgCl_2$ require more energy for recovery, negating benefits.
Lin et al., [46]	▪ China's annual desalination capacity growth is robust at about 10 000 m^3/d, with water production costs maintained between 0.74 - 1.18 USD/m^3
Hafiz et al., [47]	▪ Key challenges for wastewater treatment and desalination technology include developing a model for osmotic pressure by MNPs, evaluating membrane fouling and energy consumption, assessing economic feasibility and establishing regulations for MNPs use.
Firouzjaei et al., [48]	▪ Future development of FO membranes should focus on simplified functionalization, optimized reaction conditions, effective procedures and reagents for modification and application-specific functionalization schemes. ▪ The goal of creating anti-biofouling membranes is to achieve durable performance for real applications. ▪ However, a gap exists between lab-scale research and industrial applications due to the narrow conditions of experiments and a lack of understanding of long-term applications with complex feeds.

1.2.2 Draw solutions used in FO processes

1.2.2.1 Hydrogels

Hydrogels with thermoplastic polyurethane (TPU) microfibers were developed for improved water diffusion and swelling pressures [49]. The composite monolith (TPU-PSA) doubled the water flux and dewatering flux compared to standalone poly (sodium acrylate) (PSA), with values of 1.81 and 3.51 LMH, respectively [49]. Electro-responsive hydrogels demonstrated a water flux of 2.76 LMH and could release 71% of adsorbed water under a 15 V electric field [50]. The hydrogels maintained their efficiency for three regeneration cycles, suggesting the potential of electric fields in FO desalination [50]. A binary ionic liquid/hydrogel system enabled cost-effective, recyclable high-purity water recovery, overcoming challenges of inorganic draw solutes [51]. The system outperformed conventional methods, allowing continuous use of hydrogels. The use of solar energy for draw agent regeneration can reduce energy consumption [51]. A hydrogel-polyurethane interpenetrating network produced better water fluxes of 17.9 LMH as compared to the 2.2 LMH of pure hydrogel powders [52]. There was no observed RSF hence simplifying the operation. More work is still needed to increase dewatering efficiency in FO systems [52]. A temperature-sensitive hydrogel that incorporated poly (ethylene glycol) as a porogen enhanced the water flux and improved wastewater concentration efficiencies [52]. The use of N-isopropyl acryl-amide/sodium acrylate/poly (ethylene glycol) (PEG4000) was recommended for FO applications [52]. Sewage sludge ash (SSA) was added to thermo-responsive hydrogels, doubling the water flux to 2.33 LMH while maintaining excellent performance characteristics [53]. Significantly, the hydrogels retained 94.4% of their initial water flux even after four regeneration cycles. SSA is recommended as an effective modifier to improve permeation and energy efficiency in FO processes [53]. Nanocomposite polymer hydrogels (NPHs) were synthesized using acrylic acid and N-vinyl pyrrolidone, modifying them with clay or graphene oxide [54]. These modified NPHs exhibited increased water flux due to enhanced swelling ratio, porosity and osmotic pressure [54]. The NPHs could be reused four times without significant flux reduction, making them promising for various FO processes [54].

CO$_2$ and thermo-responsive hydrogels were developed using poly (N, N-dimethyl allylamine), which could absorb and release large amounts of water [55]. These hydrogels showed potential for extracting water from 3.5 wt.% NaCl feed solutions in FO [55]. Furthermore, electric-responsive hydrogels made from 2-Acrylamido-2-methyl-1-propanesulfonic acid (AMPS) and 2-(Dimethylamino) ethyl methacrylate (DMAEMA) demonstrated promising water fluxes during FO operation using a 2000 ppm NaCl feed solution, initially exhibiting water fluxes of 2.09 LMH and 1.63 LMH [55]. These hydrogels could simplify operations and improve efficiency [55]. A sodium alginate-graphene oxide aerogel achieved high initial water fluxes of 15.25 LMH and exhibited easy regeneration capability. Over repeated cycles, the aerogel maintained a consistent water flux of around 5 - 6.5 LMH [56]. When tested with seawater, it produced impressive water fluxes of approximately 7.49 LMH, demonstrating good desalination capacity [56]. Using this aerogel can improve efficiency and reduce energy consumption in FO [56]. A hydrogel composed of poly (vinyl alcohol) and poly (acrylic acid) (PVA-PAA) exhibited sensitivity to electric stimuli [57]. The hydrogel could expand or contract and release water when subjected to an electric field. During FO operation using deionized water and a 2000 ppm NaCl solution as feeds, the hydrogels achieved water fluxes of 1.04, 0.72, 0.73, and 0.54 LMH [57]. The use of these hydrogels could prevent reverse salt flux and improve the overall FO process performance [57]. A hybrid monolith composed of hyaluronic acid-graphene oxide/poly (vinyl alcohol) was synthesized for use as a draw agent in FO [58]. This monolith exhibited high water fluxes of 13.9 LMH with no reverse permeation when deionized water was the feed solution. The HA-GO/PVA monolith demonstrated longevity, maintaining an average water flux of approximately 6.22 LMH over 300 cycles [58]. When applied to real seawater desalination processes, the dry monolith demonstrated a capacity of about 7.2 LMH, while the wet monolith reached 3.9 LMH [58]. Regeneration involved a simple manual squeezing process, which could be accomplished quickly [58]. A gas-responsive copolymer microgel was developed as a solution to high recovery costs in industrial FO systems [59]. These microgels could absorb water when exposed to oxygen and release it when purged with nitrogen. High water fluxes of up to 29

LMH were observed while desalinating a 2000 ppm NaCl solution feed solution at ambient temperature [59].

The use of these microgels is highly recommended as draw agents in FO desalination [59]. Hydrogels in FO desalination can address the high energy consumption and costs challenges [60]. A hydrogel was synthesized from activated carbon filler (AC) blended with sodium carboxymethyl cellulose (NaCMC) and hydroxyethyl cellulose (HEC) in a 1:3 ratio, then crosslinked with citric acid [60]. This hydrogel showed improved desalination efficiency, although excess AC reduced performance [60]. Hydrogels were developed as a paste of water, reduced graphene oxide nanofillers, carboxymethyl cellulose and hydroxyethyl cellulose [61]. The crosslinking was done using citric acid solution. Evaluating desalination and antimicrobial properties revealed that a hydrogel with a swelling ratio of 1447% yielded 30% desalination efficiency [61]. A fluidic ionosilica hydrogel was synthesized for desalination and wastewater treatment applications [62]. The hydrogel exhibited high initial osmotic pressures around 10 atm that decreased over multiple cycles, necessitating further investigation [62]. The use of iodide anions showed superior osmotic properties. The hydrogels were regenerated using UF, facilitating a closed-loop operation of FO and UF [62].

1.2.2.2 Inorganic draw solutes

Table 1.2 presents an overview of the FO performance data for various inorganic draw solutes investigated since 2000.

1.2.2.3 Organic and other draw solutes

Table 1.3 presents an overview of the FO performance data for various organic and other draw solutes investigated since 2000. The tabulated information includes the year, specific draw solute employed, composition of the feed solution, properties of the draw solution (concentration and osmotic pressure), operating temperatures of the feed and draw solutions, measured water and solute flux values, type of FO membrane utilized, method employed for regenerating the draw solution (or direct

application when regeneration was not required), specific energy consumption and the total associated costs. Some of these draw solutes are depicted in Figure 1.5.
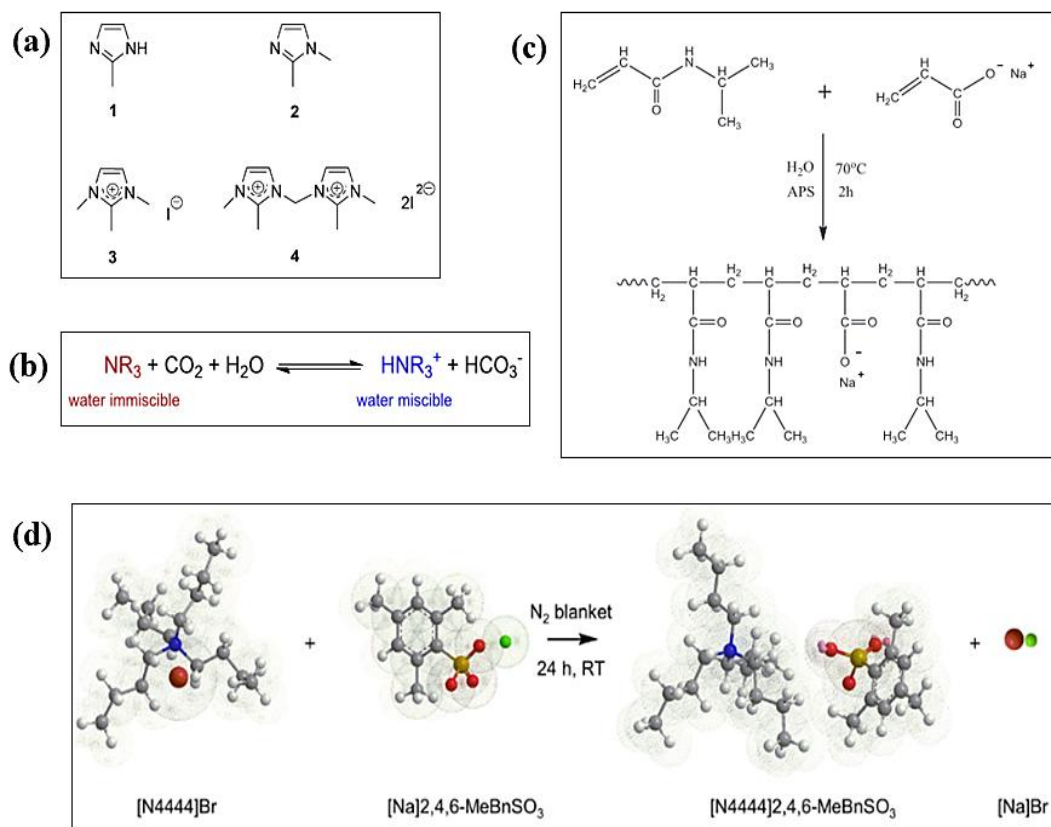
Figure 1.5: Some of the organic and other draw solutes (a) 2-Methylimidazole-based compounds, adapted from (Yen et al., [79]), (b) Switchable polarity solvents adapted from (Stone et al. [84]), (c) Thermo-sensitive polyelectrolytes adapted from (Ou et al. [85]), and (d) Monomeric thermo-responsive ionic liquid adapted from (Zeweldi et al., [107]).

The evaluation of hydrogels, inorganic, and organic draw agents requires assessment across six key criteria: osmotic pressure, water flux performance, recovery efficiency, reverse solute flux, cost, and stability. Inorganic salts usually achieve high osmotic pressures, such as 152, 112, 258.3 and 219 bar for NH_4HCO_3, $ZnSO_4$, $MgCl_2$ and NaCl, respectively [63, 65, 67]. Organic draw agents usually generate moderate pressures such as 27.1 – 54.4 bar for sucrose, methyl acetate and sodium formate [71, 81, 82]. However, it is noteworthy that an extremely high osmotic pressure of 505.1 bar has been reported for 5M fructose solution [78]. In terms of

water fluxes, inorganic draw agents usually produce better water fluxes due to the high osmotic driving forces. Organic solutions usually produce moderate fluxes, whilst hydrogels usually exhibit low performance, such as 0.72 LMH for PVA-PAA hydrogel [57], although these are also dependent on various other operating conditions. Inorganic draw agents usually offer easy recovery through energy-intensive established methods such as RO, UF and distillation [66, 70, 72, 74]. Organic draw agents show variable recovery depending on molecular properties, with some phase-separating draw agents requiring additional membrane separation processes [133]. The recovery of hydrogels can either be simple, using methods such as squeezing, or complex, requiring stimulus-responsive methods. Inorganic draw agents usually exhibit high reverse fluxes, such as 23.6 gMH for NaCl [65]. Organic draw agents usually demonstrate low reverse flux due to their larger sizes. Hydrogels usually achieve minimal or zero reverse fluxes through size exclusion [57, 58]. Inorganic draw agents are usually cheaper and readily available. Organic draw agents are usually slightly more expensive. Hydrogels may incur high costs due to synthesis requirements. Inorganic draw agents demonstrate excellent chemical stability. Organic draw agents show variable stability whilst hydrogels may experience swelling/deswelling issues. Thus, inorganic draw agents have been studied extensively for most FO applications due to their high osmotic pressure and established though energy intensive recovery methods, despite higher reverse solute flux. However, the optimal choice depends on specific application requirements and no ideal draw agent has yet been established.

A more detailed comparison of the performance of hydrogels and inorganic draw agents in FO processes was recently conducted by Hashemifard et al. [176]. In their experimental setup, the same membrane was employed for both draw agents, with NaCl selected as the inorganic draw agent and sodium acrylate superabsorbent polymer as the hydrogel draw agent. NaCl solutions of varying concentrations were used for both feed and draw solutions, with pure water also employed as feed in selected experiments. Both types of draw agents were evaluated in FO and PRO modes. The comparative analysis revealed that NaCl draw agents produced higher water fluxes than the hydrogel draw agent, although the hydrogel maintained above

zero fluxes across all tested feed solution concentrations. The osmotic pressure difference between the NaCl draw agent and pure water was greater than the swelling pressure difference between the hydrogel and pure water, thus accounting for the higher fluxes observed with NaCl draw agents. The researchers identified this performance gap as a major concern for hydrogel systems in FO processes. The results also demonstrated higher water fluxes in PRO mode compared to FO mode when using NaCl feed solutions. Increasing the quantity of hydrogels and reducing hydrogel particle size were identified as factors that enhanced water fluxes in the FO system. The authors questioned the adequacy of hydrogel draw agents for desalination processes and recommended the development of novel membranes with minimal resistance to optimize this process - a commitment they have made for their future studies. They also proposed implementing continuous day-night cycles for hydrogel draw agents, rather than single swelling-deswelling cycles, to enhance flux performance.

1.2.3   Specific energy consumption and Total costs of FO processes

Any FO process requires a minimal energy requirement of ~ 0.25 kWh m^{-3}, primarily for feed and draw solution circulation across the FO membrane [132]. The energy demands of FO with proprietary draw solutes contrasted against other desalination technologies is detailed in Table 1.4.

Table 1.2: Some of the inorganic draw solutes since 2000

Reference; Draw solute; Feed solution	Draw properties (Concentration., Osmotic pressure)	Temperature (ºC); Water flux; Solute flux; FO Membrane	Regeneration method	SEC and Cost Analysis
(McCutcheon et al., [63]); Ammonium bicarbonate; 0.5 M NaCl	6M; 150 atm	50; 6.5 μm/s; -; HTI CTA	Thermal	-
(McGinnis and Elimelech, [64]); Ammonia–CO$_2$; 1.5 M NaCl	-	Low temp; -; -; -	Thermal	Energy - 0.24 kWh/m^3
(Cornelissen et al., [65]); Magnesium sulphate; DI	1.5 M; 73 bar	20; 1.1 LMH; 0.04 gMH; TFC-NF	-	-
(Cornelissen et al., [65]); Magnesium sulphate; DI	1.5 M; 73 bar	20; 0.4 LMH; 0.01 gMH; TFC-RO	-	-
(Cornelissen et al., [65]); Sodium Nitrate; Activated sludge	1.5 M; 73 bar	20; 8.1 LMH; 66 gMH; CTA	-	-
(Cornelissen et al., [65]); Sodium chloride; Activated sludge	1 M; 49 bar	20; 7.6 LMH; 15.4 gMH; CTA	-	-
(Cornelissen et al., [65]); Sodium chloride; Activated sludge	1.5 M; 73 bar	20; 9.6 LMH; 23.6 gMH; CTA	-	-
(Cornelissen et al., [65]); Sodium chloride; Activated sludge	4.5 M; 219 bar	20; 12.9 LMH; 48.5 gMH; CTA	-	-
(Cornelissen et al., [65]); Zinc sulphate; Activated sludge	0.5 M; 24 bar	20; 2.7 LMH; 4.1 gMH; CTA	-	-
(Cornelissen et al., [65]); Zinc sulphate; Activated sludge	1 M; 49 bar	20; 3.7 LMH; 2.9 gMH; CTA	-	-
(Cornelissen et al., [65]); Zinc sulphate; Activated sludge	1.5 M; 73 bar	20; 4.2 LMH; 3.8 gMH; CTA	-	-
(Cornelissen et al., [65]); Zinc sulphate;	2.3 M; 112 bar	20; 4.8 LMH; 4.6 gMH; CTA	-	-

Activated sludge				
(Cornelissen et al., [65]); Sodium chloride; DI	0.5 M; 24 bar	20; 5.1 LMH; 7.4 gMH; CTA	-	-
(Achilli et al., [66]); Sodium sulphate; Ultrapure water	127.3 g/L; 4.2 MPa	25; 2.56× 10^{-6} m/s; 3.1 gMH; HTI CTA	RO	Cost - 0.004 $/L
(Achilli et al., [66]); Sodium bicarbonate; Ultrapure water	63.9 g/L; 2.8 MPa	25; 2.47× 10^{-6} m/s; 1.7 gMH; HTI CTA	RO	Cost - 0.009 $/L
(Achilli et al., [66]); Sodium Chloride; Ultrapure water	50.8 g/L; 4.2 MPa	25; 3.38×10^{-6} m/s; 9.1 gMH; HTI CTA	RO	Cost - 0.013 $/L
(Achilli et al., [66]); Potassium bicarbonate; Ultrapure water	99 g/L; 4.2 MPa	25; 2.80× 10^{-6} m/s; 2 gMH; HTI CTA	RO	Cost - 0.015 $/L
(Achilli et al., [66]); Magnesium sulphate; Ultrapure water	141.3 g/L; 2.8 MPa	25; 1.54×10^{-6} m/s; 1.2 gMH; HTI CTA	RO	Cost - 0.015 $/L
(Achilli et al., [66]); Magnesium chloride; Ultrapure water	47.6 g/L; 4.2 MPa	25; 2.70×10^{-6} m/s; 5.6 gMH; HTI CTA	RO	Cost - 0.018 $/L
(Achilli et al., [66]); Ammonium chloride; Ultrapure water	48.2 g/L; 4.2 MPa	25; 3.61×10^{-6} m/s; 10.2 gMH; HTI CTA	RO	Cost - 0.023 $/L
(Achilli et al., [66]); Potassium sulphate; Ultrapure water	101.4 g/L; 2.8 MPa	25; 2.52×10^{-6} m/s; 3.7 gMH; HTI CTA	RO	Cost - 0.031 $/L
(Achilli et al., [66]); Calcium chloride; Ultrapure water	62.3 g/L; 4.2 MPa	25; 3.22×10^{-6} m/s; 9.5 gMH; HTI CTA	RO	Cost - 0.032 $/L
(Achilli et al., [66]); Ammonium sulphate; Ultrapure water	109.1 g/L; 4.2 MPa	25; 2.74×10^{-6} m/s; 3.6 gMH; HTI CTA	RO	Cost - 0.033 $/L
(Achilli et al., [66]); Potassium chloride; Ultrapure water	70.3 g/L; 4.2 MPa	25; 3.74×10^{-6} m/s; 15.2 gMH; HTI CTA	RO	Cost - 0.05 $/L
(Achilli et al., [66]); Calcium nitrate; Ultrapure water	131.2 g/L; 4.2 MPa	25; 2.97×10^{-6} m/s; 6.6 gMH; HTI CTA	RO	Cost - 0.091 $/L
(Achilli et al., [66]); Ammonium bicarbonate; Ultrapure water	83.4 g/L; 4.2 MPa	25; 2.85×10^{-6} m/s; 20.6 gMH; HTI CTA	-	Cost - 0.111 $/L

(Achilli et al., [66]); Potassium bromide; Ultrapure water	104.7 g/L; 4.2 MPa	25; 3.59×10^{-6} m/s; 29.2 gMH; HTI CTA	-	Cost - 0.172 $/L
(Su et al., [67]); Magnesium chloride; Saline water	2 M; 258.3 bar	25; 7.3 LMH; 0.53 gMH; CA NF	-	-
(Phuntsho et al., [68]); Fertilizer – (KCl); DI	2 M; 89.3 atm	25; 6.337 µm/s; 0.222000 mmoles/m²s; HTI CA	Fertigation	-
(Phuntsho et al., [68]); Fertilizer – ($NaNO_3$); DI	2 M; 81.1 atm	25; 5.706 µm/s; 0.277500 mmoles/m²s; HTI CA	Fertigation	-
(Phuntsho et al., [68]); Fertilizer – (KNO_3); DI	2 M; 64.9 atm	25; 4.429 µm/s; 0.485625 mmoles/m²s; HTI CA	Fertigation	-
(Phuntsho et al., [68]); Fertilizer – (NH_4NO_3); DI	2 M; 64.9 atm	25; 4.177 µm/s; 0.790876 mmoles/m²s; HTI CA	Fertigation	-
(Phuntsho et al., [68]); Fertilizer – (NH_4Cl); DI	2 M; 87.7 atm	25; 5.348 µm/s; 0.333000 mmoles/m²s; HTI CA	Fertigation	-
(Phuntsho et al., [68]); Fertilizer – (($NH_4)_2SO_4$); DI	2 M; 92.1 atm	25; 5.391 µm/s; 0.005550 mmoles/m²s; HTI CA	Fertigation	-
(Phuntsho et al., [68]); Fertilizer – ($NH_4H_2PO_4$); DI	2 M; 86.3 atm	25; 4.349 µm/s; 0.069375 mmoles/m²s; HTI CA	Fertigation	-
(Phuntsho et al., [68]); Fertilizer – ($Ca(NO_3)_2$); DI	2 M; 108.5 atm	25; 5.022 µm/s; 0.009019 mmoles/m²s; HTI CA	Fertigation	-
(Phuntsho et al., [68]); Fertilizer – (($NH_4)_2HPO_4$); DI	2 M; 95.0 atm	25; 3.892 µm/s; 0.009713 mmoles/m²s; HTI CA	Fertigation	-
(Yangali-Quintanilla et al.,[69]); Real Red Sea seawater; Secondary wastewater effluent	-	20; 5.5 LMH; -; HTI CA	FO–LPRO	Energy consumption - 1.5 kWh/m³ Cost - 0.91 USD/m³
(Su et al., [70]); Sodium chloride; DI	0.60 M; 28 atm	25; 9.6 LMH; 9.1 gMH; HTI CTA	RO	Cost - 0.013 $/L

(Su et al., [70]); Magnesium chloride; DI	0.36 M; 28 atm	25; 8.4 LMH; 5.6 gMH; HTI CTA	RO	Cost - 0.018 $/L
(Su et al., [70]); Potassium Chloride; DI	2 M; 89.3 atm	25; 22.6 LMH; 0.222000 mmoles/m^{2}s; HTI CA	Fertigation	-
(Su et al., [70]); Ammonium bicarbonate; DI	0.67 M; 28 atm	25; 7.3 LMH; 20.6 gMH; HTI CTA	-	Cost - 0.111 $/L
(Alnaizy et al., [71]); Copper sulphate; 5050 ppm NaCl	200 000 ppm; 29.94 bar	25; 3.57 LMH; -; HTI CTA	Metathesis precipitation	-
(Amjad et al., [72]); K/CNF; DI	0.2 wt.% K/CNF and 20 vol.% TEG; 70.3 bar	25; 13.3 LMH; 0.031 g/L; pre-wetted FO flat sheet (Aquaporin Inside)	Evaporation	-
(Gulied et al., [73]); Single fertilizer draw solution; Synthetic wastewater	22 g/L has 23.73-29.04 bar	25; 4.43 LMH; varying; FTSH2 CTA	-	-
(Gulied et al., [73]); multi-component draw solution; Synthetic wastewater	200 g/L; 222 g/L - 6.64 bar	25; 14.0 LMH; varying; FTSH2 CTA	-	Energy - 0.312 kW/h m^3
	100 g/L; 222 g/L - 6.64 bar	25; 10 LMH; varying; FTSH2 CTA	-	Energy - 0.23 kW/h m^3
(Gadelha et al., [74]); Sodium dodecyl sulphate; DI	1 M; 0.35 bar	-; 2.98 × 10^{-7} mol/m^2/h; -; HTI CTA	UF	-
(Gadelha et al., [74]); 1-octane sulfonic acid sodium salt; DI	1 M; 5 bar	-; 2.01 × 10^{-6} mol/m^2/h; -; HTI CTA	UF	-
(Gadelha et al., [74]); Meristyl trimethyl ammonium bromide; DI	1 M; -	-; 6.8 × 10^{-7} mol/m^2/h; -; HTI CTA	UF	-
(Gadelha et al., [74]); Trimethyl octyl ammonium bromide; DI	1 M; 27.2 bar	-; 1.58 × 10^{-6} mol/m^2/h; -; HTI CTA	UF	-
(Gadelha et al., [74]); Tetraethyl ammonium bromide; DI	1 M; 42 bar	-; 2.28 × 10^{-6} mol/m^2/h; -; HTI CTA	UF	-
(Liu et al., [75]); NH$_4$Cl; DI	0.5 M; 22 atm	25; 2.217 μm/s; -; HTI TFC	Irrigation	-

(Liu et al., [75]); K$_2$SO$_4$; DI	0.5 M; 24 atm	25; 2.140 μm/s; -; HTI TFC	Irrigation	-
(Liu et al., [75]); KCl; DI	0.5 M; 22 atm	25; 2.012 μm/s; -; HTI TFC	Irrigation	-
(Liu et al., [75]); KNO$_3$; DI	0.5 M; 20 atm	25; 1.926 μm/s; -; HTI TFC	Irrigation	-
(Liu et al., [75]); NH$_4$NO$_3$; DI	0.5 M; 18 atm	25; 1.884 μm/s; -; HTI TFC	Irrigation	-
(Liu et al., [75]); NaCl; DI	0.5 M; 23 atm	25; 1.781 μm/s; -; HTI TFC	Irrigation	-
(Liu et al., [75]); (NH$_4$)$_2$HPO$_4$; DI	0.5 M; 27 atm	25; 1.551 μm/s; -; HTI TFC	Irrigation	-
(Liu et al., [75]); Urea; DI	0.5 M; 12 atm	25; 0.577 μm/s; -; HTI TFC	Irrigation	-
(Liu et al., [75]); NH$_4$HCO$_3$; DI	0.5 M; 20 atm	25; 1.534 μm/s; -; HTI TFC	Irrigation	-
(Liu et al., [75]); NH$_4$Cl + NH$_4$HCO$_3$; DI	0.5 M:0.5 M; 49 atm	25; 3.108 μm/s; -; HTI TFC	Irrigation	-
(Liu et al., [75]); K$_2$SO$_4$ + NH$_4$HCO$_3$; DI	0.5 M:0.5 M; 37 atm	25; 2.858 μm/s; -; HTI TFC	Irrigation	-
(Liu et al., [75]); KCl + NH$_4$HCO$_3$; DI	0.5 M:0.5 M; 50 atm	25; 3.093 μm/s; -; HTI TFC	Irrigation	-
(Liu et al., [75]); KNO$_3$ + NH$_4$HCO$_3$; DI	0.5 M:0.5 M; 38 atm	25; 3.036 μm/s; -; HTI TFC	Irrigation	-
(Liu et al., [75]); NH$_4$NO$_3$ + NH$_4$HCO$_3$; DI	0.5 M:0.5 M; 37 atm	25; 2.839 μm/s; -; HTI TFC	Irrigation	-
(Liu et al., [75]); NaCl + NH$_4$HCO$_3$; DI	0.5 M:0.5 M; 50 atm	25; 3.028 μm/s; -; HTI TFC	Irrigation	-
(Liu et al., [75]); (NH$_4$)$_2$HPO$_4$ + NH$_4$HCO$_3$; DI	0.5 M:0.5 M; 42 atm	25; 2.553 μm/s; -; HTI TFC	Irrigation	-
(Liu et al., [75]); Urea + NH$_4$HCO$_3$; DI	0.5 M:0.5 M; 32 atm	25; 2.142 μm/s; -; HTI TFC	Irrigation	-
(Qasim et al., [76]); ferric sulphate; 5000 ppm NaCl	280 000 ppm; 52.6 atm	25; 3.75 LMH; 1.88 gMH; HTI CTA	Precipitation	-
(Aende et al.,[77]); Sodium carbon nanofibers; DI	0.1 wt./vol%; 93.9 bar	25; 4.13 LMH; 0.24 gMH; FTSH2O™ CTA	Evaporation	-

Table 1.3: Organic and other draw solutes since the year 2000

Reference; Draw solute; Feed solution	Draw properties (Concentration., Osmotic pressure)	Temperature (ºC); Water flux; Solute flux; FO Membrane	Regeneration method	SEC and Cost analysis
(Tang and Ng, [78]); Fructose; 1 M NaCl	5 M; 498.5 atm	50; 15 LMH; -; CA	-	-
(Yen et al.,[79]); 2-Methylimidazole-based ($C_{11}H_{18}I_2N_4$); 3.5 wt.% NaCl	0.5 M; ~ 40 bar	23; 10.75 LMH; 0.90 gMH; HTI CTA	FO–MD	-
(Yong et al. [80]); Urea; DI	4 M; -	20; 7.5 LMH; 8 mol m^{-2}h^{-1}; HTI CTA	-	-
(Yong et al. [80]); Ethylene glycol; DI	2 M; -	20; 4 LMH; 2.1 mol m^{-2}h^{-1}; HTI CTA	-	-
(Yong et al. [80]); Glucose; DI	1 M; -	20; 3 LMH; ~0 mol m^{-2}h^{-1}; HTI CTA	-	-
(Kim et al., [81]); Methanol; -	3 M; 67.517 atm	-	Distillation	Cost - 4.512 ($/t)
(Kim et al., [81]); Ethanol; -	3 M; 62.794 atm	-	Distillation	Cost - 4.201 ($/t)
(Kim et al., [81]); 2-Butanone; -	3 M; 61.392 atm	-	Distillation	Cost - 1.372 ($/t)
(Kim et al., [81]); Methyl acetate; -	3 M; 53.657 atm	-	Distillation	Cost - 3.837 ($/t)
(Kim et al., [81]); 2-Propanol; -	3 M; 50.485 atm	-	Distillation	Cost - 4.609 ($/t)
(Bowden et al., [82]); Magnesium acetate; DI	264 g/L; 4.2 MPa	25; 2.47 m/s; 1.06 gMH; HTI CTA	RO	Cost - 0.029 ($/L)
(Bowden et al., [82]); Sodium formate; DI	70 g/L; 4.2 MPa	25; 3.25 m/s; 7.63 gMH; HTI CTA	RO	Cost - 0.090 ($/L)
(Bowden et al., [82]); Sodium acetate; DI	139 g/L; 4.2 MPa	25; 2.89 m/s; 3.55 gMH; HTI CTA	RO	Cost - 0.018 ($/L)
(Bowden et al., [82]); Sodium propionate; DI	102 g/L; 4.2 MPa	25; 2.97 m/s; 2.29 gMH; HTI CTA	RO	Cost - 0.019 ($/L)

(Ge et al., [83]); Polyelectrolytes of PAA-Na; DI	0.25 g/mL; 20 atm	25; 6 LMH; ~ 0.5 gMH; HTI CTA	UF	-
(Alnaizy et al., [71]); Sucrose; DI	1 M; 26.7 atm	25; 12.9 LMH; Minimal; CA hollow fibre	NF	-
(Su et al., [70]); PAA-Na 1200; DI	0.72 g/mL; 44 atm	25; 22 LMH; ~ 0.5 gMH; HTI CTA	UF	-
(Su et al., [70]); Poly (ethylene glycol) diacid-coated MNPs; DI	0.065 M; 73 atm	23; 13 LMH; 0 gMH; HTI CTA	Magnet	-
(Su et al., [70]); 1,2,3-Trimethylimidazolium iodide; DI	1 M; 50 atm	23; 13 LMH; 0.90 gMH; HTI CTA	FO–MD	-
(Su et al., [70]); Sodium formate; DI	0.68 M; 28 atm	25; 9.4 LMH; 7.63 gMH; HTI CTA	RO	Total cost - 0.090 ($/L)
(Su et al., [70]); Polyglycol copolymer; 3.5% NaCl	30-70%; 40-95 atm	-; $\geq$ 4 LMH; -; HTI CTA	-	-
(Su et al., [70]); Sodium hexa-carboxylatophenoxy phosphazene; DI	0.067 M; -	30; 6 LMH; -; HTI CTA	-	-
(Stone et al., [84]); Switchable polarity solvents; 1 mol/kg NaCl	7.6 mol/kg; 325 atm	30; 16 LMH; -; HTI CTA	Switching process	-
(Ou et al., [85]); Thermo-sensitive polyelectrolytes; DI	14.28 wt.%; 31.2 atm	25; 0.347 LMH; -; HTI CTA	Hot UF	Energy: (Wh·m^{-3}) - 1965.13. Cost: (RMB·ton^{-1}) - 1.18
(Yu et al., [86]); HA-GO/PVA monolith; Seawater	1:1 HA: GO (mass ratio); -	25; 7.2 LMH; 0 gMH; HTI CTA-ES	Squeezing	-
(Zhao et al., [87]); Polyacrylamide (MW - 3 000 000); RBR dye solution	20 g/L; 366 mOsm/kg	25; 3.211 LMH; 0.015 gMH; PA-based TFC	-	-
(Ray et al., [88]); Chlorhexidine gluconate-based Mouthwash; DI	25%; > 600 mOsm/kg	25; 8 LMH; SRSF - 0.07 g/L; HTI TFC	Membrane Distillation	-

(Yu et al., [89]); Ferric-lactate complex; DI	1 M; 3180 mOsm kg^{-1}	25; 18.78 LMH; 1 gMH; HTI CTA-ES	NF	-
(Long et al., [90]); Oligomeric Sodium carboxylates; 0.15 or 0.6 M NaCl	0.5 mol/kg; 143 bar	25; 23.5 LMH; 0.5 gMH; HTI-TFC	NF	-
(Ding et a., [91]); Polysaccharide derivatives; DI	40 wt.%; 65 bar	25; 24.9 LMH PRO; 0.97 gMH; PVDF-TFC	UF	SEC - low
(Wang et al., [92]); Thermo-sensitive polyelectrolyte; DI	0.20 g/ml; 72×10^{-5} Pa	25; 2.09 LMH; Very low; HTI CTA	Centrifugation	-
(Zhao et al., [93]); Thermo-responsive PSSS-PNIPAM; Seawater	33.3 wt.%; 2137 mOsm kg^{-1}.	-; 4 LMH; -; HTI TFC	Membrane distillation	Energy - 1.16 kWh/m^3 for every 1 °C MD - 29 kWh/m^3
(Orme et al., [94]); 1-Cyclohexylpiperidine; 0.5 mol/kg NaCl	5 mol/kg; > 500 atm	25; 8.5 kg/m^{2}h; 0.0040 kg/m^{2}h; Polyamide TFC	CO$_2$ removal	-
(Zhao et al., [95]); EDTA-MgNa$_2$; DI	0.5 M; 1500 mOsm/kg	25; 8 LMH; 1 gMH; HTI TFC	NF	Cost: 0.47 $/m^3
(Zhao et al., [95]); EDTA-CaNa$_2$; DI	0.5 M; 1500 mOsm/kg	25; 8 LMH; 1 gMH; HTI TFC	NF	Cost: 0.32 $/m^3
(Zhao et al., [95]); EDTA-MnNa$_2$; DI	0.5 M; 1500 mOsm/kg	25; 8 LMH; 1 gMH; HTI TFC	NF	Cost: 0.41 $/m^3
(Zhao et al., [95]); EDTA-ZnNa$_2$; DI	0.5 M; 1500 mOsm/kg	25; 8.5 LMH; 1 gMH; HTI TFC	NF	Cost: 0.30 $/m^3
(Kim et al., [96]); Poly(tetra butyl phosphonium styrene sulfonate)s; DI	20 wt.%; 20.85 atm	25; 14.50 LMH; 0.14 gMH; HTI TFC	Thermal precipitation	-
(Kumar et al., [97]); Hydrolysed poly(isobutylene-alt-maleic anhydride); DI	0.375 g/mL; 1500 mmol/kg	60; 34 LMH PRO; 0.196 gMH; HTI CTA	Membrane distillation	-
(Huang et al., [98]); Poly(4-styrenesulfonic acid-co-maleic acid)	0.25 g/ml; 32.8 bar	25; 15 LMH under PRO; 0.04 gMH; HTI TFC	NF	-

sodium salt; DI				
(Monjezi et al., [99]); Dimethyl ether (Chabahar, Iran); 0.5 wt.% NaCl	7.0 wt.%; 0.43 MPa	-	Thermal	Energy - 0.46 kWh/m^3
(Laohaprapanon et al. [100]); Natural polyelectrolyte; DI	30 wt.%; 11.91 atm	45; 4.10 LMH for PRO; 1.62 gMH; HTI TFC	UF	-
(Yang et al., [101]); Polyacrylic acid sodium salts (PAA-Na); DI	25 wt.%; -	21; 18.02 LMH; 0.110 gMH; HTI TFC	Combined pH and MF	Cost - 0.037 \$/m^3
(Zeweldi et al., [102]); Tetraethylammonium bromide ([N2222]Br) IL; DI	0.50 M; -	25; 10.65 LMH; 0.0397 molm^{-2} h^{-1}; HTI CTA	Membrane distillation	Energy - 0.5 kWhm^{-3}
(Zeweldi et al., [102]); Tetraethylammonium bromide ([N2222]Br) IL; DI	1 M; -	25; 14.20 LMH; 0.066 molm^{-2} h^{-1}; HTI CTA	Membrane distillation	Energy - 0.5 kWhm^{-3}
(Zeweldi et al., [102]); Tetraethylammonium bromide ([N2222]Br) IL; DI	2 M; -	25; 21.27 LMH; 0.086 molm^{-2} h^{-1}; HTI CTA	Membrane distillation	Energy - 0.5 kWhm^{-3}
(Zeweldi et al., [102]); Tetraethylammonium bromide ([N2222]Br) IL; DI	4 M; 167.8 bar	25; 26.46 LMH; 0.1128 molm^{-2} h^{-1}; HTI CTA	Membrane distillation	Energy - 0.5 kWhm^{-3}
(Huang et al., [103]); Sodium phytate; DI	0.45M; 76.38 bar	25; 19.02 LMH in PRO; 0.51 gMH; HTI TFC	Dilution	-
(Huang et al., [103]); Sodium phytate; DI	0.45M; 76.38 bar	25; 30.35 LMH in PRO; 0.61 gMH; HPAN-TFC	Dilution	-
(Islam et al., [104]); Potassium acetate (KAc); DI	0.66 M; 28 bar	24; 15.48 LMH; 0.021-0.04 mol/m^2.h; HTI TFC	Membrane distillation	-
(Islam et al., [104]); Ammonium acetate (NH$_4$Ac); DI	0.91 M; 28 bar	24; 15.86 LMH; 0.021-0.04 mol/m^2.h; HTI TFC	Membrane distillation	-
(Islam et al., [104]); Ammonium carbamate (NH$_4$Car); DI	0.38 M; 28 bar	24; 16.56 LMH; 0.021-0.04 mol/m^2.h; HTI TFC	Membrane distillation	-

(Islam et al., [104]); Ammonium formate (NH$_4$For); DI	0.62 M; 28 bar	24; 16.92 LMH; 0.021-0.04 mol/m^2.h; HTI TFC	Membrane distillation	-
(Islam et al., [104]); Potassium formate (KFor); DI	0.68 M; 28 bar	24; 17.15 LMH; 0.021-0.04 mol/m^2.h; HTI TFC	Membrane distillation	-
(Islam et al., [104]); Sodium propionate (NaPro); DI	0.69 M; 28 bar	24; 19.71 LMH; 0.021-0.04 mol/m^2.h; HTI TFC	Membrane distillation	-
(Islam et al., [104]); Sodium glycolate (NaGly); DI	0.73 M; 28 bar	24; 18.47 LMH; 0.021-0.04 mol/m^2.h; HTI TFC	Membrane distillation	-
(Kim et al., [105]); Ethanol; DI	10 wt.%; 46.7 bar	25; 17 LMH; 240 g/m^1.h^1; Porifera Inc. TFC	Vacuum distillation	Energy - 8.8 kWh/m^3
(Shokrollahzadeh et al., [106]); Itaconic acid-choline chloride (IA-CC); DI	1.2 mol/L; 204.1 atm	25; 32.8 LMH; 1.4 gMH; HTI CTA	Phase separation at 5 ℃	-
(Zeweldi et al., [107]); Tetrabutylammonium 2,4,6-trimethylbenzenesulfonate; DI	2 M; 58.92 bar	25; 12.3 LMH in PRO; 0.006 mol/m^2.h^1; TFC	Thermal precipitation	Energy - 9.95 kWh m^{-3} Cost – 0.756 \$/m^3
(Nguyen et al., [108]); Mixed trivalent draw solution containing of EDTA–2Na and Na$_3$PO$_4$; DI	0.3 M EDTA–2Na and 0.55 M Na$_3$PO$_4$; 50 atm	25; 9.17 LMH; 0.053 g/L; HTI CTA	Membrane distillation	-
(Kamel et al., [109]); Sodium carbon quantum dots; DI	0.5 g/ml; 113.9967 bar	29; 11.935 LMH; 0.0621 gMH; CTA-FO	Thermal	-
(Kamel et al., [109]); Potassium carbon quantum dots; DI	0.5 g/ml; 121.0399 bar	29; 13.924 LMH; 0.0253 gMH; CTA-FO	Thermal	-
(Ge et al., [110]); Poly(ethylene glycol) diacid-coated MNPs; DI	0.065 M; 73 atm	23; 16.2 LMH; 0 gMH; HTI CTA	Magnetic	-
(Guizani et al., [111]); Polyethylene glycol 4000 coated MNPs; Urine	9.6 g/L; 14.9 atm	25; > 1 LMH; 0 gMH; FTSH2O™ CTA	Magnetic	-
(Hafiz et al., [47]); Polyethylene glycol 5000 coated MNPs; DI	1800 ppm; 14.6 Pa	25; 1.16 LMH; 0 gMH; Porifera	Magnetic	-

(Mishra et al., [112]); Polyethylene glycol coated MNPs; DI	0.08 M; -	25; 11.30 LMH; -; HTI CTA	Electromagnet	-
(Mishra et al., [112]); Polyacrylic acid coated MNPs; DI	0.08 M; -	25; 13.85 LMH; -; -	-	-
(Ling et al., [113]); Polyacrylic acid coated MNPs; -	-; 6 atm	22; 0 gMH; HTI CTA	-	-
(Ling et al., [114]); Polyacrylic acid coated MNPs; DI	-; -	22; 10.4 LMH; 0 gMH; HTI CTA	Magnetism	-
(Ling et al., [115]); MNPs capped with Tri ethylene glycol; DI	0.23 mol/L; 70 atm	22; 7 LMH; -; HTI CTA	Magnetic / UF	-
(Ling et al., [116]); MNPs functionalized with poly(N-isopropyl acrylamide) and triethylene glycol; DI	-	22; 1.2 LMH; 0 gMH; HTI CTA	Magnetic	-
(Yang et al., [117]); Hyperbranched Polyglycerol Carboxylate-Coated MNPs; DI	500 g/L; 16 atm	25; 7.2 LMH; 0 gMH; HTI CTA	UF	-
(Yang et al., [118]); Hyperbranched polyglycerol-coated MNPs; DI	400 g/L; 10 atm	25; 3.0 LMH; 0 gMH; HTI CTA	UF	-
(Ban et al., [119]); Poly-Sodium-Acrylate (PSA)-Coated MNPs; DI	7 wt.%; 8.8 atm	23; 3.8 LMH; 0.05 gMH; AIM Aquaporin	UF	-
(Zhou et al., [120]); Poly(N-isopropylacrylamide-co-sodium 2-acrylamido-2-methylpropane sulfonate) magnetic nanogels; DI	20 g/L; 3.3 atm	25; 0.25 LMH; -; HTI CTA	Thermal – Magnetic	-
(Zhao et al., [121]); Fe_3O_4 NPs grafted with copolymer poly(sodium styrene-4-sulfonate)-co-poly(N-isopropylacrylamide; DI	33 wt.%; 55 atm	25; 14.9 LMH; -; HTI CTA	Magnetic / UF	-
(Shakeri et al., [122]); MNP-	-; -	25; 5.72 LMH; -; TFC-FO	Magnetic	-

crosslinked ferro hydrogel; DI				
(Bai et al., [123]); Dextran coated Fe₃O₄ MNPs; DI	2.0 M; -	22; 9.0 LMH; 0 gMH; HTI CTA	Magnetic	-
(Attallah et al., [124]); Pectin-coated MNPs; Well water	2 wt.%; -	25; 0.4 LMH; -; PES Aquaporin	Magnetic	-
(Tayel et al., [125]); Pectin-coated MNPs; 1% NaCl	0.5 wt.%; -	25; 7 LMH; -; Porifera	Magnetic	-
(Shabani et al., [126]); Chitosan and dehydroascorbic acid-coated MNPs; DI	0.06 g/L; -	25; 5.3 LMH; -; CA/CTA	Magnetic	-
(Azadi et al., [127]); Gelatin-Coated MNPs; DI	14.3 g/L; -	30; 1.54 LMH; -; HTI CTA	Magnetic	-
(Khazaie et al., [128]); Sulfonated sodium alginate MNPs; DI	60 g/L; 117.2 atm	25; 12.8 LMH; 1.5 gMH; CTA	Magnetic	-
(Na et al., [129]); Citrate coated MNPs; DI	20 mg/L; -	25; 13 LMH; -; HTI CTA	Magnetic	-
(Ge et al., [130]); Citric acid coated MNPs; DI	0.8 g/mL; 68 atm	23; 12.6 LMH; 0.08–0.09 gMH; TFC-PES	Magnetic, then NF	-
(Ge et al., [130]); Oxalic acid coated MNPs; DI	0.8 g/mL; 56 atm	23; 10.2 LMH; 0.08–0.09 gMH; TFC-PES	Magnetic, then NF	-
(Ge et al., [130]); EDTA coated MNPs; DI	0.8 g/mL; 40 atm	23; 8.2 LMH; 0.08–0.09 gMH; TFC-PES	Magnetic, then NF	-
(Khazaie et al.,[131]); Sodium alginate sulphate; DI	0.11 g/mL; 219.89 atm	25; 28.5 LMH; 3.4 gMH; CTA	RO	-
(Zeweldi et al., [132]); Supramolecular host-guest complex of methylated β-cyclodextrin with polymerized ionic liquid ([vbim]TFSI)n; DI	0.5 M; 7 Osm/kg	25; 13.73 LMH PRO; 4.41×10^{-3} mol/m².h[1]; TFC	Heating, then NF	Energy - 5.54 kWh m⁻³ Cost - $ 0.42 m⁻³

Table 1.4: SEC, in kWh/m³ of various desalination technologies compared to FO, adapted from (Colciaghi et al., [133])

Desalination technology	Electrical (kWh_{ele}/m^3)	Thermal (kWh_{ther}/m^3)	Total electricity (kWh_{ele}/m^3)
Multi-stage flash distillation (MSF)	$2.5 - 5$	$53 - 65$	$19.6 - 27.3$
Multiple effect distillation (MED)	$2 - 2.5$	$40 - 64$	$14.5 - 21.4$
Mechanical vapour compression (MVC)	$7 - 12$	-	$7 - 12$
Thermal vapour compression (TVC)	$1.8 - 1.6$	63	16.3
Reverse osmosis (RO)	$4 - 6$	-	$4 - 6$
Electrodialysis (ED)	$2.6 - 5.5$	-	$2.6 - 5.5$
Forward osmosis (FO) using PAGB	$0.5 - 1.9$	$39.5 - 123$	$6.7 - 21.8$
Forward osmosis (FO) using AB	> 3.51	> 442	> 90.6

The energy consumption is quantified as: [91]

$$E_{FO} = \frac{1}{\eta_{pump}} \times Q_{draw} \times (P_{FO} - P_0) + \frac{1}{\eta_{pump}} \times Q_{feed} \times (P_{FO} - P_0) \qquad (1.1)$$

where, Q_{draw}, Q_{feed}, P_{FO}, P_0 and η_{pump} are the draw solution flow rate in the module, feed solution flow rate in the module, operating pressure, ambient pressure and efficiency of the pump, respectively. The Specific Energy Consumption (SEC), quantified in kWh/m³, is determined as follows: [91]

$$SEC = \frac{E}{Q_P} \qquad (1.2)$$

$$Q_P = J_w \times A_m \qquad (1.3)$$

where, Q_P is the flow rate of the permeate.

In developing the SEC equation, the key assumptions include an infinite membrane area, water recovery (Y) determined as the ratio of permeate flow rate to feed solution flow rate, pump efficiency assumed to be 100% to consume the lowest

electrical energy, and negligible pressure drops in FO modules due to extremely low flow velocities [91]. It should be noted that some of these assumptions represent highly idealized conditions that do not reflect real-world operational parameters. In practice, pump efficiencies typically range from 70 - 85% for centrifugal pumps depending on design or sizes. The pressure drops, while minimal in FO systems, are not negligible in large-scale installations. These simplifications result in SEC estimates that represent theoretical lower bounds rather than realistic energy consumption values. The actual energy requirements would be higher due to pump inefficiencies and system pressure losses, with the magnitude of increase depending on specific system design and operating conditions.

RO is energy-demanding due to its requirement for substantial hydraulic pressure to overcome the seawater's osmotic pressure [93]. Basing on thermodynamic analysis and presuming 3.5% salinity and 50% water recovery, the RO process's practical minimum energy is nearly 1.5 kWh/m^3 [93]. Typically, the energy requirement ranges between 3-7 kWh/m^3 for RO [93]. In turn, for FO processes to rival existing RO in energy consumption, the comprehensive energy demand, including the draw solute recovery system must not exceed 4 kWh/m^3 [93]. This implies that the energy expenditure for the draw solute regeneration process should remain under 3.75 kWh/m^3 [93]. However, as discernible from Tables 1.2 and 1.3, the majority of scholars overlooked the energy expenditure and overall cost of FO processes in their investigations.

1.2.4   FO Membranes

Any material exhibiting characteristics such as high density, non-porosity and selective permeability can theoretically be suitable for use as a FO membrane [134]. Traditional RO membranes are suboptimal for FO applications due to fundamental structural differences. RO membranes require substantial mechanical strength to withstand applied hydrostatic pressures [134, 172]. This is achieved through a composite structure comprising a dense sponge-like support layer reinforced with a loose mesh backing. The support layer exhibits increasing density toward the active layer to provide a smooth substrate for active layer formation [134, 172]. Conversely,

FO membranes operate without external hydraulic pressure, thus eliminating the need for high mechanical strength. This allows FO membranes to use a single, thinner support layer with a more open pore structure. The reduced thickness and enhanced porosity significantly enhance FO performance while minimizing ICP. [134, 172].

Figure 1.6 shows an HTI cellulose acetate FO membrane with a thickness of less than 50 μm and a magnification of 263X.
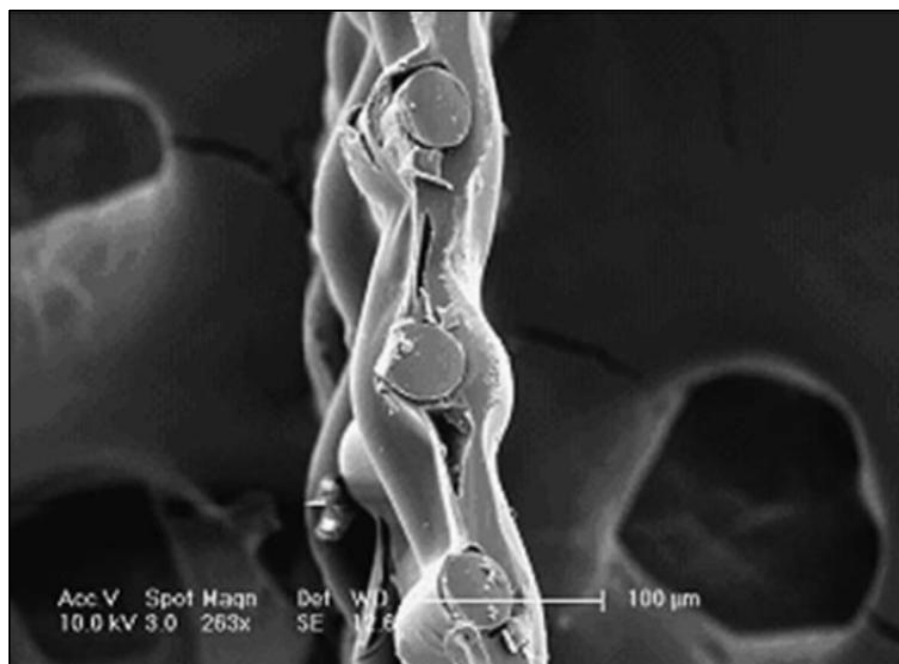
Figure 1.6: HTI CTA membrane adapted from (Cath et al., [134])

Efficient desalination using FO requires membranes that exhibit high water flux, thus necessitating membranes with elevated water permeability and low structural parameters [134]. The ideal semipermeable FO membranes would completely restrict solute permeation into the feed solution. However, absolute barrier properties are unattainable, allowing minor solute transport across the membrane [135]. Thin-film composite polyamide membranes demonstrated superior water flux, solute rejection, pH stability, and hydrolysis and biological degradation resistance compared to CTA FO membranes [136]. Fouling in FO processes can be grouped into four categories according to the type of foulant [137]. These four categories of fouling are colloidal (deposition of colloidal particles), organic (adsorption of macromolecular organics),

inorganic scaling (precipitation of sparingly soluble inorganics) and biofouling (microbial adhesion and biofilm formation) [137]. An osmotic-resistance filtration model was advanced to elucidate the implications of fouling [137]. The HTI CTA membrane shown in Figure 1.6 exhibited better performance than RO membranes employed in FO processes. This superior performance is attributed to the HTI CTA membrane's relatively thin structure and the absence of a fabric support layer [134]. Based on the information in Tables 1.2 and 1.3, most researchers utilized the HTI CTA membrane, which has since been discontinued.   As a result, researchers have developed various novel FO membranes to compete with the former industry standard. Figure 1.7 highlights some of these innovative FO membrane designs.
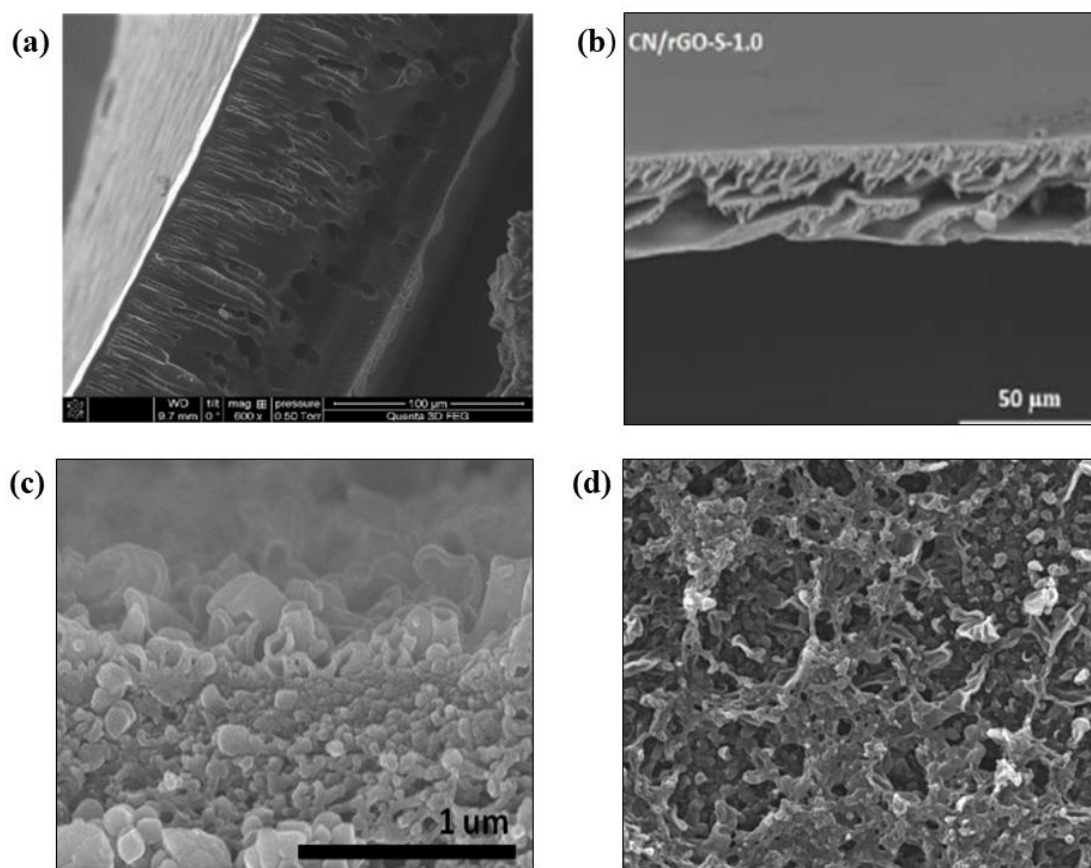
Figure 1.7: SEM micrographs of (a) asymmetric polybenzimidazole flat sheet membrane adapted from (Flanagan et al., [138]), (b) Reduced graphene oxide modified graphitic carbon nitride TFC polyamide membrane adapted from (Wang et al., [139]), (c) Polyamide TFC membranes based on carboxylated polysulfone microporous support membrane adapted from (Cho et al., [140]), and (d) Thin film

nanocomposite (TFN) FO membranes using functionalized multi-walled carbon nanotubes adapted from (Amini et al., [141]).

The polybenzimidazole membrane exhibited enhanced performance in terms of both water flux and salt rejection [138]. The hybrid TFC membrane, modified with reduced graphene oxide and carbon nitride, showed great water transport during the FO process [139]. This suggests incorporating such nanosheets could be a promising approach for creating high-performance FO membranes [139]. FO membranes with a carboxylated polysulfone microporous support layer were found to be more favourable than unmodified polysulfone [140]. Their high porosity and hydrophilicity led to higher water fluxes, making them a better support material choice [140]. Membranes incorporating functionalized multi-walled carbon nanotubes exhibited superior potential for FO applications due to their enhanced structural and separation performance [141].

1.3 Current studies on FO processes

1.3.1 Number of publications on FO

Figure 1.8 shows the ScienceDirect publication counts from 2000 to mid-2024 for the keyword's "desalination" and "forward osmosis". The data illustrates a sustained upward trend in the number of research outputs focused on FO since the beginning of the 21st century. However, it is evident that FO constitutes a relatively modest fraction of the overall scientific literature encompassing desalination technologies and processes during this timeframe.
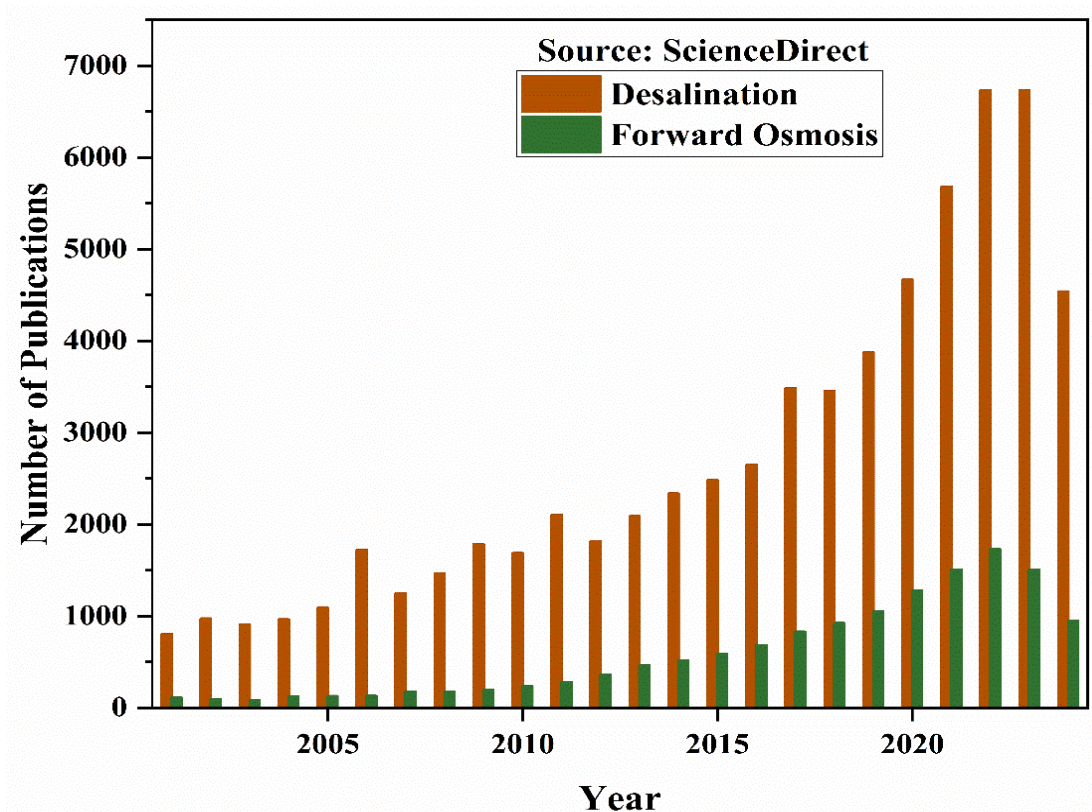
Figure 1.8: Number of publications per year from ScienceDirect

Recent FO research from 2023 onwards has focused on four key areas: developing novel draw solutes, fabricating improved FO membranes, applying machine learning for process optimization and investigating hybrid desalination systems integrating FO with other technologies like RO and MD [142 – 171]. Figure 1.9 summarizes the main research focus areas of FO desalination from 2023 onwards.
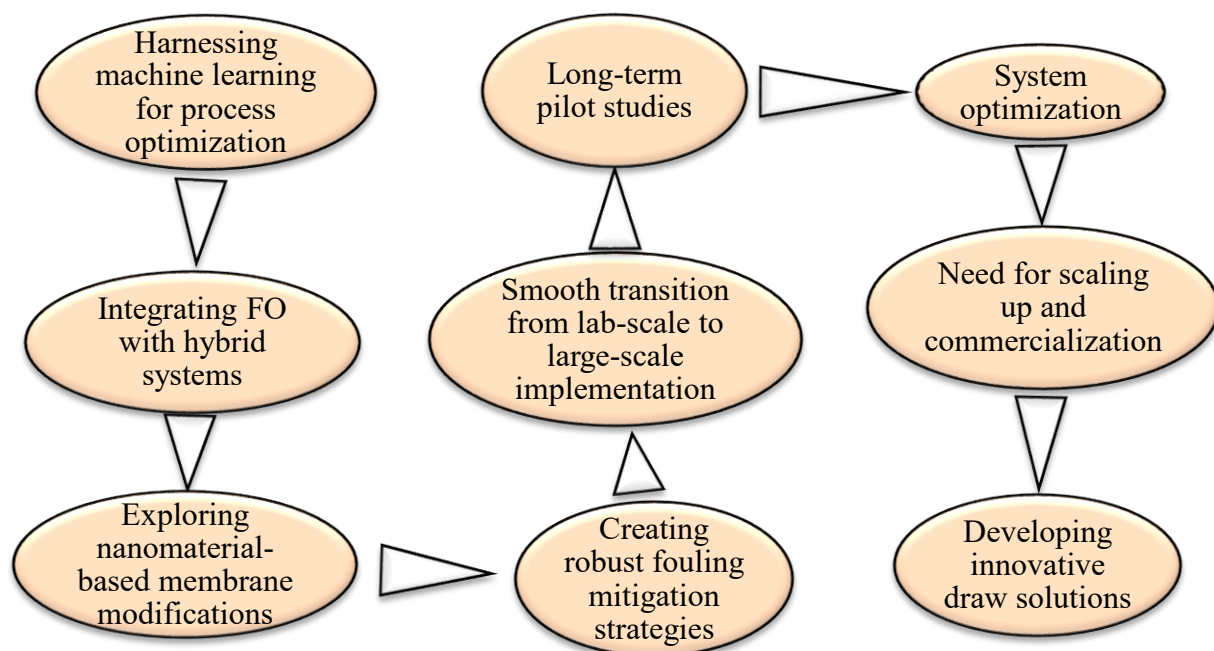
Figure 1.9: Main research focus areas of FO desalination from 2023 onwards

1.3.2   Novel draw solutes

A thermo-responsive ionic liquid-based draw solute exhibited LCSTs between 6 and 34 $^\circ$C, at various concentrations, allowing for draw solution recovery [142]. The water fluxes achieved were 11.26, 8.01 and 6.76 LMH when using distilled water, 2000 ppm NaCl and 20 wt.% orange juice as feeds, respectively [142]. A new draw solute using poly (amidoamine) dendrimer coated magnetic nanoparticles produced an initial water flux of 12.9 LMH [143]. However, the flux decreased over time due to solution dilution. The nanoparticles could be recovered using a magnet for reuse. After four FO cycles, the water flux was reduced by approximately 25% due to membrane fouling effects [143]. Zinc sulphate was explored for its potential as a draw solute for desalinating brackish water [144]. Fresh water was generated from the diluted solution through reagent precipitation (RP) and nanofiltration, yielding product water with 9.8 and 360 ppm total dissolved solids, respectively [144]. The diluted draw solution was regenerated by adding sulphuric acid. The specific energy consumption and water production cost for the FO-RP process were estimated around 0.5 kWh/m^3 and $ 0.09/m^3, respectively [144]. Five commercial thermo-responsive polyalkylene glycols (PAGs) were tested as draw agents in FO [145]. The

water flux varied between 1.5 - 2.0 LMH, while the reverse solute flux ranged from 0.04 - 0.4 gMH [145]. All PAG solutions could be recovered and reused below 100 °C, making them promising for systems utilizing low-grade waste heat [145]. Specifically, regenerated Pluronic® L-35 showed recovery rates of 91.1%, 93.1%, and 91.9% across three FO cycles [145]. CO_2-responsive polymers were used as a draw solute in FO [146]. The 50 wt.% poly (N, N-dimethyl allylamine) draw agent produced an osmotic pressure over 170 bars [146]. Using a cellulose triacetate membrane, the highest observed water flux was 89 LMH for a 0.2 wt.% NaCl feed solution [146]. Slightly lower fluxes of 81 and 77 LMH were produced for higher 1.75 and 3.5 wt.% NaCl feeds, respectively [146]. Afterwards, the draw agent was regenerated through heating to remove CO_2, precipitating the polymer for easy recovery [146]. This left around 2 wt.% residual in the water-rich phase, which was subsequently removed using RO to yield clean water [146]. Development of a cost-effective draw solution was accomplished using a mixture of NaCl and the polyethylene glycol tert-octyl phenyl ether surfactant TX114 [147]. Compared to NaCl alone, this mixture improved the water flux to 21.26 LMH and reduced salt leakages (J_s/J_w = 1.82 g/L) [147]. The draw solution was efficiently recovered using membrane distillation powered by solar or waste heat [147]. The hybrid FO/MD process showed a stable 6 LMH water flux, excellent ~100% salt rejection for 25 hours and resistance to membrane fouling, making it promising for seawater desalination [147]. Thermo-responsive magnetic ionic liquids (TMILs) were developed for seawater desalination [148]. The TMILs possessed tunable LCSTs, making them ideal FO draw solutes [148]. Over 43% of the TMILs could be magnetically extracted above their LCSTs, demonstrating an easy draw solution regeneration method [148]. A 25 wt.% $D-Bu-FeX_4$ draw solution achieved a water flux of 4.5 LMH. The TMILs' ionic, thermo-, and magnetic-responsive properties make them promising FO draw solutes for desalination and wastewater reclamation [148].

A review was performed on thermally responsive draw solutes (TRDS) like ionic liquids (ILs) and hydrogels for sustainable FO desalination [149]. TRDS offer improved water recovery and draw solute regeneration by leveraging low-grade and

renewable heat sources [149]. The design and synthesis of TRDS, balancing hydrophilic and hydrophobic components, were discussed. Compared to non-responsive draw solutes, TRDS have shown higher water flux, better recovery rates, lower energy demands, and greater economic feasibility [149]. TRDS demonstrate potential for contributing to more sustainable desalination processes [149]. Green hydrogels from flaxseed gum and sodium alginate were developed for FO desalination [150]. The hydrogel, crosslinked with epichlorohydrin and semi-interpenetrated with polyethylene glycol, was optimized for high swelling capacity [150]. When tested in a batch FO unit, the hydrogel showed enhanced water flux with increased feed temperature, reduced concentration and smaller particle size [150]. The optimal formulation achieved swelling ratios of 1800% after 1 hour and 5300% at equilibrium [150]. Another hydrogel was fabricated from sodium alginate and polyvinyl alcohol and crosslinked with epichlorohydrin for FO applications [151]. The hydrogel composition was optimized based on swelling capacity and evaluated in a batch FO unit with a cellulose triacetate membrane [151]. The optimal 25% polyvinyl alcohol hydrogel with 0.8 crosslinking ratio achieved 5228% equilibrium swelling [151]. Using distilled water feed, 60 μm hydrogel particles and 40 ºC feed temperature yielded the maximum water flux of 0.845 LMH [151].

1.3.3   Hybrid processes involving FO with other desalination technologies

Several studies have explored various hybrid processes for desalinating brackish and saline waters. A melamine sponge loaded with polypyrrole solar evaporator was used in a forward osmosis-solar evaporation (FO-SE) process, achieving a maximum evaporation flux of 17.4 LMH for a 2 M NaCl draw solution [152]. A high-temperature forward osmosis/crystallization/reverse osmosis (FO/Cry/RO) process was developed that outperformed conventional RO in recovery, cost, and energy consumption [153]. Integrating photocatalysis and forward osmosis (PFO) using a simple photocatalytic hydrogel film decomposed 90% of organic pollutants in the feed solution while maintaining a sustainable water flux of 11.8 LMH, without significant fouling [154].

The use of a reverse electrodialysis-forward osmosis (RED-FO) hybrid system for agricultural fertigation and power generation demonstrated high salinity power generation [155]. Evaluating the impact of feed and draw solution concentrations on a pilot-scale forward osmosis-air gap membrane distillation (FO-AGMD) system for desalination showed the highest recoveries at a fixed draw solution concentration of 70 000 ppm NaCl [156]. A mathematical model to optimize FO, reverse osmosis and their hybrid system was developed [157]. The model confirmed the FO-RO system's greater energy efficiency compared to RO alone, with energy savings of 87.57% to 87.81% [157]. Development was made of a graphene oxide-enhanced forward osmosis membrane (GFO), integrating it with membrane distillation (FO-MD) for textile wastewater treatment [158]. The GFO-based FO-MD system achieved over 80% water recovery and nearly 100% rejection of contaminants [158]. A techno-economic study showed lower water production costs for the GFO-MD system ($5.73 m^{-3}) compared to the commercial FO membrane-MD system ($6.48 m^{-3}) [158]. However, the water flux has to be maintained above 10 LMH for economic viability [158]. Studies on solar-assisted humidification-dehumidification (HDH) and FO were done for desalinating brackish water [159]. Two hybrid configurations, HDH-FO and FO-HDH showed FO to be crucial contributing over 90% to productivity in both configurations [159]. Despite a lower inlet flow rate, the HDH-FO system outperformed a conventional FO unit [159]. A pilot scale forward osmosis integrated air gap membrane distillation (FO-AGMD) system for desalinating Arabian Gulf seawater was designed and tested [160]. The water flux remained stable within the range of 6.3 - 7.3 LMH for the FO process, while the MD process exhibited a stable water flux between 3.75 - 4.0 LMH [160]. The main energy consumption was from heating the feed and cooling the permeate [160]. Integrated FO and Capacitive Deionization (CDI) in four configurations produced ultrapure water and achieved up to 90% water recovery [161]. Exploring a combined FO and temperature swing solvent extraction (TSSE) yielded water fluxes up to 7.5 LMH against artificial seawater [162].

1.3.4 FO membrane modifications

A highly efficient thin film composite polyamide-based FO membrane was developed, achieving an impressive water flux of 60.94 ± 3.5 LMH and a solute flux of 1.52 ± 0.08 gMH [163]. Critically reviewing the surface tailoring of FO membranes identified knowledge gaps [164]. These included the need for large-scale production feasibility studies, long-term performance assessments and exploration of novel materials and modification techniques [164]. The design of thin film membranes manipulated the substrate membrane structure to optimize the final composite membrane [165]. The substrate structure and MAX phase (Ti_3AlC_2) significantly improved the membrane's morphological characteristics and performance, outperforming the pure PES membrane [165]. Fabricated double-sided coated polyethyleneimine crosslinked reduced graphene oxide, PEI:rGO, membranes exhibited superior salt rejection (95%) than single-sided ones (90.1%) [166]. However, they were slightly lower than of a commercial CTA-FO membrane (99.3%) [166]. Under an electric field, both PEI:rGO membranes demonstrated improved antifouling properties due to electro-oxidation and unique nanocomposite structure [166]. Fabrication of MoS_2-Ag nanofillers used photochemical deposition and incorporated them into thin-film composite membranes for FO water treatment [167]. Incorporating the MoS_2-Ag nanofillers smoothened the active layer surface, reducing roughness from 40.09 ± 1.39 nm (TFC) to 15.53 ± 0.17 nm (TFN), and decreased contact angle from $79.0 \pm 2.0^{\circ}$ (TFC) to $52.2 \pm 0.7^{\circ}$ (TFN) [167]. This surface modification improved water flux by 35.2% [167].

1.3.5 Machine learning and FO process modeling

Artificial neural network (ANN) data-driven and Spiegler-Kedem transport models for FO and NF membranes have been developed [168]. ANN exhibited superior fit (R^2 between 0.9 - 0.65) over other machine learning techniques [168]. Optimized ANN models showed high R^2 (95.03% FO, 96.08% NF) but higher errors (5-12%) than transport models (2%) due to limited training data variation [168]. However, ANN competently predicted suitable draw solutes and feed responses [168]. The process development of an upgraded temperature and agent-dependent FO model was performed and calibrated using NaCl and validated with $MgCl_2$ [169].

The process showed good agreement (relative index > 0.99) between simulated and measured performance [169]. Optimizing for maximum water flux, minimum reverse solute flux under constraints increased the water flux/reverse solute flux ratio by 40% for NaCl and 20% for $MgCl_2$, while improving effective osmotic pressure difference 2 - 3.8 times [169]. Assessment of machine learning methods like artificial neural networks, XGBoost, CatBoost, Random Forest, and linear regression for predicting ICP in FO processes was performed [170]. CatBoost outperformed other methods based on R^2 and mean square error [170]. CatBoost accurately predicted ICP on non-training data, showing better generalizability than solution diffusion models [170]. Machine learning algorithms offered insights into major input features affecting ICP modeling [170]. Developing a machine learning approach using supervised CatBoost algorithm accurately predicted reverse solute flux in FO [171]. CatBoost achieved high accuracy with R^2 of 0.94 and RMSE of 0.44 on actual versus predicted data [171]. Simulations on real experimental data showed minimal 0 - 2% error compared to experimental RSF [171]. This demonstrates machine learning's potential to save time while precisely predicting RSF based solely on FO process, membrane permeability inputs and valuable for applications involving reverse salt flux [171].

A highly accurate integrated machine learning and explainable artificial intelligence (ML-XAI) model was developed for predicting permeate fluxes in FO [173]. The XGBoost, LightGBM and CatBoost models demonstrated excellent predictive performance, with XGBoost achieving an R^2 of 0.9716 [173]. Analysis revealed that differences in osmotic pressure and water permeability were the most critical factors influencing water flux predictions [173].

Response surface methodology (RSM) was employed to optimize reverse solute fluxes in FO processes [174]. The parameters identified as critical for Na^+ reverse diffusion included the electrical conductivity of the draw solution, feed solution conductivity, interactions between solution flow rates, and interactions between draw solution flow rate and operating time [174]. RSM yielded R^2 values of 0.948 and 0.958, compared to R^2 values of 0.984 and 0.968 for ANN models. Consequently, ANN models were recommended for use in future studies [174].

Various artificial intelligence techniques, including ANN and Gradient Boosting Regressor (GBR), were used to predict the performance of commercial FO membranes in removing micropollutants [175]. GBR achieved an R^2 of 0.98 and RMSE of 0.54 for water flux prediction, and an R^2 of 0.81 and RMSE of 7.65 for rejection rate prediction [175]. In comparison, ANN demonstrated superior performance with an R^2 of 1 and RMSE of 0.22 for water flux, and an R^2 of 0.89 and RMSE of 5.99 for rejection rate [175]. Based on these results, ANN was identified as the optimal machine learning approach, demonstrating exceptionally high prediction accuracy [175].

1.4 Research gaps

FO desalination has gained significant traction in the 21st century as an energy-efficient technology which has the potential to complement existing desalination processes. Future research areas were identified to unlock FO's full potential including:

- Need to harness machine learning techniques to optimize FO
- Need to develop innovative, high-performing and sustainable draw solutions for FO systems.
- Need to create robust and effective fouling mitigation strategies to enhance the long-term operational stability of FO processes.
- To address the need for scaling up FO technology and facilitating its commercialization.
- Need to advocate for long-term pilot studies to better understand the real-world applicability and reliability of FO systems.
- Need to investigate the economic viability of harnessing waste heat and renewable energy sources for FO desalination

As the global water crisis intensifies, FO desalination stands out as a promising solution – sustainable, energy-efficient and economically viable, provided cheaper draw solution recovery strategies are devised. By addressing these identified challenges and capitalizing on such exciting opportunities, FO desalination can play

a pivotal role in securing the availability of pure drinking water for generations to come.

1.5 Research objectives

This research work aimed to **develop novel phase separating draw solutions for desalinating brackish water or seawater using FO**. The detailed objectives of the present study are as follows:

- To identify new draw solutes with high osmotic pressure for osmotic driven processes.
- To test the identified draw solutes on membrane test cells for osmotic driven processes.
- To undertake mathematical modeling of the process and estimation of transport parameters.
- Use the Artificial Neural Network based approach to model the forward osmosis with the new identified draw solutions
- To perform a feasibility and economic analysis of the process with new draw solutes.

1.6 Overview of the Thesis

To fulfil the above objectives, the work embodied in the thesis entitled **"Studies on water desalination using osmotic pressure-driven processes"** has been divided into **SEVEN** chapters.

Chapter 1 introduces the thesis on osmotic pressure-driven water desalination. It provides an overview, identifies research gaps and establishes the significance of the proposed work. The chapter defines the research problems, objectives and thesis structure. It also presents a comprehensive literature review on the progress, challenges and future of forward osmosis (FO) desalination. Analyzing FO as an emerging energy-efficient solution, the chapter evaluates technological advancements, membrane properties and comparative performance. It highlights critical research gaps to position FO as a viable, efficient and sustainable approach to the global water crisis.

Chapter 2 focuses on the theoretical foundations and modeling approaches for FO desalination processes, with a particular emphasis on data-driven techniques using Artificial Neural Networks (ANN). This work acknowledges the limitations of the traditional solution-diffusion (S-D) model, especially for multi-component and neutral draw solutions, as well as the lack of diffusion coefficient data for the developed systems. To address these challenges, the chapter employs ANN modeling as a robust and flexible alternative to the S-D model. The theoretical underpinnings and assumptions of the ANN approach are presented in detail, along with the governing equations and computational frameworks utilized. Furthermore, the chapter delves into the theoretical aspects of the techno-economic assessment for the FO process, providing a comprehensive treatment of the models and equations used to estimate both operating expenditures (OPEX) and capital expenditures (CAPEX). By establishing this robust theoretical framework, Chapter 2 lays the groundwork for the successful implementation and analysis of data-driven FO desalination models within the broader context of the thesis.

Chapter 3 details the materials, methodology, experimental setup and characterization techniques employed in the development and analysis of novel organic draw solution systems for FO desalination of brackish and seawater. The chapter outlines the specific organic compounds used as potential draw solutes. It then describes the step-by-step experimental procedures for preparing, optimizing and testing these draw solution formulations. The experimental setup is comprehensively covered, including the FO membrane, test cells, feed and draw solution circulation systems, analytical instruments and other key components. Emphasis is placed on the design considerations, operational parameters and control mechanisms to ensure data reliability. Furthermore, the chapter discusses the extensive characterization techniques employed to analyze the physico-chemical properties and osmotic performance, such as measurements of osmotic pressure, viscosity, concentration, pH, density, cloud point determinations and compatibility of the novel organic draw solutions and the FO membrane.

Chapter 4 investigates novel polyelectrolyte-glycol ether ternary phase-separating draw solutions for FO desalination. The chapter systematically evaluates 4 binary

and 6 ternary systems incorporating sodium carboxymethyl cellulose (NaCMC) and propylene glycol propyl ether (PGPE), utilizing their lower critical solution temperature (LCST) behaviour for draw solution regeneration. Experiments were conducted using a custom FO setup with a harvested HTI CTA membrane in AL-FS mode. Optimal draw solutions were selected based on osmotic pressure, viscosity and cloud point measurements.

Chapter 5 investigates the enhancement of FO desalination of brackish water through the development and application of phase-separating ternary organic draw solutions incorporating hydroxypropyl cellulose (HPC) and propylene glycol propyl ether (PGPE). The study systematically evaluates sixteen distinct draw solution compositions, including single-solute and ternary mixtures with varying HPC (0.25 – 2 wt.%) and PGPE (1.25 - 3.75 M) concentrations. Notably, the study established the feasibility of draw solution regeneration through the lower critical solution temperature (LCST) behaviour.

Chapter 6 discusses the results of modeling using Artificial Neural Networks (ANN) and a techno-economic evaluation of the FO-PS desalination process. The ANN model incorporates nine input parameters - FO run details, temperatures, concentrations, flow rates and draw solution molecular weights - to predict permeate fluxes. The model was developed using 312 experimental data points collected during 120-minute FO runs with various draw solutions. The techno-economic assessment evaluates both operating expenditures (OPEX) and capital expenditures (CAPEX) for the FO process and phase separation (PS) draw regeneration.

Chapter 7 presents the conclusions and major findings of the research on phase-separating organic draw solutions in FO desalination. The chapter outlines significant research outcomes and provides recommendations for future applications. Key suggestions are presented to guide researchers interested in advancing the study of phase-separating organic draw solutions in FO desalination. The thesis utilizes a chapter-wise reference system to ensure clear organization and easy access to source materials.

1.7 References

1. Jury, W. A., & Vaux, H. (2005). The role of science in solving the world's emerging water problems. Proceedings of the National Academy of Sciences, 102(44), 15715–15720. https://doi.org/10.1073/pnas.0506467102

2. Vushe, A. (2021). Proposed research, science, technology, and innovation to address current and future challenges of climate change and water resource management in Africa. In Springer eBooks (pp. 489–518). https://doi.org/10.1007/978-3-030-61225-2_21

3. Mekonnen, M. M., & Hoekstra, A. Y. (2016). Four billion people facing severe water scarcity. Science Advances, 2(2). https://doi.org/10.1126/sciadv.1500323

4. Mahato, A., Upadhyay, S., & Sharma, D. (2022). Global water scarcity due to climate change and its conservation strategies with special reference to India: A review. Plant archives, 64–69. https://doi.org/10.51470/plantarchives.2022.v22.no1.009

5. Abou-Shady, A., Siddique, M. S., & Yu, W. (2023). A critical review of recent progress in global water reuse during 2019–2021 and perspectives to overcome future water crisis. Environments, 10(9), 159. https://doi.org/10.3390/environments10090159

6. Manju, S., & Sagar, N. (2017). Renewable energy integrated desalination: A sustainable solution to overcome future fresh-water scarcity in India. Renewable and Sustainable Energy Reviews, 73, 594–609. https://doi.org/10.1016/j.rser.2017.01.164

7. Olatunji, G., Kokori, E., Moradeyo, A., Olatunji, D., Ajibola, F., Otolorin, O., & Aderinto, N. (2023). A perspective on the 2023 cholera outbreaks in Zimbabwe: Implications, response strategies, and policy recommendations. Journal of Epidemiology and Global Health, 14(1), 243–248. https://doi.org/10.1007/s44197-023-00165-6

8. Nabhan, G. P., Richter, B. D., Riordan, E. C., & Tornbom, C. (2023). Toward water-resilient agriculture in Arizona: Future scenarios addressing water scarcity. Lincoln Institute of Land Policy, Cambridge, MA, USA.

9. Sirkar, K. K. (1997). Membrane separation technologies: Current developments. Chemical Engineering Communications, 157(1), 145–184. https://doi.org/10.1080/00986449708936687

10. Yang, J., Monnot, M., Ercolei, L., & Moulin, P. (2020). Membrane-based processes used in municipal wastewater treatment for water reuse: State-of-the-art and performance analysis. Membranes, 10(6), 131. https://doi.org/10.3390/membranes10060131

11. Alawad, S. M., Mansour, R. B., Al-Sulaiman, F. A., & Rehman, S. (2023). Renewable energy systems for water desalination applications: A comprehensive review. Energy Conversion and Management, 286, 117035. https://doi.org/10.1016/j.enconman.2023.117035

12. Yusuf, A., Sodiq, A., Giwa, A., Eke, J., Pikuda, O., De Luca, G., . . . Chakraborty, S. (2020). A review of emerging trends in membrane science and technology for

sustainable water treatment. Journal of Cleaner Production, 266, 121867. https://doi.org/10.1016/j.jclepro.2020.121867

13. Strathmann, H. (2001). Membrane separation processes: Current relevance and future opportunities. AIChE Journal, 47(5), 1077–1087. https://doi.org/10.1002/aic.690470514

14. Kwarciak-Kozlowska, A., & Wlodarczyk, R. (2020). Treatment of waterborne pathogens by microfiltration. In Elsevier eBooks (pp. 81–103). https://doi.org/10.1016/b978-0-12-818783-8.00005-0

15. Teow, Y. H., Sum, J. Y., Ho, K. C., & Mohammad, A. W. (2021). Principles of nanofiltration membrane processes. In Elsevier eBooks (pp. 53–95). https://doi.org/10.1016/b978-0-12-821016-1.00014-0

16. Chen, J. P., Chian, E. S. K., Sheng, P., Nanayakkara, K. G. N., Wang, L. K., & Ting, Y. (2010). Desalination of seawater by reverse osmosis. In Humana Press eBooks (pp. 559–601). https://doi.org/10.1007/978-1-59745-278-6_13

17. Zubair, M. M., Saleem, H., & Zaidi, S. J. (2023). Recent progress in reverse osmosis modeling: An overview. Desalination, 564, 116705. https://doi.org/10.1016/j.desal.2023.116705

18. Qasim, M., Badrelzaman, M., Darwish, N. N., Darwish, N. A., & Hilal, N. (2019). Reverse osmosis desalination: A state-of-the-art review. Desalination, 459, 59–104. https://doi.org/10.1016/j.desal.2019.02.008

19. Lim, W. J., & Ooi, B. S. (2022). Applications of responsive hydrogel to enhance the water recovery via membrane distillation and forward osmosis: A review. Journal of Water Process Engineering, 47, 102828. https://doi.org/10.1016/j.jwpe.2022.102828

20. McGovern, R. K., & Lienhard, J. H., V (2014). On the potential of forward osmosis to energetically outperform reverse osmosis desalination. Journal of Membrane Science, 469, 245–250. https://doi.org/10.1016/j.memsci.2014.05.061

21. Han, G., Zhang, S., Li, X., & Chung, T. (2015). Progress in pressure retarded osmosis (PRO) membranes for osmotic power generation. Progress in Polymer Science, 51, 1–27. https://doi.org/10.1016/j.progpolymsci.2015.04.005

22. Rastgar, M., Moradi, K., Burroughs, C., Hemmati, A., Hoek, E., & Sadrzadeh, M. (2023). Harvesting blue energy based on salinity and temperature gradient: Challenges, solutions, and opportunities. Chemical Reviews, 123(16), 10156–10205. https://doi.org/10.1021/acs.chemrev.3c00168

23. Zou, S., Qin, M., & He, Z. (2018). Tackle reverse solute flux in forward osmosis towards sustainable water recovery: Reduction and perspectives. Water Research, 149, 362–374. https://doi.org/10.1016/j.watres.2018.11.015

24. Tharayil, J. M., Manaf, A., & J, N. J. (2020). Sustainable forward osmosis desalination: A review on polymeric membranes and flux parameters. International Journal of Environmental & Analytical Chemistry, 102(16), 4412–4439. https://doi.org/10.1080/03067319.2020.1784414

25. Li, L., Shi, W., & Yu, S. (2019). Research on forward osmosis membrane technology still needs improvement in water recovery and wastewater treatment. Water, 12(1), 107. https://doi.org/10.3390/w12010107

26. Wang, J., Gao, S., Tian, J., Cui, F., & Shi, W. (2020). Recent developments and future challenges of hydrogels as draw solutes in forward osmosis process. Water, 12(3), 692. https://doi.org/10.3390/w12030692

27. Yadav, S., Ibrar, I., Bakly, S., Khanafer, D., Altaee, A., Padmanaban, V. C., . . . Hawari, A. H. (2020). Organic fouling in forward osmosis: A comprehensive review. Water, 12(5), 1505. https://doi.org/10.3390/w12051505

28. Abu-Zurayk, R., Alnairat, N., Khalaf, A., Ibrahim, A. A., & Halaweh, G. (2023). Cellulose acetate membranes: Fouling types and antifouling strategies - A brief review. Processes, 11(2), 489. https://doi.org/10.3390/pr11020489

29. Ibrar, I., Yadav, S., Naji, O., Alanezi, A. A., Ghaffour, N., Déon, S., . . . Altaee, A. (2022). Development in forward osmosis-membrane distillation hybrid system for wastewater treatment. Separation and Purification Technology, 286, 120498. https://doi.org/10.1016/j.seppur.2022.120498

30. Ahmed, F. E., Khalil, A., & Hilal, N. (2021). Emerging desalination technologies: Current status, challenges and future trends. Desalination, 517, 115183. https://doi.org/10.1016/j.desal.2021.115183

31. Zhan, M., Kim, Y., & Hong, S. (2021). Comprehensive review of osmotic dilution/concentration using FO membranes for practical applications. Desalination, 515, 115190. https://doi.org/10.1016/j.desal.2021.115190

32. Panagopoulos, A., & Haralambous, K. (2020). Environmental impacts of desalination and brine treatment - Challenges and mitigation measures. Marine Pollution Bulletin, 161, 111773. https://doi.org/10.1016/j.marpolbul.2020.111773

33. Chiao, Y., Sengupta, A., Ang, M. B. M. Y., Chen, S., Haan, T. Y., Almodovar, J., . . . Wickramasinghe, S. R. (2021). Application of zwitterions in forward osmosis: A short review. Polymers, 13(4), 583. https://doi.org/10.3390/polym13040583

34. Mohammadifakhr, M., De Grooth, J., Roesink, H. D. W., & Kemperman, A. J. B. (2020). Forward osmosis: A critical review. Processes, 8(4), 404. https://doi.org/10.3390/pr8040404

35. Ibraheem, B. M., Aani, S. A., Alsarayreh, A. A., Alsalhy, Q. F., & Salih, I. K. (2023). Forward osmosis membrane: Review of fabrication, modification, challenges and potential. Membranes, 13(4), 379. https://doi.org/10.3390/membranes13040379

36. Salamanca, M., Peña, M., Hernandez, A., Prádanos, P., & Palacio, L. (2023). Forward osmosis application for the removal of emerging contaminants from municipal wastewater: A review. Membranes, 13(7), 655. https://doi.org/10.3390/membranes13070655

37. Park, J., & Lee, S. (2022). Desalination technology in South Korea: A comprehensive review of technology trends and future outlook. Membranes, 12(2), 204. https://doi.org/10.3390/membranes12020204

38. Singh, S. K., Sharma, C., & Maiti, A. (2021). A comprehensive review of standalone and hybrid forward osmosis for water treatment: Membranes and recovery strategies of draw solutions. Journal of Environmental Chemical Engineering, 9(4), 105473. https://doi.org/10.1016/j.jece.2021.105473

39. Mahto, A., Aruchamy, K., Meena, R., Kamali, M., Nataraj, S. K., & Aminabhavi, T. M. (2020). Forward osmosis for industrial effluents treatment – Sustainability

considerations. Separation and Purification Technology, 254, 117568. https://doi.org/10.1016/j.seppur.2020.117568

40. Xu, Y., Zhu, Y., Chen, Z., Zhu, J., & Chen, G. (2022). A comprehensive review on forward osmosis water treatment: Recent advances and prospects of membranes and draw solutes. International Journal of Environmental Research and Public Health, 19(13), 8215. https://doi.org/10.3390/ijerph19138215

41. Suwaileh, W., Pathak, N., Shon, H., & Hilal, N. (2020). Forward osmosis membranes and processes: A comprehensive review of research trends and future outlook. Desalination, 485, 114455. https://doi.org/10.1016/j.desal.2020.114455

42. Wang, J., & Liu, X. (2020). Forward osmosis technology for water treatment: Recent advances and future perspectives. Journal of Cleaner Production, 280, 124354. https://doi.org/10.1016/j.jclepro.2020.124354

43. Ahmed, F. E., Hashaikeh, R., & Hilal, N. (2020). Hybrid technologies: The future of energy efficient desalination – A review. Desalination, 495, 114659. https://doi.org/10.1016/j.desal.2020.114659

44. Skuse, C., Gallego-Schmid, A., Azapagic, A., & Gorgojo, P. (2020). Can emerging membrane-based desalination technologies replace reverse osmosis? Desalination, 500, 114844. https://doi.org/10.1016/j.desal.2020.114844

45. Giagnorio, M., Casasso, A., & Tiraferri, A. (2021). Environmental sustainability of forward osmosis: The role of draw solute and its management. Environment International, 152, 106498. https://doi.org/10.1016/j.envint.2021.106498

46. Lin, S., Zhao, H., Zhu, L., He, T., Chen, S., Gao, C., & Zhang, L. (2020). Seawater desalination technology and engineering in China: A review. Desalination, 498, 114728. https://doi.org/10.1016/j.desal.2020.114728

47. Hafiz, M., Hassanein, A., Talhami, M., Al-Ejji, M., Hassan, M. K., & Hawari, A. H. (2022). Magnetic nanoparticles draw solution for forward osmosis: Current status and future challenges in wastewater treatment. Journal of Environmental Chemical Engineering, 10(6), 108955. https://doi.org/10.1016/j.jece.2022.108955

48. Firouzjaei, M. D., Seyedpour, S. F., Aktij, S. A., Giagnorio, M., Bazrafshan, N., Mollahosseini, A., . . . Rahimpour, A. (2019). Recent advances in functionalized polymer membranes for biofouling control and mitigation in forward osmosis. Journal of Membrane Science, 596, 117604. https://doi.org/10.1016/j.memsci.2019.117604

49. McLeod, A., Jefferson, B., & McAdam, E. J. (2016). Toward gas-phase controlled mass transfer in micro-porous membrane contactors for recovery and concentration of dissolved methane in the gas phase. Journal of Membrane Science, 510, 466–471. https://doi.org/10.1016/j.memsci.2016.03.030

50. Luo, H., Wu, K., Wang, Q., Zhang, T. C., Lu, H., Rong, H., & Fang, Q. (2019). Forward osmosis with electro-responsive P(AMPS-co-AM) hydrogels as draw agents for desalination. Journal of Membrane Science, 593, 117406. https://doi.org/10.1016/j.memsci.2019.117406

51. Hsu, C., Ma, C., Bui, N., Song, Z., Wilson, A. D., Kostecki, R., . . . Urban, J. J. (2019). Enhanced forward osmosis desalination with a hybrid ionic liquid/hydrogel thermoresponsive draw agent system. ACS Omega, 4(2), 4296–4303. https://doi.org/10.1021/acsomega.8b02827

52. Le, Y., Yun, Y., Wang, M., Liu, W., Dong, S., Yang, K., . . . Liu, G. (2021). N-isopropyl acrylamide/sodium acrylate hydrogel as draw agent for forward osmosis to concentrate esterification wastewater. Korean Journal of Chemical Engineering, 38(5), 975–981. https://doi.org/10.1007/s11814-021-0779-3

53. Pan, Z., Guo, H., Yu, H., Wen, G., Qu, F., Huang, T., & He, J. (2021). Sewage sludge ash-based thermo-responsive hydrogel as a novel draw agent towards high performance of water flux and recovery for forward-osmosis. Desalination, 512, 115147. https://doi.org/10.1016/j.desal.2021.115147

54. Vafaei, M. A., Shakeri, A., Salehi, H., Razavi, S. R., & Salari, N. (2021). The effect of nanosheets on polymer hydrogels performance in rhodamine B dye removal by forward osmosis process. Journal of Water Process Engineering, 44, 102351. https://doi.org/10.1016/j.jwpe.2021.102351

55. Ellis, S. N., Cunningham, M. F., & Jessop, P. G. (2021). A forward osmosis hydrogel draw agent that responds to both heat and CO_2. Desalination, 510, 115074. https://doi.org/10.1016/j.desal.2021.115074

56. Yu, M., Zhang, H., & Yang, F. (2017). Hydrophilic and compressible aerogel: A novel draw agent in forward osmosis. ACS Applied Materials & Interfaces, 9(39), 33948–33955. https://doi.org/10.1021/acsami.7b10229

57. Cui, H., Zhang, H., & Yang, F. (2017). Preparation and properties of electric-sensitive poly(vinyl alcohol)/poly(acrylic acid) IPN hydrogels as draw agent for forward osmosis. Desalination and Water Treatment, 71, 280–288. https://doi.org/10.5004/dwt.2017.20539

58. Yu, M., Zhang, H., Wang, Y., Zhao, R., Xu, X., Ge, C., . . . Yang, F. (2020). Hyaluronic acid-graphene oxide/PVA hybrid monolith: A hydrophilic and compressible solid draw agent in forward osmosis. Applied Surface Science, 531, 147235. https://doi.org/10.1016/j.apsusc.2020.147235

59. Rabiee, H., Jin, B., Yun, S., & Dai, S. (2019). O_2/N_2-responsive microgels as functional draw agents for gas-triggering forward osmosis desalination. Journal of Membrane Science, 595, 117584. https://doi.org/10.1016/j.memsci.2019.117584

60. Obra, J. B., Maranan, J. Q., & Tumolva, T. (2021). Synthesis and characterization of NaCMC/HEC/Activated carbon hydrogel composites for the desalination of seawater. Engineering, Materials Science 7th GoGreen Summit 2021. https://doi.org/10.36647/978-93-92106-02-6.16

61. Tumolva, T., Madamba, K. C., Nunag, I. G., & Villanueva, V. G. (2021). Developing a HEC/CMC-reduced graphene oxide hydrogel nanocomposite for seawater desalination. Diffusion and Defect Data, Solid State Data. Part B, Solid State Phenomena/Solid State Phenomena, 324, 173–178. https://doi.org/10.4028/www.scientific.net/ssp.324.173

62. Rodrigues, A. D., Jacob, M., Gauchou, V., Durand, J., Trens, P., & Hesemann, P. (2020). Quaternary ammonium-based ionosilica hydrogels as draw solutes in forward osmosis. Molecules, 25(24), 5987. https://doi.org/10.3390/molecules25245987

63. McCutcheon, J. R., McGinnis, R. L., & Elimelech, M. (2005). A novel ammonia - carbon dioxide forward (direct) osmosis desalination process. Desalination, 174(1), 1–11. https://doi.org/10.1016/j.desal.2004.11.002

64. McGinnis, R. L., & Elimelech, M. (2007). Energy requirements of ammonia–carbon dioxide forward osmosis desalination. Desalination, 207(1–3), 370–382. https://doi.org/10.1016/j.desal.2006.08.012

65. Cornelissen, E., Harmsen, D., Dekorte, K., Ruiken, C., Qin, J., Oo, H., & Wessels, L. (2008). Membrane fouling and process performance of forward osmosis membranes on activated sludge. Journal of Membrane Science, 319(1–2), 158–168. https://doi.org/10.1016/j.memsci.2008.03.048

66. Achilli, A., Cath, T. Y., & Childress, A. E. (2010). Selection of inorganic-based draw solutions for forward osmosis applications. Journal of Membrane Science, 364(1–2), 233–241. https://doi.org/10.1016/j.memsci.2010.08.010

67. Su, J., Yang, Q., Teo, J. F., & Chung, T. (2010). Cellulose acetate nanofiltration hollow fibre membranes for forward osmosis processes. Journal of Membrane Science, 355(1–2), 36–44. https://doi.org/10.1016/j.memsci.2010.03.003

68. Phuntsho, S., Shon, H. K., Hong, S., Lee, S., & Vigneswaran, S. (2011). A novel low energy fertilizer driven forward osmosis desalination for direct fertigation: Evaluating the performance of fertilizer draw solutions. Journal of Membrane Science, 375(1–2), 172–181. https://doi.org/10.1016/j.memsci.2011.03.038

69. Yangali-Quintanilla, V., Li, Z., Valladares, R., Li, Q., & Amy, G. (2011). Indirect desalination of Red Sea water with forward osmosis and low-pressure reverse osmosis for water reuse. Desalination, 280(1–3), 160–166. https://doi.org/10.1016/j.desal.2011.06.066

70. Su, J., Chung, T., Helmer, B. J., & De Wit, J. S. (2012). Enhanced double-skinned FO membranes with inner dense layer for wastewater treatment and macromolecule recycle using sucrose as draw solute. Journal of Membrane Science, 396, 92–100. https://doi.org/10.1016/j.memsci.2012.01.001

71. Alnaizy, R., Aidan, A., & Qasim, M. (2013). Copper sulphate as draw solute in forward osmosis desalination. Journal of Environmental Chemical Engineering, 1(3), 424–430. https://doi.org/10.1016/j.jece.2013.06.005

72. Amjad, M., Gardy, J., Hassanpour, A., & Wen, D. (2018). Novel draw solution for forward osmosis based solar desalination. Applied Energy, 230, 220–231. https://doi.org/10.1016/j.apenergy.2018.08.021

73. Gulied, M., Momani, F. A., Khraisheh, M., Bhosale, R., & AlNouss, A. (2019). Influence of draw solution type and properties on the performance of forward osmosis process: Energy consumption and sustainable water reuse. Chemosphere, 233, 234–244. https://doi.org/10.1016/j.chemosphere.2019.05.241

74. Gadelha, G., Nawaz, M. S., Hankins, N. P., Khan, S. J., Wang, R., & Tang, C. Y. (2014). Assessment of micellar solutions as draw solutions for forward osmosis. Desalination, 354, 97–106. https://doi.org/10.1016/j.desal.2014.09.009

75. Liu, P., Gao, B., Shon, H. K., Ma, D., Rong, H., Zhao, P., . . . Li, Q. (2014). Water flux behaviour of blended solutions of ammonium bicarbonate mixed with eight salts respectively as draw solutions in forward osmosis. Desalination, 353, 39–47. https://doi.org/10.1016/j.desal.2014.09.011

76. Qasim, M., Mohammed, F., Aidan, A., & Darwish, N. A. (2017). Forward osmosis desalination using ferric sulphate draw solute. Desalination, 423, 12–20. https://doi.org/10.1016/j.desal.2017.08.019

77. Aende, A., Gardy, J., Edokali, M., Harbottle, D., & Hassanpour, A. (2024). Sodium functionalised carbon nanofibers draw solution for a solar-thermal forward osmosis water desalination system. Process Safety and Environmental Protection, 203, 130–139. https://doi.org/10.1016/j.cherd.2024.01.017

78. Tang, W., & Ng, H. Y. (2008). Concentration of brine by forward osmosis: Performance and influence of membrane structure. Desalination, 224(1–3), 143–153. https://doi.org/10.1016/j.desal.2007.04.085

79. Yen, S. K., N, F. M. H., Su, M., Wang, K. Y., & Chung, T. (2010). Study of draw solutes using 2-methylimidazole-based compounds in forward osmosis. Journal of Membrane Science, 364(1–2), 242–252. https://doi.org/10.1016/j.memsci.2010.08.021

80. Yong, J. S., Phillip, W. A., & Elimelech, M. (2011). Coupled reverse draw solute permeation and water flux in forward osmosis with neutral draw solutes. Journal of Membrane Science, 392–393, 9–17. https://doi.org/10.1016/j.memsci.2011.11.020

81. Kim, T., Park, S., & Yeh, K. (2013). Cost-effective design of a draw solution recovery process for forward osmosis desalination. Desalination, 327, 46–51. https://doi.org/10.1016/j.desal.2013.07.020

82. Bowden, K. S., Achilli, A., & Childress, A. E. (2012). Organic ionic salt draw solutions for osmotic membrane bioreactors. Bioresource Technology, 122, 207–216. https://doi.org/10.1016/j.biortech.2012.06.026

83. Ge, Q., Su, J., Amy, G. L., & Chung, T. (2011). Exploration of polyelectrolytes as draw solutes in forward osmosis processes. Water Research, 46(4), 1318–1326. https://doi.org/10.1016/j.watres.2011.12.043

84. Stone, M. L., Rae, C., Stewart, F. F., & Wilson, A. D. (2012). Switchable polarity solvents as draw solutes for forward osmosis. Desalination, 312, 124–129. https://doi.org/10.1016/j.desal.2012.07.034

85. Ou, R., Wang, Y., Wang, H., & Xu, T. (2013). Thermo-sensitive polyelectrolytes as draw solutions in forward osmosis process. Desalination, 318, 48–55. https://doi.org/10.1016/j.desal.2013.03.022

86. Yu, M., Zhang, H., Wang, Y., Zhao, R., Xu, X., Ge, C., . . . Yang, F. (2020). Hyaluronic acid-graphene oxide/PVA hybrid monolith: A hydrophilic and compressible solid draw agent in forward osmosis. Applied Surface Science, 531, 147235. https://doi.org/10.1016/j.apsusc.2020.147235

87. Zhao, P., Gao, B., Xu, S., Kong, J., Ma, D., Shon, H. K., . . . Liu, P. (2014). Polyelectrolyte-promoted forward osmosis process for dye wastewater treatment – Exploring the feasibility of using polyacrylamide as draw solute. Chemical Engineering Journal, 264, 32–38. https://doi.org/10.1016/j.cej.2014.11.064

88. Ray, S. S., Chen, S., Nguyen, N. C., Nguyen, H. T., Li, C., Wang, J., & Yan, B. (2016). Forward osmosis desalination by utilizing chlorhexidine gluconate-based mouthwash as a reusable draw solute. Chemical Engineering Journal, 304, 962–969. https://doi.org/10.1016/j.cej.2016.07.023

89. Yu, M., Zhang, H., & Yang, F. (2016). A study of a ferric-lactate complex as draw solute in forward osmosis. Chemical Engineering Journal, 314, 132–138. https://doi.org/10.1016/j.cej.2016.12.100

90. Long, Q., Huang, J., Xiong, S., Shen, L., & Wang, Y. (2018). Exploration of oligomeric sodium carboxylates as novel draw solutes for forward osmosis. Process Safety and Environmental Protection, 138, 77–86. https://doi.org/10.1016/j.cherd.2018.08.020

91. Ding, C., Zhang, X., Shen, L., Huang, J., Lu, A., Zhong, F., & Wang, Y. (2019). Application of polysaccharide derivatives as novel draw solutes in forward osmosis for desalination and protein concentration. Process Safety and Environmental Protection, 146, 211–220. https://doi.org/10.1016/j.cherd.2019.04.005

92. Wang, Y., Yu, H., Xie, R., Zhao, K., Ju, X., Wang, W., . . . Chu, L. (2015). An easily recoverable thermo-sensitive polyelectrolyte as draw agent for forward osmosis process. Chinese Journal of Chemical Engineering, 24(1), 86–93. https://doi.org/10.1016/j.cjche.2015.11.015

93. Zhao, D., Wang, P., Zhao, Q., Chen, N., & Lu, X. (2014). Thermoresponsive copolymer-based draw solution for seawater desalination in a combined process of forward osmosis and membrane distillation. Desalination, 348, 26–32. https://doi.org/10.1016/j.desal.2014.06.009

94. Orme, C. J., & Wilson, A. D. (2015). 1-Cyclohexylpiperidine as a thermolytic draw solute for osmotically driven membrane processes. Desalination, 371, 126–133. https://doi.org/10.1016/j.desal.2015.05.024

95. Zhao, Y., Ren, Y., Wang, X., Xiao, P., Tian, E., Wang, X., & Li, J. (2015). An initial study of EDTA complex based draw solutes in forward osmosis process. Desalination, 378, 28–36. https://doi.org/10.1016/j.desal.2015.09.006

96. Park, H., Cho, S., Kim, K., & Kwon, Y. (2015). Effect of feed spacer thickness on the fouling behaviour in reverse osmosis process — A pilot scale study. Desalination, 379, 155–163. https://doi.org/10.1016/j.desal.2015.11.011

97. Kumar, R., Al-Haddad, S., Al-Rughaib, M., & Salman, M. (2016). Evaluation of hydrolyzed poly(isobutylene-alt-maleic anhydride) as a polyelectrolyte draw solution for forward osmosis desalination. Desalination, 394, 148–154. https://doi.org/10.1016/j.desal.2016.05.012

98. Huang, J., Long, Q., Xiong, S., Shen, L., & Wang, Y. (2017). Application of poly (4-styrenesulfonic acid-co-maleic acid) sodium salt as novel draw solute in forward osmosis for dye-containing wastewater treatment. Desalination, 421, 40–46. https://doi.org/10.1016/j.desal.2017.01.039

99. Monjezi, A. A., Mahood, H. B., & Campbell, A. (2017). Regeneration of dimethyl ether as a draw solute in forward osmosis by utilising thermal energy from a solar pond. Desalination, 415, 104–114. https://doi.org/10.1016/j.desal.2017.03.034

100. Laohaprapanon, S., Fu, Y., Hu, C., You, S., Tsai, H., Hung, W., . . . Lai, J. (2017). Evaluation of a natural polymer-based cationic polyelectrolyte as a draw solute in forward osmosis. Desalination, 421, 72–78. https://doi.org/10.1016/j.desal.2017.04.027

101. Yang, Y., Chen, M., Zou, S., Yang, X., Long, T. E., & He, Z. (2017). Efficient recovery of polyelectrolyte draw solutes in forward osmosis towards sustainable water treatment. Desalination, 422, 134–141. https://doi.org/10.1016/j.desal.2017.08.024

102.	Zeweldi, H. G., Limjuco, L. A., Bendoy, A. P., Kim, H., Park, M. J., Shon, H. K., . . . Nisola, G. M. (2018). The potential of monocationic imidazolium-, phosphonium-, and ammonium-based hydrophilic ionic liquids as draw solutes for forward osmosis. Desalination, 444, 94–106. https://doi.org/10.1016/j.desal.2018.07.017

103.	Huang, J., Xiong, S., Long, Q., Shen, L., & Wang, Y. (2018). Evaluation of food additive sodium phytate as a novel draw solute for forward osmosis. Desalination, 448, 87–92. https://doi.org/10.1016/j.desal.2018.10.004

104.	Islam, M. S., Sultana, S., McCutcheon, J. R., & Rahaman, M. S. (2018). Treatment of fracking wastewaters via forward osmosis: Evaluation of suitable organic draw solutions. Desalination, 452, 149–158. https://doi.org/10.1016/j.desal.2018.11.010

105.	Kim, J., Kim, J., Lim, J., & Hong, S. (2019). Evaluation of ethanol as draw solute for forward osmosis (FO) process of highly saline (waste)water. Desalination, 456, 23–31. https://doi.org/10.1016/j.desal.2019.01.012

106.	Shokrollahzadeh, S., Bide, Y., & Gholami, S. (2020). Enhancing forward osmosis performance via an oligomeric deep eutectic solvent as a draw solute. Desalination, 491, 114473. https://doi.org/10.1016/j.desal.2020.114473

107.	Zeweldi, H. G., Bendoy, A. P., Park, M. J., Shon, H. K., Kim, H., Johnson, E. M., . . . Nisola, G. M. (2020). Tetrabutylammonium 2,4,6-trimethylbenzenesulfonate as an effective and regenerable thermo-responsive ionic liquid drawing agent in forward osmosis for seawater desalination. Desalination, 495, 114635. https://doi.org/10.1016/j.desal.2020.114635

108.	Nguyen, N. C., Duong, H. C., Nguyen, H. T., Chen, S., Le, H. Q., Ngo, H. H., . . . Bui, X. T. (2020). Forward osmosis–membrane distillation hybrid system for desalination using mixed trivalent draw solution. Journal of Membrane Science, 603, 118029. https://doi.org/10.1016/j.memsci.2020.118029

109.	Kamel, A. H., Alsalhy, Q. F., Ibrahim, S. S., Faneer, K. A., Hashemifard, S. A., Jangizehi, A., . . . Bantz, C. (2023). Novel sodium and potassium carbon quantum dots as forward osmosis draw solutes: Synthesis, characterization and performance testing. Desalination, 567, 116956. https://doi.org/10.1016/j.desal.2023.116956

110.	Ge, Q., Su, J., Chung, T., & Amy, G. (2010). Hydrophilic superparamagnetic nanoparticles: Synthesis, characterization, and performance in forward osmosis processes. Industrial & Engineering Chemistry Research, 50(1), 382–388. https://doi.org/10.1021/ie101013w

111.	Guizani, M., Endo, T., Ito, R., & Funamizu, N. (2020). Polyethylene glycol-coated magnetic nanoparticles-based draw solution for forward osmosis. Sanitation Value Chain, 4, 27 – 37. https://doi.org/10.34416/svc.00017

112.	Mishra, T., Ramola, S., Shankhwar, A. K., & Srivastava, R. K. (2015). Use of synthesized hydrophilic magnetic nanoparticles (HMNPs) in forward osmosis for water reuse. Water Science & Technology Water Supply, 16(1), 229–236. https://doi.org/10.2166/ws.2015.131

113.   Ling, M. M., Chung, T., & Lu, X. (2011). Facile synthesis of thermosensitive magnetic nanoparticles as "smart" draw solutes in forward osmosis. Chemical Communications, 47(38), 10788. https://doi.org/10.1039/c1cc13944d

114.   Ling, M. M., Wang, K. Y., & Chung, T. (2010). Highly water-soluble magnetic nanoparticles as novel draw solutes in forward osmosis for water reuse. Industrial & Engineering Chemistry Research, 49(12), 5869–5876. https://doi.org/10.1021/ie100438x

115.   Ling, M. M., & Chung, T. (2011). Desalination process using super hydrophilic nanoparticles via forward osmosis integrated with ultrafiltration regeneration. Desalination, 278(1–3), 194–202. https://doi.org/10.1016/j.desal.2011.05.019

116.   Ling, M. M., & Chung, T. (2011). Novel dual-stage FO system for sustainable protein enrichment using nanoparticles as intermediate draw solutes. Journal of Membrane Science, 372(1–2), 201–209. https://doi.org/10.1016/j.memsci.2011.02.003

117.   Yang, H., Park, C. W., Han, M. J., Seo, B., Moon, J., & Lee, K. (2016). Hyperbranched polyglycerol carboxylate-coated magnetic nanoparticles as a draw solute in a combined forward osmosis and ultrafiltration process. Journal of Nanoscience and Nanotechnology, 16(10), 10858–10863. https://doi.org/10.1166/jnn.2016.13253

118.   Yang, H., Choi, H. M., Jang, S., Han, M. J., Seo, B., Moon, J., & Lee, K. (2015). Succinate functionalization of hyperbranched polyglycerol-coated magnetic nanoparticles as a draw solute during forward osmosis. Journal of Nanoscience and Nanotechnology, 15(10), 8279–8284. https://doi.org/10.1166/jnn.2015.11244

119.   Ban, I., Markuš, S., Gyergyek, S., Drofenik, M., Korenak, J., Helix-Nielsen, C., & Petrinić, I. (2019). Synthesis of poly-sodium-acrylate (PSA)-coated magnetic nanoparticles for use in forward osmosis draw solutions. Nanomaterials, 9(9), 1238. https://doi.org/10.3390/nano9091238

120.   Zhou, A., Luo, H., Wang, Q., Chen, L., Zhang, T. C., & Tao, T. (2015). Magnetic thermoresponsive ionic nanogels as novel draw agents in forward osmosis. RSC Advances, 5(20), 15359–15365. https://doi.org/10.1039/c4ra12102c

121.   Zhao, Q., Chen, N., Zhao, D., & Lu, X. (2013). Thermoresponsive magnetic nanoparticles for seawater desalination. ACS Applied Materials & Interfaces, 5(21), 11453–11461. https://doi.org/10.1021/am403719s

122.   Shakeri, A., Salehi, H., Khankeshipour, N., Nakhjiri, M. T., & Ghorbani, F. (2018). Magnetic nanoparticle-crosslinked ferrohydrogel as a novel class of forward osmosis draw agent. Journal of Nanoparticle Research, 20(12), 325. https://doi.org/10.1007/s11051-018-4437-6

123.   Bai, H., Liu, Z., & Sun, D. D. (2011). Highly water soluble and recovered dextran coated Fe_3O_4 magnetic nanoparticles for brackish water desalination. Separation and Purification Technology, 81(3), 392–399. https://doi.org/10.1016/j.seppur.2011.08.007

124.   Attallah, O. A., Al-Ghobashy, M. A., Nebsen, M., El-Kholy, R., & Salem, M. Y. (2018). Assessment of pectin-coated magnetite nanoparticles in low-energy

water desalination applications. Environmental Science and Pollution Research, 25(19), 18476–18483. https://doi.org/10.1007/s11356-018-2060-9

125.	Tayel, A., Nasr, P., & Sewilam, H. (2019). Forward osmosis desalination using pectin-coated magnetic nanoparticles as a draw solution. Clean Technologies and Environmental Policy, 21(8), 1617–1628. https://doi.org/10.1007/s10098-019-01738-5

126.	Shabani, Z., & Rahimpour, A. (2016). Chitosan- and dehydroascorbic acid-coated Fe_3O_4 nanoparticles: Preparation, characterization and their potential as draw solute in forward osmosis process. Iranian Polymer Journal, 25(10), 887–895. https://doi.org/10.1007/s13726-016-0474-0

127.	Azadi, F., Karimi-Jashni, A., & Zerafat, M. M. (2020). Desalination of brackish water by gelatin-coated magnetite nanoparticles as a novel draw solute in forward osmosis process. Environmental Technology, 42, 4094–4104. https://doi.org/10.1080/09593330.2020.1717642

128.	Khazaie, F., Shokrollahzadeh, S., Bide, Y., Sheshmani, S., & Shahvelayati, A. S. (2020). Forward osmosis using highly water dispersible sodium alginate sulfate coated-Fe_3O_4 nanoparticles as innovative draw solution for water desalination. Process Safety and Environmental Protection, 146, 789–799. https://doi.org/10.1016/j.psep.2020.12.010

129.	Na, Y., Yang, S., & Lee, S. (2014). Evaluation of citrate-coated magnetic nanoparticles as draw solute for forward osmosis. Desalination, 347, 34–42. https://doi.org/10.1016/j.desal.2014.04.032

130.	Ge, Q., Yang, L., Cai, J., Xu, W., Chen, Q., & Liu, M. (2016). Hydroacid magnetic nanoparticles in forward osmosis for seawater desalination and efficient regeneration via integrated magnetic and membrane separations. Journal of Membrane Science, 520, 550–559. https://doi.org/10.1016/j.memsci.2016.07.033

131.	Khazaie, F., Shokrollahzadeh, S., Bide, Y., Sheshmani, S., & Shahvelayati, A. S. (2021). High-flux sodium alginate sulphate draw solution for water recovery from saline waters and wastewaters via forward osmosis. Chemical Engineering Journal, 417, 129250. https://doi.org/10.1016/j.cej.2021.129250

132.	Zeweldi, H. G., Bendoy, A. P., Park, M. J., Shon, H. K., Kim, H., Johnson, E. M., . . . Nisola, G. M. (2021). Supramolecular host-guest complex of methylated β-cyclodextrin with polymerized ionic liquid ([vbim]TFSI) as highly effective and energy-efficient thermo-regenerable draw solutes in forward osmosis. Chemical Engineering Journal, 411, 128520. https://doi.org/10.1016/j.cej.2021.128520

133.	Colciaghi, R., Simonetti, R., Molinaroli, L., Binotti, M., & Manzolini, G. (2021). Potentialities of thermal responsive polymer in forward osmosis (FO) process for water desalination. Desalination, 519, 115311. https://doi.org/10.1016/j.desal.2021.115311

134.	Cath, T., Childress, A., & Elimelech, M. (2006). Forward osmosis: Principles, applications, and recent developments. Journal of Membrane Science, 281(1–2), 70–87. https://doi.org/10.1016/j.memsci.2006.05.048

135.	Phillip, W. A., Yong, J. S., & Elimelech, M. (2010). Reverse draw solute permeation in forward osmosis: Modeling and experiments. Environmental Science & Technology, 44(13), 5170–5176. https://doi.org/10.1021/es100901n

136.   Gu, Y., Wang, Y., Wei, J., & Tang, C. Y. (2013). Organic fouling of thin-film composite polyamide and cellulose triacetate forward osmosis membranes by oppositely charged macromolecules. Water Research, 47(5), 1867–1874. https://doi.org/10.1016/j.watres.2013.01.008

137.   She, Q., Wang, R., Fane, A. G., & Tang, C. Y. (2015). Membrane fouling in osmotically driven membrane processes: A review. Journal of Membrane Science, 499, 201–233. https://doi.org/10.1016/j.memsci.2015.10.040

138.   Flanagan, M. F., & Escobar, I. C. (2013). Novel charged and hydrophilized polybenzimidazole (PBI) membranes for forward osmosis. Journal of Membrane Science, 434, 85–92. https://doi.org/10.1016/j.memsci.2013.01.039

139.   Wang, Y., Ou, R., Wang, H., & Xu, T. (2014). Graphene oxide modified graphitic carbon nitride as a modifier for thin film composite forward osmosis membrane. Journal of Membrane Science, 475, 281–289. https://doi.org/10.1016/j.memsci.2014.10.028

140.   Cho, Y. H., Han, J., Han, S., Guiver, M. D., & Park, H. B. (2013). Polyamide thin-film composite membranes based on carboxylated polysulfone microporous support membranes for forward osmosis. Journal of Membrane Science, 445, 220–227. https://doi.org/10.1016/j.memsci.2013.06.003

141.   Amini, M., Jahanshahi, M., & Rahimpour, A. (2013). Synthesis of novel thin film nanocomposite (TFN) forward osmosis membranes using functionalized multi-walled carbon nanotubes. Journal of Membrane Science, 435, 233–241. https://doi.org/10.1016/j.memsci.2013.01.041

142.   Moon, J., & Kang, H. (2023). Thermo-responsive tributyl-4-vinylbenzylphosphonium alkanesulfonate ionic liquid-based draw solute for forward osmosis. Journal of Industrial and Engineering Chemistry, 129, 413–423. https://doi.org/10.1016/j.jiec.2023.09.001

143.   Hassanein, A., Hafiz, M., Hassan, M. K., Ba-Abbad, M. M., Al-Ejji, M., Alfahel, R., . . . Hawari, A. H. (2023). Developing sustainable draw solute for forward osmosis process using poly(amidoamine) dendrimer coated magnetic nanoparticles. Desalination, 564, 116800. https://doi.org/10.1016/j.desal.2023.116800

144.   Khan, B. E., Mahmood, A., Zaman, M., & Lee, K. (2023). Zinc sulphate as a draw solute in forward osmosis and its regeneration by reagent precipitation. Desalination, 571, 117087. https://doi.org/10.1016/j.desal.2023.117087

145.   Petrinic, I., Jancic, N., Van Vuuren, R. D. J., & Buksek, H. (2024). Commercial thermo-responsive polyalkylene glycols as draw agents in forward osmosis. Desalination, 582, 117576. https://doi.org/10.1016/j.desal.2024.117576

146.   Ramezani, M., Ellis, S. N., Riabtseva, A., Cunningham, M. F., & Jessop, P. G. (2023). CO_2-responsive low molecular weight polymer with high osmotic pressure as a draw solute for forward osmosis. ACS Omega, 8(51), 49259–49269. https://doi.org/10.1021/acsomega.3c07644

147.   Nguyen, H. T., Nguyen, N. C., Chen, S., Duong, H. C., Nguyen, M. L., Tran, C., & Nguyen, P. (2023). Exploration of a cost-effective draw solution based on mixing surfactant and sodium chloride for forward osmosis desalination process.

Environmental Technology & Innovation, 30, 103088.
https://doi.org/10.1016/j.eti.2023.103088

148.	Zhao, Q., & Zhao, D. L. (2023). Thermoresponsive magnetic ionic liquids as forward osmosis draw solutes for seawater desalination. Chemical Engineering Journal Advances, 14, 100446. https://doi.org/10.1016/j.ceja.2023.100446

149.	Reddy, A. S., Wanjari, V. P., & Singh, S. P. (2023). Design, synthesis, and application of thermally responsive draw solutes for sustainable forward osmosis desalination: A review. Chemosphere, 317, 137790.
https://doi.org/10.1016/j.chemosphere.2023.137790

150.	Saad, M. A., Sadik, E. R., Eldakiky, B. M., He, Z., Elashtoukhy, E. Z., Khalifa, R. E., . . . Moustafa, H. (2024). Synthesis and characterization of an innovative sodium alginate/flaxseed gum green hydrogel for forward osmosis desalination. Applied Water Science, 14(2), 40. https://doi.org/10.1007/s13201-023-02080-4

151.	Saad, M. A., Sadik, E. R., Eldakiky, B. M., Moustafa, H., Fadl, E., He, Z., . . . Zewail, T. M. M. (2024). Synthesis and characterization of an innovative sodium alginate/polyvinyl alcohol bioartificial hydrogel for forward-osmosis desalination. Scientific Reports, 14(1), 58533. https://doi.org/10.1038/s41598-024-58533-6

152.	Zhang, Z., Ma, T., Gao, B., Wang, H., Yue, Q., & Gao, Y. (2024). A feasibility study of hybrid forward osmosis-solar evaporation process using melamine sponge loaded with polypyrrole (PPy@MS) solar evaporator for desalination of brackish water. Separation and Purification Technology, 343, 127074. https://doi.org/10.1016/j.seppur.2024.127074

153.	Moon, J., Kim, D. Y., Kim, J. H., & Park, K. (2024). Cost-based optimization, feasibility study, and sensitivity analysis of forward osmosis/crystallization/reverse osmosis with high-temperature operation for high-salinity seawater desalination. Desalination, 580, 117531.
https://doi.org/10.1016/j.desal.2024.117531

154.	Lu, M., Zhang, H., Tian, Y., Yao, W., Wang, J., & Wang, Y. (2023). Photocatalytic hydrogel film assisted forward osmosis (PFO) for water treatment: Sustainable performance and contaminant control. Journal of Hazardous Materials, 460, 132364. https://doi.org/10.1016/j.jhazmat.2023.132364

155.	Elmakki, T., Zavahir, S., Gulied, M., Qiblawey, H., Hammadi, B., Khraisheh, M., . . . Han, D. S. (2023). Potential application of hybrid reverse electrodialysis (RED)-forward osmosis (FO) system to fertilizer-producing industrial plant for efficient water reuse. Desalination, 550, 116374.
https://doi.org/10.1016/j.desal.2023.116374

156.	Ahmed, M. (2024). A study on the influence of feed and draw solution concentrations on the performance of the pilot-scale forward osmosis-membrane distillation system. Desalination and Water Treatment, 317, 100225.
https://doi.org/10.1016/j.dwt.2024.100225

157.	Saeed, R., Konsowa, A., Shalaby, M. S., Mansour, M. S., & Eloffy, M. (2022). Optimization of integrated forward – reverse osmosis desalination processes for brackish water. Alexandria Engineering Journal, 63, 89–102.
https://doi.org/10.1016/j.aej.2022.07.054

158. Wu, X., Ma, S., Ng, D., Acharya, D., Fan, L., & Xie, Z. (2024). Enhancing water recovery through integrated graphene oxide-modified forward osmosis and membrane distillation for real textile wastewater treatment. Journal of Environmental Chemical Engineering, 12(3), 112512. https://doi.org/10.1016/j.jece.2024.112512

159. Tashtoush, B., & Al-Omari, J. (2023). Solar-assisted hybrid integration of humidification-dehumidification and forward osmosis for brackish water desalination: A parametric study. Case Studies in Chemical and Environmental Engineering, 8, 100500. https://doi.org/10.1016/j.cscee.2023.100500

160. Ahmed, M., Alambi, R. K., Bhadrachari, G., Al-Muqahwi, S., & Thomas, J. P. (2023). Design and optimization of a unique pilot scale forward osmosis integrated membrane distillation system for seawater desalination. Journal of Environmental Chemical Engineering, 11(3), 109949. https://doi.org/10.1016/j.jece.2023.109949

161. Saleem, M. W., Ali, S., Usman, M., Chaudhary, T. N., Ullah, A., Arslan, M., & Hameed, A. U. (2024). Integration of capacitive deionization and forward osmosis for high water recovery and ultrapure water production: Concept, modelling and performance analysis. Environmental Technology, 45(28), 6136–6157. https://doi.org/10.1080/09593330.2024.2326798

162. Frauholz, J., Roth, H., & Wessling, M. (2023). Seawater desalination by forward-osmosis-assisted temperature swing solvent extraction. Desalination, 564, 116697. https://doi.org/10.1016/j.desal.2023.116697

163. Singh, S. K., Sharma, C., Mahadeva, R., Patole, S. P., & Maiti, A. (2024). Predicting forward osmosis performance with synthesized polyamide-based membrane: An integrated machine learning (MATLAB and ANN) and economic analysis framework. Journal of Cleaner Production, 444, 141285. https://doi.org/10.1016/j.jclepro.2024.141285

164. Farahbakhsh, J., Golgoli, M., Khiadani, M., Najafi, M., Suwaileh, W., Razmjou, A., & Zargar, M. (2023). Recent advances in surface tailoring of thin film forward osmosis membranes: A review. Chemosphere, 346, 140493. https://doi.org/10.1016/j.chemosphere.2023.140493

165. Abdul-Hussein, S. T., Alsalhy, Q. F., Al-Furaiji, M. H., Russo, F., Chiappetta, G., Di Luca, G., & Figoli, A. (2023). Systematic investigation of MAX phase (Ti_3AlC_2) modified polyethersulfone membrane performance for forward osmosis applications in desalination. Arabian Journal of Chemistry, 17(1), 105475. https://doi.org/10.1016/j.arabjc.2023.105475

166. Edokali, M., Mehrabi, M., Cespedes, O., Sun, C., Collins, S. M., Harbottle, D., . . . Hassanpour, A. (2024). Antifouling and stability enhancement of electrochemically modified reduced graphene oxide membranes for water desalination by forward osmosis. Journal of Water Process Engineering, 59, 104809. https://doi.org/10.1016/j.jwpe.2024.104809

167. Kim, T., Lee, Y., Kim, E., & Kim, K. (2023). Fouling-resistant surface modification of forward osmosis membranes using MoS_2-Ag nanofillers. Surfaces and Interfaces, 38, 102844. https://doi.org/10.1016/j.surfin.2023.102844

168.   Mahawer, K., Mutto, A., & Gupta, S. K. (2023). A modeling-based comparison study of data-driven and transport models for forward osmosis-nanofiltration hybrid system. Desalination, 574, 117251. https://doi.org/10.1016/j.desal.2023.117251

169.   Kegl, T., Korenak, J., Bukšek, H., & Petrinić, I. (2024). Modeling and multi-objective optimization of forward osmosis process. Desalination, 580, 117550. https://doi.org/10.1016/j.desal.2024.117550

170.   Ibrar, I., Yadav, S., Braytee, A., Altaee, A., HosseinZadeh, A., Samal, A. K., . . . Fantozzi, F. (2022). Evaluation of machine learning algorithms to predict internal concentration polarization in forward osmosis. Journal of Membrane Science, 646, 120257. https://doi.org/10.1016/j.memsci.2022.120257

171.   Ibrar, I., Yadav, S., Altaee, A., Braytee, A., Samal, A. K., Zaid, S. M. J., & Hawari, A. H. (2023). A machine learning approach for prediction of reverse solute flux in forward osmosis. Journal of Water Process Engineering, 54, 103956. https://doi.org/10.1016/j.jwpe.2023.103956

172.   Perry, M. (2019, May 20). General intro to forward osmosis membranes and processes. ForwardOsmosisTech. https://www.forwardosmosistech.com/forward-osmosis-membranes-and-membrane-processes/

173.   Song, Y., Moon, J., & Park, K. (2025). Explainable AI for permeate flux prediction in forward osmosis: SHAP interpretability and theoretical validation for enhanced predictive reliability. Desalination, 601, 118551. https://doi.org/10.1016/j.desal.2025.118551

174.   Hosseinzadeh, A., Altaee, A., Ibra, I., & Zhou, J. L. (2024). Modeling and optimization of reverse salt diffusion and water flux in forward osmosis by response surface methodology and artificial neural network. Chemical Engineering and Processing - Process Intensification, 208, 110140. https://doi.org/10.1016/j.cep.2024.110140

175.   Jafari, M., Tzirtzipi, C., Aghdam, A. M., Chahartagh, N. M., & Castro Dominguez, B. (2025). AI-assisted prediction and optimization of micropollutants removal with forward osmosis membranes. Available at SSRN: https://ssrn.com/abstract=5134015 or https://doi.org/10.2139/ssrn.5134015

176.   Hashemifard, S. A., Ghanavatyan, M. A., Jangizehi, A., Salehi, H., Shakeri, A., Alsalhy, Q. F., Al-Timimi, D., Bantz, C., Maskos, M., & Seiffert, S. (2024). Challenges of forward osmosis desalination processes using hydrogels as draw agents. Journal of Membrane Science, 714, 123408. https://doi.org/10.1016/j.memsci.2024.123408

CHAPTER 2

THEORY AND MODELING

The initial section of this chapter centres on the theoretical foundations and underlying assumptions of the data-driven modeling approach employed for FO desalination, specifically the utilization of Artificial Neural Networks (ANNs). The latter portions of the chapter delve into the theory and assumptions underpinning the techno-economic assessment of the forward osmosis-phase separation system.

2.1 Modeling of FO desalination processes

2.1.1 Introduction

The modeling of FO processes can be approached through two primary methods: transport-based models and data-driven models [1]. The transport-based models include the Solution-Diffusion (S-D) and Spiegler-Kedem (S-K) models, which rely on theoretical principles of solute and solvent transport [1]. In contrast, data-driven models leverage machine learning techniques to derive predictive relationships from empirical data [1].

2.1.2 Transport-based models

2.1.2.1 Solution-Diffusion model

The solution-diffusion model is widely used to explain mass transport in membrane separation processes like RO [2]. It postulates that the membrane's internal pressure is uniform [2]. Furthermore, the model stipulates that the chemical potential gradient across the membrane manifests solely as a variation in concentration [2]. This model adopts the solution-diffusion mechanism to describe the transport of water and solutes across the membrane [2]. The permeating species initially dissolves into the membrane material, followed by diffusion through the membrane due to a driving force [2, 3].
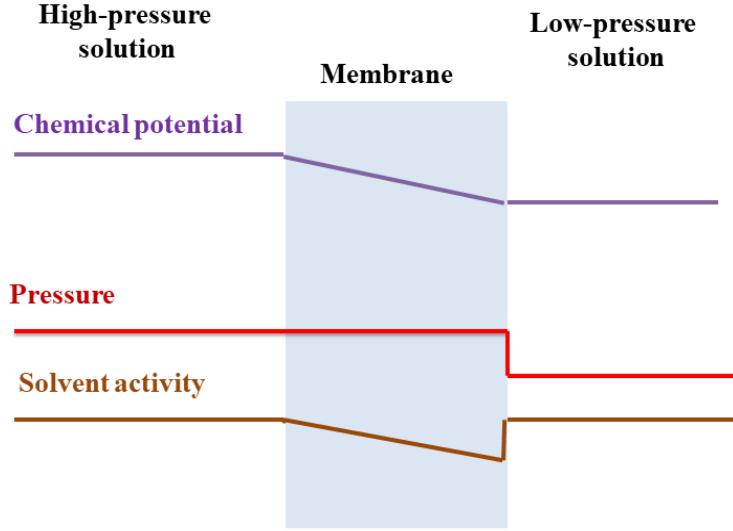
Figure 2.1: Solution-diffusion model (Source: Wijmans & Baker [2])

Using the classical solution diffusion model for FO processes, the water flux can be expressed using the equation [4 – 9].

$$J_W = A\delta(\pi_D - \pi_F) = A\delta\Delta\pi = A\Delta\pi \tag{2.1}$$

where, J_W is the water flux (L/m²h or LMH), A is the membrane hydraulic permeability coefficient (L m^{-2} h^{-1} bar^{-1}), δ is the reflection coefficient of the FO membrane, π_D is the osmotic pressure of the draw solution (bar) at the membrane surface, π_F is the osmotic pressure of the feed solution (bar) at the membrane surface and $\Delta\pi$ is the net osmotic pressure (bar).

The Van't Hoff equation establishes a quantitative relationship between a solution's osmotic pressure and its solute concentration [10 – 12]

$$\pi_{F_b} = nmRT \tag{2.2}$$

where, π_{F_b} is the bulk osmotic pressure of the feed solution (bar), m is the solute molar concentration, n is the Van't Hoff factor (i.e. 2 for NaCl), R is the universal gas constant (0.08206 L-atm/mol/K) and T is the temperature in Kelvin.

The osmotic pressure of the draw or feed solutions can also be determined from the water activity using the equation [13]

$$\pi = -\frac{RT}{V_i} \ln a_i \tag{2.3}$$

where π is the osmotic pressure of the solution, R is gas constant (J/mol.K), T is the temperature of solution (K), V_i is the molar volume, and a_i is the water activity of solution in m^3/mole. Since pure water has a water activity of 1, its osmotic pressure is inherently zero. Therefore, when using distilled water as the feed in FO or PRO, the driving force, represented by the difference in osmotic pressure, can be approximated as solely arising from the draw solution's osmotic pressure [13].

The solute flux (J_s) is given by the expression

$$J_s = B\Delta C \tag{2.4}$$

where B is the solute permeability coefficient, and ΔC is the concentration difference between the draw and feed solutions [14, 15]

While the solution-diffusion model offers advantages in simplicity and aligns with basic mass transfer principles, it possesses limitations. Notably, it does not account for concentration polarization phenomena [16]. Phuntsho et al. [17] presented expressions to capture the influence of both ECP and internal concentration polarization (ICP) of asymmetric FO membranes

$$\pi_{F,m} = \pi_{F,b} \exp\left(\frac{J_w}{k_f}\right) \tag{2.5}$$

$$\pi_{D,i} = \pi_{D,b} \exp(-J_w K_D) \tag{2.6}$$

where, $\pi_{F,m}$ denotes the osmotic pressure of the feed solution on the FO membrane active layer, $\pi_{F,b}$ represents the bulk osmotic pressure of the feed solution and k_f is the mass transfer coefficient of the feed side boundary layer, $\pi_{D,i}$ is the osmotic pressure inside the porous support layer, $\pi_{D,b}$ and K_D is the solute resistivity for diffusion of draw solutes within the porous support layer. The solute resistance to diffusion within the membrane support layer is given by the equation [17, 18].

$$K_D = \frac{t\tau}{D_D \varepsilon} \tag{2.7}$$

where t is the thickness of the FO membrane support layer, τ is the tortuosity of the membrane support layer, ε is the porosity of the membrane support and D_D is the diffusion coefficient of the draw solution. The mass transfer coefficient of the feed solution, k_f is given by the equation [17]

$$k_f = \frac{Sh D_F}{d_h} \tag{2.8}$$

where Sh is the Sherwood number, D_F is the diffusion coefficient of the feed solution and d_h is the hydraulic diameter of the feed channel. The Sherwood number can be expressed on whether the fluid flow is laminar or turbulent using the equations [19]

$$Sh = 1.85 \left(Re \frac{\eta_F}{\rho_F D_F} \frac{d_h}{P} \right)^{0.33} \text{ for laminar flow} \tag{2.9}$$

$$Sh = 0.04 Re \left(\frac{\eta_F}{\rho_F D_F} \right)^{0.33} \text{ for turbulent flow} \tag{2.10}$$

where Re is the Reynolds number, η_F is the absolute viscosity of the feed solution, ρ_F is the density of the feed solution and P is the channel length (m). The Reynolds number is given by the expression [20, 21]

$$Re_F = \frac{d_h v_F \rho_F}{\eta_F} \tag{2.11}$$

The Diffusion coefficient of NaCl feed solutions, D_F can also be determined using OLI Stream Analyzer™ (OLI Systems, Inc.), with the average diffusion coefficient value, $D_{F_{avg}}$, expressed using the equation [22]

$$D_{F_{avg}} = \frac{|Z_1| + |Z_2|}{\left(\frac{|Z_2|}{D_1} \right) + \left(\frac{|Z_1|}{D_2} \right)} \tag{2.12}$$

where Z_1 is the sodium ion charge, Z_2 is the chloride ion charge, D_1 is the diffusion coefficient of sodium ion and D_2 is the diffusion coefficient of chloride ion.

The diffusion coefficients of draw solutions can be estimated using the Wilke-Chang equation [23 – 28].

$$D_{12} = 7.4 \times 10^{-8} \frac{(\emptyset M_1)^{0.5} T}{\mu_1 (V_{Tc,bp,2})^{0.6}} \qquad (2.13)$$

$$V_{Tc,bp,2} = 0.285 \times V_{c,2}^{1.048} \qquad (2.14)$$

where D_{12} is the binary diffusion coefficient in cm^2/s, $\emptyset$ is the association factor of the solvent (2.26 for water), T is the temperature (K), M_1 is the molecular weight of the solvent (18 g/mol for water), μ_1 is the solvent viscosity (0.7972 cP for water at 303K), $V_{Tc,bp,2}$ is the solute molar volume at normal boiling temperature in cm^3/mol and $V_{c,2}$ is the solute critical volume in cm^3/mol i.e. $\frac{molar\ mass\ of\ solute\ (\frac{g}{mol})}{mass\ density\ of\ solute\ (\frac{g}{cm^3})}$

The water and solute fluxes are then predicted using the equations [17, 18]

$$J_w = A\sigma \left[\pi_D \exp(-J_w K_D) - \pi_F \exp\left(\frac{J_w}{k_f}\right) \right] \qquad (2.15)$$

$$J_s = B \left[\frac{\left(\pi_D \exp(-J_w K_D) - \pi_F \exp\left(-\frac{J_w}{k_f}\right) \right)}{1 + \frac{B}{J_w} \left(\exp\left(-\frac{J_w}{k_f}\right) - \exp(-J_w K_D) \right)} \right] \qquad (2.16)$$

2.1.2.2 Limitations of the Solution-Diffusion model

Yong et al. [29] investigated the water fluxes produced by three neutral draw solutes - urea, ethylene glycol and glucose - using a commercial asymmetric FO membrane. The experimental measurements showed that the water fluxes generated by these solutes were consistently lower than the theoretical predictions of the established models. This discrepancy persisted even after accounting for the impact of external concentration polarization (ECP).

Yong et al. [29] attributed this behaviour to a coupling between the forward water flux and the reverse solute flux and they introduced a reflection coefficient to capture this solute-solvent coupling.

The elegance of the solution-diffusion (S-D) model lies in its simplicity, providing an intuitive approach to membrane transport phenomena [2, 30]. However, the applicability of Equations 2.15 and 2.16 in the S-D model is primarily limited to

binary draw solutes. Foo et al. [31] noted that the model's accuracy diminishes for ternary or multi-component draw solutions, with errors reaching up to 66%. To address this limitation, Foo et al. developed a multicomponent solution-diffusion model, an extension of the binary model, which incorporated multicomponent diffusion theory. With access to the necessary multicomponent diffusion coefficients, their model's average absolute deviation was reduced from 21% to 3% for seven distinct ternary mixtures [31].

Ibrar et al. [32] further emphasized that the limited availability of data on the diffusion coefficients of multi-component electrolyte draw solutions complicates the determination of mass transfer coefficients and solute resistance to diffusion in the FO process.

Given the inadequacy of the S-D model in addressing multi-component draw solution systems, as demonstrated by Foo et al. [31] and Ibrar et al. [32], as well as its limitations in modeling neutral draw solutions, as shown by Yong et al. [29], this work presents an alternative approach to modeling novel binary and ternary organic draw solutions developed in our studies. Specifically, this work opts for data-driven modeling utilizing Artificial Neural Networks (ANNs), given the lack of literature data on the diffusion coefficients of the novel binary mono propylene glycol propyl ether (PGPE) and the ternary systems of hydroxypropyl cellulose–propylene glycol propyl ether (HPC–PGPE) and sodium carboxymethyl cellulose–propylene glycol propyl ether (NaCMC–PGPE).

2.1.3 Introduction to data-driven modeling

2.1.3.1 Artificial neural networks (ANN)

ANN is one of the foremost data-driven approaches to modeling membrane-based systems. ANNs have emerged as powerful tools for modeling and optimizing these complex systems by effectively capturing intricate relationships between various operating parameters. ANN algorithm learns the basic relationship present in terms of input data and utilizes that knowledge to predict the output data. The satisfactory

performance of ANN in giving accurate predictions from non-linear complex datasets makes it more suitable for membrane-based operations.

2.1.3.2 Fundamental principles of ANNs

ANNs mimic biological neural systems through layers of interconnected neurons that process information through weighted connections [1]. The network architecture consists of an input layer, hidden layers containing multiple neurons and an output layer, all connected by adjustable weights [1]. During training, data flows through the network and the system compares predictions to actual values, continuously adjusting weights to minimize errors [1]. Key parameters such as activation functions, layer configuration, learning rate and weight coefficients are fine-tuned throughout this process [1]. By iteratively adjusting these parameters using training data, the network learns to recognize patterns and improves its predictive accuracy for complex problems [1].

The basic architecture of ANNs consists of interconnected neurons organized into three main layers:

- Input Layer: receives initial data for processing
- Hidden Layers: processes inputs through one or more intermediate layers
- Output Layer: produces the final predictions

The neurons are connected through weighted links, which are adjusted during training to optimize predictions. The activation functions comprise of non-linear functions that enable the network to capture complex patterns in the data. The log-sigmoid and tan-sigmoid transfer functions are given using the equations [1]

$$Log - sigmoid = \frac{1}{1-e^{-z}} \tag{2.17}$$

$$Tan - sigmoid = \frac{e^{2z}-1}{e^{2z}+1} \tag{2.18}$$

where z represents the initialized weight of the neuron.

2.1.3.3 Core assumptions

- Black-box modeling: ANNs learn patterns from data without explicitly representing underlying physical processes

- Nonlinear relationships: The network can capture complex, nonlinear interactions common in FO processes

- Data requirements:
    - Sufficient quantity and quality of training data
    - Statistical independence of training samples
    - Generalization capability to unseen scenarios

2.1.4   Implementation procedure

The following section describes the procedures followed in modeling the novel phase-separating draw solutions for FO processes using ANNs in this work.

2.1.4.1 Data gathering

The dataset used in this study comprises 312 experimental data points, which are presented in ***Table AP-1 Appendix section***. These data were obtained from FO experiments using binary or ternary organic draw solutions, including 0.25HPC-3.75PGPE, 0.5HPC-3.75PGPE, 0.75HPC-3.75PGPE, 0.5NaCMC-3.75PGPE, 40PGPE and 0.5NaCMC-20PGPE. Each FO experiment, an FO run, was conducted for 120 minutes, with the number of runs varying for each specific draw solution. The experimental water flux was measured at 10-minute intervals throughout each 120-minute FO run, providing the data points used for modeling. Table 2.1 presents the input variables and their respective ranges employed in the modeling process.

Table 2.1: Input variables of the dataset

Input variables	Range	Units
FO runs	1 – 4	-
Time for each FO run	120	mins
Feed side temperature	25 – 30	°C
Feed side concentration	0.0181 – 0.6519	M
Feed side flow rate	9 – 24	L/h
Draw side temperature	25 – 30	°C
Draw side concentration	1.9598 – 38.4661	M
Draw side molecular weight	118.17 - 120.17	g mol^{-1}
Draw side flow rate	9 – 24	L/h

The molecular weights of the draw solutions were determined by calculating the weighted average of their constituent components' molecular masses, defined as the ratio of total molecular mass to the total number of molecules in the system. The molecular weights for 0.25HPC-3.75PGPE, 0.5HPC-3.75PGPE, 0.75HPC-3.75PGPE, 0.5NaCMC-3.75PGPE, 40PGPE and 0.5NaCMC-20PGPE were 118.84, 119.50, 120.17, 119.50, 118.17 and 118.42 g mol^{-1}, respectively. Notably, these values closely approximate the molecular weight of PGPE.

2.1.4.2 Pre-processing step: Normalizing data

The data can be normalized by employing the equation [1]

$$y = \left[\frac{(y_{max} - y_{min})(x - x_{min})}{(x_{max} - x_{min})} \right] + y_{min} \tag{2.19}$$

where y represents the normalised x value, x_{max} represents the maximum value of the dataset, x_{min} is the minimum value of the dataset, y_{max} is 1 and y_{min} is 0.

2.1.4.3 Pre-processing step: Data splitting

The normalized dataset was imported into MATLAB and partitioned into three subsets: training, validation and test sets as shown in Table 2.2

Table 2.2: Data partitioning

FO raw dataset	1st Ratios	2nd Ratios	3rd Ratios
Training	70%	80%	90%
Validation	15%	10%	5%
Testing	15%	10%	5%

2.1.4.4 Network Architecture Design

The input, hidden and output layers of the ANN network consisting of neurons are shown in Figure 2.2.
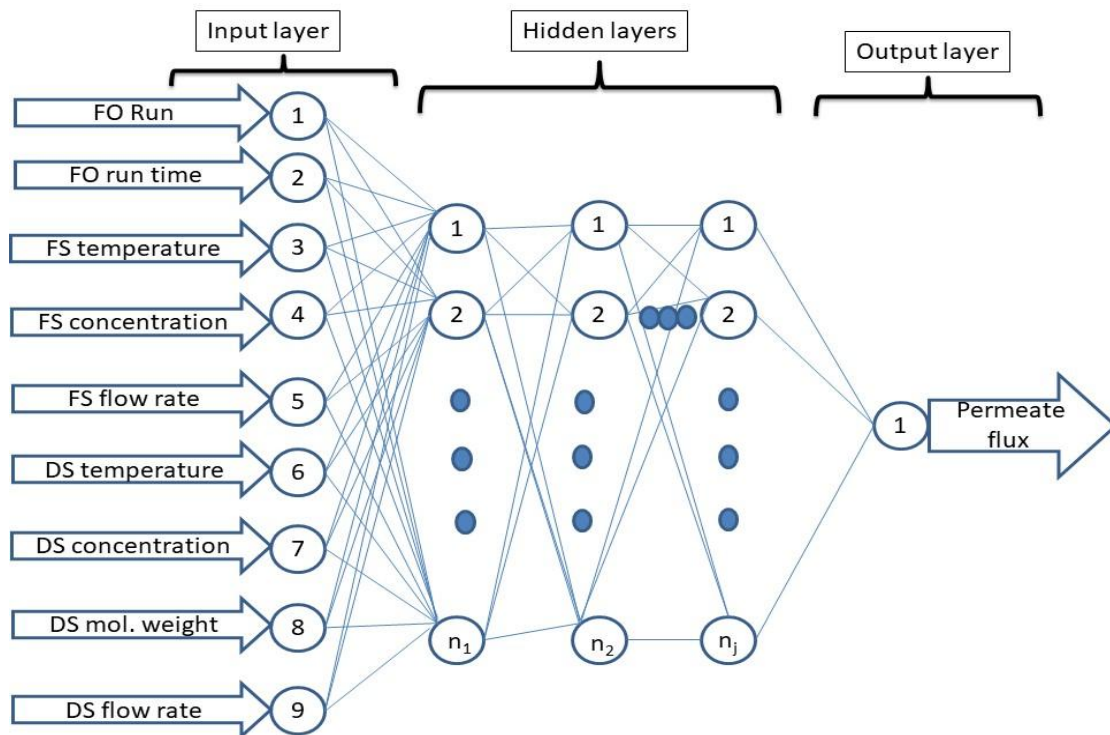
Figure 2.2: Artificial neural network architecture

2.1.4.5 ANN training

The artificial neural network was trained using the Levenberg-Marquardt algorithm implemented in MATLAB R2022a. The training process encompassed weight and

bias initialization, forward and backward propagation, optimization, convergence monitoring, hyperparameter tuning and regularization to mitigate overfitting. In this work, the ANN training was done following the procedures from Mahawer et al. [1] as shown in Figure 2.3

1 • Normalize the training data

2 • Define the training algorithm and transfer functions

3 • Initialize the number of Neurons (N) and Hidden Layers (HL)

4 • Start training

5 • Initialize the random values to weight parameters

6 • Perform feed forward computation for validation set

7 • Calculate validation error

8 • If desired accuracy is **achieved**, then STOP training and get ready for testing

9 • If desired accuracy is **not achieved**, perform feed forward computation for training set, calculate training error, compute the derivatives of training error, update weight parameters using backpropagation
• Then go back to step 6

Figure 2.3: ANN training procedure adapted from [1]

2.1.4.6 Model validation and evaluation

The ANN model was evaluated using the R^2 values and mean square errors [33 – 35]

$$R^2 = 1 - \frac{\sum_{i=1}^{n}(\widehat{Y_i} - Y_t)^2}{\sum_{i=1}^{n}(\widehat{Y_i} - \bar{Y})^2} \tag{2.20}$$

$$Root\ mean\ square\ error\ (RMSE) = \sqrt{\frac{1}{n}\sum_{i=1}^{n}(\widehat{Y_i} - Y_t)^2} \tag{2.21}$$

where n represents the total data points, $\widehat{Y_i}$ is the predicted value, Y_t is the target result and $\bar{Y}$ is the mean of the data. The coefficient of determination, R^2, is a crucial metric for assessing model performance. Models that exhibit R^2 values greater than 0.9 are generally regarded as highly satisfactory, indicating strong predictive capability [33]. Those with R^2 values ranging from 0.8 to 0.9 are considered acceptable, while models yielding R^2 values below 0.8 are typically deemed unsatisfactory [33].

2.2 Techno-economic assessment (TEA)

Most assumptions and formulas used for the techno-economic assessment of the ternary HPC-PGPE, NaCMC-PGPE and binary PGPE organic draw systems were based on previous methodologies [36 – 39]. The TEA assumed a full-scale FO plant with an operational capacity of 160 m^3 d^{-1}, positing that membrane parameters derived from laboratory-scale experimental data could be directly extrapolated to full-scale operations. The ternary 0.5NaCMC-20PGPE draw solution was chosen as the draw solution for desalinating seawater. Figure 2.4 illustrates the schematic of the FO-PS process used for the economic evaluation.

The calculation of CAPEX and OPEX for both the FO and PS processes was predicated on multiple assumptions comprehensively presented in Table 2.3. The efficiency of the FO-PS system was contingent upon the regeneration and reuse of draw solutions and the utilization of industrial waste energy as the thermal source for the phase separation process.
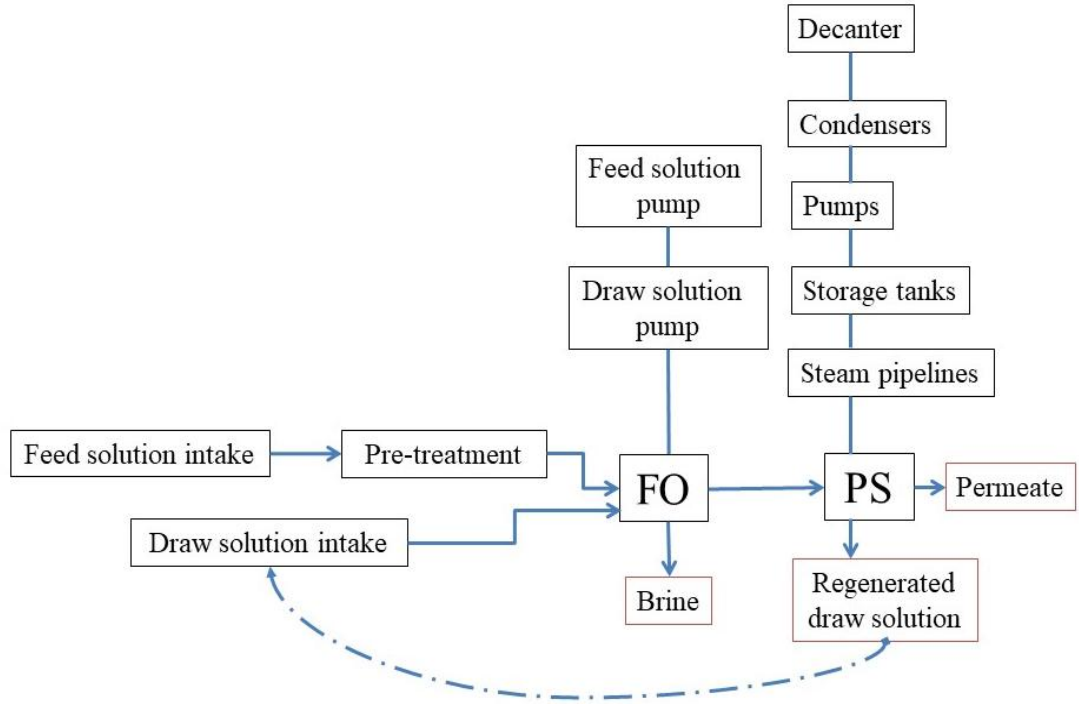
Figure 2.4: Schematic of FO-PS process used for economic evaluation

Table 2.3: Assumptions for OPEX and CAPEX calculations

Economic or Plant parameter	Value	Unit	Ref
FO plant capacity	160	$m^3 \ d^{-1}$	[36]
FO plant lifetime, n	20	yr	[36]
FO Interest rate, i	6	%	[36]
FO electricity cost, D_{Ele}	0.08	$\$ \ kWh^{-1}$	[36]
Unit cost of the FO membrane, $C_{membrane}$	30	$\$ \ m^{-2}$	[40]
Total area of the FO membrane, $Area_{membrane}$	27	m^2	[36]
Feed solution flow rate, Q_{FS}	75	$m^3 \ h^{-1}$	-
Draw solution flow rate, Q_{DS}	100	$m^3 \ h^{-1}$	-
Pressure drop for FS pump, p_{FS}	2	bar	[36]
Pressure drop for DS pump, p_{DS}	0.5	bar	[36]
Annual operating cost of pre-treatment, $OC_{pre_{FO}}$	0.15	kWh m^{-3} of feed	[36]

FO operation time per day, t	20	h	[36]
Cost of the draw solution, C_{DS}	1.73	$ kg^{-1}	-
FO pump efficiency, η_{pump}	0.85	-	[36]
Lifetime of the FO membrane, n_{Mem}	5	yr	[36]
Draw solution drainage frequency per day, f_{DS}	1	-	[36]
Molar mass of the ternary draw solution, M_{DS}	118.42	g mol^{-1}	-
Plant loading factor, PLF	0.91		[41]
PS maintenance costs	4	%	[41]
PS operator costs	84 103.25	$ yr^{-1}	[41]
PS plant operating hours per year	8000	h	[41]

The TEA contains several inherent limitations that must be acknowledged. The CAPEX and OPEX formulas for the stand-alone FO process were adapted from Zarebska-Mølgaard et al. [36], while the corresponding PS draw regeneration process formulas were based on industrial waste heat recovery systems [41]. Since FO technology has not been commercialized at scale, all cost equations derive from theoretical projections rather than actual commercial plant operations. The linear scaling relationships employed may not accurately represent the true nature of scale during the transition from laboratory scale to full commercial scale. Membrane performance parameters were extrapolated from short-term laboratory studies and may not reflect long-term commercial operation conditions, where membrane fouling, degradation, and replacement cycles could differ substantially from controlled experimental conditions. The model assumes constant values for critical economic parameters such as a 6% interest rate, $ 0.08/kWh electricity cost and 20-year plant lifetime without accounting for market volatility or regional variations that significantly impact project economics. Additionally, the model assumes continuous operation at design capacity with fixed operational parameters, which does not reflect real-world variability including maintenance downtime, process optimization adjustments and variable feed water quality. The absence of commercial FO plants

eliminates benchmarking opportunities against actual operational data, preventing validation of cost estimates or identification of systematic modeling biases.

2.2.1 CAPEX for stand-alone FO process

The capital cost for the stand-alone FO process was contingent upon both direct and indirect capital costs [36]. The pumping costs for both feed and draw solution pumps, $CC_{pumpFS/DS}$ ($), depended on the applied pressures, $p_{FS/DS}$ (bar) and the flow rates, $Q_{FS/DS}$ (m³ h⁻¹)

$$CC_{pumpFS/DS} = 52 \times (p_{FS/DS} \times Q_{FS/DS}) \tag{2.22}$$

$$CC_{pumpFS/DS} = 81 \times (Q_{FS/DS} \times p_{FS/DS})^{0.96} \tag{2.23}$$

Equation 2.22 is applicable for pump flow rates less than 200 m³ h⁻¹, while Equation 2.23 applies for pump flow rates exceeding 200 m³ h⁻¹ but less than 450 m³ h⁻¹ [40].

The capital cost of the FO membrane, $CC_{Mem_{FO}}$ ($), was calculated based on the total area of the FO membrane, $Area_{membrane}$ (m²) and the unit cost of the FO membrane, $C_{membrane}$ ($ m⁻²)

$$CC_{Mem_{FO}} = Area_{membrane} \times C_{membrane} \tag{2.24}$$

The capital cost of the equipment, $CC_{Equipment_{FO}}$ ($), encompassed the sum of the capital costs of the individual feed and draw solution pumps and the FO membrane

$$CC_{Equipment_{FO}} = CC_{pump_{FS}} + CC_{pump_{DS}} + CC_{Mem_{FO}} \tag{2.25}$$

The capital cost of site development, $CC_{Site_{FO}}$ ($), was assumed to be 20% of the capital cost of the equipment

$$CC_{Site_{FO}} = CC_{Equipment_{FO}} \times 0.2 \tag{2.26}$$

The direct capital cost, DCC_{FO} ($), was the aggregate of the capital cost of the equipment and the capital cost of site development

$$DCC_{FO} = CC_{Equipment_{FO}} + CC_{Site_{FO}} \tag{2.27}$$

The indirect capital costs, ICC_{FO} ($), were assumed to constitute 30% of the direct capital cost

$$ICC_{FO} = DCC_{FO} \times 0.3 \qquad (2.28)$$

The total capital costs, TCC_{FO} ($), of the FO process was the sum of the direct and indirect capital costs

$$TCC_{FO} = DCC_{FO} + ICC_{FO} \qquad (2.29)$$

The total annual capital cost, ACC_{FO} ($), was determined from the total capital costs, the lifetime of the plant, n, and the interest rate, i.

$$ACC_{FO} = TCC_{FO} \frac{i(1+i)^n}{(1+i)^n - 1} \qquad (2.30)$$

2.2.2 OPEX for stand-alone FO process

The operating cost associated with power consumption during the standalone FO, $OC_{Power_{FO}}$ ($), was a function of the annual operating cost of pre-treatment, $OC_{pre_{FO}}$, operating cost of the feed solution pump, $OC_{pump_{FS}}$ and operating cost of the draw solution pump $OC_{pump_{DS}}$

$$OC_{Power_{FO}} = \left(OC_{pre_{FO}} + OC_{pump_{FS}} + OC_{pump_{DS}}\right) \times 365 \qquad (2.31)$$

The operating cost of the feed or draw solution pumps, $OC_{pump_{FS/DS}}$, was a function of the extrapolated pressure drop, $\Delta P_{FO_{FS/DS}}$, operation time, t, the efficiency of the pumps, η_{pump}, FO electricity cost, D_{Ele} and the Plant loading factor, PLF [39]

$$OC_{pump_{FS/DS}} = \frac{0.028 \times \Delta P_{FO_{FS/DS}} \times Q_{FS/DS} \times t \times D_{Ele} \times PLF}{\eta_{pump}} \qquad (2.32)$$

The operating cost of membrane replacement, $OC_{MR_{FO}}$ ($), was determined from the capital cost of the FO membrane, interest rate and the lifetime of the FO membrane, n_{Mem}.

$$OC_{MR_{FO}} = \frac{CC_{Mem_{FO}} \times i}{[1-(1+i)^{-n_{Mem}]}} \qquad (2.33)$$

The operating cost of the draw solution, OC_{DS}, was a function of the frequency of draw solution drainage per day, f_{DS}, cost of the 0.5NaCMC-20PGPE draw solution, c_{DS}, the concentration of the draw solution at the inlet, C_{DS} and the molar mass of the ternary draw solution, M_{DS}.

$$OC_{DS} = f_{DS} \times C_{DS} \times Q_{DS} \times M_{DS} \times c_{DS} \tag{2.34}$$

The operating costs associated with other ancillary parameters, including labour, maintenance and cleaning chemicals, were estimated to constitute 55% of the total operating capital cost.

$$OC_{etc_{FO}} = \frac{OC_{MR_{FO}} + OC_{DS} + OC_{pre_{FO}} + OC_{pump_{FS/DS}}}{45\%} \times (1 - 45\%) \tag{2.35}$$

The annual operating cost, AOC_{FO}, was the total costs associated with power consumption, membrane replacement and other operational costs.

$$AOC_{FO} = OC_{Power_{FO}} + OC_{MR_{FO}} + OC_{etc_{FO}} \tag{2.36}$$

Thus, for the standalone FO process, the total water production cost, WC_{FO}, was based on the total annual capital cost, annual operating cost, permeate flow (m^3 d^{-1}) and the plant loading factor, PLF.

$$WC_{FO} = \frac{ACC_{FO} + AOC_{FO}}{365 \times Q_p \times PLF} \tag{2.37}$$

2.2.3 CAPEX for PS draw regeneration process

Using waste heat can appreciably decrease the overall cost associated with the draw regeneration process of the novel organic draw solute systems. The installed equipment cost was contingent upon the cost and installation factor for each. The installation factors for the steam pipelines, storage tanks, heat exchangers, pumps and condensers were 1.60, 6.13, 3.45 – 4.90, 12.24 and 9.84, respectively [41].

$$Equipment\ Installed\ Cost\ (\$) = Equipment\ cost\ (\$) \times$$
$$Individual\ Installation\ factor \tag{2.38}$$

$$Total\ Installed\ Cost\ (\$) = \sum(Installed\ costs\ of\ all\ equipment\ items) \tag{2.39}$$

The yearly CAPEX ($ yr^{-1}) depended upon the total installed cost and an annualized factor.

$$Annualized\ factor\ =\ \sum_{24}^{n=1}\left[\frac{1}{(1+p)^n}\right] \tag{2.40}$$

where, p is the interest rate.

$$Annualized\ CAPEX\ =\ \frac{Total\ Installed\ Cost}{Annualized\ factor} \tag{2.41}$$

2.2.4 OPEX for PS draw regeneration process

The PS process's annual OPEX was contingent upon maintenance, operators, electricity and cooling costs.

$$Yearly\ Electricity\ Cost\ \left(\frac{\$}{yr}\right) = Pump\ Effect\ (kW) \times \frac{Oper.hrs}{year} \times$$
$$El.price\ \left(\frac{\$}{kWh}\right) \tag{2.42}$$

$$Yearly\ Cooling\ Cost\ \left(\frac{\$}{yr}\right) = Cooling\ water\ \left(\frac{m^3}{hr}\right) \times \frac{Oper.hrs}{year} \times$$
$$Cooling\ water\ price\ \left(\frac{\$}{m^3}\right) \tag{2.43}$$

$$Yearly\ operational\ cost\ (\$) = \sum(Yearly\ maintenance\ cost\ +$$
$$Yearly\ operator\ cost + Yearly\ electricity\ cost + Yearly\ cooling\ cost) \tag{2.44}$$

$$Total\ yearly\ costs\ \left(\frac{\$}{yr}\right) = CAPEX\ \left(\frac{\$}{yr}\right) + OPEX\ \left(\frac{\$}{yr}\right) \tag{2.45}$$

The cost of steam ($ ton^{-1}) depended on the total yearly costs, the amount of steam produced and the total operating hours of the plant.

$$Steam\ cost\ \left(\frac{\$}{ton}\right) = \frac{Yearly\ cost\ \left(\frac{\$}{yr}\right)}{Steam\ produced\ \left(\frac{ton}{hr}\right) \times Plant\ operating\ hours\ \left(\frac{hrs}{year}\right)} \tag{2.46}$$

2.3 References

1. Mahawer, K., Mutto, A., & Gupta, S. K. (2023). A modeling-based comparison study of data-driven and transport models for forward osmosis-nanofiltration hybrid system. Desalination, 574, 117251. https://doi.org/10.1016/j.desal.2023.117251

2. Wijmans, J., & Baker, R. (1995). The solution-diffusion model: A review. Journal of Membrane Science, 107(1–2), 1–21. https://doi.org/10.1016/0376-7388(95)00102-i

3. Mccutcheon, J. R., & Elimelech, M. (2007). Modeling water flux in forward osmosis: Implications for improved membrane design. AIChE Journal, 53(7), 1736–1744. https://doi.org/10.1002/aic.11197

4. Zhao, S., & Zou, L. (2011). Relating solution physicochemical properties to internal concentration polarization in forward osmosis. Journal of Membrane Science, 379(1–2), 459–467. https://doi.org/10.1016/j.memsci.2011.06.021

5. Gruber, M., Johnson, C., Tang, C., Jensen, M., Yde, L., & Hélix-Nielsen, C. (2011). Computational fluid dynamics simulations of flow and concentration polarization in forward osmosis membrane systems. Journal of Membrane Science, 379(1–2), 488–495. https://doi.org/10.1016/j.memsci.2011.06.022

6. Wang, K. Y., Teoh, M. M., Nugroho, A., & Chung, T. (2011). Integrated forward osmosis–membrane distillation (FO–MD) hybrid system for the concentration of protein solutions. Chemical Engineering Science, 66(11), 2421–2430. https://doi.org/10.1016/j.ces.2011.03.001

7. Zhao, S., & Zou, L. (2011). Effects of working temperature on separation performance, membrane scaling and cleaning in forward osmosis desalination. Desalination, 278(1–3), 157–164. https://doi.org/10.1016/j.desal.2011.05.018

8. Kim, T., Kim, Y., Yun, C., Jang, H., Kim, W., & Park, S. (2011). Systematic approach for draw solute selection and optimal system design for forward osmosis desalination. Desalination, 284, 253–260. https://doi.org/10.1016/j.desal.2011.09.008

9. Field, R. W., & Wu, J. J. (2013). Mass transfer limitations in forward osmosis: Are some potential applications overhyped? Desalination, 318, 118–124. https://doi.org/10.1016/j.desal.2013.01.025

10. Grim, E. (1953). Relation between pressure and concentration difference across membranes permeable to solute and solvent. Experimental Biology and Medicine, 83(2), 195–200. https://doi.org/10.3181/00379727-83-20306

11. Grattoni, A., Merlo, M., & Ferrari, M. (2007). Osmotic pressure beyond concentration restrictions. The Journal of Physical Chemistry B, 111(40), 11770–11775. https://doi.org/10.1021/jp075834j

12. Fritz, C. J., Scalia, J., Shackelford, C. D., & Malusis, M. A. (2019). Determining maximum chemico-osmotic pressure difference across clay membranes. Journal of Geotechnical and Geoenvironmental Engineering, 146(1), 04019126. https://doi.org/10.1061/(asce)gt.1943-5606.0002196

13. Yu, Q., Gutierrez, M. T. G., & Hägg, M. (2018). Using an osmotic membrane pressure actuator (OMPA) for enhanced oil and gas recovery – The concept.

International Journal of Petrochemical Science & Engineering, 3(2), 76–78. https://doi.org/10.15406/ipcse.2018.03.00076

14. Greisner, B., Mauer, D., Rögener, F., & Lerch, A. (2023). Predicting water flux in forward osmosis with unknown feed solution composition: An empirical approach based on thermodynamical properties. Membranes, 13(4), 427. https://doi.org/10.3390/membranes13040427

15. D'Haese, A. K., Motsa, M. M., Van Der Meeren, P., & Verliefde, A. R. (2016). A refined draw solute flux model in forward osmosis: Theoretical considerations and experimental validation. Journal of Membrane Science, 522, 316–331. https://doi.org/10.1016/j.memsci.2016.08.053

16. Su, J., & Chung, T. (2011). Sublayer structure and reflection coefficient and their effects on concentration polarization and membrane performance in FO processes. Journal of Membrane Science, 376(1–2), 214–224. https://doi.org/10.1016/j.memsci.2011.04.031

17. Phuntsho, S., Hong, S., Elimelech, M., & Shon, H. K. (2013). Osmotic equilibrium in the forward osmosis process: Modelling, experiments and implications for process performance. Journal of Membrane Science, 453, 240–252. https://doi.org/10.1016/j.memsci.2013.11.009

18. Kim, W., & Heldman, D. R. (2020). A mathematical estimation of the structural parameter for prediction of forward osmosis (FO) performance. Journal of Water Process Engineering, 39, 101719. https://doi.org/10.1016/j.jwpe.2020.101719

19. Phuntsho, S., Vigneswaran, S., Kandasamy, J., Hong, S., Lee, S., & Shon, H. K. (2012). Influence of temperature and temperature difference in the performance of forward osmosis desalination process. Journal of Membrane Science, 415–416, 734–744. https://doi.org/10.1016/j.memsci.2012.05.065

20. Wei, T., & Willmarth, W. W. (1989). Reynolds-number effects on the structure of a turbulent channel flow. Journal of Fluid Mechanics, 204, 57–95. https://doi.org/10.1017/s0022112089001667

21. Schultz, M. P., & Flack, K. A. (2013). Reynolds-number scaling of turbulent channel flow. Physics of Fluids, 25(2), 025101. https://doi.org/10.1063/1.4791606

22. Park, M., Lee, J. J., Lee, S., & Kim, J. H. (2011). Determination of a constant membrane structure parameter in forward osmosis processes. Journal of Membrane Science, 375(1–2), 241–248. https://doi.org/10.1016/j.memsci.2011.03.052

23. Sassiat, P. R., Mourier, P., Caude, M. H., & Rosset, R. H. (1987). Measurement of diffusion coefficients in supercritical carbon dioxide and correlation with the equation of Wilke and Chang. Analytical Chemistry, 59(8), 1164–1170. https://doi.org/10.1021/ac00135a020

24. Chang, P., & Wilke, C. R. (1955). Some measurements of diffusion in liquids. The Journal of Physical Chemistry, 59(7), 592–596. https://doi.org/10.1021/j150529a005

25. Miyabe, K., & Isogai, R. (2011). Estimation of molecular diffusivity in liquid phase systems by the Wilke–Chang equation. Journal of Chromatography A, 1218(38), 6639–6645. https://doi.org/10.1016/j.chroma.2011.07.018

26. Reddy, K. A., & Doraiswamy, L. K. (1967). Estimating liquid diffusivity. Industrial & Engineering Chemistry Fundamentals, 6(1), 77–79. https://doi.org/10.1021/i160021a012

27. Sitaraman, R., Ibrahim, S. H., & Kuloor, N. R. (1963). A generalized equation for diffusion in liquids. Journal of Chemical & Engineering Data, 8(2), 198–201. https://doi.org/10.1021/je60017a017

28. Miyabe, K. (2011). Estimation of molecular diffusivity in aqueous solution of acetonitrile by the Wilke–Chang equation. Journal of Separation Science, 34(19), 2674–2679. https://doi.org/10.1002/jssc.201100385

29. Yong, J. S., Phillip, W. A., & Elimelech, M. (2011). Coupled reverse draw solute permeation and water flux in forward osmosis with neutral draw solutes. Journal of Membrane Science, 392–393, 9–17. https://doi.org/10.1016/j.memsci.2011.11.020

30. Paul, D. (2004). Reformulation of the solution-diffusion theory of reverse osmosis. Journal of Membrane Science, 241(2), 371–386. https://doi.org/10.1016/j.memsci.2004.05.026

31. Foo, Z. H., Rehman, D., Coombs, O. Z., Deshmukh, A., & Lienhard, J. H. (2021). Multicomponent Fickian solution-diffusion model for osmotic transport through membranes. Journal of Membrane Science, 640, 119819. https://doi.org/10.1016/j.memsci.2021.119819

32. Ibrar, I., Yadav, S., Altaee, A., Hawari, A., Nguyen, V., & Zhou, J. (2020). A novel empirical method for predicting concentration polarization in forward osmosis for single and multicomponent draw solutions. Desalination, 494, 114668. https://doi.org/10.1016/j.desal.2020.114668

33. Nurhayati, M., Jeong, K., Lee, H., Park, J., Hong, B. U., Kang, H. G., . . . Lee, S. (2024). Predicting and optimizing forward osmosis membrane operation using machine learning. Desalination, 591, 118154. https://doi.org/10.1016/j.desal.2024.118154

34. Ma, S., Wu, X., Fan, L., & Xie, Z. (2024). Predicting water flux and reverse solute flux in forward osmosis processes using artificial neural networks (ANN) modelling with structural parameters. Separation and Purification Technology, 351, 128092. https://doi.org/10.1016/j.seppur.2024.128092

35. Ibrar, I., Yadav, S., Altaee, A., Braytee, A., Samal, A. K., Zaid, S. M. J., & Hawari, A. H. (2023). A machine learning approach for prediction of reverse solute flux in forward osmosis. Journal of Water Process Engineering, 54, 103956. https://doi.org/10.1016/j.jwpe.2023.103956

36. Zarebska-Mølgaard, A., Li, K., Niedzielska, A., Schneider, C., Yangali-Quintanilla, V., Tsapekos, P., . . . Helix-Nielsen, C. (2021). Techno-economic assessment of a hybrid forward osmosis and membrane distillation system for agricultural water recovery. Separation and Purification Technology, 283, 120196. https://doi.org/10.1016/j.seppur.2021.120196

37. Linares, R. V., Li, Z., Yangali-Quintanilla, V., Ghaffour, N., Amy, G., Leiknes, T., & Vrouwenvelder, J. (2015). Life cycle cost of a hybrid forward osmosis – low pressure reverse osmosis system for seawater desalination and wastewater

recovery. Water Research, 88, 225–234.
https://doi.org/10.1016/j.watres.2015.10.017

38. Osipi, S. R., Secchi, A. R., & Borges, C. P. (2020). Cost analysis of forward osmosis and reverse osmosis in a case study. In Elsevier eBooks (pp. 305–324). https://doi.org/10.1016/b978-0-12-816777-9.00013-7

39. Choi, Y., Cho, H., Shin, Y., Jang, Y., & Lee, S. (2015). Economic evaluation of a hybrid desalination system combining forward and reverse osmosis. Membranes, 6(1), 3. https://doi.org/10.3390/membranes6010003

40. Patel, D., Mudgal, A., Patel, V., Patel, J., Park, K., Davies, P., & Alegre, R. R. (2023). Energy, exergy, economic and environment analysis of standalone forward osmosis (FO) system for domestic wastewater treatment. Desalination, 567, 116995. https://doi.org/10.1016/j.desal.2023.116995

41. Ali, H., Eldrup, N. H., Normann, F., Andersson, V., Skagestad, R., Mathisen, A., & Øi, L. E. (2018). Cost estimation of heat recovery networks for utilization of industrial excess heat for carbon dioxide absorption. International Journal of Greenhouse Gas Control, 74, 219–228.
https://doi.org/10.1016/j.ijggc.2018.05.003

CHAPTER 3

EXPERIMENTAL SETUP AND PROCEDURE

3.1 Raw materials/chemicals

In this study, the following raw materials/chemicals were employed

- Propylene glycol propyl ether (PGPE)
- Hydroxypropyl cellulose (HPC)
- Sodium carboxymethyl cellulose (NaCMC)
- Sodium chloride (NaCl)
- Commercial asymmetric cellulose triacetate (CTA) membrane

3.1.1 Specification and Sources of raw materials/chemicals

Specifications and sources of the raw materials and chemicals used in the development and analysis of novel phase-separating organic draw solutions are given in Table 3.1

Table 3.1: Specification and sources of raw materials/chemicals

Sr. No.	Chemical/Raw material	Source	Specification
1.	Propylene glycol propyl ether	Sigma-Aldrich, India	molecular weight of 118.17 Da, 99% purity, viscosity of 2.389 mPa.s at 25 ºC and density of 0.885 g/mL at 25 ºC
2.	Hydroxypropyl cellulose	ThermoFisher Scientific, India	molecular weight of 100 000 and viscosity of 75 – 150 mPa.s for 5% aqueous solution
3.	Sodium carboxymethyl cellulose	Sigma-Aldrich, India	molecular weight of 90 000, 0.7 carboxymethyl groups per anhydro glucose unit, density of 1.59 g/cm^3, viscosity of 50 – 200 mPa.s for 4% in water at 25 ºC
4.	Sodium chloride	ThermoFisher Scientific, India	Analytical reagent grade and > 99.5% purity
5.	CTA membrane	Hydration Technology Inc., Albany, OR, USA	Harvested commercial OsMem2521FO-MS-CTA-P-3H membrane

3.2 Research Methodology

The methodology used to achieve the objectives of the research work is divided into the following sections

- Preparation and nomenclature of draw solutions
- Properties of the feed solution
    - Concentration
    - Osmotic pressure
    - Density
- Properties of the draw solution
    - Osmotic pressure
    - Dynamic viscosity
    - pH
    - Density and Concentration
- Draw solution regeneration potential
- FO membrane and draw solution compatibility study
    - Using Scanning Electron Microscopy (SEM)
    - Using ImageJ software
- Phase-separation tests
- Membrane parameters
    - Membrane hydraulic permeability constant
    - Solute permeability coefficient
    - Reflection coefficient

3.2.1 Preparation and nomenclature of draw solutions

The draw solutes were dissolved in double RO water. Equal volumes of the cellulose derivative solution and the PGPE solution were dissolved separately. These two solutions were then combined and allowed to dissolve together at room temperature to form the final designated ternary draw solution.

In the nomenclature of the draw solutions, the numerical value preceding the polyelectrolyte, NaCMC, or the cellulose derivative, HPC, signifies its weight percentage (wt.%). The numerical value before PGPE denotes its molarity (M).

For instance, the draw solution designated as "0.5NaCMC-3.75PGPE" represents a draw solution comprising 0.5wt.% NaCMC and 3.75 M PGPE solution.

Four binary and six ternary draw solutions were prepared using various combinations of PGPE and NaCMC for the NaCMC-PGPE system in desalinating brackish water. The binary draw solutions were 0.5NaCMC, 1NaCMC, 2NaCMC and 3.75PGPE. The ternary draw solutions were 1NaCMC-1.25PGPE, 1NaCMC-2.5PGPE, 1NaCMC-3.75PGPE, 0.25NaCMC-1.25PGPE, 0.5NaCMC-2.5PGPE and 0.5NaCMC-3.75PGPE. For seawater desalination, higher concentration draw solutions of 40PGPE and 0.5NaCMC-20PGPE were prepared. For the HPC-PGPE system, a total of sixteen distinct single-solute and ternary organic draw mixtures were prepared. These draw solutions were named 0.5HPC, 1HPC, 1.5HPC, 2HPC, 0.25HPC-1.25PGPE, 0.5HPC-1.25PGPE, 0.75HPC-1.25PGPE, 1HPC-1.25PGPE, 0.25HPC-2.5PGPE, 0.5HPC-2.5PGPE, 0.75HPC-2.5PGPE, 1HPC-2.5PGPE, 0.25HPC-3.75PGPE, 0.5HPC-3.75PGPE, 0.75HPC-3.75PGPE and 1HPC-3.75PGPE.

3.2.2   Properties of the feed solution

3.2.2.1 Concentration

The present work adopted the method proposed by Di Noto and Mecozzi [1] for determining NaCl concentrations, which was thoroughly analyzed through experimentation and modeling by Peters [2]. At a wavelength of 206 nm, Peters demonstrated a linear relationship between molarity and absorbance for NaCl solutions, with an R^2 value of 0.9836. Di Noto and Mecozzi, as well as Peters, reported a maximum absorbance for NaCl solutions around 200 nm. On the other hand, Tong et al. [3] observed the peak at 197 nm.

The feed solution concentrations were determined using an Eppendorf Bio Spectrometer for the 5000 ppm and 35 000 ppm NaCl solutions. The concentration of the 1000 ppm NaCl brackish feed solution was determined using a Shimadzu UV-1800 UV/Visible Scanning Spectrophotometer at 228.4 nm.

The absorbance values of the feed solution were catalogued, and the results of the absorbance versus wavelength are shown in Figure 3.1a. The standard curve, shown in Figure 3.1b, served as a reference for estimating the feed solution's concentration based on its corresponding absorbance value. The relationship between the brackish feed solution's concentration and its osmotic pressure is shown in Figure 3.1c.
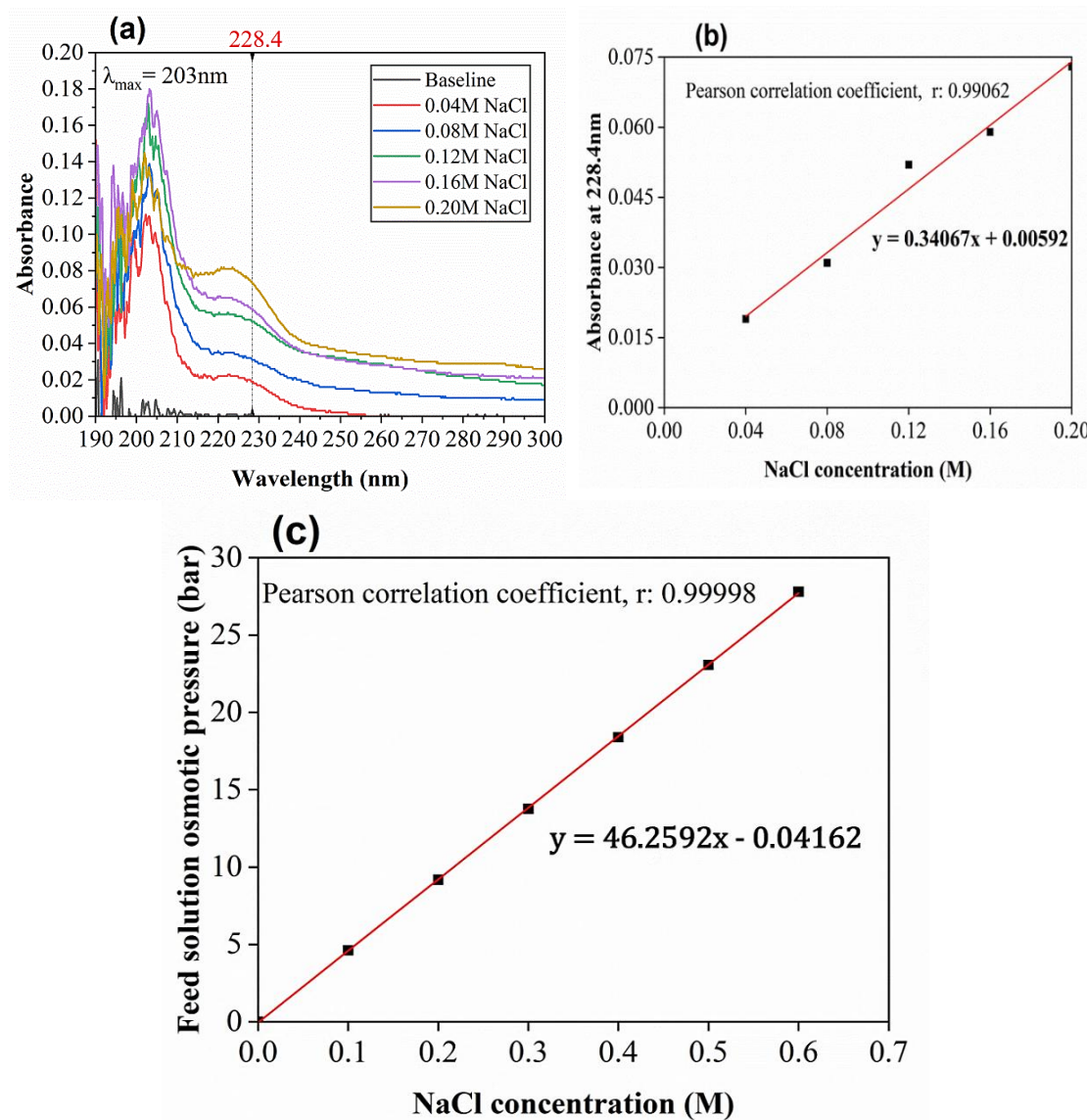
Figure 3.1: Feed solution calibration curves

3.2.2.2 Osmotic pressure

The osmotic pressures of the NaCl feed solutions were determined from OLI Analyzer software.

3.2.2.3 Density

The densities of the feed solutions were determined using a density bottle.

3.2.3　Properties of the draw solution

3.2.3.1 Osmotic pressure

The draw solution's osmolality was measured using freezing point depression osmometry. The osmometer was a Semi-Micro Osmometer K-7400 (Knauer Inc., Germany), with a measuring range from 0 – 2000 mOsm/kg. The osmolality (in Osmoles/kg) was converted to osmotic pressure using the equation

$$\text{Osmotic pressure} = RTc \tag{3.1}$$

where, R is the universal gas constant (0.083144598 L.bar.K^{-1}.mol^{-1}), T is the absolute temperature in Kelvin, and c (Osmoles/L) is the osmolarity calculated from the osmolality given by the osmometer.

Figure 3.2: Freezing point depression osmometer

3.2.3.2 Dynamic viscosity

The dynamic viscosities of the draw solutions were determined using an Anton Paar MCR 302 Modular Compact Rheometer at different temperatures.

Figure 3.3: Anton Paar MCR 302 Modular Compact Rheometer

3.2.3.3 pH

The pH of the draw solutions was determined using an esaw pH meter at a temperature of 15 ºC.

3.2.3.4 Density and Concentration

The densities of the draw solutions were determined using a density bottle. The concentrations of the various draw solutions were determined by refractive index determinations.

3.2.4   Draw solution regeneration potential

The thermal reversibility of the draw solutions was evaluated by visually determining the cloud point temperatures. Samples were heated in a water bath at various temperatures of 25 ℃, 32 ℃, 40 ℃, 45 ℃ and 50 ℃ for 30 minutes each.

Subsequent visual inspection, conducted using a high-grade camera, aimed to detect any cloudiness or phase separation. This approach provided a preliminary assessment of the draw solutions' thermal stability and reversibility.

3.2.5   FO membrane and draw solution compatibility study

3.2.5.1 Morphological analysis by SEM

Morphological studies were conducted to assess the compatibility of the FO membrane with the organic draw solutions after a 21-day immersion period. Three identical membranes were immersed in solutions of 0.5NaCMC, 3.75PGPE and 0.5NaCMC-3.75PGPE, with one unimmersed membrane serving as a control. Following the immersion period, the membranes were rinsed with distilled water and then sputter-coated using an Emitech K550X coater. The membranes were imaged using a JSM-7800F Prime Field Emission Scanning Electron Microscope at 100x, 250x, 1 000x and 10 000x magnifications.

3.2.5.2 Morphological analysis by ImageJ software

ImageJ software was used to analyse the SEM micrographs for morphological parameters such as size and surface roughness. The SEM micrographs of the FO membranes, taken at a magnification of 10 000x were further analysed using ImageJ to determine the compatibility of the membranes with the draw solutions. The analysis process involved opening all four membranes in ImageJ, scaling and colour adjusting them using the Huang thresholding method, and then converting them into binary form. Various parameters of the membranes, including total count, total area, perimeter, average size, mean gray value, modal gray value (corresponding to the highest peak in the histogram), circularity (which indicates the shape with a value between 0 and 1, where 1 represents a perfect circle), solidity,

Feret diameter, integrated intensity, and kurtosis, were determined. These morphological parameters were then compared for all the FO membranes.

Surface roughness of the FO membranes was quantified using ImageJ software. SEM micrographs were initially converted to 8-bit grayscale images. The waviness and roughness plugin were then utilized with a cut-off value of 40 pixels.

This plugin converts the SEM micrograph into separate surface roughness and waviness plots. The roughness profile for each FO membrane was then plotted as a function of gray value against distance.

3.2.6   Phase-separation tests

Phase-separation was induced by heating the draw solutions at a temperature above the cloud point temperature for 1 hour.

3.2.7   Membrane parameters

3.2.7.1 Membrane hydraulic permeability constant

The hydraulic permeability coefficient, A, of the FO membrane was determined on a RO system by measuring the water fluxes at pressures of 2, 3 and 4 kg/cm^2. The value of A was determined as the slope of the water flux (LMH) versus applied pressure (bar) linear fit.

3.2.7.2 Solute permeability and Reflection coefficient

The solute permeability coefficient and reflection coefficients of the draw solutions were evaluated using the Spiegler-Kedem mathematical model for FO processes. Model equations were coded in the MATLAB. Steady-state experimental data were fitted in the model equations by minimizing the errors between experimental results and model predictions.

3.3 Experimental setup and procedure

3.3.1 Experimental setup

Figure 3.4 depicts a schematic representation of the self-assembled FO experimental setup used for the NaCMC-PGPE draw solutions

No.	Equipment
1	Weighing scale
2	Draw solution tank
3	Feed solution tank
4	Submersible pump
5	Non-submersible pump
6	Valve
7	Rotameter
8	FO test cell with membrane
9	Rotameter
10	Valve
11	Valve
12	Rotameter
13	H198130 waterproof pH, EC/TDS and temperature tester.
14	Digital thermometer
15	Refractometer
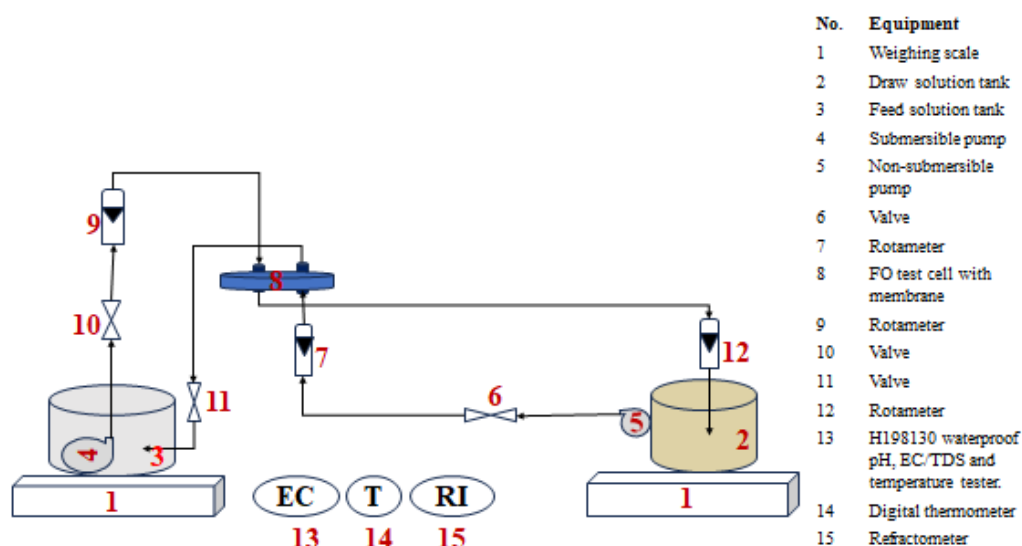
Figure 3.4: Schematic representation of the self-assembled laboratory FO experimental setup for the NaCMC-PGPE draws solution system

The FO setup consisted of a 10L plastic feed tank connected to a submersible pump capable of providing a maximum hydraulic head of 1.65m. The feed and draw solution temperatures were monitored using a waterproof LABART^{TM} digital thermometer with a range of -50 to 300 °C. A 10L plastic draw solution tank was coupled to a 12V high-pressure Generic^{TM} non-submersible pump. Rotameters with a maximum flow range of 1 LPM were employed to measure the flow rates of the draw solution entering and exiting the FO test cell, as well as the feed solution entering the cell. The mass changes of the draw and feed solutions were recorded using a Cynor CY-04 electronic weighing scale and an Eminent SS electronic weighing machine, respectively.

Figure 3.5 shows the schematic of the self-assembled FO experimental setup for the HPC-PGPE draw solution system
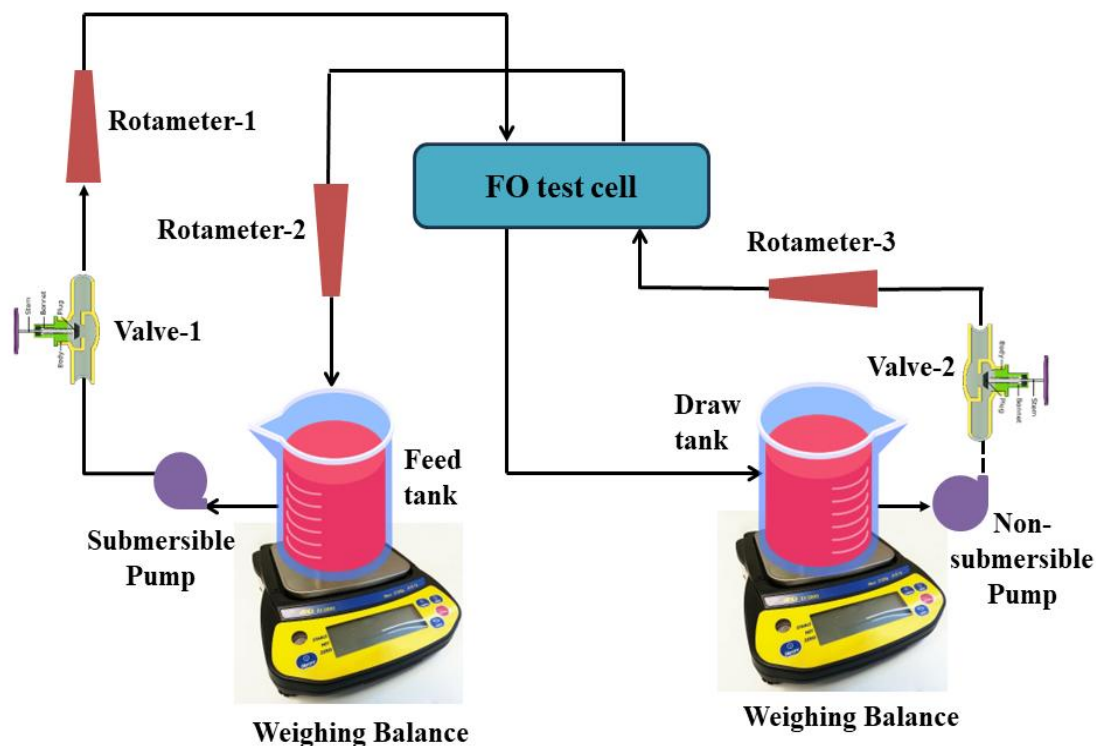
Figure 3.5: Schematic of the self-assembled FO laboratory setup for the HPC-PGPE draw solution system

3.3.2 Experimental procedure

3.3.2.1 NaCMC-PGPE draw solution systems

The self-assembled FO setup equipped with the harvested HTI CTA membrane employed the AL-FS mode. In this configuration, the feed solution was in direct contact with the active layer of the FO membrane. The feed and draw solutions were kept at controlled temperatures of 25 ± 1 °C or 30 ± 1 °C for 120 minutes. The fluctuations in the weights of both the feed and draw solutions were monitored every 10 minutes. The experiment was initiated by pumping the draw solution into the system, followed by the feed solution one minute later. After stabilizing the flow rates, the experiment commenced and afterwards, the setup was disassembled. The FO membrane was cleaned using double RO water and immersed in distilled water for 24 hours before reuse. The same membrane was used for all the experiments reported in this work. Feed and draw spacers were used to mitigate ECP effects.

The experimental water and solute fluxes were then determined by

$$J_{w-exp} = \frac{m}{\rho_F \times A_m \times t} \qquad (3.2)$$

where J_{w-exp} is the experimental water flux (LMH), m is the gain in the mass of the draw solution (kg), ρ_F is the density of the feed solution (kg/L), A_m is the active area of the FO membrane (m^2) and t is time (hours).

$$J_{s-exp} = \frac{C_t V_t - C_o V_o}{A_m \times t} \qquad (3.3)$$

where J_{s-exp} is the experimental solute flux (gMH), C_t and C_o are the final and initial feed solution concentrations (g/L) whilst V_t and V_o are the volumes (L) of the final and initial feed solutions.

3.3.2.2 HPC-PGPE draw solution systems

Both the feed solution and draw solutions were kept at a controlled temperature of 25 $\pm$ 1 °C throughout the experiment. The initial volume of the feed solution was 5 L, and the weight loss of the feed solution was monitored every 10 minutes for a total duration of 120 minutes. The draw solution had an initial volume of 3.5 L, and the weight gain of the draw solution was continuously monitored every 10 minutes for the same 120-minute duration. To initiate the experiment, the draw solution was first pumped into the system using a non-submersible high-pressure pump, followed by the feed solution a minute later. The volumetric flow rates of both solutions were measured using rotameters and expressed in litres per minute. The flow rates of the draw solution were initially set at 0.20 LPM and were increased to 0.40 LPM for the more viscous draw solutions. The experimental water flux was calculated using the Equation 3.2. The experimental solute flux (in gMH) was determined by checking the concentrations of the feed solution at regular intervals and calculated using the Equation 3.3.

3.4 References

1. Di Noto, V., & Mecozzi, M. (1997). Determination of seawater salinity by ultraviolet spectroscopic measurements. Applied Spectroscopy, 51(9), 1294–1302. https://doi.org/10.1366/0003702971942295
2. Peters, R. D. (2016, September 26). Using spectral measurements to differentiate between aqueous NaCl and aqueous KCL in dual-salt solutions. Retrieved from https://harvest.usask.ca/handle/10388/7489
3. Tong, A., Tang, X., Zhang, F., & Wang, B. (2020). Study on the shift of ultraviolet spectra in aqueous solution with variations of the solution concentration. Spectrochimica Acta Part A, Molecular and Biomolecular Spectroscopy, 234, 118259. https://doi.org/10.1016/j.saa.2020.118259

CHAPTER 4

NOVEL POLYELECTROLYTE-GLYCOL ETHER TERNARY PHASE-SEPARATING DRAW SOLUTIONS FOR DESALINATION USING FORWARD OSMOSIS

4.1 Introduction

The progress of FO has been hindered by several challenges, including the lack of an ideal draw solution and expensive regeneration methods [1]. Although inorganic draw solutes like NaCl, KCl and NH_4HCO_3 have been explored, they suffer from high reverse salt fluxes and limited biodegradability, prompting research into novel organic draw solutes [2, 3]. Most organic draw solutions, such as polysaccharides, possess high viscosities, which contribute to internal concentration polarization (ICP) effects and bio fouling [4].

Researchers are actively engaged in the development of novel organic draw solutes with tailored and customizable properties for optimal performance. Advancements in FO membrane technology hold promise for overcoming the limitations of traditional FO desalination systems [5]. As a result, FO is strategically positioned to lead research efforts in addressing global water scarcity [6].

Extensive work has been conducted using binary organic draw solutions incorporating food additives [7], molasses [8], ethanol [9], polyacrylamide [10], micellar solution [11] and dimethyl ether [12]. However, the high costs of some of these materials, ICP and fouling effects posed major drawbacks on the water flux performance. Researchers then explored the use of ternary (three components) or quaternary (four components) systems in order to mitigate the drawbacks associated with binary (two component) draw solutions. Some of these multi-component systems include a ternary combination of ionic liquid and hydrogel [13], various mixtures of magnesium chloride, sodium chloride, sucrose and maltose [14], a ternary system comprising sodium acetate and glucose in calcium chloride [15] and the addition of aluminium sulphate to magnesium chloride [16]. These combined draw solutions exhibited improved water fluxes and reduced reverse solute fluxes. However, their major drawback was the inefficiency of the draw solution

regeneration processes. Cellulose derivatives have been widely used in areas like medicine and biotechnology [17]. Sodium carboxymethyl cellulose is a specialized material that is characterized as both a polyelectrolyte and a cellulose derivative.

Darvishmanesh et al. [18] investigated the potential of using mixtures of two distinct glycol ethers, tripropylene glycol methyl ether (TPM, molecular weight 206.27 Da) and tripropylene glycol n-butyl ether (TPnB, molecular weight 248.35 Da), as draw agents. Despite generating high osmotic pressures, the draw agents caused substantial initial reductions in the transmembrane water and solute fluxes. The water flux was hindered by concentration polarization (CP) stemming from the high viscosities of the draw solutions and the adsorption of glycol ether onto the dense layer of the FO membrane. Additionally, the reverse solute fluxes in all FO modes were reported to be greater than 2.9 gMH. Inada et al. [19] used mass spectrometry to demonstrate that polyalkylene glycol draw solutes with molecular weights below 1250 Da permeated the FO membrane. Draw solutes with a molecular weight of 1810 – 3911 Da exhibited the lowest J_s/J_w ratio. This suggests that lower molecular weight glycol ether draw solutes, while being less viscous and exerting greater osmotic pressures, produce higher solute fluxes [19]. On the other hand, glycol ethers with higher molecular weights are more viscous but yield relatively lower solute fluxes. The solute permeability coefficient of draw solutions can be evaluated using a Spiegler-Kedem mathematical model for FO processes [20].

In the present study, the feasibility of employing PGPE and NaCMC solutions as draw agents for FO desalination was investigated. These solutions exhibit LCST behaviour, enabling facile regeneration through moderate heating. Initially, binary and ternary solutions were evaluated based on their osmotic pressures and viscosities. Cloud point measurements were performed to determine the LCST and assess the regeneration potential. The most promising solutions were subsequently tested in a laboratory-scale FO setup for water recovery from model brackish water (5 000 ppm NaCl) and model seawater (35 000 ppm NaCl).

4.2 Results and Discussion

4.2.1 Draw solutions' properties

The densities, dynamic viscosities, pH, freezing point depressions and osmolalities of the binary draw solutions are shown in Tables 4.1.

Table 4.1: Binary draw system's properties

Draw solution	Density (g/ml)	Dynamic viscosity (mPa.s)	pH at 15 ºC	Freezing point depression (ºC)	Osmolality (mOsm/kg)	Osmotic pressure at 25 ºC (bar)
0.5NaCMC	0.9657	1.9197	7.45	-0.020	11	0.272
1NaCMC	0.9786	4.6843	7.48	-0.039	21	0.520
2NaCMC	0.9855	11.8860	7.49	-0.049	26	0.644
3.75PGPE	0.9649	3.1354	5.85	-2.107	1133	28.1

The dynamic viscosities, pH, freezing point depressions and osmolalities of the ternary draw solutions are shown in Tables 4.2.

Table 4.2: Ternary draw system's properties

Draw solution	Dynamic viscosity (mPa.s)	pH at 15 ºC	Freezing point depression (ºC)	Osmolality (mOsm/kg)	Osmotic pressure at 25 ºC (bar)
1NaCMC-1.25PGPE	6.0074	7.14	-1.146	718	17.8
1NaCMC-2.5PGPE	6.9824	7.11	-2.409	1295	32.1
1NaCMC-3.75PGPE	7.9458	7.10	-2.738	1477	36.7
0.25NaCMC-1.25PGPE	2.2470	7.35	-1.079	582	14.4
0.5NaCMC-2.5PGPE	3.6481	7.25	-1.952	1053	26.1
0.5NaCMC-3.75PGPE	4.2369	7.23	-2.538	1369	33.9

It is evident from Tables 4.1 and 4.2 that the addition of NaCMC in PGPE solutions significantly increases the osmotic pressure, while the pH remains almost constant. However, the ternary solutions have higher dynamic viscosities compared to the binary draw solutions, which may cause high pressure drops in the system and increased concentration polarization. Therefore, the amount of NaCMC in the draw solution needs to be optimized to improve the water flux in the FO system.

4.2.2 Selection of favourable draw solutions

NaCMC solutions have an entanglement concentration (c_e), beyond which their specific viscosities exhibit a substantial increase [21 – 23]. The dynamic viscosities and osmolalities of the binary and ternary draw solutions from Tables 4.1 and 4.2 were used to select the best solutions for further investigation. The chosen draw solution for FO runs against 1000 ppm and 5000 ppm NaCl brackish feed solutions was the ternary 0.5NaCMC-3.75PGPE. The 0.5NaCMC-3.75PGPE draw solution generated comparable osmotic pressures to 1NaCMC-3.75PGPE, while requiring a lower NaCMC concentration, potentially lowering costs and environmental impact. For desalinating 35 000 ppm NaCl feed solution, the concentrated solutions 40PGPE and 0.5NaCMC-20PGPE were chosen due to their significantly higher osmotic pressures of 130.297 and 59.455 bars, respectively, as detailed in Table 4.3. This selection aimed to achieve sufficient driving force for water transport against the high salinity feed solution.

Table 4.3: Osmotic pressures of 0.5NaCMC-20PGPE and 40PGPE draw solutions.

Draw solution	Freezing point depression (ºC)	Average freezing point depression (ºC)	Osmolality (mOsm/kg)	Average Osmolality (mOsm/kg)		Osmotic pressure (bar)
40PGPE	-2.409[#]	-2.394[#]	1305[#]	1293[#]	5172	130.297
	-2.378[#]		1281[#]			
0.5NaCMC-20PGPE	-2.180[*]	-2.187[*]	1176[*]	1180[*]	2360	59.455
	-2.193[*]		1183[*]			

[#] Represents readings after 1:3 dilution of draw solution with water

[*] Represents readings after 1:1 dilution of draw solution with water

4.2.3 Dynamic viscosities of the favourable draw solutions

The dynamic viscosities of the pure 0.5NaCMC, 1NaCMC and 2NaCMC solutions are shown in Figure 4.1a. Their respective dynamic viscosities at 100 s^{-1} shear rate were 1.797, 4.6031 and 14.342 mPa.s. The dynamic viscosities of the 0.5NaCMC-3.75PGPE and 1NaCMC-3.75PGPE draw solutions at temperatures of 25, 30, 32, 35, 40, 45 and 50 ºC are shown in Figures 4.1b and 4.1c, respectively.
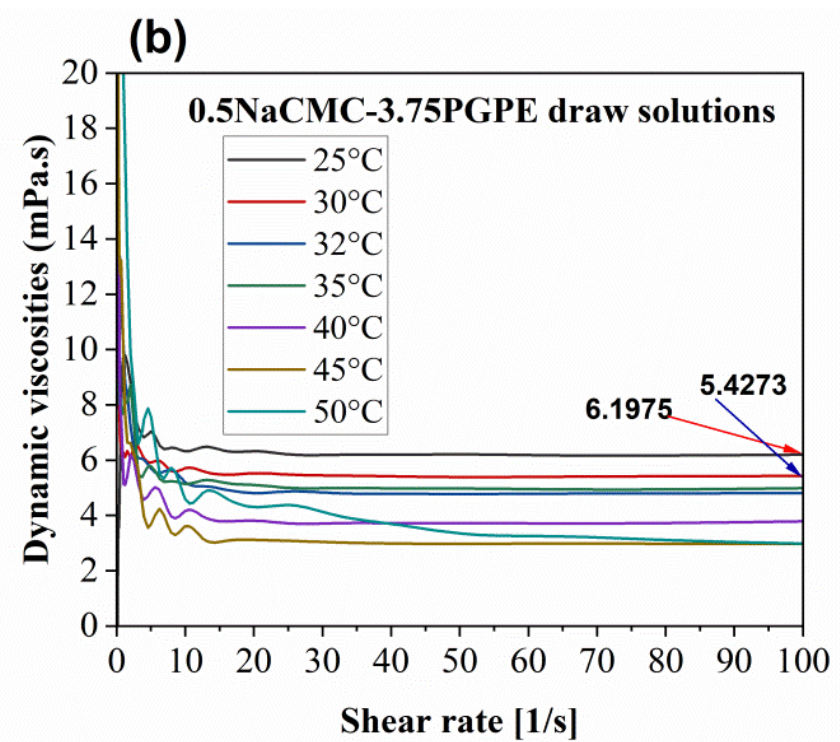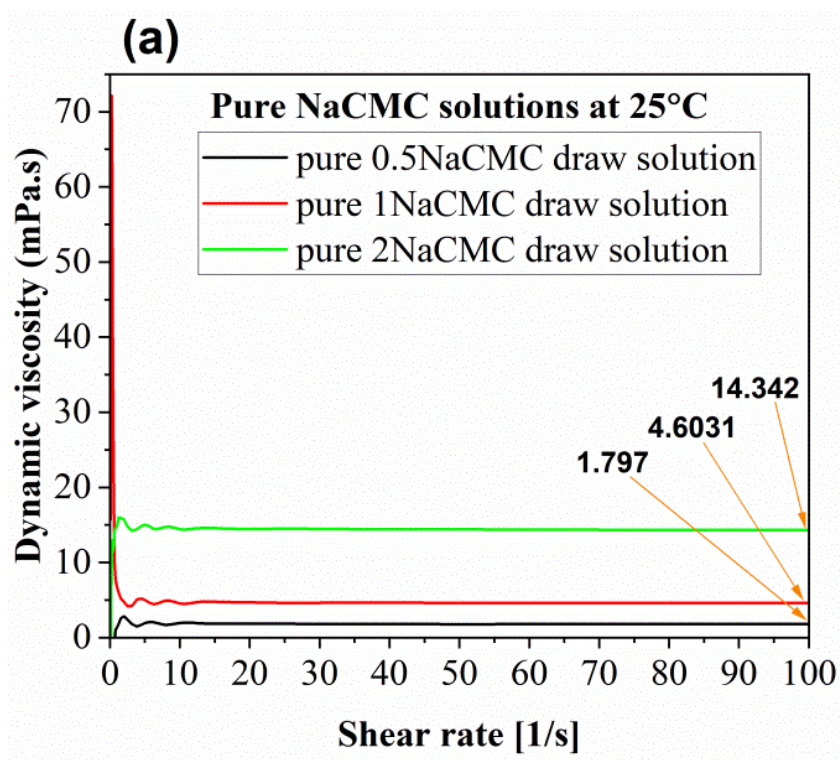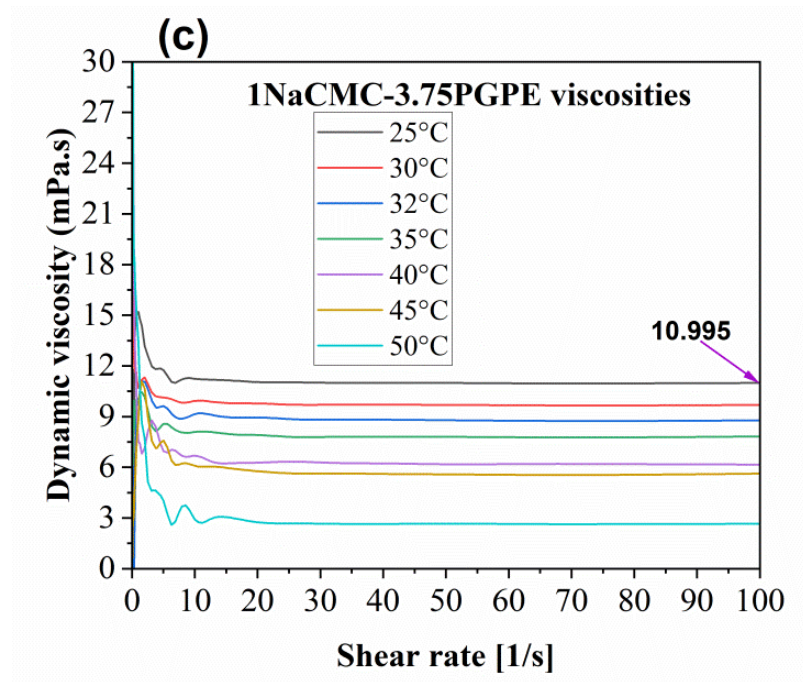
Figure 4.1: Dynamic viscosities of the organic draw solutions

The dynamic viscosities of the 40PGPE and 0.5NaCMC-20PGPE draw solutions as a function of shear rate are shown in Figure 4.2
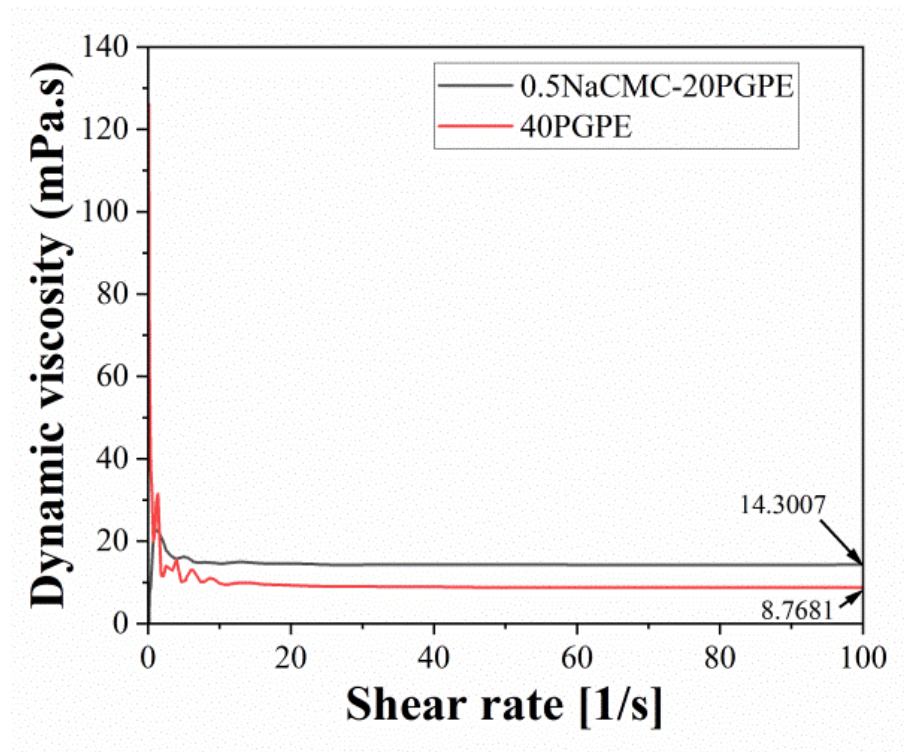
Figure 4.2: Dynamic viscosities of 40PGPE and 0.5NaCMC-20PGPE draw solutions

Figures 4.1 and 4.2 clearly show that adding NaCMC to PGPE solutions significantly increases the viscosity of the solutions. However, these solutions can still be used as draw solutions because they provide high osmotic pressures (as shown in Tables 4.1 and 4.2). The dynamic viscosities at a shear rate of 100 s^{-1} were 8.768 and 14.301 mPa.s for the respective solutions. It is clear from Figures 4.2 and 4.3 that all the draw solutions exhibit non-Newtonian behaviour up to very low shear rates (< 10 s^{-1}). Therefore, for draw solution applications, these solutions can be considered as Newtonian fluids only.

4.2.4   Phase-Separation Tests

Figure 4.3 shows phase separation induced by heating at 70 $^{\circ}$C for the 3.75PGPE, 0.5NaCMC-3.75PGPE, 40PGPE and 0.5NaCMC-20PGPE draw solutions.

(a)

(b)

(c)

(d)
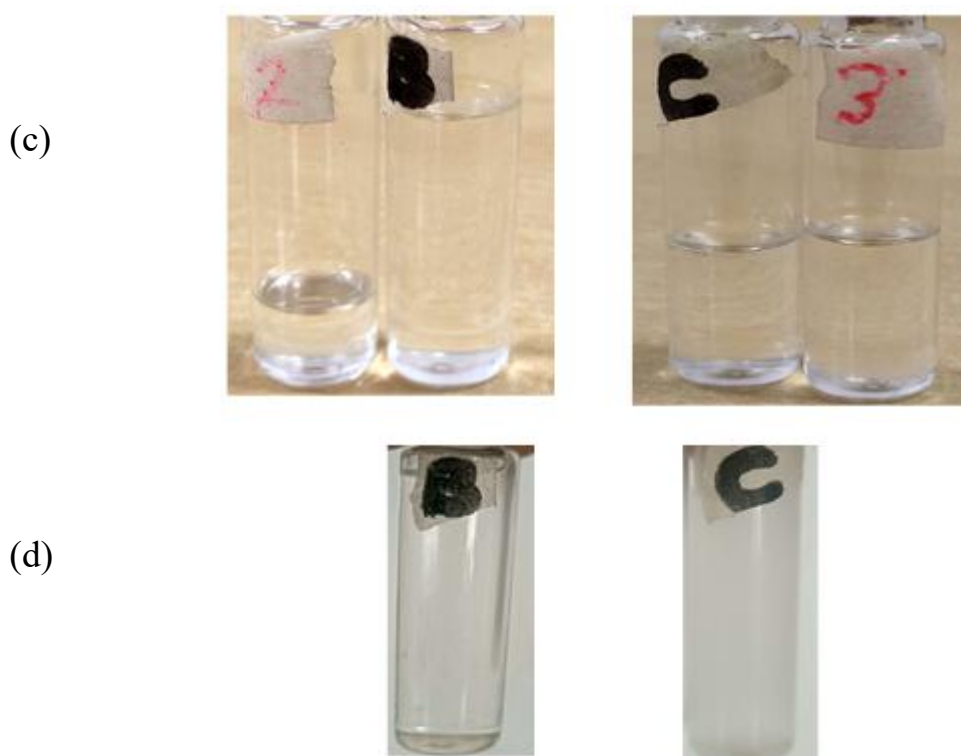
Figure 4.3: Phase separation induced by heating for 1 hour at 70 °C for the 0.5NaCMC-3.75PGPE (shown as A), 3.75PGPE (shown as B) and 0.5NaCMC-20PGPE (shown as C) draw solutions. (a) Homogeneous solutions at room temperature. (b) Phase-separated solutions after heating. (c) Distinct separated phases for 3.75PGPE (left) and 0.5NaCMC-20PGPE (right). (d) Regenerated homogeneous solutions at room temperature.

The binary 3.75PGPE solution was successfully regenerated. However, no visible phase separation occurred at 70 °C for the more concentrated 40PGPE solution, underscoring the critical influence of concentration on the phase separation behaviour. The dilution of the 40PGPE draw solution during FO processes may thus facilitate phase separation. These results confirm that the 3.75PGPE, 0.5NaCMC-3.75PGPE and 0.5NaCMC-20PGPE draw solutions can be regenerated by heating the solutions at a temperature of 70 °C. The same method was also proposed by Darvishmanesh et al. [18] for mixtures of two different glycol ethers, tripropylene glycol methyl ether and tripropylene glycol n-butyl ether.

4.2.5 Solute permeability and Reflection coefficient

The FO membrane hydraulic permeability constant, A, was determined to be 0.78274 L m^{-2} hr^{-1} bar^{-1}. The steady-state experimental data (Table 4.4) was fitted in the Spiegler-Kedem model to calculate the solute permeability and reflection coefficient.

Table 4.4: Experimental data at steady state used to estimate the solute permeability coefficient for the 0.5NaCMC-3.75PGPE draw solution

FO Run	$Q_{F_{in}}$ (LPH)	$Q_{D_{in}}$ (LPH)	$C_{F_{in}}$ (g/L)	Feed osmotic pressure (bar)	Draw osmotic pressure (bar)	$Q_{p_{exp}}$ (LPH×10^2)	$Q_{p_{the}}$ (LPH×10^2)
1	12	9	5	4.34	33.9	4.8779	4.6669
2	12	12	5	4.34	33.9	4.8779	4.6590
3	12	15	5	4.34	33.9	5.4876	4.6537
4	9	12	5	4.34	33.9	6.0975	4.6590

The estimated values of the solute permeability coefficient and reflection coefficient for the 0.5NaCMC-3.75PGPE draw solution were 1.24×10^{-8} m/s and 0.999, respectively. The reported solute permeability and reflection coefficients of NaCl for the same membrane are 1.14×10^{-7} m/s and 0.988 [20].

The results demonstrate that the permeability of the 0.5NaCMC-3.75PGPE solution was considerably lower than the reported value for NaCl, likely attributable to the larger molecular sizes of NaCMC and PGPE compared to NaCl.

4.2.6 FO performances of 0.5NaCMC-3.75PGPE desalinating 1000 ppm NaCl brackish feed solution

Figure 4.4a shows the FO performances when the 0.5NaCMC-3.75PGPE draw solution was used to desalinate 1000 ppm NaCl brackish feed solution. An FO run constitutes a complete 120-minute forward osmosis experiment. Runs 1, 2, 3 and 4 represent sequential independent experiments, with Run 1 denoting the initial 120-minute trial, followed consecutively by Runs 2, 3 and 4. The feed and draw flow rates were set at 0.15 LPM and 0.20 LPM, respectively, with the experiment conducted at 25 °C. The average experimental water fluxes for the four runs were

12.173, 11.899, 10.140 and 8.772 LMH. Their corresponding solute fluxes were 2.737, 2.654, 2.393 and 2.316 gMH, respectively, as shown in Figure 4.4b.
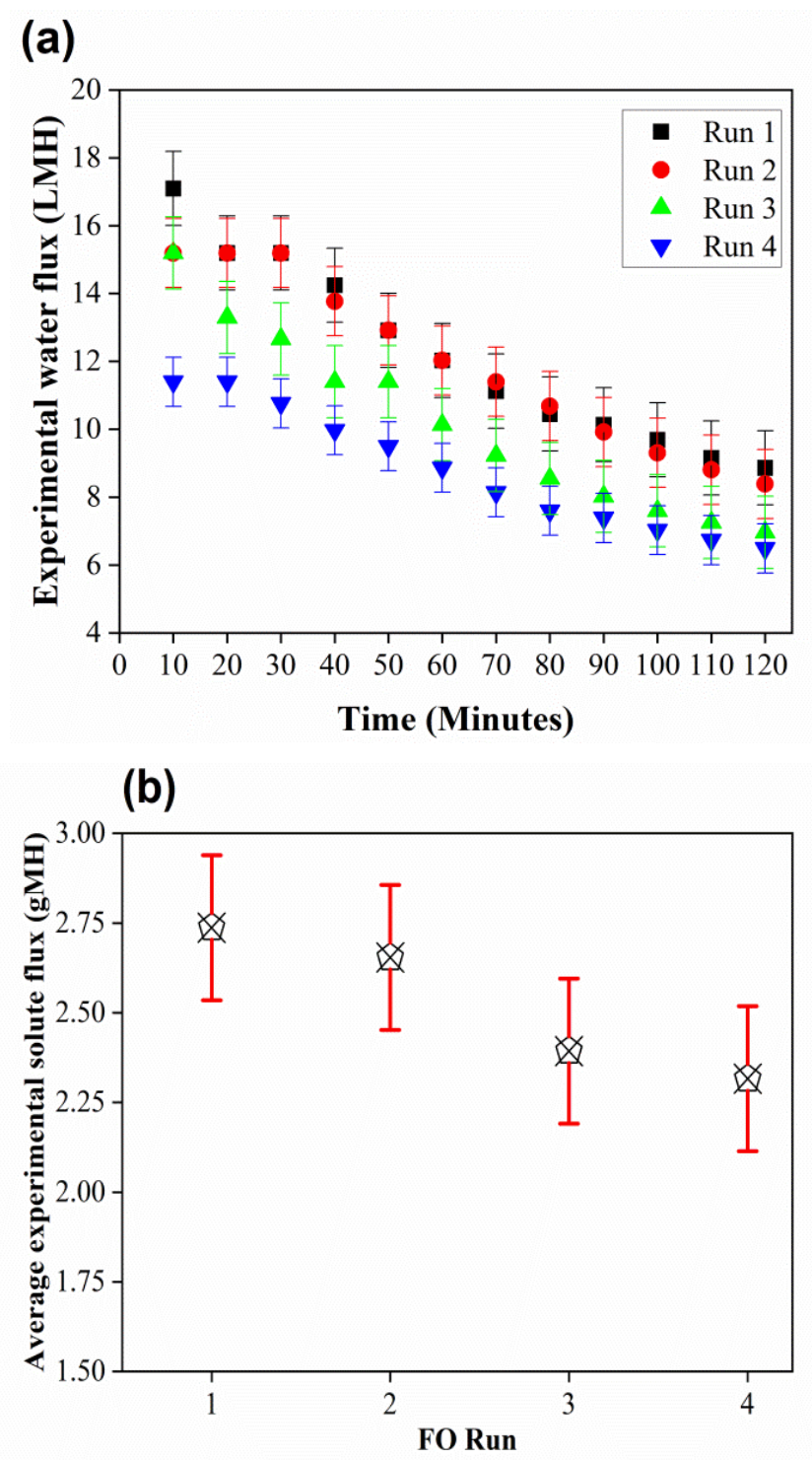
Figure 4.4: 0.5NaCMC-3.75PGPE desalinating 1000 ppm NaCl brackish feed solution. (a) Water flux; (b) Solute flux; (Error bars represent the standard deviation).

4.2.7 FO performances of 0.5NaCMC-3.75PGPE desalinating 5 000 ppm NaCl brackish feed solution

The experimental results of the 0.5NaCMC-3.75PGPE draw solution against 5 000 ppm NaCl brackish feed solutions are shown in Figure 4.5a for two FO runs. The feed flow rate was 0.15 LPM and the draw flow rate was 0.20 LPM at a temperature of 25 ºC for 2 hours. The average experimental water flux for runs 1 and 2 were 7.629 and 7.760 LMH respectively. The solute fluxes for the two runs were 2.255 and 2.479 gMH, as shown in Figure 4.5b.
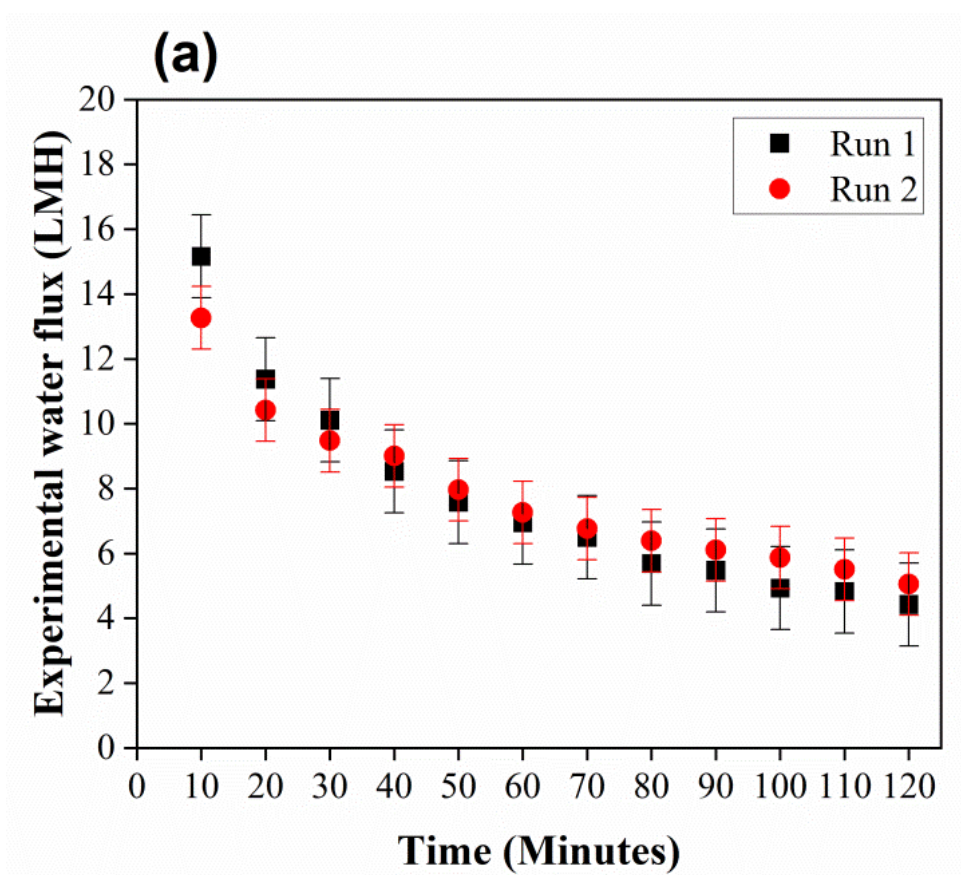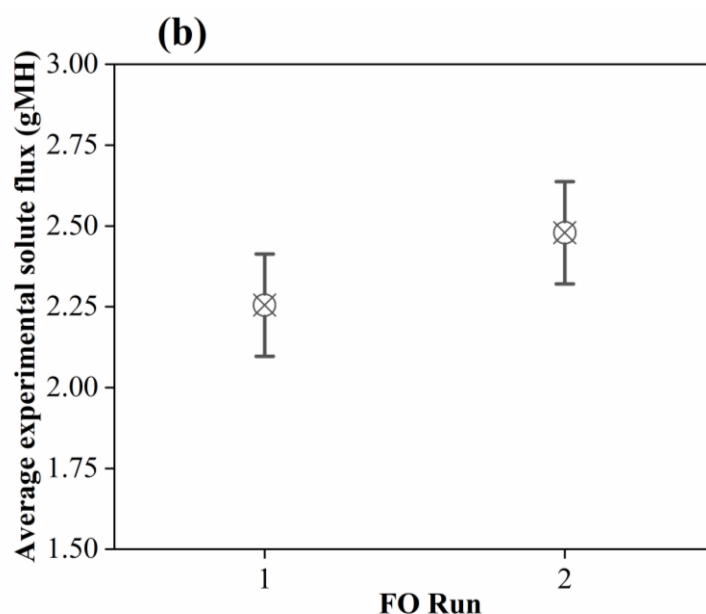
Figure 4.5: 0.5NaCMC-3.75PGPE desalinating 5 000 ppm NaCl brackish feed solutions. (a) Water flux; (b) Solute flux; (Errors bars represent the standard deviation).

4.2.8 FO performances of 0.5NaCMC-3.75PGPE desalinating 5 000 ppm NaCl solution at varying flow rates

Figure 4.6a shows the experimental results of the 0.5NaCMC-3.75PGPE draw solution desalinating 5 000 ppm NaCl brackish feed solutions for three FO runs using a feed flow rate of 0.20 LPM and a draw flow rate of 0.15 LPM.
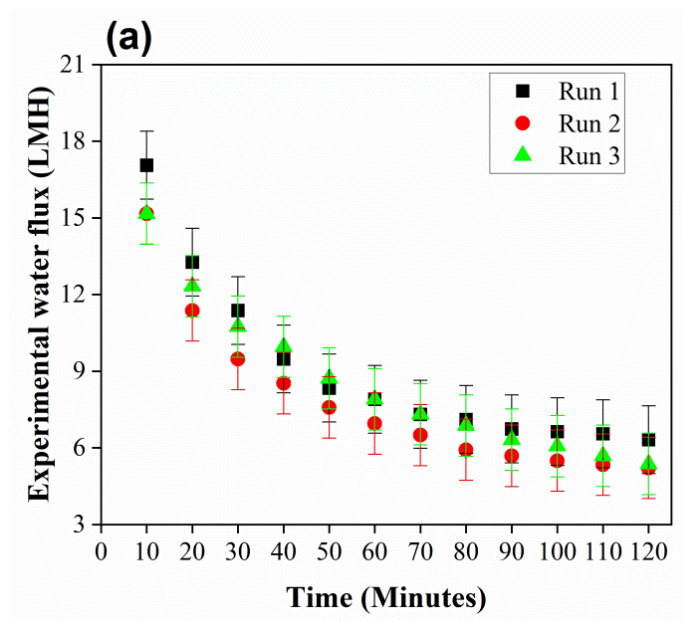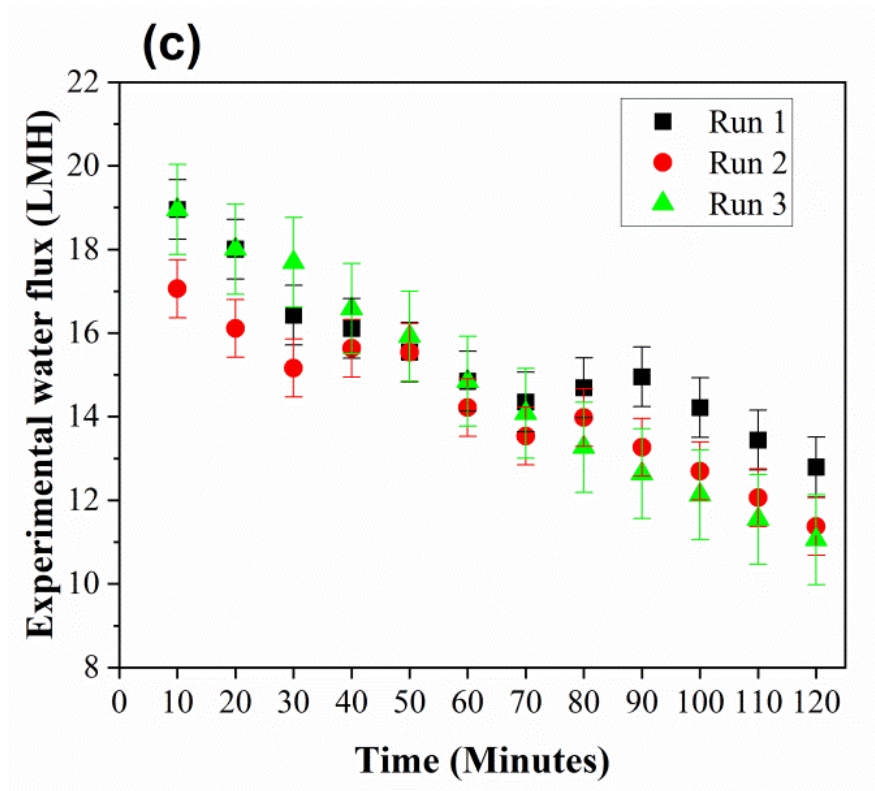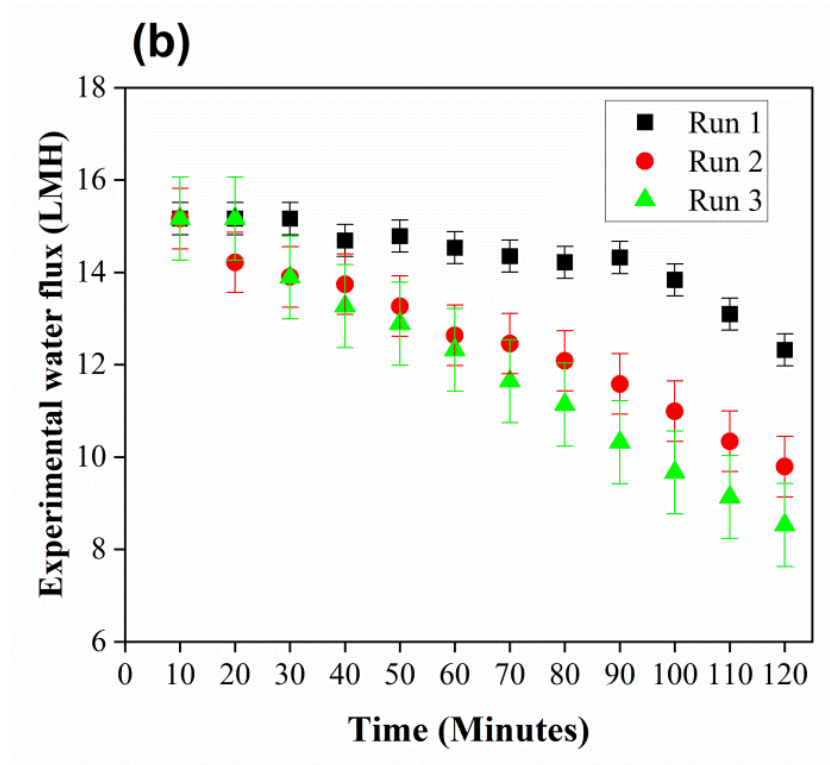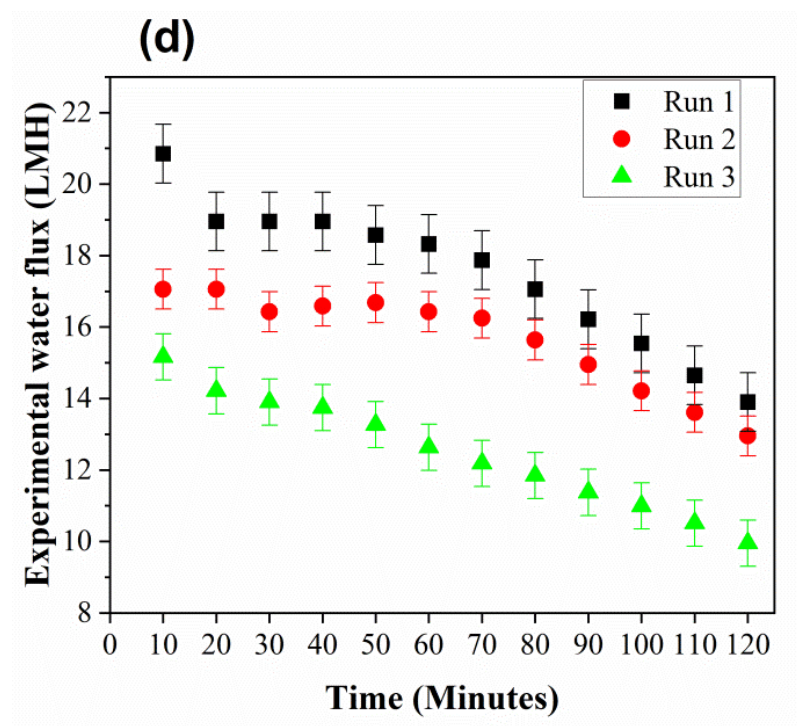
Figure 4.6: Experimental water fluxes of 0.5NaCMC-3.75PGPE against 5 000 ppm NaCl at 30 °C at (a) draw flow rate of 0.15 LPM. (b) draw flow rate of 0.20 LPM (c) draw flow rate of 0.25 LPM (d) draw flow rate of 0.20 LPM and feed flow rate of 0.15 LPM. Errors bars represent the standard deviation.

The temperature was kept at 30 °C for 2 hours. The average experimental water flux for runs 1, 2 and 3 were 9.006, 7.769 and 8.534 LMH respectively. The percentage difference in the water flux values decreased more than tenfold from the initial 10 minutes to the final 120-minute readings, showing that there was a considerable decline in the experimental water fluxes as the experiment progressed. The corresponding solute fluxes for the three runs were 2.025, 2.021 and 2.030 gMH.

The experimental results of the 0.5NaCMC-3.75PGPE draw solution against 5 000 ppm NaCl brackish feed solutions for three FO runs at a feed flow rate of 0.20 LPM and a draw flow rate of 0.20 LPM are shown in Figure 4.6b. The experiment was done at a temperature of 30 °C for 2 hours. The average experimental water fluxes for runs 1, 2 and 3 were 14.303, 12.514 and 11.927 LMH respectively. The corresponding experimental solute fluxes were 2.875, 3.054 and 2.996 gMH, respectively as shown in Figure 4.7.

The experimental results of the 0.5NaCMC-3.75PGPE draw solution against 5 000 ppm NaCl brackish feed solutions for three FO runs using a feed flow rate of 0.20 LPM and a draw flow rate of 0.25 LPM are shown in Figure 4.6c. The experiment was performed at a temperature of 30 °C for 2 hours. The average experimental water flux for runs 1, 2 and 3 were 15.361, 14.221 and 14.727 LMH respectively. There was minimal deviation in the percentage water flux differences in all three FO runs. However the trend in which the experimental water fluxes declined with time was still observed, although not as much as at a draw flow rate of 0.15 LPM (Figure 4.6a). The corresponding solute fluxes were 3.246, 3.380 and 3.393 gMH, respectively.

The experimental results for the 0.5NaCMC-3.75PGPE draw solution against 5 000 ppm NaCl brackish feed solutions for three FO runs for a feed flow rate of 0.15 LPM and a draw flow rate of 0.20 LPM are shown in Figure 4.6d. The temperature was maintained at 30 °C for 2 hours. The average experimental water flux for runs 1, 2 and 3 were 17.487, 15.654 and 12.482 LMH respectively. The first FO run had the least percentage differences in the water fluxes of all the experiments, although the same trend in which the experimental water fluxes declined with time was observed. The solute fluxes for the three runs were 3.057, 3.194 and 3.390 gMH. In all instances observed in Figures 4.6, the water fluxes declined over time suggesting potential membrane fouling or concentration polarization. Minimal water flux decline at the higher draw flow rate of 0.25 LPM compared to those at 0.15 LPM suggests reduced concentration polarization at higher draw flow rates.

The solute fluxes of the 0.5NaCMC-3.75PGPE ternary draw solution when desalinating 5000 ppm NaCl brackish feed solution at varying flow rates at 30 °C are shown in Figure 4.7.
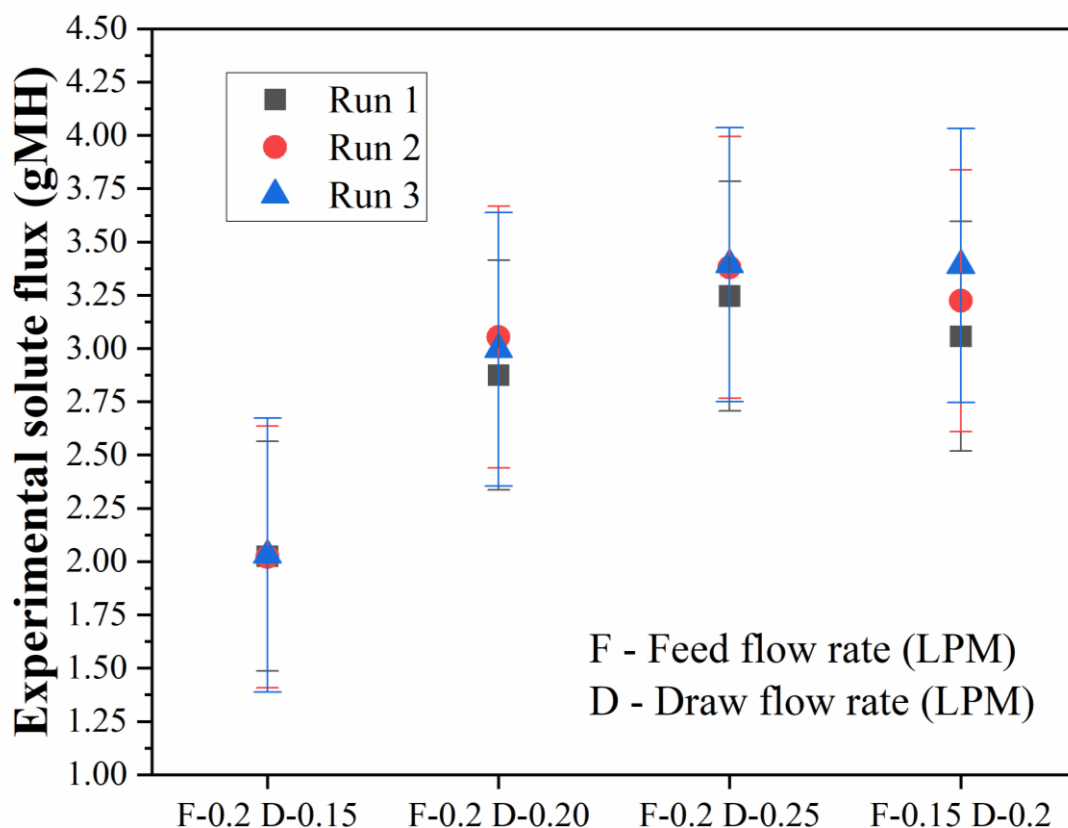
Figure 4.7: Solute fluxes of 0.5NaCMC-3.75PGPE at varying flow rates at 30 °C. Errors bars represent the standard deviation.

4.2.9 FO performances of 40PGPE desalinating 35 000 ppm NaCl feed solution

The experimental results of the 40PGPE draw solution in desalinating 35 000 ppm NaCl feed solution are shown in Figure 4.8 for two FO runs. The feed flow rate was 0.15 LPM and the draw flow rate was 0.20 LPM at a temperature of 30 °C for 2 hours.

The average experimental water fluxes for runs 1 and 2 were 22.436 and 19.738 LMH. There was great percentage difference in the water fluxes caused by the draw solution not remaining totally homogenous as the experiment progressed. Thus, for future work it is recommended that a continuous stirring system be used with this organic draw solution.
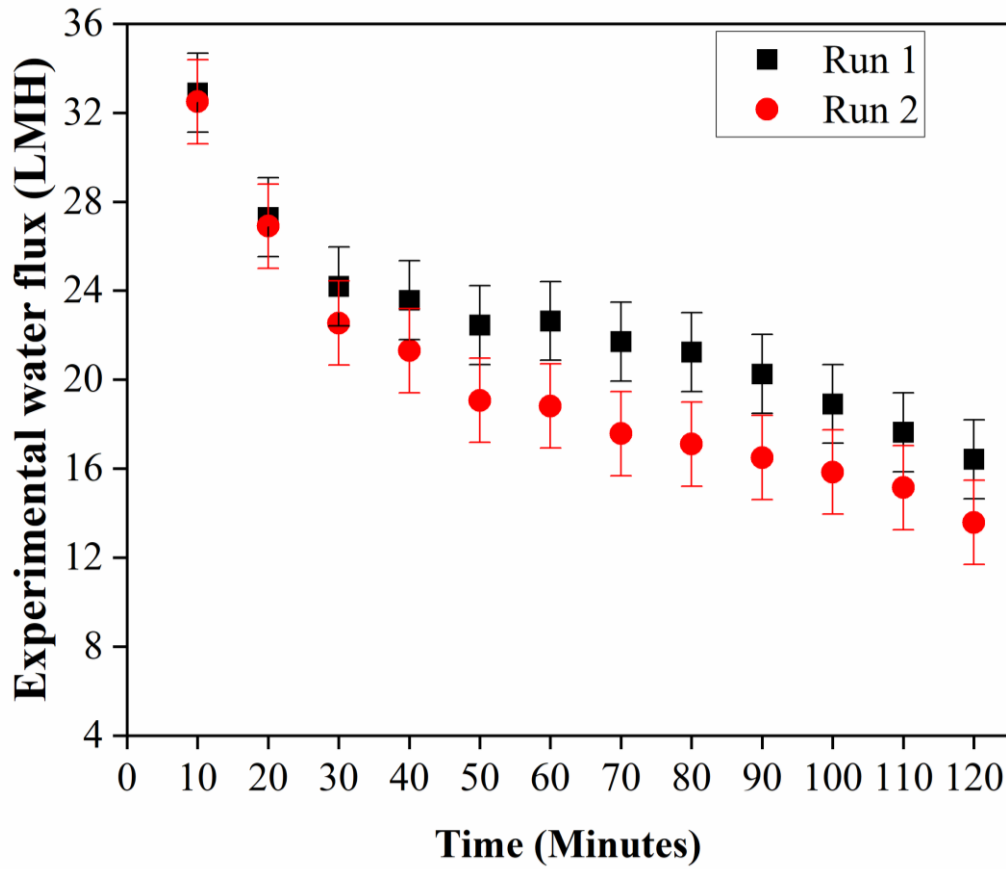
Figure 4.8: Binary 40PGPE draw solution against 35 000 ppm NaCl feed solution. Errors bars represent the standard deviation

4.2.10 FO performances of 0.5NaCMC-20PGPE desalinating 35 000 ppm NaCl feed solution

The experimental results of the 0.5NaCMC-20PGPE ternary draw solution against 35 000 ppm NaCl feed solution are shown in Figure 4.9 for two FO runs. The feed flow rate was 0.15 LPM and the draw flow rate was 0.20 LPM at a temperature of 30 °C for 2 hours. The average experimental water flux for runs 1 and 2 were 13.975 and 14.284 LMH respectively.
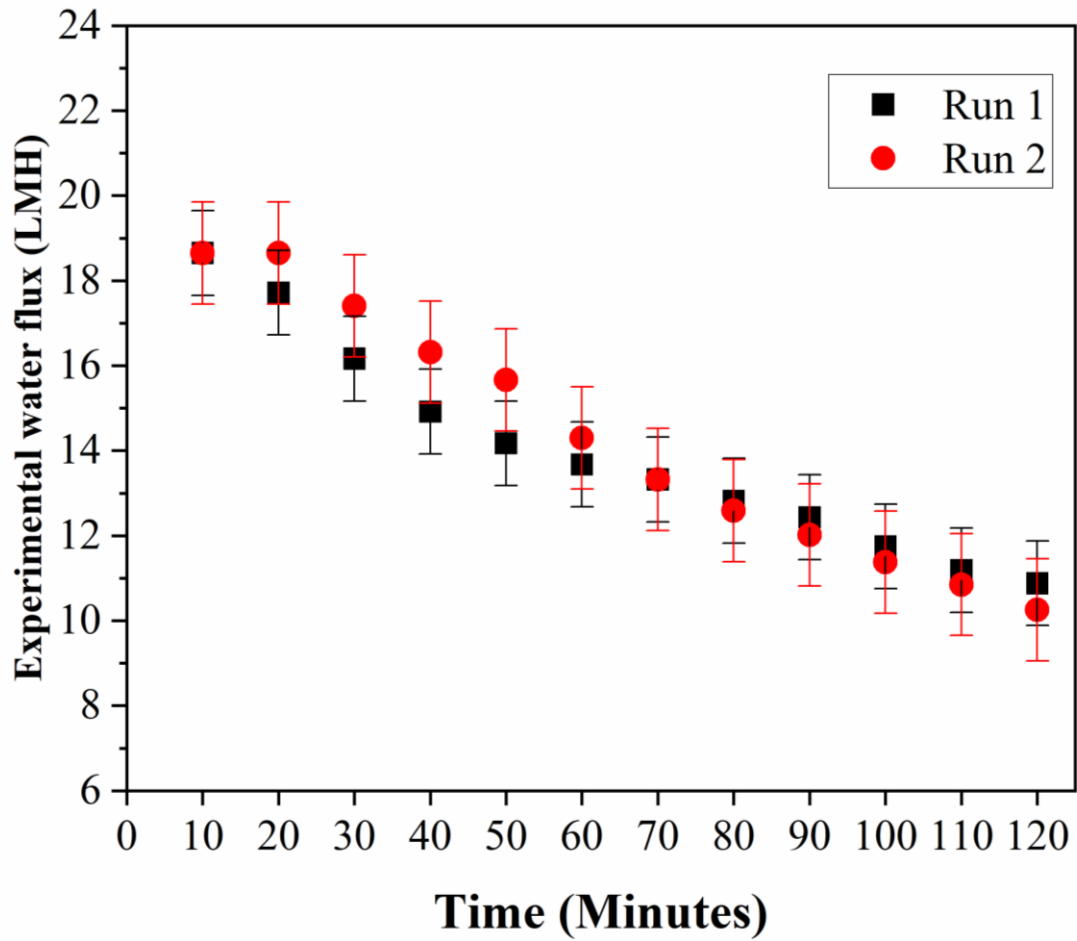
Figure 4.9: Ternary 0.5NaCMC-20PGPE draw solution against 35 000 ppm NaCl feed solution. Errors bars represent the standard deviation.

The solute fluxes of the binary 40PGPE draw solution surpassed those of the ternary 0.5NaCMC-20PGPE for both FO runs. The experimental solute fluxes for the 40PGPE draw solution were 8.958 and 7.469 gMH for both FO runs, whist those of the 0.5NaCMC-20PGPE draw solution were 4.763 and 4.511 gMH. This demonstrated that the binary 40PGPE draw solution, with a lower molecular weight, allowed more solutes to permeate back to the feed solution compared to the ternary solution. The findings corroborate the observations of Inada et al. [19], who reported that glycol ether draw solutes with molecular weights below 1250 Da exhibited FO membrane permeation and higher J_s/J_w ratios compared to those with molecular weights ranging from 1810 to 3911 Da. However, significantly higher water fluxes were observed with the binary 40PGPE draw solution compared to the ternary

0.5NaCMC-20PGPE draw solution. Both organic draw solutions necessitate the implementation of a continuous stirring system to guarantee solution homogeneity throughout the FO runs.

4.2.11 FO Membrane and Organic draw solutions compatibility study

Various parameters of the membranes, including total count, total area, perimeter, average size, mean gray value, modal gray value (corresponding to the highest peak in the histogram), circularity (which indicates the shape with a value between 0 and 1, where 1 represents a perfect circle), solidity, Feret diameter, integrated intensity, and kurtosis, were determined. These morphological parameters were then compared for all the FO membranes as shown in Table 4.5

Table 4.5: Comparison of morphological parameters of the FO membranes after immersion in draw solutions

Membrane	Original	0.5NaCMC	3.75PGPE	0.5NaCMC-3.75PGPE
Count	26376	35580	34056	31099
Total Area	179128.4	199219.2	120661.9	134926.3
Average Size	6.791	5.599	3.543	4.339
Mean	254.549	254.386	254.560	254.529
Mode	255	255	255	255
Perimeter	6.552	6.789	5.683	5.861
Circularity	0.911	0.891	0.898	0.904
Solidity	0.916	0.899	0.904	0.909
Feret	2.305	2.500	2.308	2.281
Integrated intensity	1543	1268	818	989
Kurtosis	11	10	9	8

As indicated in Table 4.5, minor morphological variations were observed, particularly for the membrane immersed in the binary 3.75PGPE solution, compared to the original membrane. These slight alterations are also evident in the SEM micrographs of the membranes presented in Figure 4.10

Magnification
of 10 000x
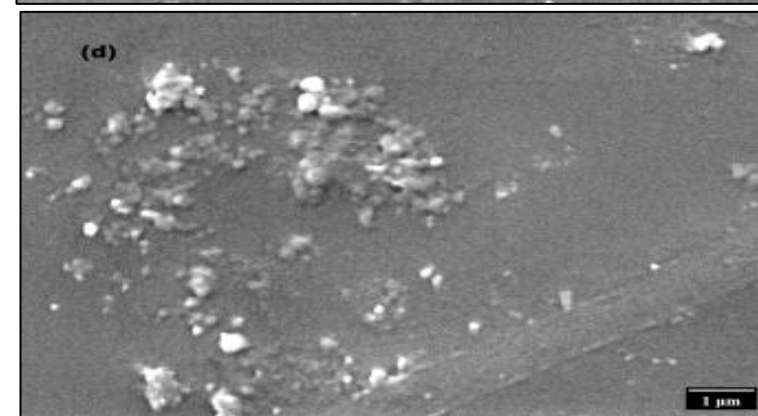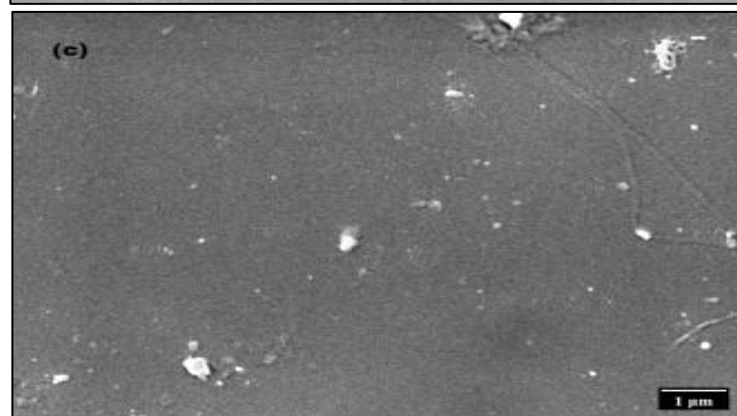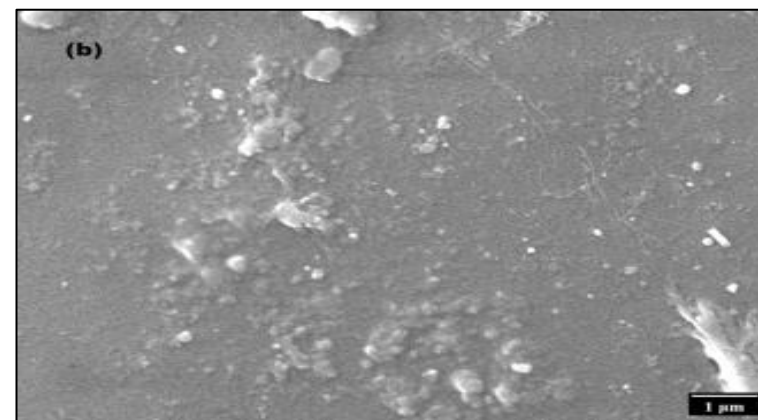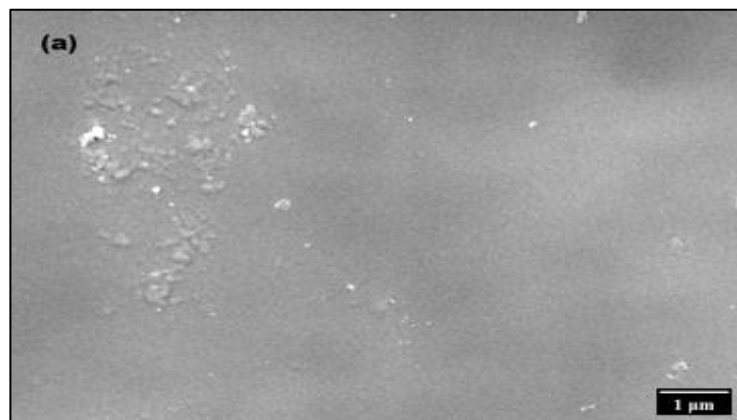
Magnification
of 1 000x
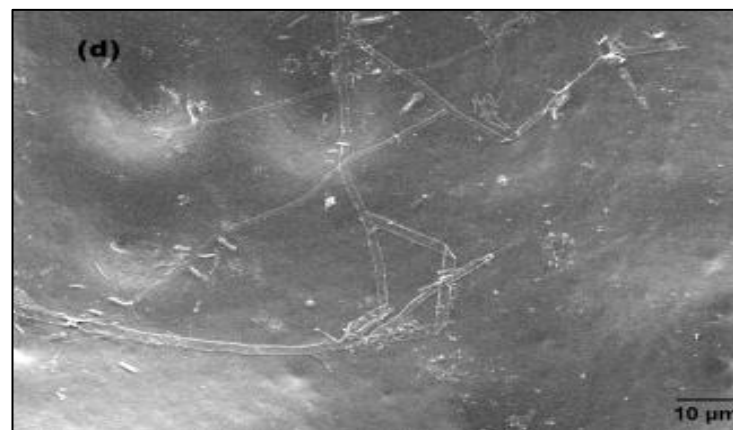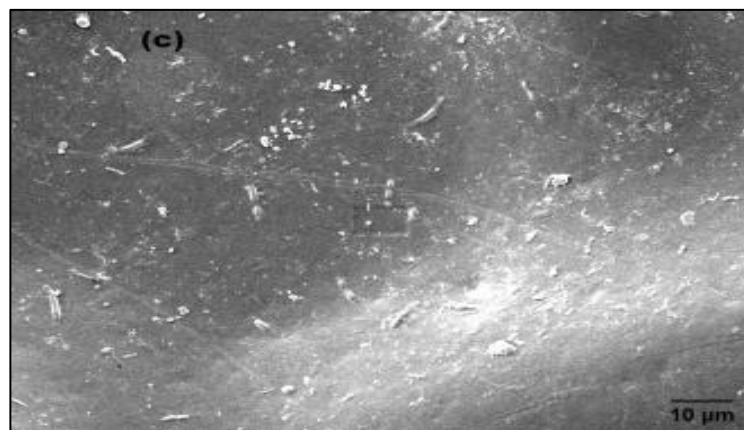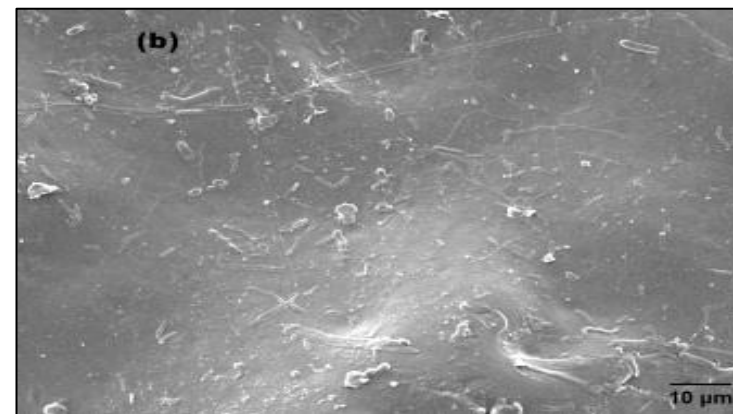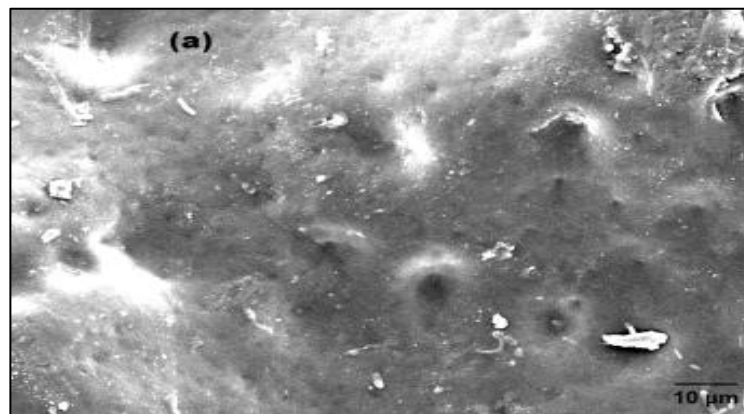
Magnification
of 250x
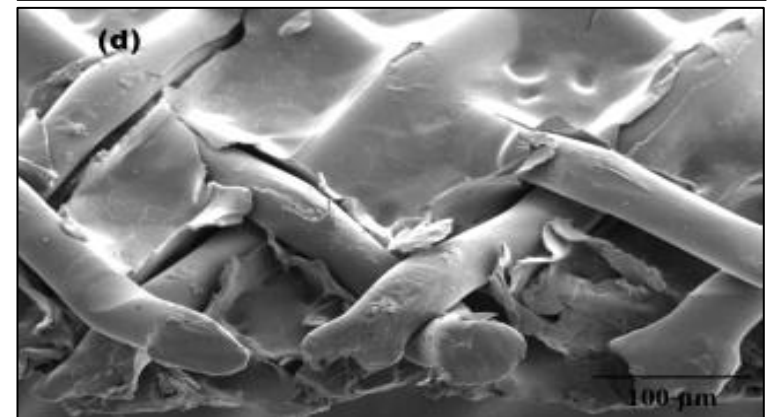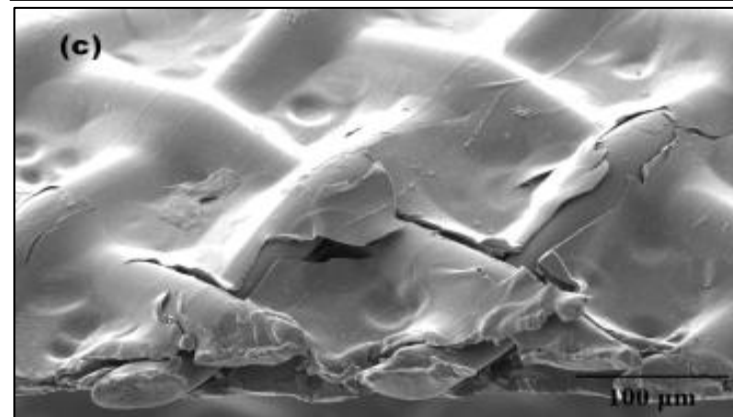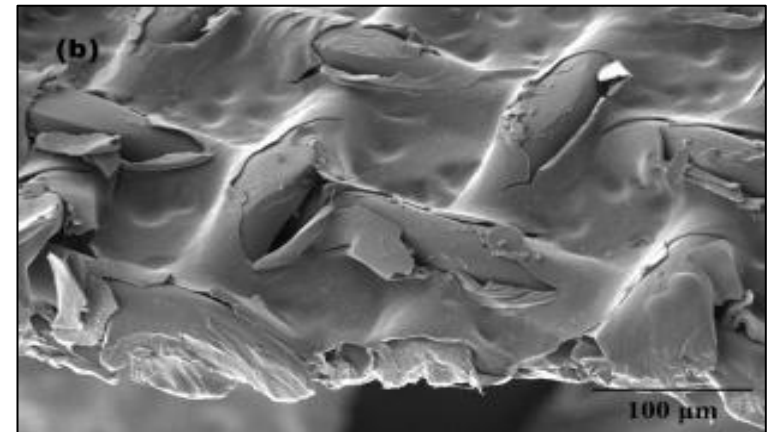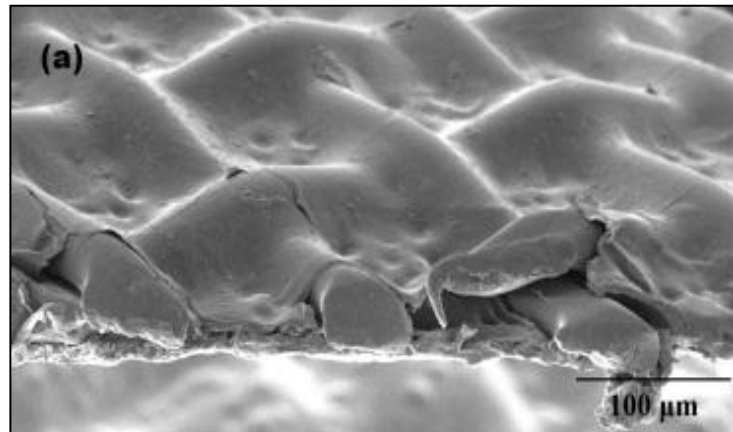
Roughness
8-bit
ImageJ

(a)

(b)

(c)

(d)
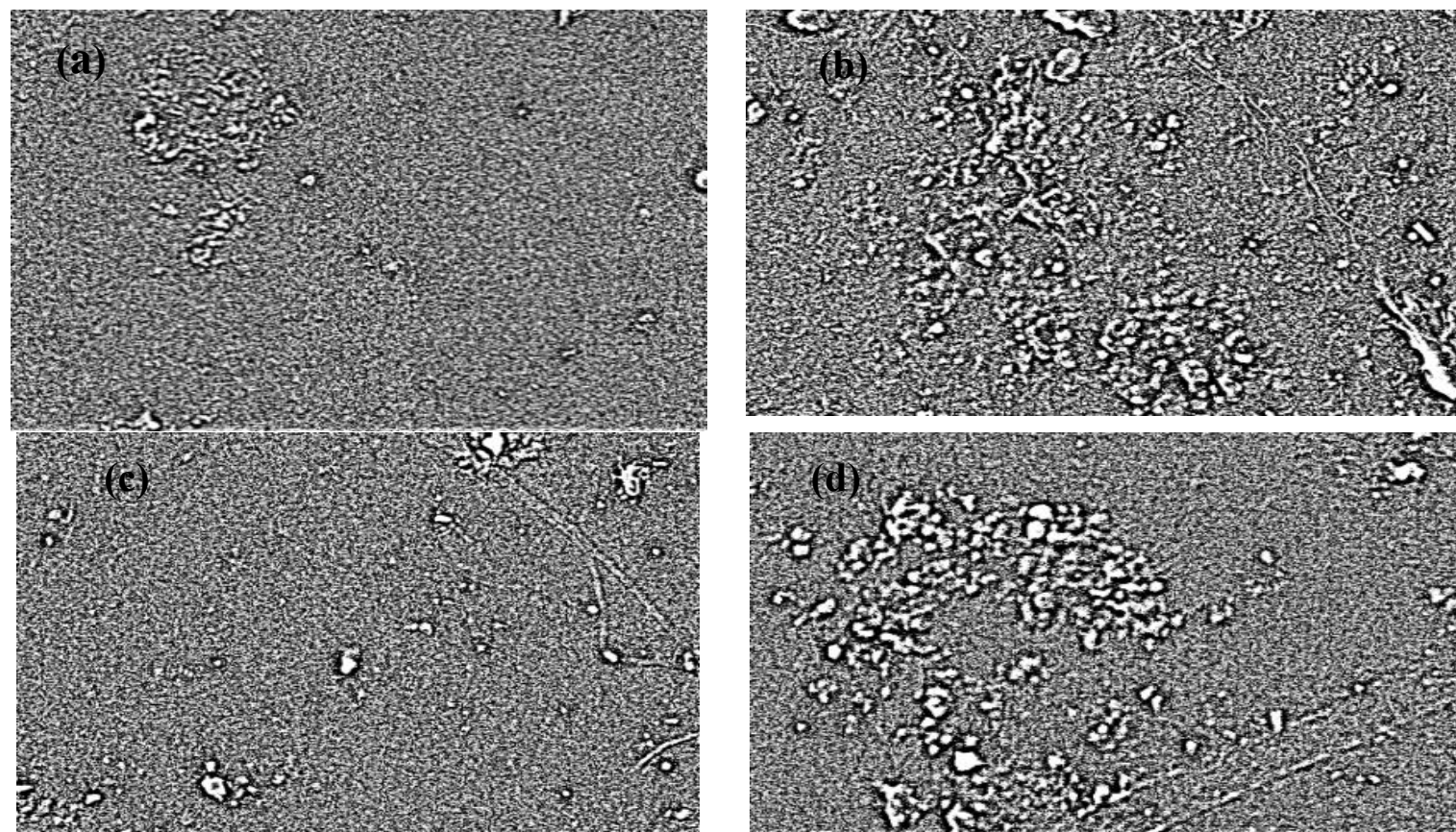
Figure 4.10: SEM micrographs of FO membrane before and after immersion in the organic draw solutions (a) Original FO membrane (b) FO membrane after immersion in 0.5NaCMC (c) FO membrane after immersion in 3.75PGPE (d) FO membrane after immersion in

0.5NaCMC-3.75PGPE

The roughness profile for each FO membrane was plotted as a function of gray value against distance.
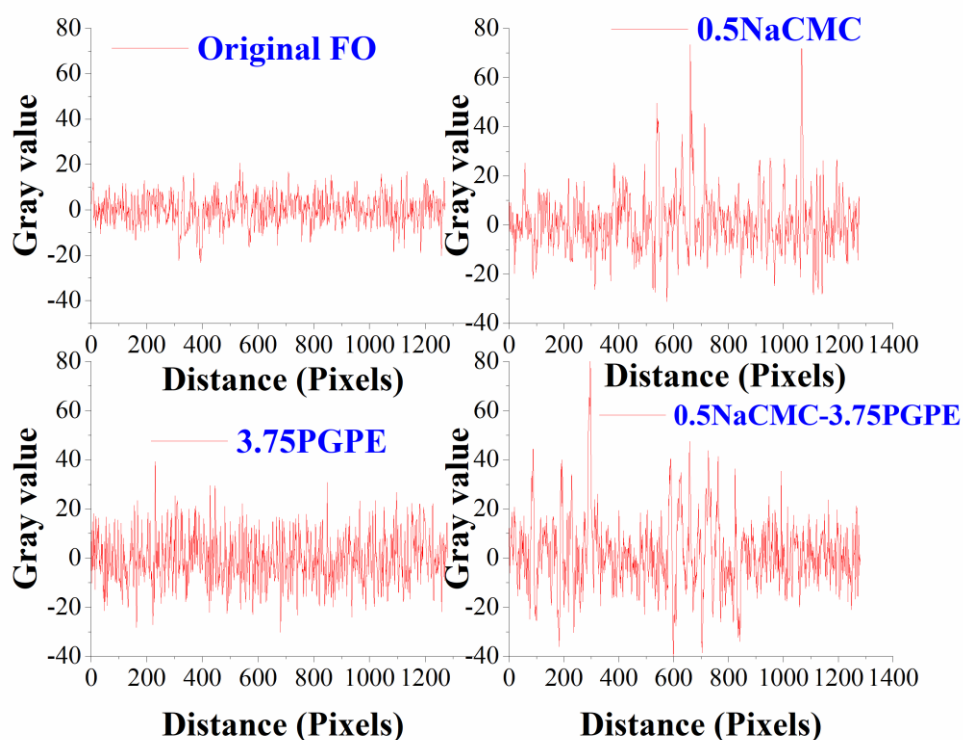
Figure 4.11: Gray value vs distance plots for roughness of FO membranes

The results from Table 4.5 on morphological parameters showed that the immersed membranes generally exhibited smaller average sizes compared to the original, suggesting potential alterations in pore structure or surface area. Grayscale intensity remained consistent across all membranes, indicating similar material compositions. Parameters like circularity and solidity showed slight variations but remained close to the original. The Feret diameter experienced minor alterations. Additionally, the immersed membranes exhibited lower integrated density values, implying changes in material distribution. Analysis of the gray value profiles in Figure 4.11 revealed distinct surface characteristics across the membrane treatments. The original FO membrane exhibited a relatively uniform pattern with minimal fluctuations, indicating a smooth surface texture. Upon immersion in 0.5NaCMC, the membrane surface demonstrated pronounced high-frequency oscillations with substantial

amplitude variations, suggesting significantly enhanced surface roughness compared to the original membrane. The FO membrane treated with 3.75PGPE displayed an intermediate texture profile, characterized by increased frequency variations relative to the original membrane, albeit with smaller magnitude changes than those observed in the 0.5NaCMC-treated membrane. When exposed to the ternary 0.5NaCMC-3.75PGPE solution, the membrane manifested a complex texture profile incorporating both high and low-frequency variations in gray values, indicative of a heterogeneous surface with multiscale roughness features. Despite these alterations, the membranes generally maintained compatibility with their respective draw solutions. Notably, the membrane's overall shape and integrity were preserved after immersion in the draw solution.

4.2.12 Comparative studies of the novel draw solutions with literature

Table 4.6 presents a comparative summary of the FO performance achieved by various inorganic, organic, and polyelectrolyte draw solutes reported in the literature. The table highlights their performances against the novel binary or ternary draw solutes investigated in this study; 40PGPE, 0.5NaCMC-3.75PGPE, and 0.5NaCMC-20PGPE. Analysis of Table 4.6 reveals that the draw solutes developed in this work exhibit competitive FO performance. Notably, the 40PGPE draw solution produced the second-highest comparative osmotic pressure, surpassed only by the 143 bars achieved by oligomeric carboxylate draw solutes. Additionally, all three draw solutions demonstrated significantly higher osmotic pressures and performance compared to traditional non-polyelectrolyte organic draw solutes like fructose, glucose, and sucrose, which exhibit significantly lower reported water fluxes of 7.50, 0.24, and 0.35 LMH, respectively. Furthermore, the performance of these draw solutes aligns well with those of existing polyelectrolyte-based draw solutes, such as Poly (isobutylene-alt-maleic acid) Sodium salt and Polyelectrolyte polyacrylic acid sodium salts. These established polyelectrolyte solutions exhibit similarly high osmotic pressures and low reverse solute fluxes, demonstrating the promising potential of the novel draw solutes developed in this study.

Table 4.6: Comparison study of the draw solutions with other draw solutes from literature

Feed	Draw solute	FO Membrane	Concentration	Osmotic pressure	FO Performance		Ref
					J_w (LMH)	J_s (gMH)	
Seawater	Modified potassium carbon quantum dots	CTA	0.5 g/L	121.0399 atm	5.371	0.391	[24]
DI	Modified potassium carbon quantum dots	CTA	0.5 g/L	121.0399 atm	13.924	-	[24]
DI	PIAM-Na	CTA	0.375 g/mL	-	34	0.196	[25]
Seawater	Multicomponent fertilizer	CTA	22 g/L	-	4.3	0.80	[26]
DI	2-Methylimidazole-based	CTA	0.5 M	-	10.75	0.90	[27]
DI	Polyelectrolyte polyacrylic acid sodium salts (PAA-NA), 1200 Da	CTA	0.72 g/mL	44 atm	21.6	1.7	[28]
Seawater	Polyelectrolyte polyacrylic acid sodium salts (PAA-NA), 1200Da	CTA	0.72 g/mL	44 atm	6.5	-	[28]
DI	Sodium formate	CTA	46 g/L	28 atm	9.36	6.04	[29]
DI	Sodium acetate	CTA	91 g/L	28 atm	9.00	2.73	[29]
DI	Sodium propionate	CTA	66 g/L	28 atm	8.68	1.47	[29]
DI	Magnesium acetate	CTA	166 g/L	28 atm	8.10	1.07	[29]
DI	Oligomeric carboxylates	TFC	0.5 mol/kg	143 bar	19	0.8	[30]
DI	NaCl	CTA	35.2 g/L	28 atm	9.6	7.2	[31]
DI	KCl	CTA	47.0 g/L	28 atm	10.9	12.3	[31]

DI	NH$_4$HCO$_3$	CTA	52.8 g/L	28 atm	7.3	18.2	[31]
DI	Fructose	CTA	360 g/L	55.02 atm	7.50	-	[32]
DI	Glucose	CTA	360 g/L	55.03 atm	0.24	-	[32]
DI	Sucrose	CTA	684 g/L	56.81 atm	0.35	-	[32]
DI	Ethanol	CTA	92 g/L	43.93 atm	-	-	[32]
1 000 ppm NaCl	0.5NaCMC-3.75PGPE	CTA	0.5wt.% NaCMC and 3.75M PGPE	33.9942 bars	12.17	2.737	This work
5 000 ppm NaCl	0.5NaCMC-3.75PGPE	CTA	0.5wt.% NaCMC and 3.75M PGPE	33.9942 bars	7.629	2.255	This work
35 000 ppm NaCl	40PGPE	CTA	40M PGPE	130.297 bars	22.44	8.958	This work
35 000 ppm NaCl	0.5NaCMC-20PGPE	CTA	0.5wt.% NaCMC and 20M PGPE	59.455 bars	13.98	4.763	This work

4.3 References

1. Skuse, C., Gallego-Schmid, A., Azapagic, A., & Gorgojo, P. (2020). Can emerging membrane-based desalination technologies replace reverse osmosis? Desalination, 500, 114844. https://doi.org/10.1016/j.desal.2020.114844

2. Rufuss, D. D. W., Hosseinipour, E., Arulvel, S., & Davies, P. (2022). Complete parametric investigation of a forward osmosis process using sodium chloride draw solution. Desalination, 547, 116218. https://doi.org/10.1016/j.desal.2022.116218

3. Al-Hemiri, A. A., Sharil, A. O., & Hussein, M. (2009). A study of forward osmosis using various drawing agent. Iraqi Journal of Chemical and Petroleum Engineering, 10(3), 51–56. https://doi.org/10.31699/ijcpe.2009.3.7

4. Yadav, S., Ibrar, I., Bakly, S., Khanafer, D., Altaee, A., Padmanaban, V. C., . . . Hawari, A. H. (2020). Organic fouling in forward osmosis: A comprehensive review. Water, 12(5), 1505. https://doi.org/10.3390/w12051505

5. Xu, Y., Zhu, Y., Chen, Z., Zhu, J., & Chen, G. (2022). A comprehensive review on forward osmosis water treatment: Recent advances and prospects of membranes and draw solutes. International Journal of Environmental Research and Public Health, 19(13), 8215. https://doi.org/10.3390/ijerph19138215

6. Li, L., Shi, W., & Yu, S. (2019). Research on forward osmosis membrane technology still needs improvement in water recovery and wastewater treatment. Water, 12(1), 107. https://doi.org/10.3390/w12010107

7. Yang, S., Lee, S., & Hong, S. (2021). Enhancing the applicability of forward osmosis membrane process utilizing food additives as draw solutes. Journal of Membrane Science, 638, 119705. https://doi.org/10.1016/j.memsci.2021.119705

8. Bagheri, B., Karimi-Jashni, A., & Zerafat, M. M. (2019). Application of molasses as draw solution in forward osmosis desalination for fertigation purposes. Environmental Technology, 42(5), 764–774. https://doi.org/10.1080/09593330.2019.1645215

9. Kim, J., Kim, J., Lim, J., & Hong, S. (2019). Evaluation of ethanol as draw solute for forward osmosis (FO) process of highly saline (waste)water. Desalination, 456, 23–31. https://doi.org/10.1016/j.desal.2019.01.012

10. Zhao, P., Gao, B., Xu, S., Kong, J., Ma, D., Shon, H. K., . . . Liu, P. (2014). Polyelectrolyte-promoted forward osmosis process for dye wastewater treatment – Exploring the feasibility of using polyacrylamide as draw solute. Chemical Engineering Journal, 264, 32–38. https://doi.org/10.1016/j.cej.2014.11.064

11. Roach, J. D., Al-Abdulmalek, A., Al-Naama, A., & Haji, M. (2014). Use of micellar solutions as draw agents in forward osmosis. Journal of Surfactants and Detergents, 17(6), 1241–1248. https://doi.org/10.1007/s11743-014-1638-6

12. Monjezi, A. A., Mahood, H. B., & Campbell, A. (2017). Regeneration of dimethyl ether as a draw solute in forward osmosis by utilising thermal energy from a solar pond. Desalination, 415, 104–114. https://doi.org/10.1016/j.desal.2017.03.034

13. Hsu, C., Ma, C., Bui, N., Song, Z., Wilson, A. D., Kostecki, R., . . . Urban, J. J. (2019). Enhanced forward osmosis desalination with a hybrid ionic

liquid/hydrogel thermoresponsive draw agent system. ACS Omega, 4(2), 4296–4303. https://doi.org/10.1021/acsomega.8b02827

14. Hamdan, M., Sharif, A. O., Derwish, G., Al-Aibi, S., & Altaee, A. (2015). Draw solutions for forward osmosis process: Osmotic pressure of binary and ternary aqueous solutions of magnesium chloride, sodium chloride, sucrose and maltose. Journal of Food Engineering, 155, 10–15. https://doi.org/10.1016/j.jfoodeng.2015.01.010

15. Farman, A. A., Irfan, M., Amin, N. U., Jahan, Z., Song, X., Jiang, H., & Gul, S. (2022). Evaluation of sodium acetate and glucose as minor additives with calcium chloride as optimum mixed draw solutes for fruit juice concentration via forward osmosis. Korean Journal of Chemical Engineering, 39(11), 3102–3108. https://doi.org/10.1007/s11814-022-1228-7

16. Nguyen, N. C., Chen, S., Jain, S., Nguyen, H. T., Ray, S. S., Ngo, H. H., . . . Duong, H. C. (2017). Exploration of an innovative draw solution for a forward osmosis-membrane distillation desalination process. Environmental Science and Pollution Research, 25(6), 5203–5211. https://doi.org/10.1007/s11356-017-9192-1

17. Shibata, T. (2011). Cellulose and its derivatives in medical use. In The Royal Society of Chemistry eBooks (pp. 48–87). https://doi.org/10.1039/9781849733519-00048

18. Darvishmanesh, S., Pethica, B. A., & Sundaresan, S. (2017). Forward osmosis using draw solutions manifesting liquid-liquid phase separation. Desalination, 421, 23–31. https://doi.org/10.1016/j.desal.2017.05.036

19. Inada, A., Kumagai, K., & Matsuyama, H. (2020). Effect of the molecular weights of thermoresponsive polyalkylene glycol draw solutes on forward osmosis performance. Separation and Purification Technology, 252, 117462. https://doi.org/10.1016/j.seppur.2020.117462

20. Attarde, D., Jain, M., & Gupta, S. K. (2016). Modeling of a forward osmosis and a pressure-retarded osmosis spiral wound module using the Spiegler-Kedem model and experimental validation. Separation and Purification Technology, 164, 182–197. https://doi.org/10.1016/j.seppur.2016.03.039

21. Lopez, C. G., Colby, R. H., Graham, P., & Cabral, J. T. (2016). Viscosity and scaling of semiflexible polyelectrolyte NaCMC in aqueous salt solutions. Macromolecules, 50(1), 332–338. https://doi.org/10.1021/acs.macromol.6b02261

22. Jimenez, L. N., Narváez, C. D. V. M., & Sharma, V. (2020). Capillary breakup and extensional rheology response of food thickener cellulose gum (NaCMC) in salt-free and excess salt solutions. Physics of Fluids, 32(1), 012113. https://doi.org/10.1063/1.5128254

23. Lopez, C. G., & Richtering, W. (2018). Influence of divalent counterions on the solution rheology and supramolecular aggregation of carboxymethyl cellulose. Cellulose, 26(3), 1517–1534. https://doi.org/10.1007/s10570-018-2158-8

24. Kamel, A. H., Alsalhy, Q. F., Ibrahim, S. S., Faneer, K. A., Hashemifard, S. A., Jangizehi, A., . . . Bantz, C. (2023). Novel sodium and potassium carbon quantum dots as forward osmosis draw solutes: Synthesis, characterization and

performance testing. Desalination, 567, 116956.
https://doi.org/10.1016/j.desal.2023.116956

25. Kumar, R., Al-Haddad, S., Al-Rughaib, M., & Salman, M. (2016). Evaluation of hydrolyzed poly(isobutylene-alt-maleic anhydride) as a polyelectrolyte draw solution for forward osmosis desalination. Desalination, 394, 148–154. https://doi.org/10.1016/j.desal.2016.05.012

26. Gulied, M., Momani, F. A., Khraisheh, M., Bhosale, R., & AlNouss, A. (2019). Influence of draw solution type and properties on the performance of forward osmosis process: Energy consumption and sustainable water reuse. Chemosphere, 233, 234–244.
https://doi.org/10.1016/j.chemosphere.2019.05.241

27. Yen, S. K., N, F. M. H., Su, M., Wang, K. Y., & Chung, T. (2010). Study of draw solutes using 2-methylimidazole-based compounds in forward osmosis. Journal of Membrane Science, 364(1–2), 242–252.
https://doi.org/10.1016/j.memsci.2010.08.021

28. Ge, Q., Su, J., Amy, G. L., & Chung, T. (2011). Exploration of polyelectrolytes as draw solutes in forward osmosis processes. Water Research, 46(4), 1318–1326. https://doi.org/10.1016/j.watres.2011.12.043

29. Bowden, K. S., Achilli, A., & Childress, A. E. (2012). Organic ionic salt draw solutions for osmotic membrane bioreactors. Bioresource Technology, 122, 207–216. https://doi.org/10.1016/j.biortech.2012.06.026

30. Long, Q., Huang, J., Xiong, S., Shen, L., & Wang, Y. (2018). Exploration of oligomeric sodium carboxylates as novel draw solutes for forward osmosis. Process Safety and Environmental Protection, 138, 77–86.
https://doi.org/10.1016/j.cherd.2018.08.020

31. Achilli, A., Cath, T. Y., & Childress, A. E. (2010). Selection of inorganic-based draw solutions for forward osmosis applications. Journal of Membrane Science, 364(1–2), 233–241. https://doi.org/10.1016/j.memsci.2010.08.010

32. Akther, N., Sodiq, A., Giwa, A., Daer, S., Arafat, H., & Hasan, S. (2015). Recent advancements in forward osmosis desalination: A review. Chemical Engineering Journal, 281, 502–522. https://doi.org/10.1016/j.cej.2015.05.080

CHAPTER 5

ENHANCED FORWARD OSMOSIS DESALINATION OF BRACKISH WATER USING PHASE SEPARATING TERNARY ORGANIC DRAW SOLUTIONS OF HYDROXYPROPYL CELLULOSE AND PROPYLENE GLYCOL PROPYL ETHER

5.1 Introduction

In areas with freshwater scarcity, the desalination of brackish water plays a critical role in providing a sustainable freshwater supply [1]. Forward osmosis (FO) is a promising membrane separation system based on the osmotic pressure gradient, thus requiring lesser energy requirements than reverse osmosis (RO) [2]. Cath et al. [3] have reported the advantages of FO over pressure-driven membrane processes. As FO uses minimal hydraulic pressures, the equipment is relatively cheaper, simpler and gives less membrane fouling compared to RO. Much attention has been paid to inorganic draw solutions, especially sodium chloride, while low molecular weight glycol ethers have produced promising results as organic draw solutions [4]. However, some organic compounds have good potential as draw solutes because they dissolve easily in water, resulting in high osmotic pressures [5]. Chu et al. [6] have shown that citric acid produces better water fluxes of 4.5 LMH despite having lesser osmotic pressures of 22.29 bar compared to 22.63 and 53.24 bar of 1M potassium sorbate and sodium benzoate, respectively. A good organic draw solution should possess high osmotic pressure and low dynamic viscosity. Hsu et al. [7] have successfully utilized a 70 wt.% ternary ionic liquid (IL) and hydrogel draw solution for the effective desalination of 0.15 to 0.3 M saline feed solutions. In their study, Hamdan et al. [8] have reported on the osmotic pressures of binary and ternary draw solutions containing magnesium chloride, sodium chloride, sucrose, and maltose. Their findings have shown that the ternary solutions had higher osmotic pressures compared to the binary solutions. Farman et al. [9] have incorporated organic compounds, sodium acetate and glucose, in a calcium chloride draw solution. Introducing 5% sodium acetate to calcium chloride has delivered better water fluxes of 23.9 LMH and solute fluxes of 6.64 gMH. Nguyen et al. [10] have lowered the reverse solute flux while keeping the water fluxes relatively high by adding 0.05 M

aluminium sulphate to 0.5 M magnesium chloride draw solution. Given the impressive osmotic pressures demonstrated by multi-component solutions, as highlighted by Hamdan et al. [8], and the reduced reverse solute fluxes, as evidenced by Nguyen et al. [10], it is worth noting that the primary drawback lies in the regeneration process of the draw solution.

In the continuous pursuit of innovative draw solutions, Ahangar and Taghavijeloudar [11] have conducted an investigation into rhamnolipid biosurfactants, which have been found to generate osmotic pressures up to 29 bar. Volpin et al. [12] have conducted a study on the potential use of human urine in the dewatering of microalgae through FO. The hydrolyzed urine has been able to generate osmotic pressures exceeding 20 bars. During the course of a 20-hour FO operation, there has been no significant fouling observed in the support layer.

Thermally responsive IL's have shown promising potential as effective draw solutes for FO processes. Zeweldi et al. [13] have employed a stable, low-toxicity tetrabutylammonium 2,4,6-trimethyl benzenesulfonate IL draw solute, which has generated an osmotic pressure of 58.92 bar. The IL solution has exhibited 98% recovery upon heating above its LCST of 57 $^\circ$C, with the remaining residuals recovered by RO. Zhong et al. [14] have utilized 3.2 M protonated betaine bis (trifluoromethyl sulfonyl) imide draw solution with LCST maintained above 56 $^\circ$C. In a similar study, Yang et al. [15] have investigated various thermoresponsive phosphonium and ammonium-based ILs draw solutes with different cation-anion pairs for FO processes. Moon and Kang [16] have developed tetrabutylphosphonium-based ILs exhibiting LCST for use in FO processes. The thermoresponsive ILs, [P4444][MBS] and [P4444][EBS], have exhibited LCSTs of 36 $^\circ$C and 25 $^\circ$C respectively in 20 wt.% aqueous solutions, facilitating draw solute recovery through liquid-liquid phase separation.

As reported above, thermally responsive solutions exhibit significant potential as draw solutions due to their high osmotic pressure and facile regeneration using low-grade heat [12 – 15], which can be readily obtained from renewable energy sources or waste heat from thermal and nuclear power plants. This chapter investigates novel

ternary draw solutions with promising properties for FO applications. Mitigating the drawbacks of single glycol ether draw solutes, the developed ternary HPC-PGPE solutions demonstrate potential for enhanced performance and regeneration capabilities. The systematic approach, encompassing the determination of osmotic pressures, viscosities, and experimental evaluation of water and solute fluxes, provides a comprehensive understanding of these novel draw solutions. Moreover, the investigation of regeneration potential through phase separation further augments the practical applicability of these ternary solutions.

5.2 Results and discussion

5.2.1   Osmotic pressure analysis

The osmolalities of the organic draw solutions, as determined using Freezing point osmometry, are shown in Table 5.1

Table 5.1: Osmotic pressures of organic draw solutions

Draw solution	Freezing point depression (°C)	Osmolality (mOsm/kg)	Osmotic pressure (bar)
0.5HPC	-0.003	1	0.02
1HPC	-0.013	7	0.17
1.5HPC	-0.015	8	0.19
2HPC	-0.030	16	0.40
0.25HPC-1.25PGPE	-1.105	596	14.8
0.5HPC-1.25PGPE	-1.153	622	15.4
0.75HPC-1.25PGPE	-1.218	657	16.3
1HPC-1.25PGPE	-1.255	677	16.8
0.25HPC-2.5PGPE	-1.843	994	24.6
0.5HPC-2.5PGPE	-1.869	1008	25.0
0.75HPC-2.5PGPE	-2.093	1129	28.0
1HPC-2.5PGPE	-2.229	1202	29.8
0.25HPC-3.75PGPE	-2.343	1264	31.3
0.5HPC-3.75PGPE	-2.581	1392	34.5
0.75HPC-3.75PGPE	-2.629	1418	35.1
1HPC-3.75PGPE	-2.753	1485	36.8

Pure HPC draw solutions exhibited low osmolalities, ranging from 1 to 16 mOsm/kg. This rendered them unsuitable for any FO desalination processes.

However, incorporating PGPE significantly increased osmolalities to levels appropriate for FO applications, as shown in Figure 5.1. Seven combinations of HPC and PGPE produced osmolalities greater than 1000 mOsm/kg. These draw solutions were 0.25HPC-2.5PGPE, 0.75HPC-2.5PGPE, 1HPC-2.5PGPE, 0.25HPC-3.75PGPE, 0.5HPC-3.75PGPE, 0.75HPC-3.75PGPE and 1HPC-3.75PGPE with osmolalities of 1008, 1129, 1202, 1264, 1392, 1418 and 1485 mOsm/kg respectively. From these seven draw solutions, three were selected for FO experiments against 1 g/L NaCl brackish feed solution. The draw solutions that produced the highest osmotic pressures were preferred. These chosen draw solutions were 0.25HPC-3.75PGPE, 0.5HPC-3.75PGPE and 0.75HPC-3.75PGPE.
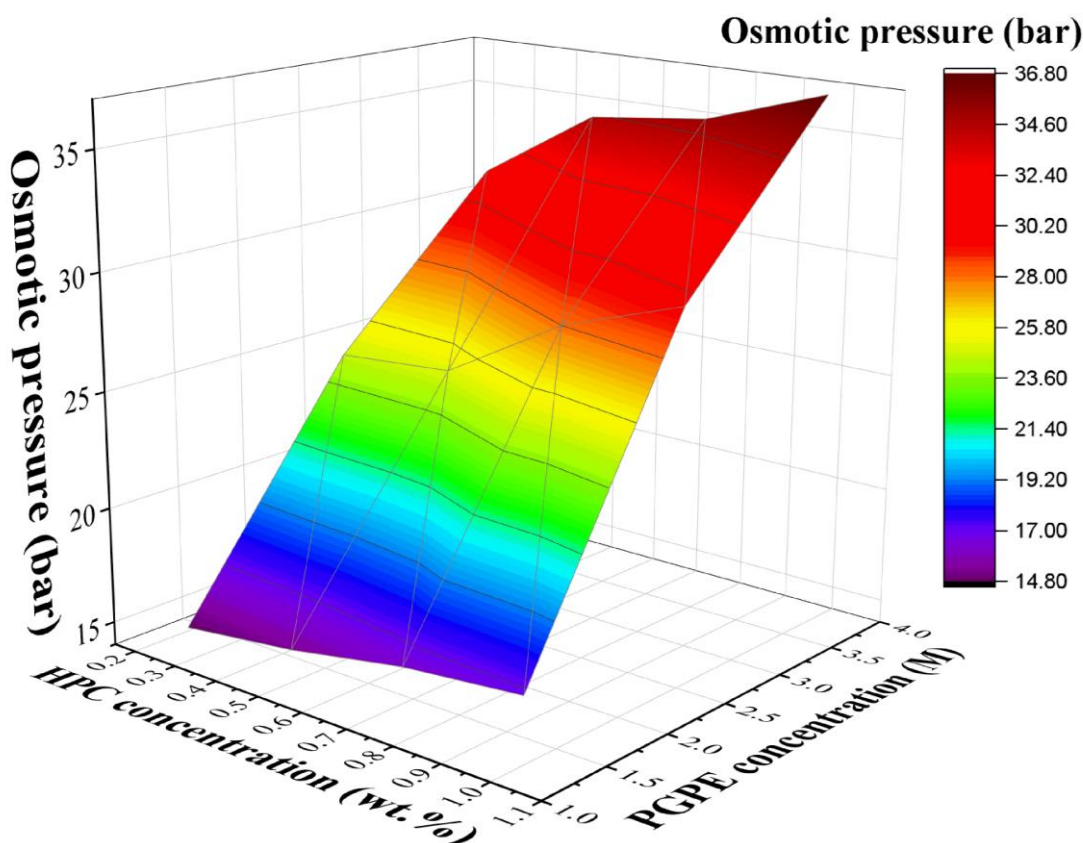
Figure 5.1: Relationship between HPC, PGPE and overall osmotic pressures

The dynamic viscosities, pH and osmotic pressures of these three favourable ternary draw solutions are shown in Table 5.2

Table 5.2: Properties of the chosen draw solutions

Draw solution	Dynamic viscosity (mPa.s)	pH at 15 °C	Osmotic pressure (bar)
0.25HPC-3.75PGPE	4.20	8.17	31.3
0.5HPC-3.75PGPE	9.16	7.95	34.5
0.75HPC-3.75PGPE	19.5	7.86	35.1

5.2.2 Dynamic viscosities of draw solutions

The dynamic viscosities of the pure single-solute 0.5 wt.% HPC, 1 wt.% HPC, 1.5 wt.% HPC and 2 wt.% HPC draw solutions are shown in Figure 5.2a. Figure 5.2b depicts the corresponding viscosities of the ternary draw solutions 0.25HPC-3.75PGPE, 0.5HPC-3.75PGPE and 0.75HPC-3.75PGPE at 25 °C. A notable observation is the substantial increase in dynamic viscosities of the pure HPC solutions upon incorporating PGPE. At a shear rate of 100 s^{-1}, the addition of 3.75M PGPE solutions increased the dynamic viscosities of the pure 0.5 wt.% HPC from 5.48 mPa.s to 14.271 mPa.s. This substantial increase may be due to the addition of a polymeric substance [17 – 19].
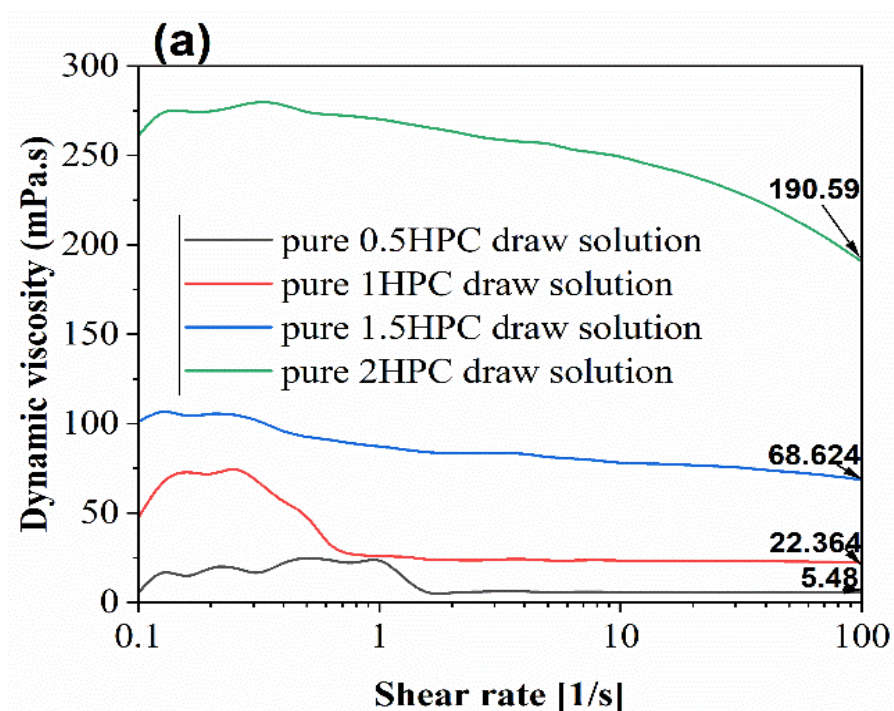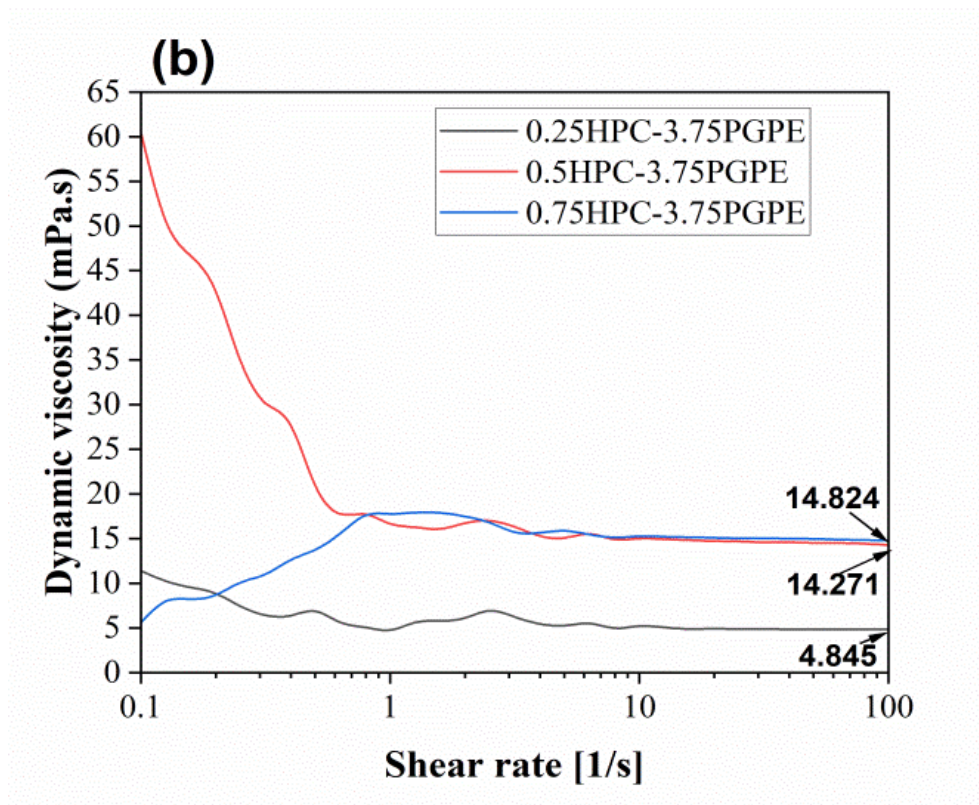
Figure 5.2: Dynamic viscosities of pure HPC solutions (a) and ternary solutions (b)

The dynamic viscosities of the 0.25HPC-3.75PGPE, 0.5HPC-3.75PGPE and 0.75HPC-3.75PGPE ternary draw solutions at different temperatures are shown in Figure 5.3.

Figure 5.3 clearly shows significant reductions in the viscosity of all ternary solutions with increasing temperature. These results suggest that running the FO experiments at slightly higher temperatures will reduce the pressure drop in the draw solution channel while significantly reducing concentration polarization, as higher viscosity reduces turbulence in the fluid and enhances concentration polarization.

(c)

Dynamic viscosities at 35°C

0.25HPC-3.75PGPE
0.5HPC-3.75PGPE
0.75HPC-3.75PGPE

3.8374
1.7902
1.9794

(d)

Dynamic viscosities at 40°C

0.25HPC-3.75PGPE
0.5HPC-3.75PGPE
0.75HPC-3.75PGPE

1.8563
1.7531
2,7244
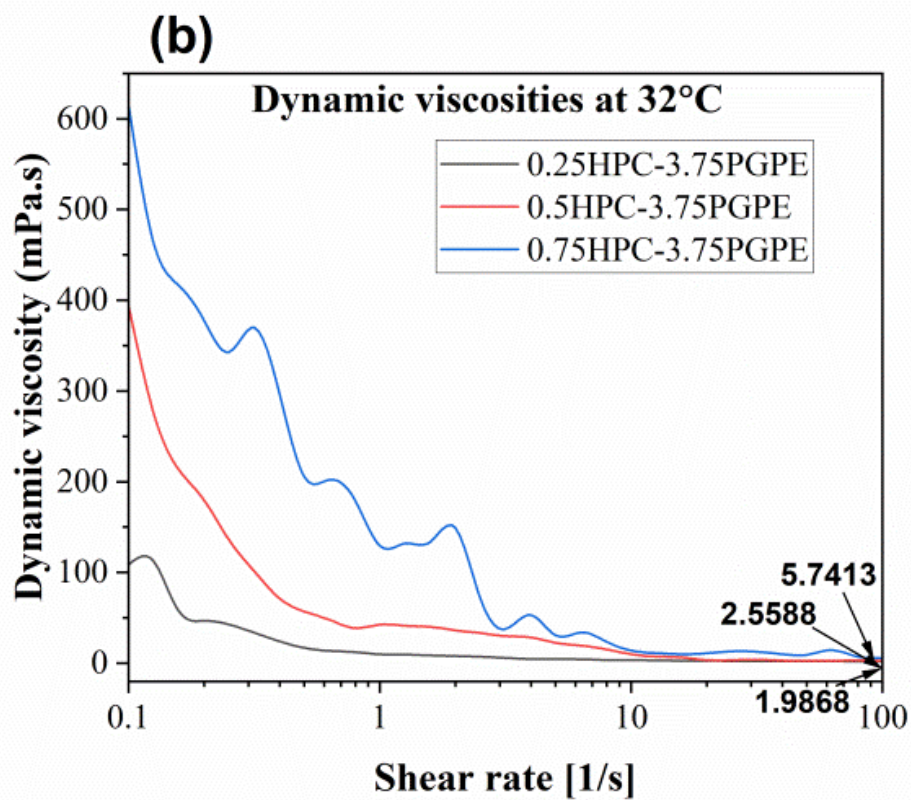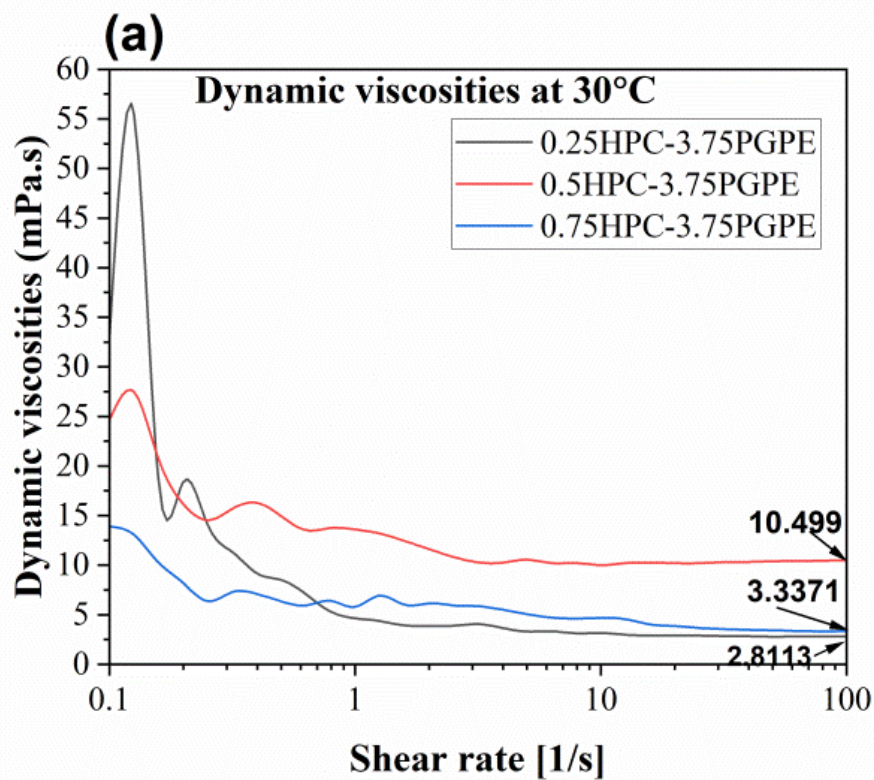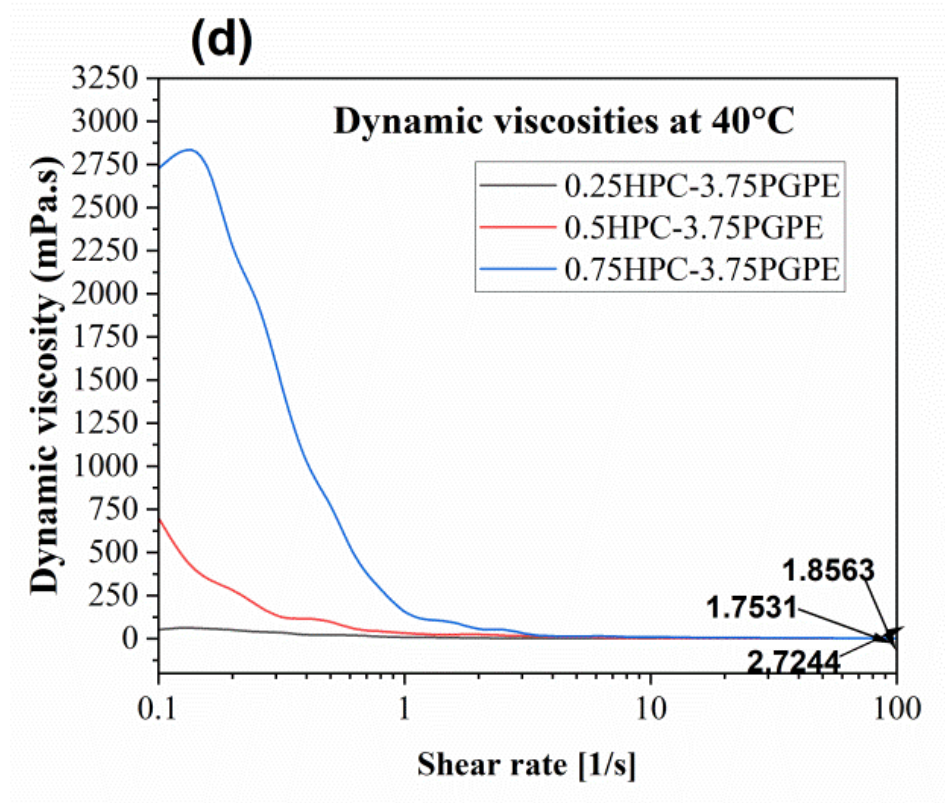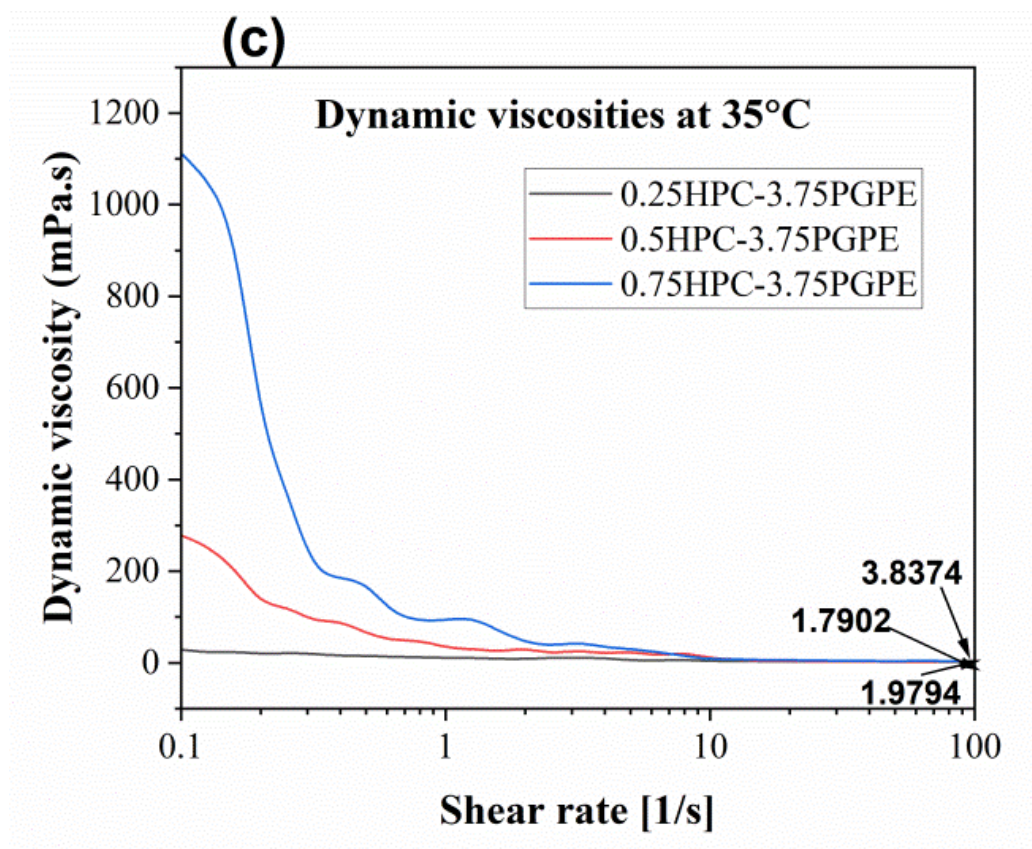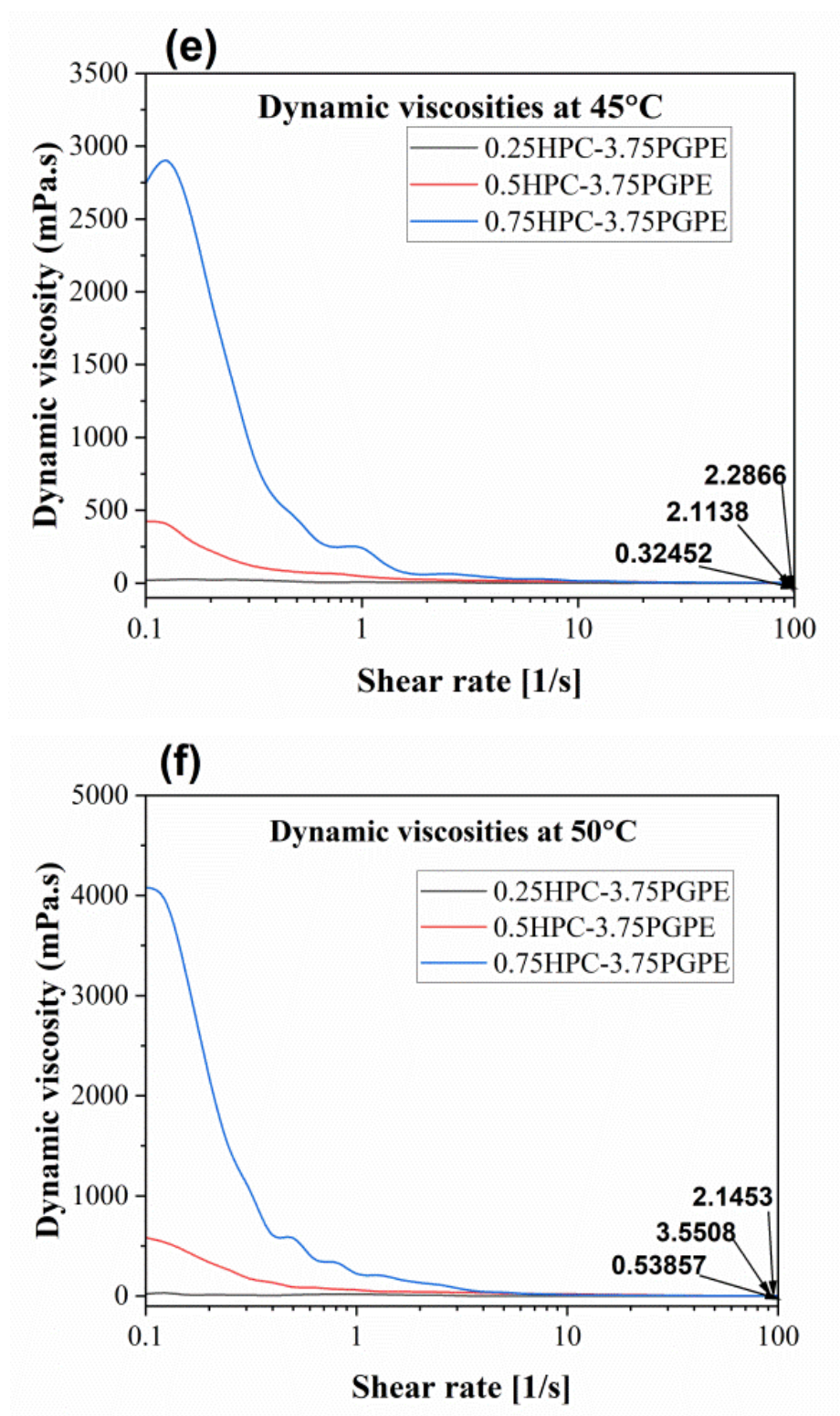
Figure 5.3: Dynamic viscosities of the three ternary draw solutions at different temperatures

5.2.3 Solute permeability coefficient of HPC-PGPE solutions

Table 5.3 shows the steady state experimental data used in estimating the solute permeability coefficient of the ternary draw solutions. These results were fitted in the Spiegler-Kedem model to determine the values of solute permeability and reflection coefficient [20].

Table 5.3: Steady-state experimental data used to estimate the solute permeability coefficient of HPC-PGPE draw solutions

FO Run	$Q_{F_{in}}$ (LPH)	$Q_{D_{in}}$ (LPH)	$C_{F_{in}}$ (g/L)	Feed osmotic pressure (bar)	$C_{D_{in}}$	Draw osmotic pressure (bar)	$Q_{p_{exp}}$ (LPH ×10²)	$Q_{p_{the}}$ (LPH ×10²)
1	24	12	1	0.85	0.25HPC-3.75PGPE	31.3	4.877	7.63
2	24	12	1	0.85	0.25HPC-3.75PGPE	31.3	4.275	7.63
3	24	24	1	0.85	0.5HPC-3.75PGPE	34.5	9.775	7.63
4	24	24	1	0.85	0.5HPC-3.75PGPE	34.5	7.637	7.63
5	24	24	1	0.85	0.75HPC-3.75PGPE	35.1	2.443	7.63
6	24	24	1	0.85	0.75HPC-3.75PGPE	35.1	2.749	7.63

Based on this model, the solute permeability coefficient and the reflection coefficient of the HPC-PGPE draw solutions were determined to be 4.05×10^{-8} m/s and 0.999, respectively. In contrast, the solute permeability and reflection coefficient of NaCl for the same membrane were reported as 1.14×10^{-7} m/s and 0.988, respectively [20]. Thus, the solute permeability of these HPC-PGPE solutions is significantly lower than that of NaCl, attributable to the larger molecular sizes of HPC and PGPE compared to NaCl.

5.2.4 FO performances of 0.25HPC-3.75PGPE draw solution

Figure 5.4 presents the experimental water fluxes achieved with a 0.25HPC-3.75PGPE ternary draw solution while desalinating 1 g/L NaCl brackish feed solutions across three FO runs. The first run employed the original draw solution, while the second and third runs utilized a regenerated draw solution obtained using vacuum distillation. The average experimental water fluxes for the first, second and third runs were 11.062, 9.852 and 9.242 LMH, respectively.
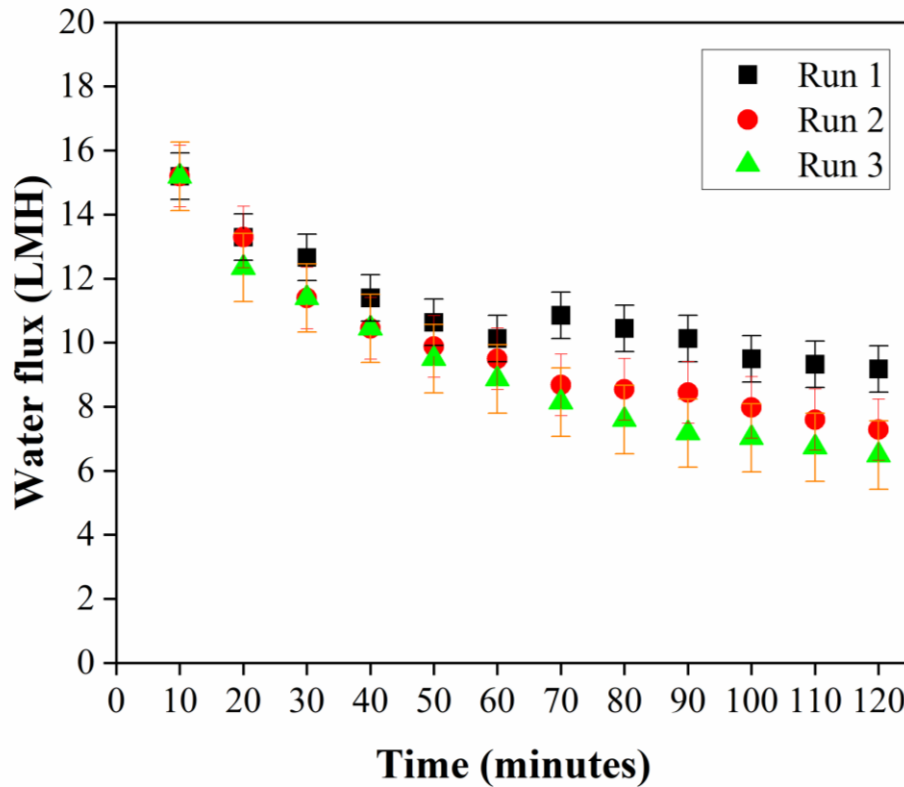
Figure 5.4: Experimental water fluxes of the 0.25HPC-3.75PGPE draw solution. Error bars represent the standard deviation

Figure 5.4 shows a decreasing trend in experimental water fluxes with the 0.25HPC-3.75PGPE draw solution across multiple FO runs. The initial fluxes were observed to be 15.194 LMH at 10 minutes, which declined steadily to 9.18, 7.281 and 6.489 LMH for runs 1, 2, and 3, respectively, by 120 minutes. Interestingly, run 1 exhibited an atypical rise in flux between 60 and 70 minutes before returning to the decreasing trend. In contrast, run 3, which utilized a regenerated draw solution, demonstrated a more consistent flux pattern. The observed decrease in water fluxes with successive FO runs may be due to dilutive ICP effects [21]. The solute fluxes were 2.753, 2.443 and 2.058 gMH across the three separate runs.

5.2.5 FO performances of 0.5HPC-3.75PGPE draw solution

Figure 5.5 illustrates the experimental water fluxes of the 0.5HPC-3.75PGPE ternary draw solution against 1 g/L NaCl brackish feed solutions for two FO runs.

The draw flow rate was set at 0.40 LPM, twice that of the 0.25HPC-3.75PGPE solution, due to the higher viscosities, as shown in Figure 5.2b. The feed flow rate was maintained at 0.40 LPM at a temperature of 25 °C. The average experimental water fluxes for the two runs were 19.793 and 13.618 LMH.
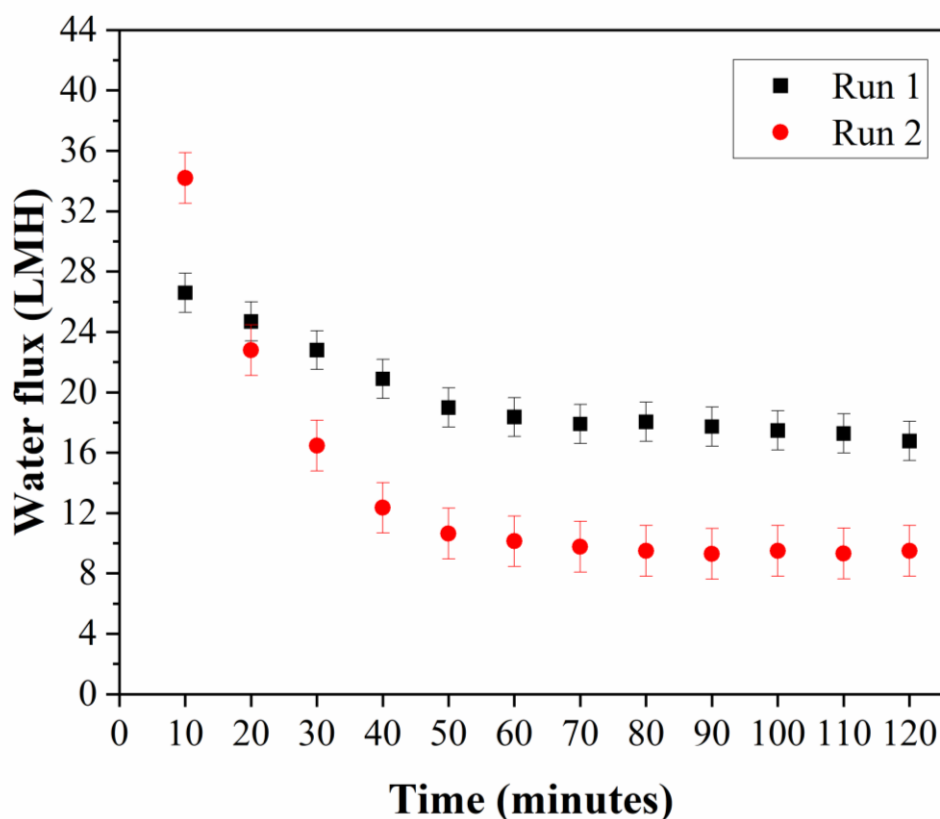
Figure 5.5: Experimental water fluxes of the 0.5HPC-3.75PGPE draw solution. Error bars represent the standard deviation.

Figure 5.5 reveals unusually high initial water fluxes, which then reduced rapidly, especially for the second run in the first 50 minutes. These results suggest that the second run was subjected to greater concentration polarization effects compared to the first, albeit still lower than those observed with the 0.25HPC-3.75PGPE solution tested at a lower flow rate. The solute fluxes were 2.615 and 2.789 gMH for the two runs. The draw solution exhibited inhomogeneity and required higher flow rates of 0.40 LPM due to increased viscosity. This suggests the need for modifications to improve its stability for practical applications.

5.2.6 FO performances of 0.75HPC-3.75PGPE draw solution

Figure 5.6 shows the experimental water fluxes of the 0.75HPC-3.75PGPE ternary draw solution against 1 g/L NaCl brackish feed solutions for two FO runs. The flow rates were the same as those of the 0.5HPC-3.75PGPE solution. The average experimental water fluxes for the two runs were 8.612 and 8.093 LMH.
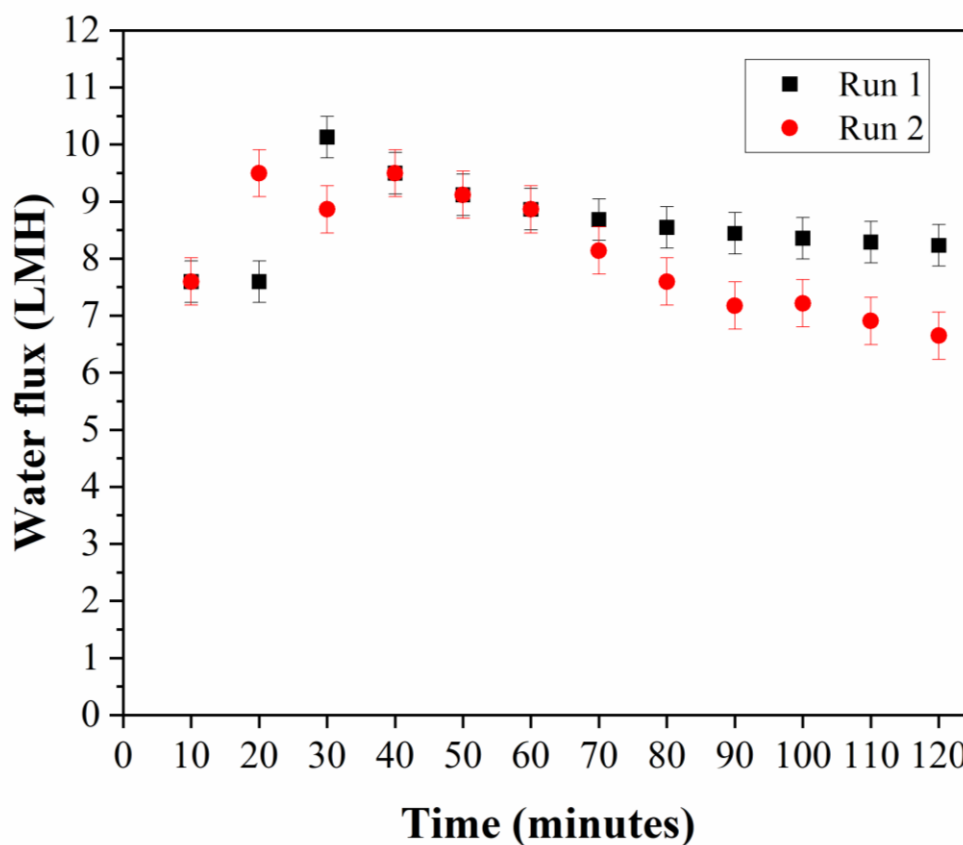
Figure 5.6: Experimental water fluxes of the 0.75HPC-3.75PGPE draw solution. Error bars represent the standard deviation.

The solute fluxes were 2.613 and 2.309 gMH, but the draw solution faced similar challenges with viscosity and inhomogeneity, requiring the use of a higher flow rate of 0.40 LPM. While the draw solution offered the easiest regeneration process, its current form is unsuitable for any FO desalination processes. Among the draw solutions, only the 0.25HPC-3.75PGPE exhibited favourable characteristics, maintaining homogeneity throughout FO runs at a lower flow rate of 0.20 LPM.

5.2.7   Comparative study with the other draw solutions from literature

The FO performances of these draw solutions were compared with those from the literature, as shown in Table 5.4. As can be seen, several prior studies have explored promising avenues for FO desalination by using phase separation of the draw solutes. However, Darvishmanesh et al. [23] highlighted the limitations of solely using glycol ether draw solutes, like PGPE. These included aggregate formation after phase separation thus reducing the osmotic pressures, decreasing initial water fluxes, an increase in irreversible membrane resistances, lower water fluxes compared to inorganic draw solutions, appreciable reverse solute fluxes and requiring RO to fully remove residual glycol ether from water. In our study, the glycol ether was combined with a cellulose derivative, which mitigated some of these drawbacks addressed by Darvishmanesh et al. [23], potentially leading to improved FO performance and broader applicability. The draw solutions used in this work have comparable FO performances with the draw solutes shown in Table 5.4, although further modifications need to be done to maintain the homogeneities of the more viscous 0.5HPC-3.75PGPE and 0.75HPC-3.75PGPE draw solutions.

Table 5.4: Comparison study of the draw solutions with other draw solutes from literature

Draw solution	Feed solution	Membrane Orientation	FO Performance		Separation Method	Ref
			Jw (LMH)	Js (gMH)		
Tetrabutylphosphonium mesitylenesulfonate	0.6 M NaCl	AL-FS	2	NR	Thermal phase separation employing cheap low-grade heat plus Nanofiltration	[22]
Mixtures of two different glycol ethers	0.6 M NaCl	AL-FS	1.3	4.9	Removal of residual glycol ethers after phase separation using RO	[23]
Choline Chloride- Ethylene Glycol	Seawater	AL-FS	2.6	NR	Using freezing due to solid-liquid separation at -7 ºC	[24]
$[P_{4446}]$ $[C_3S]$	DI water	AL-FS	3.98	1.03	LCST-type phase separation	[25]
Monocationic and dicationic phosphonium-based ILs	DI water	AL-FS	3.5	NR	Phase separation into IL-rich layer and water-rich layer above LCST	[26]
UCST ionic liquid	0.17 M NaCl	AL-FS	0.85	0.98	When cooled to room temperature, phase separated IL-rich phase was used directly as the draw solution in the next FO runs.	[14]
Chitosan derivative	DI water	AL-FS	9.1	NR	Utilizing LCST as it undergoes a phase transition separation when the temperature changes	[27]
Switchable polarity solvents	0.5 M NaCl	AL-FS	18.8	NR	Phase switching from a high osmotic pressure aqueous solution to purified water and a nonpolar liquid, which can be physically separated	[28]
PSSS-PNIPAM	0.6 M NaCl	AL-FS	3.5	2	The use of MD as the decreased osmotic pressure allows higher water vapour pressure and favours the separation of water	[29]

Trimethylamine–carbon dioxide	DI water	AL-FS	14.5	0.1 to 0.2 mol m^{-2} h^{-1}	Thermal separation using low-temperature vacuum distillation utilizing low-grade heat sources.	[30]
2-(meth-acryloyloxy) ethyl] trimethyl ammonium chloride (MTAC) and 2-(2-methoxyethoxy) ethyl methacylate (MEO)	NR	AL-FS	5.45	NR	Thermal precipitation followed by a microfiltration process at 51 ºC	[31]
Rhamnolipid biosurfactants	NR	AL-FS	7.7	0.01	Direct use for agricultural irrigation	[11]
Real fresh human urine	NR	AL-FS	9.5	NR	NR	[12]
Real hydrolysed urine	NR	AL-FS	16.7	NR	NR	[12]
Sodium chloride	Activated sludge	AL-FS	7.6 LMH	15.4 gMH	NR	[32]
Zinc sulphate	Activated sludge	AL-FS	2.7 LMH	4.1	NR	[32]
Sodium chloride	DI	AL-FS	5.1 LMH	7.4	NR	[32]
Sodium sulphate	Ultrapure water	AL-FS	2.56×10^{-6} m/s	3.1	Reverse Osmosis	[33]
Sodium bicarbonate	Ultrapure water	AL-FS	2.47×10^{-6} m/s	1.7	Reverse Osmosis	[33]
Sodium Chloride	Ultrapure water	AL-FS	3.38×10^{-6} m/s	9.1	Reverse Osmosis	[33]
Potassium Bicarbonate	Ultrapure water	AL-FS	2.80×10^{-6} m/s	2	Reverse Osmosis	[33]
Magnesium sulphate	Ultrapure water	AL-FS	1.54×10^{-6} m/s	1.2	Reverse Osmosis	[33]
Magnesium chloride	Ultrapure water	AL-FS	2.70×10^{-6} m/s	5.6	Reverse Osmosis	[33]
Ammonium chloride	Ultrapure	AL-FS	3.61×10^{-6}	10.2	Reverse Osmosis	[33]

	water			m/s		
Potassium sulphate	Ultrapure water	AL-FS	2.52×10^{-6} m/s	3.7	Reverse Osmosis	[33]
Calcium chloride	Ultrapure water	AL-FS	3.22×10^{-6} m/s	9.5	Reverse Osmosis	[33]
Ammonium sulphate	Ultrapure water	AL-FS	2.74×10^{-6} m/s	3.6	Reverse Osmosis	[33]
Potassium chloride	Ultrapure water	AL-FS	3.74×10^{-6} m/s	15.2	Reverse Osmosis	[33]
Calcium nitrate	Ultrapure water	AL-FS	2.97×10^{-6} m/s	6.6	Reverse Osmosis	[33]
Ammonium bicarbonate	Ultrapure water	AL-FS	2.85×10^{-6} m/s	20.6	NR	[33]
Potassium bromide	Ultrapure water	AL-FS	3.59×10^{-6} m/s	29.2	NR	[33]
0.25HPC-3.75PGPE	1 g/L NaCl	AL-FS	11.062	2.753	Heating at 80 ºC, then using RO to remove the residual draw solutes in the water	This work
0.5HPC-3.75PGPE	1 g/L NaCl	AL-FS	19.793	2.615	Heating at 80 ºC, then using RO to remove the residual draw solutes in the water	This work
0.75HPC-3.75PGPE	1 g/L NaCl	AL-FS	8.612	2.613	Heating at 80 ºC, then using RO to remove the residual draw solutes in the water	This work

NR: Not reported

5.2.8 Draw solution regeneration potential

Figure 5.7 demonstrates the effective reversibility of phase transitions in pure HPC solutions due to temperature changes. The pure solutions exhibit clear homogeneity and miscibility below the LCST of 45 °C, while above this temperature, the solutions become completely immiscible and phase-separated.
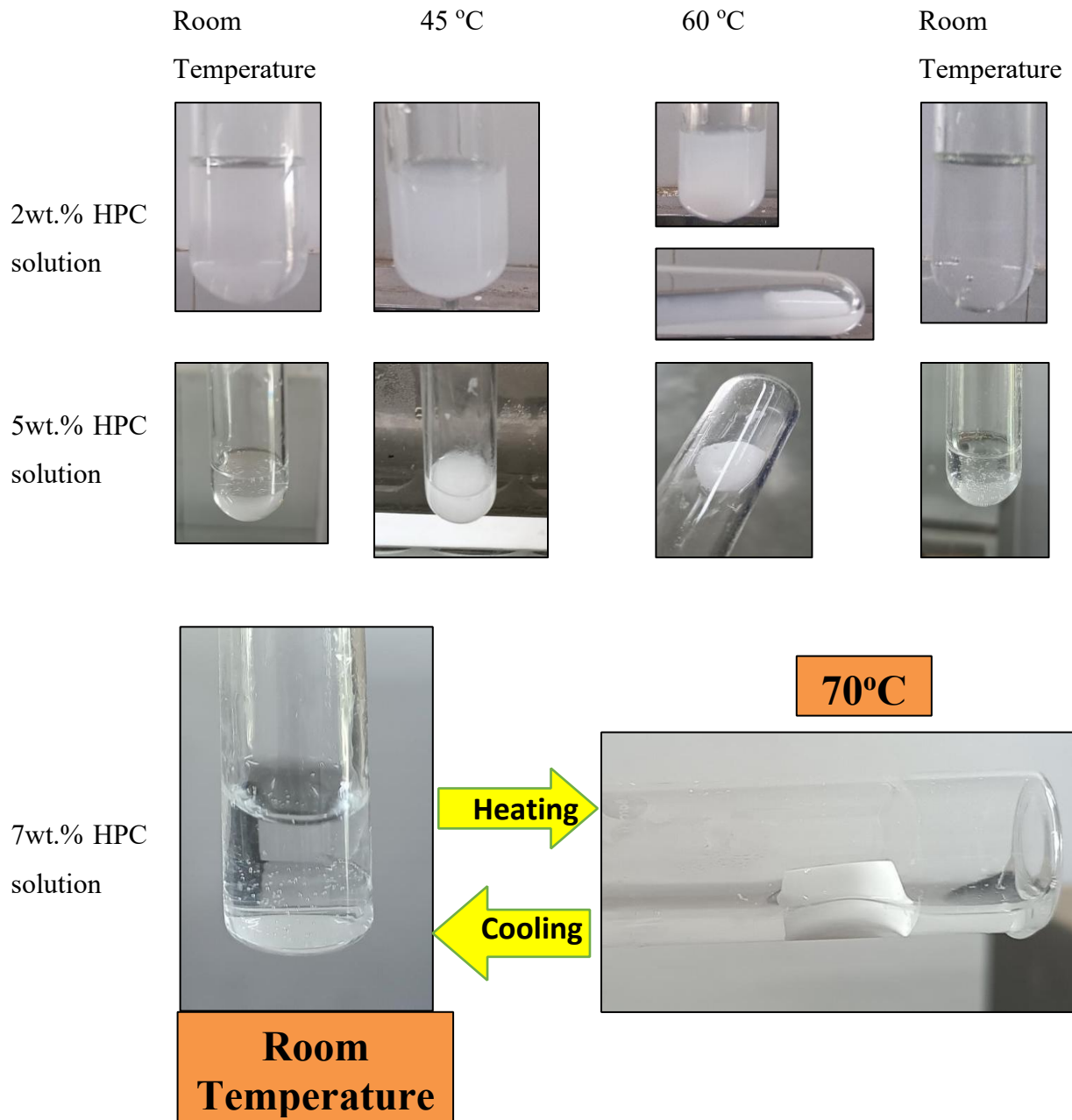
Figure 5.7: Thermoreversibility of pure HPC solutions

The cloud point temperature of the 5 M and 7.5 M PGPE draw solutions was shown to be 32 °C. On the other hand, the 2.5 M PGPE draw solution remained clear at 32 °C but lost its clarity at 48 °C. The 0.5wt.%, 1wt.%, 1.5wt.% and 2wt.% HPC concentrations all had a cloud point temperature of 45 °C. This is in agreement with the cloud point temperature of HPC solutions from the literature [34]. The images taken for the three chosen draw solutions at different temperatures are shown in Figure 5.8.

Room temperature (25 °C)

32 °C

40 °C

45 °C

50 °C

Room temperature (25°C)
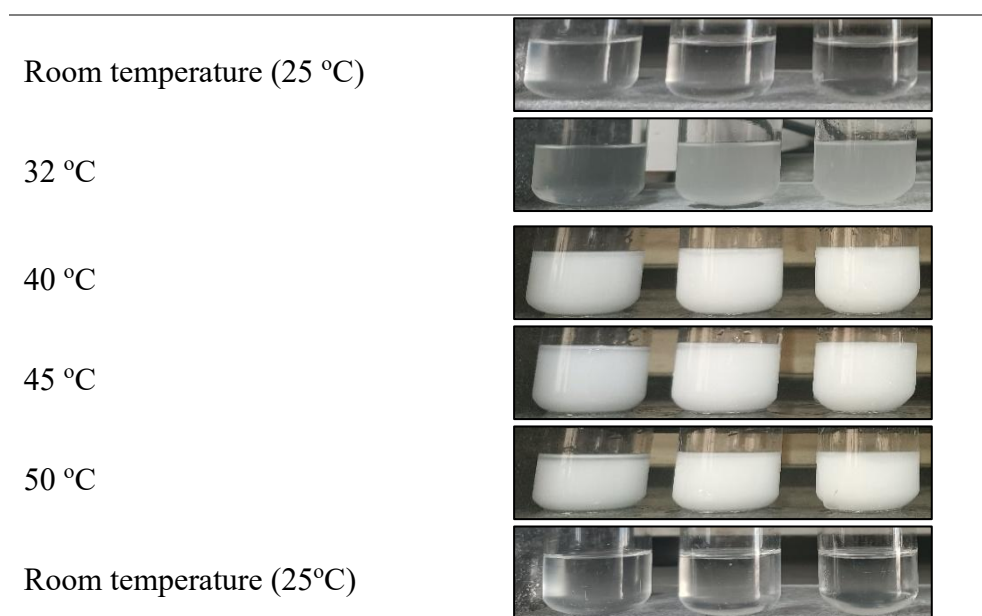
Figure 5.8: Cloud point temperatures of the selected organic draw solutions. From LEFT to RIGHT: 0.25HPC-3.75PGPE, 0.5HPC-3.75PGPE and 0.75HPC-3.75PGPE.

The results in Figure 5.8 demonstrate the potential of using the LCST behaviour of the investigated draw solutions to facilitate regeneration. At a temperature of 50 °C, the solutions would have already undergone phase separation. Figure 5.9 highlights the phase separation induced in the 0.25HPC-3.75PGPE ternary draw solution upon heating at 80 °C for 1 hour.

(a)

(b)

(c)
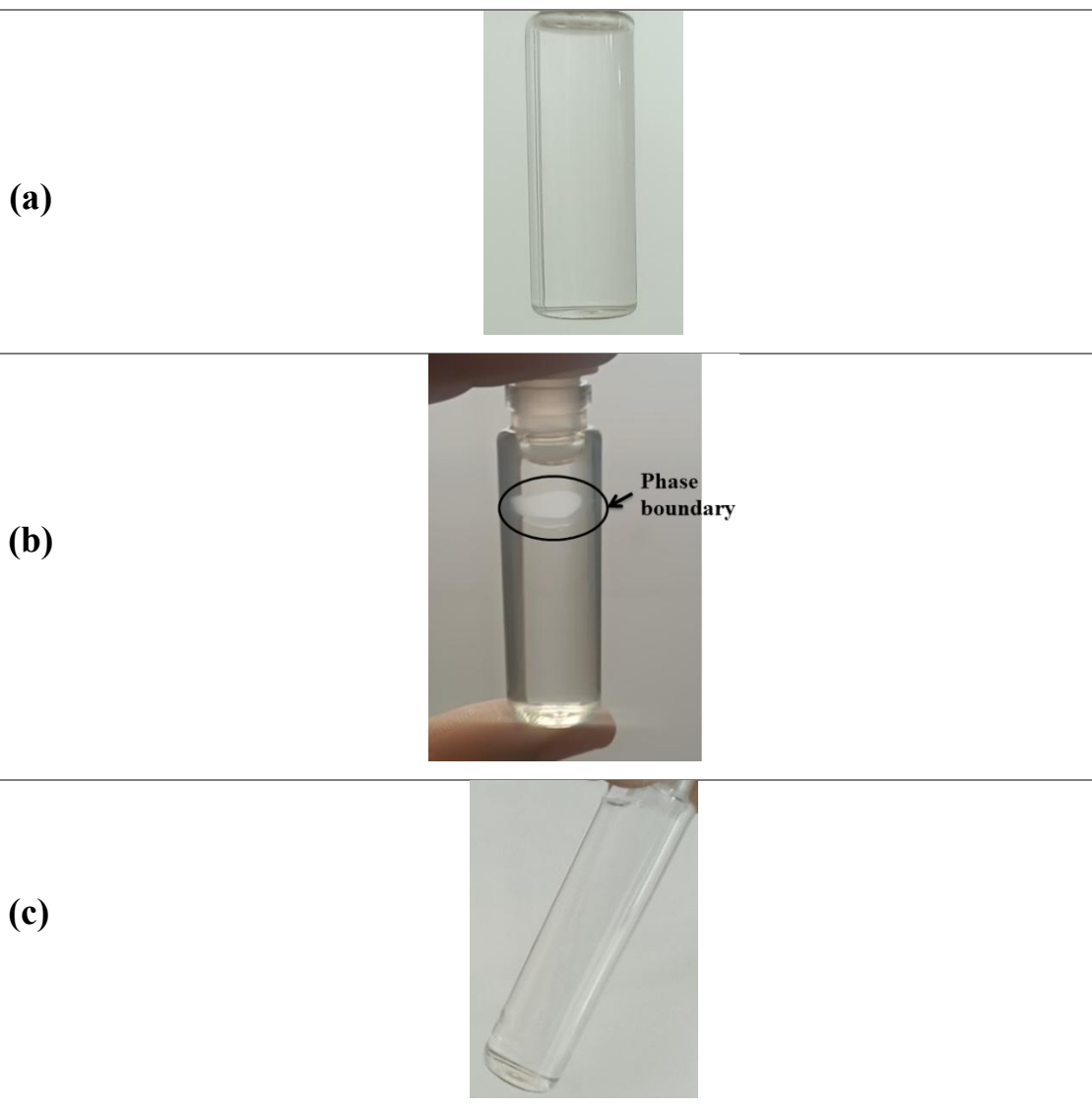
Figure 5.9: Phase behaviours of 0.25HPC-3.75PGPE ternary draw solution. (a) Homogenous draw solution at room temperature. (b) Phase separation observed after heating the solution at 80 ºC for 1 hour. (c) Regenerated homogeneous solution at room temperature after cooling

The results illustrated in Figure 5.9 demonstrate the successful regeneration of the draw solution upon heating above the cloud point temperatures determined in Figure 5.8. Of notable interest is the presence of three distinct phases conspicuously visible in Figure 5.9(b), comprising insoluble white HPC precipitates and the separated PGPE and water liquid phases.

5.3 References

1. Meerganz von Medeazza, G. (2004). Water desalination as a long-term sustainable solution to alleviate global freshwater scarcity? A North-South approach. Desalination, 169(3), 287–301. https://doi.org/10.1016/j.desa1.2004.04.001

2. Ndiaye, I., Vaudreuil, S., & Bounahmidi, T. (2019). Forward osmosis process: State-of-the-art of membranes. Separation and Purification Reviews, 50(1), 53–73. https://doi.org/10.1080/15422119.2019.1622133

3. Cath, T., Childress, A., & Elimelech, M. (2006). Forward osmosis: Principles, applications, and recent developments. Journal of Membrane Science, 281(1–2), 70–87. https://doi.org/10.1016/j.memsci.2006.05.048

4. Nakayama, D., Mok, Y., Noh, M., Park, J., Kang, S., & Lee, Y. (2014). Lower critical solution temperature (LCST) phase separation of glycol ethers for forward osmotic control. Physical Chemistry Chemical Physics, 16(11), 5319–5325. https://doi.org/10.1039/c3cp55467h

5. She, Q., Wang, R., Fane, A. G., & Tang, C. Y. (2015). Membrane fouling in osmotically driven membrane processes: A review. Journal of Membrane Science, 499, 201–233. https://doi.org/10.1016/j.memsci.2015.10.040

6. Chu, H., Zhang, Z., Zhong, H., Yang, K., Sun, P., Liao, X., & Cai, M. (2022). Athermal concentration of blueberry juice by forward osmosis: Food additives as draw solution. Membranes, 12(8), 808. https://doi.org/10.3390/membranes12080808

7. Hsu, C., Ma, C., Bui, N., Song, Z., Wilson, A. D., Kostecki, R., . . . Urban, J. J. (2019). Enhanced forward osmosis desalination with a hybrid ionic liquid/hydrogel thermoresponsive draw agent system. ACS Omega, 4(2), 4296–4303. https://doi.org/10.1021/acsomega.8b02827

8. Hamdan, M., Sharif, A. O., Derwish, G., Al-Aibi, S., & Altaee, A. (2015). Draw solutions for forward osmosis process: Osmotic pressure of binary and ternary aqueous solutions of magnesium chloride, sodium chloride, sucrose and maltose. Journal of Food Engineering, 155, 10–15. https://doi.org/10.1016/j.jfoodeng.2015.01.010

9. Farman, A. A., Irfan, M., Amin, N. U., Jahan, Z., Song, X., Jiang, H., & Gul, S. (2022). Evaluation of sodium acetate and glucose as minor additives with calcium chloride as optimum mixed draw solutes for fruit juice concentration via forward osmosis. Korean Journal of Chemical Engineering, 39(11), 3102–3108. https://doi.org/10.1007/s11814-022-1228-7

10. Nguyen, N. C., Chen, S., Jain, S., Nguyen, H. T., Ray, S. S., Ngo, H. H., . . . Duong, H. C. (2017). Exploration of an innovative draw solution for a forward osmosis-membrane distillation desalination process. Environmental Science and Pollution Research, 25(6), 5203–5211. https://doi.org/10.1007/s11356-017-9192-1

11. Ahangar, A. K., & Taghavijeloudar, M. (2023). Desalination and extraction of high value bio-products from algal-rich seawater using rhamnolipid as a

bio draw solution in forward osmosis. Desalination, 568, 117017. https://doi.org/10.1016/j.desal.2023.117017

12. Volpin, F., Yu, H., Cho, J., Lee, C., Phuntsho, S., Ghaffour, N., . . . Shon, H. K. (2019). Human urine as a forward osmosis draw solution for the application of microalgae dewatering. Journal of Hazardous Materials, 378, 120724. https://doi.org/10.1016/j.jhazmat.2019.06.001

13. Zeweldi, H. G., Bendoy, A. P., Park, M. J., Shon, H. K., Kim, H., Johnson, E. M., . . . Nisola, G. M. (2020). Tetrabutylammonium 2,4,6-trimethylbenzenesulfonate as an effective and regenerable thermo-responsive ionic liquid drawing agent in forward osmosis for seawater desalination. Desalination, 495, 114635. https://doi.org/10.1016/j.desal.2020.114635

14. Zhong, Y., Feng, X., Chen, W., Wang, X., Huang, K., Gnanou, Y., & Lai, Z. (2015). Using UCST ionic liquid as a draw solute in forward osmosis to treat high-salinity water. Environmental Science & Technology, 50(2), 1039–1045. https://doi.org/10.1021/acs.est.5b03747

15. Yang, D., & Kang, H. (2022). Thermoresponsive ionic liquid with different cation–anion pairs as draw solutes in forward osmosis. Molecules, 27(24), 8869. https://doi.org/10.3390/molecules27248869

16. Moon, J., & Kang, H. (2023). Anion effect on forward osmosis performance of tetrabutylphosphonium-based draw solute having a lower critical solution temperature. Membranes, 13(2), 211. https://doi.org/10.3390/membranes13020211

17. Waghorne, W. E. (2001). Viscosities of electrolyte solutions. Philosophical Transactions of the Royal Society A: Mathematical Physical and Engineering Sciences, 359(1785), 1529–1543. https://doi.org/10.1098/rsta.2001.0864

18. Hoernschemeyer, D. (1974). The influence of solvent type on the viscosity of concentrated polymer solutions. Journal of Applied Polymer Science, 18(1), 61–75. https://doi.org/10.1002/app.1974.070180105

19. Kol, R., Nachtergaele, P., De Somer, T., D'hooge, D. R., Achilias, D. S., & De Meester, S. (2022). Toward more universal prediction of polymer solution viscosity for solvent-based recycling. Industrial & Engineering Chemistry Research, 61(30), 10999–11011. https://doi.org/10.1021/acs.iecr.2c01487

20. Attarde, D., Jain, M., & Gupta, S. K. (2016). Modeling of a forward osmosis and a pressure-retarded osmosis spiral wound module using the Spiegler-Kedem model and experimental validation. Separation and Purification Technology, 164, 182–197. https://doi.org/10.1016/j.seppur.2016.03.039

21. Singh, S. K., Sharma, C., & Maiti, A. (2021). A comprehensive review of standalone and hybrid forward osmosis for water treatment: Membranes and recovery strategies of draw solutions. Journal of Environmental Chemical Engineering, 9(4), 105473. https://doi.org/10.1016/j.jece.2021.105473

22. Cai, Y., Shen, W., Wei, J., Chong, T. H., Wang, R., Krantz, W. B., . . . Hu, X. (2015). Energy-efficient desalination by forward osmosis using

responsive ionic liquid draw solutes. Environmental Science Water Research & Technology, 1(3), 341–347. https://doi.org/10.1039/c4ew00073k

23. Darvishmanesh, S., Pethica, B. A., & Sundaresan, S. (2017). Forward osmosis using draw solutions manifesting liquid-liquid phase separation. Desalination, 421, 23–31. https://doi.org/10.1016/j.desal.2017.05.036

24. Mahto, A., Mondal, D., Polisetti, V., Bhatt, J., R, N. M., Prasad, K., & Nataraj, S. K. (2017). Sustainable water reclamation from different feed streams by forward osmosis process using deep eutectic solvents as reusable draw solution. Industrial & Engineering Chemistry Research, 56(49), 14623–14632. https://doi.org/10.1021/acs.iecr.7b03046

25. Moon, J., & Kang, H. (2023). Effect of cation alkyl chain length on 3-sulfopropylmethacrylate-based draw solutes having lower critical solution temperature. RSC Advances, 13(12), 8291–8298. https://doi.org/10.1039/d2ra08068k

26. Liu, P., Wang, D. C., Ho, C., Chen, Y., Chung, L., Liang, T., . . . Horng, R. (2020). Exploring the performance-affecting factors of monocationic and dicationic phosphonium-based thermosresponsive ionic liquid draw solutes in forward osmosis. Desalination and Water Treatment, 200, 1–7. https://doi.org/10.5004/dwt.2020.25987

27. Lecaros, R. L. G., Syu, Z., Chiao, Y., Wickramasinghe, S. R., Ji, Y., An, Q., . . . Lai, J. (2016). Characterization of a thermoresponsive chitosan derivative as a potential draw solute for forward osmosis. Environmental Science & Technology, 50(21), 11935–11942. https://doi.org/10.1021/acs.est.6b02102

28. Stone, M. L., Rae, C., Stewart, F. F., & Wilson, A. D. (2012). Switchable polarity solvents as draw solutes for forward osmosis. Desalination, 312, 124–129. https://doi.org/10.1016/j.desal.2012.07.034

29. Zhao, D., Wang, P., Zhao, Q., Chen, N., & Lu, X. (2014). Thermoresponsive copolymer-based draw solution for seawater desalination in a combined process of forward osmosis and membrane distillation. Desalination, 348, 26–32. https://doi.org/10.1016/j.desal.2014.06.009

30. Boo, C., Khalil, Y. F., & Elimelech, M. (2014). Performance evaluation of trimethylamine–carbon dioxide thermolytic draw solution for engineered osmosis. Journal of Membrane Science, 473, 302–309. https://doi.org/10.1016/j.memsci.2014.09.026

31. Kim, J., Chung, J., Kang, H., Yu, Y. A., Choi, W. J., Kim, H. J., & Lee, J. (2014). Thermo-responsive copolymers with ionic group as novel draw solutes for forward osmosis processes. Macromolecular Research, 22(9), 963–970. https://doi.org/10.1007/s13233-014-2142-6

32. Cornelissen, E., Harmsen, D., Dekorte, K., Ruiken, C., Qin, J., Oo, H., & Wessels, L. (2008). Membrane fouling and process performance of forward osmosis membranes on activated sludge. Journal of Membrane Science, 319(1–2), 158–168. https://doi.org/10.1016/j.memsci.2008.03.048

33. Achilli, A., Cath, T. Y., & Childress, A. E. (2010). Selection of inorganic-based draw solutions for forward osmosis applications. Journal of

Membrane Science, 364(1–2), 233–241.
https://doi.org/10.1016/j.memsci.2010.08.010

34. Khuman, P., Singh, W. B. K., Devi, S. D., & Naorem, H. (2014). Viscosity-Temperature behaviour of hydroxypropyl cellulose solution in presence of an electrolyte or a surfactant: A convenient method to determine the cloud point of polymer solutions. Journal of Macromolecular Science Part A, 51(11), 924–930. https://doi.org/10.1080/10601325.2014.953377

CHAPTER 6

DATA-DRIVEN MODELING AND TECHNO-ECONOMIC ASSESSMENT FOR FORWARD OSMOSIS-PHASE SEPARATION DESALINATION PROCESSES USING NOVEL TERNARY ORGANIC DRAW SOLUTIONS

6.1 Introduction

Mathematical modeling has been extensively used in the study of membrane separation processes, encompassing reverse osmosis (RO) [1], nanofiltration (NF) [2], ultrafiltration (UF) [3], forward osmosis (FO) [4 – 7] and hybrid systems [8, 9]. The researchers have implemented diverse, innovative techniques, including machine learning algorithms, three-dimensional multiscale models, and methodologies for addressing scenarios with limited critical data, such as mass diffusivity. These approaches have been applied to both single-solute and multi-component systems. FO modeling can either be transport-based, such as the Solution-Diffusion (S-D) and Spiegler-Kedem (S-K) models, or data-driven models that make use of machine learning techniques [9]. The S-D model has been extensively used to predict water and solute fluxes in FO, particularly in single-solute inorganic draw solution systems. The S-D model assumes that permeants initially dissolve into the membrane material and diffuse through the membrane in response to a concentration gradient [10]. Despite its widespread use, some researchers deemed the S-D model inadequate for FO processes, citing flawed underlying assumptions [11]. The S-D model was deemed insufficient for multi-component draw solutions, as it failed to account for the transport coupling of the various species [12, 13]. This limitation highlighted the need for more comprehensive modeling approaches in complex FO systems. To address this deficiency, Foo et al. [12] developed a modified S-D model for multi-component systems. Their approach incorporated solute coupling effects, significantly improving the predictive accuracy. In a water-sodium chloride-ethanol ternary FO system, the modified model reduced average absolute deviations from 66.1% to 7.2%, demonstrating a substantial enhancement in modeling precision for the multi-component draw solutions. Ibrar et al. [13] propounded that the limited availability of data concerning the diffusion coefficients of multi-component electrolyte draw solutions complicated the determination of mass transfer

coefficients and solute resistance to diffusion in the FO process. Yong et al. [14] demonstrated that experimental water fluxes for organic draw solutions, such as urea, ethylene glycol, and glucose, were lower than the theoretical fluxes observed in the FO process. To address this limitation, they postulated that this discrepancy indicated a coupling between the forward water flux and reverse solute flux. Consequently, they introduced a reflection coefficient to account for this solute-solvent coupling.

This chapter presents an approach to modeling novel binary and ternary organic draw solutions developed in our previous studies [15, 16]. Foo et al. [12] and Ibrar et al. [13] emphasize that the S-D model exhibits inadequacy when applied to multi-component draw solution systems. Similarly, it falls short in addressing neutral draw solutions, as demonstrated by Yong et al. [14]. Given the lack of literature data on the diffusion coefficients of the novel binary mono propylene glycol propyl ether (PGPE) and the ternary systems of hydroxypropyl cellulose–propylene glycol propyl ether (HPC–PGPE) and sodium carboxymethyl cellulose–propylene glycol propyl ether (NaCMC–PGPE), this work opts instead for data-driven modeling making use of ANN. The input parameters include FO runs, time, temperatures of both feed and draw solutions, concentrations of both feed and draw solutions, flow rates of both feed and draw solutions and the molecular weights of the draw solutions. These inputs are used to predict permeate fluxes in the system. This chapter also conducts a comprehensive techno-economic assessment (TEA), incorporating operating expenditures (OPEX) and capital expenditures (CAPEX) calculations for both the stand-alone FO process and the phase-separating (PS) draw regeneration processes. Notably, the study emphasizes the use of waste heat energy to enhance the economic viability of the FO-PS hybrid process, recognizing that the draw regeneration process is the most energy-intensive component of the overall desalination process.

6.2 Results and discussion

6.2.1   Comparison of predictive models

To determine the most effective predictive model for the process, a comparative analysis of seven distinct machine learning algorithms: Linear regression models,

Regression Tree models, Support Vector Machine models, Gaussian Process Regression models, Kernel Approximation Regression models, Ensemble of Trees models and Neural Networks models, was performed. These algorithms were implemented and evaluated using the Regression Learner application within MATLAB R2022a. To ensure a fair comparison, identical datasets were utilized across all seven algorithms throughout the model development and assessment process. The comparisons for the predictive models are shown in Table 6.1 in terms of the root mean square error, R-squared, mean squared error and mean absolute error.

Table 6.1: Comparison of predictive models using Regression learner

Prediction model	Last change	RMSE	R^2	MSE	MAE
Linear regression models	Linear	0.066632	0.84	0.0044398	0.044924
	Interactions linear	0.048858	0.91	0.0023872	0.030912
	Robust linear	0.068209	0.83	0.0046525	0.045083
	Stepwise linear	0.053034	0.90	0.0028126	0.034795
Regression Trees models	Fine Tree	0.087492	0.72	0.0076549	0.051194
	Medium Tree	0.10465	0.60	0.010952	0.069175
	Coarse Tree	0.12806	0.39	0.0164	0.093808
Support Vector Machines models	Linear SVM	0.067625	0.83	0.0045732	0.044863
	Quadratic SVM	0.057856	0.88	0.0033473	0.034164
	Cubic SVM	0.038261	0.95	0.0014639	0.020507
	Fine Gaussian SVM	0.064581	0.85	0.0041708	0.032285
	Medium Gaussian SVM	0.065479	0.84	0.0042874	0.038943
	Coarse Gaussian SVM	0.099816	0.63	0.0099632	0.065151
Gaussian Process	Rational	0.024266	0.98	0.00058884	0.012962

Regression models	Quadratic GPR				
	Squared Exponential GPR	0.024035	0.98	0.00057769	0.013263
	Matern 5/2 GPR	0.024865	0.98	0.00061825	0.013028
	Exponential GPR	0.034278	0.96	0.001175	0.017291
Kernel Approximation Regression models	SVM Kernel	0.045715	0.92	0.0020899	0.027433
	Least Squares Regression Kernel	0.084529	0.74	0.0071452	0.056967
Ensemble of Trees models	Boosted Trees	0.06686	0.83	0.0044702	0.04386
	Bagged Trees	0.087349	0.72	0.0076298	0.057206
Neural Networks models	Narrow Neural Networks	0.041787	0.94	0.0017461	0.026341
	Medium Neural Networks	0.03357	0.96	0.001127	0.020699
	Wide Neural Networks	0.028479	0.97	0.00081108	0.017985
	Bilayered Neural Networks	0.038757	0.94	0.0015021	0.022288
	Trilayered Neural Networks	0.028679	0.97	0.0008225	0.016483

The Predicted vs. True response curves of output flux for linear regression models are shown in Figure 6.1
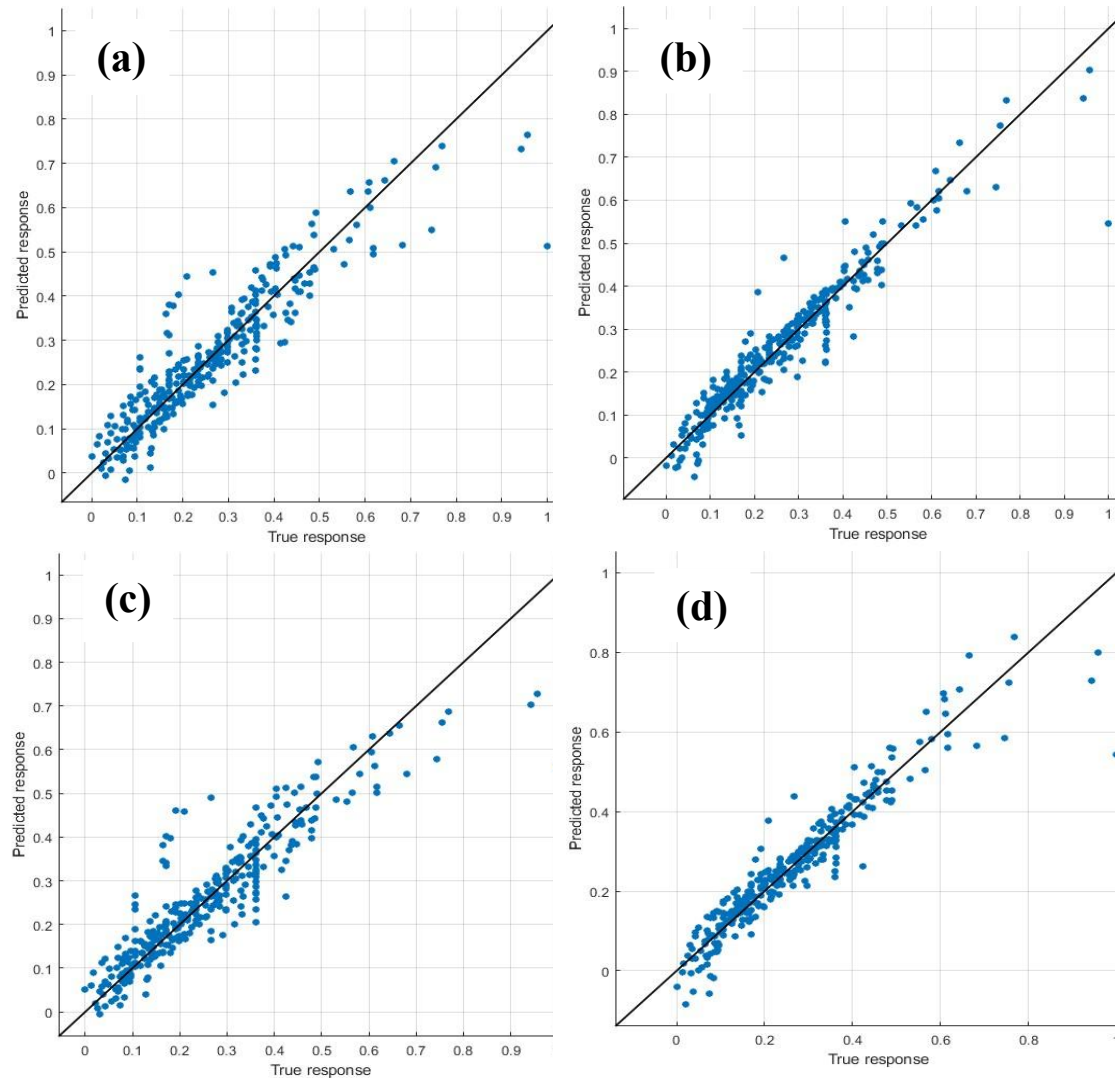
Figure 6.1: Predicted vs. True response curves of output flux for linear regression of the training and validation (a) Linear (b) Interactions linear (c) Robust linear (d) Stepwise linear

The Predicted vs. True response curves of output flux for regression tree models are shown in Figure 6.2
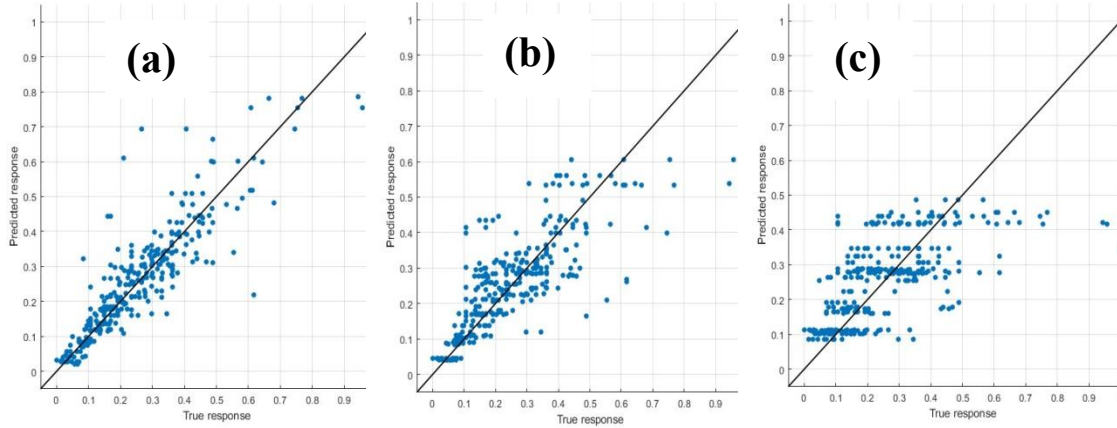
Figure 6.2: Predicted vs. True response curves of output flux for regression trees of the training and validation (a) Fine Tree (b) Medium Tree (c) Coarse Tree

The Predicted vs. True response curves of output flux for support vector machine models are shown in Figure 6.3
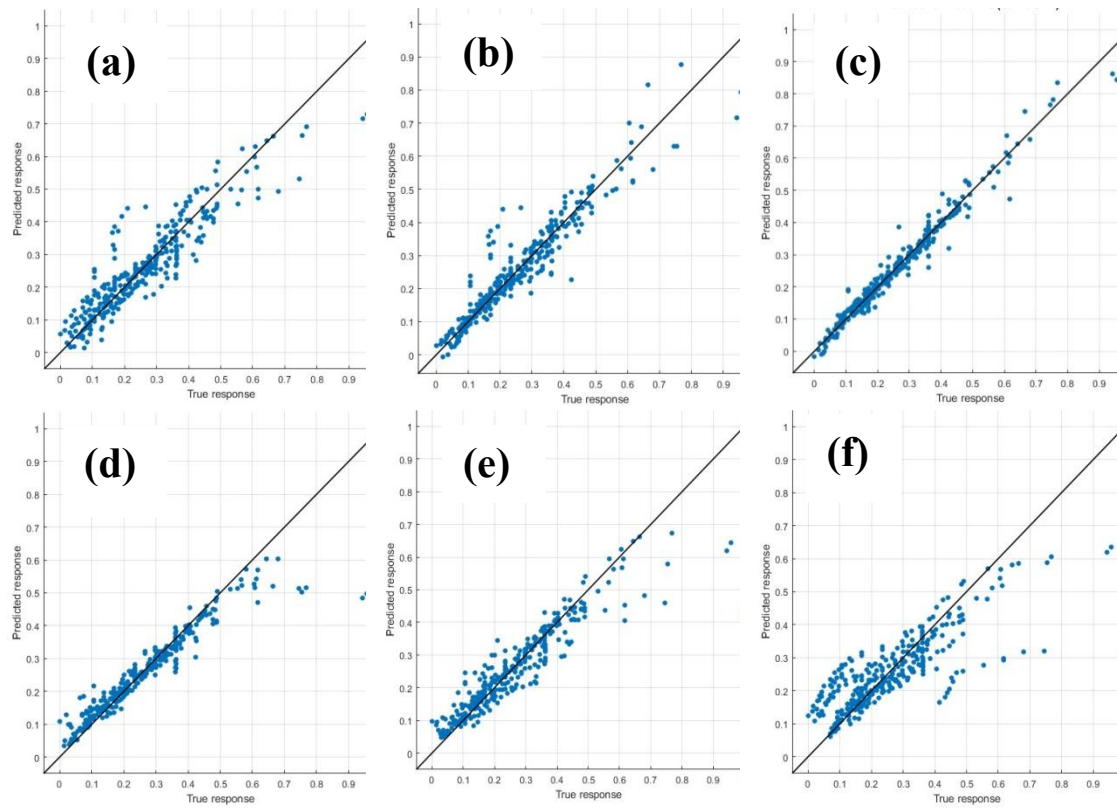
Figure 6.3: Predicted vs. True response curves of output flux for support vector machines of the training and validation (a) Linear SVM (b) Quadratic SVM (c)

Cubic SVM (d) Fine Gaussian SVM (e) Medium Gaussian SVM (f) Coarse Gaussian SVM

The Predicted vs. True response curves of output flux for Gaussian process regression models are shown in Figure 6.4
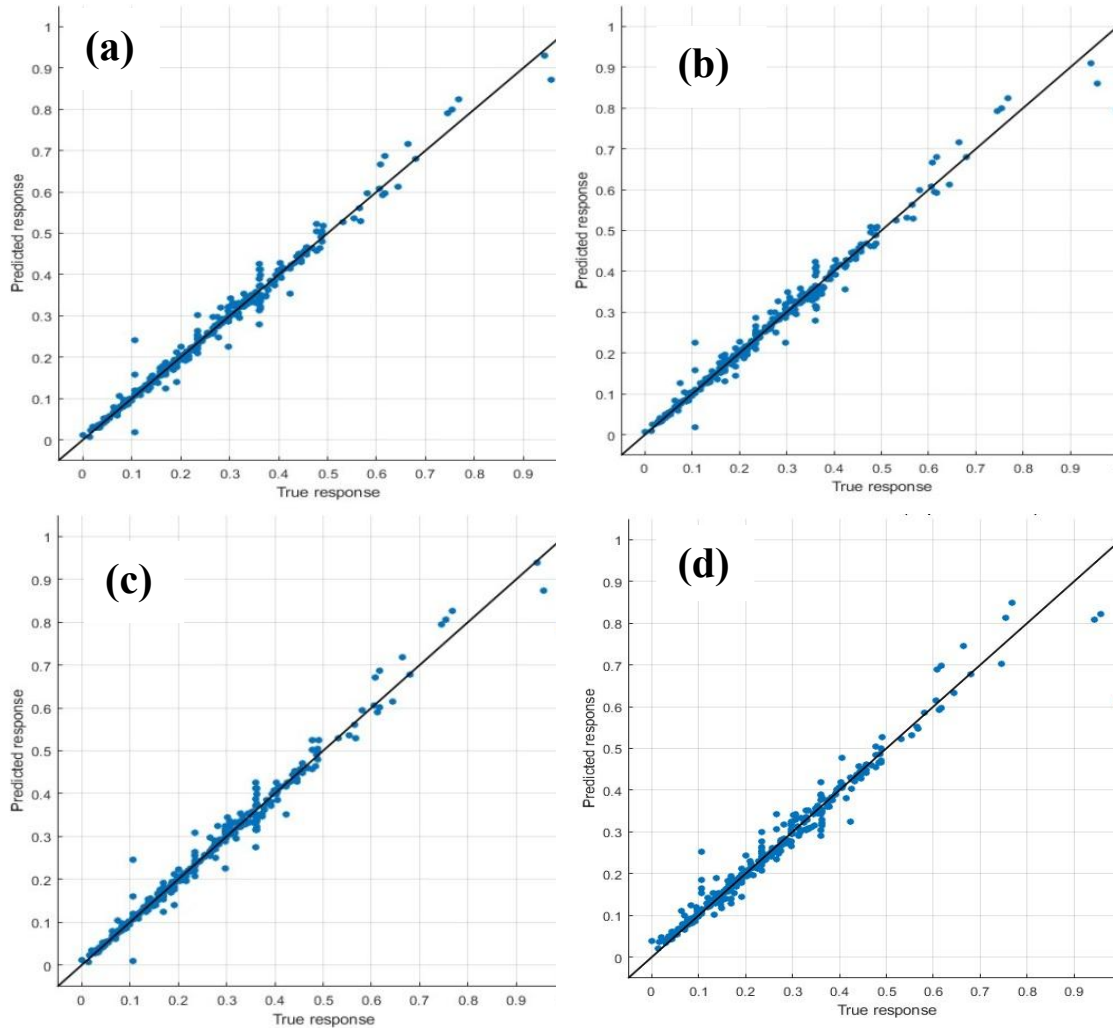
Figure 6.4: Predicted vs. True response curves of output flux for Gaussian process regression models of the training and validation (a) Rational Quadratic GPR (b) Squared Exponential GPR (c) Matern 5/2 GPR (d) Exponential GPR

The Predicted vs. True response curves of output flux for Kernel approximation regression models are shown in Figure 6.5
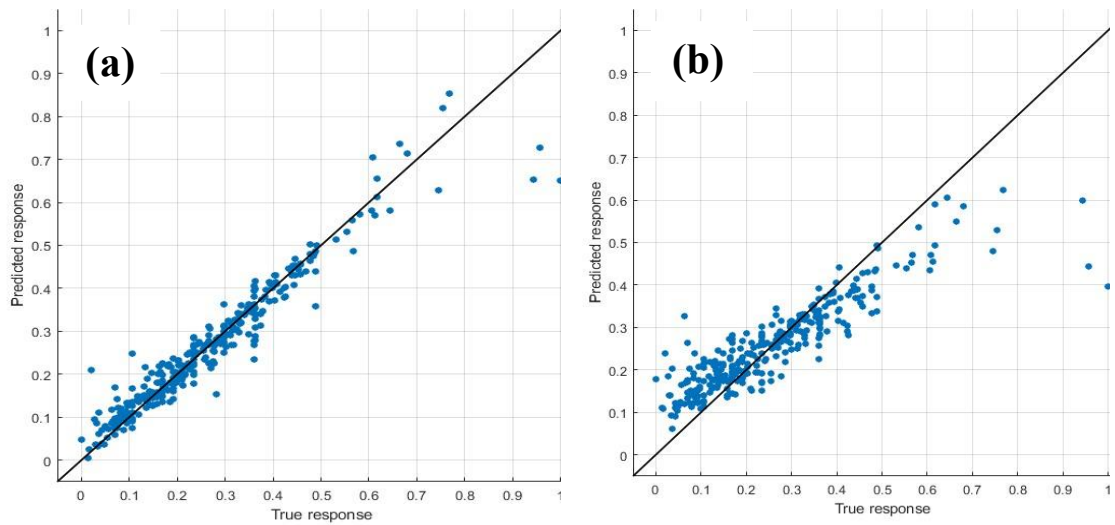
Figure 6.5: Predicted vs. True response curves of output flux for Kernel approximation regression models of the training and validation (a) SVM Kernel (b) Least Squares Regression Kernel

The Predicted vs. True response curves of output flux for Ensemble of Trees models are shown in Figure 6.6
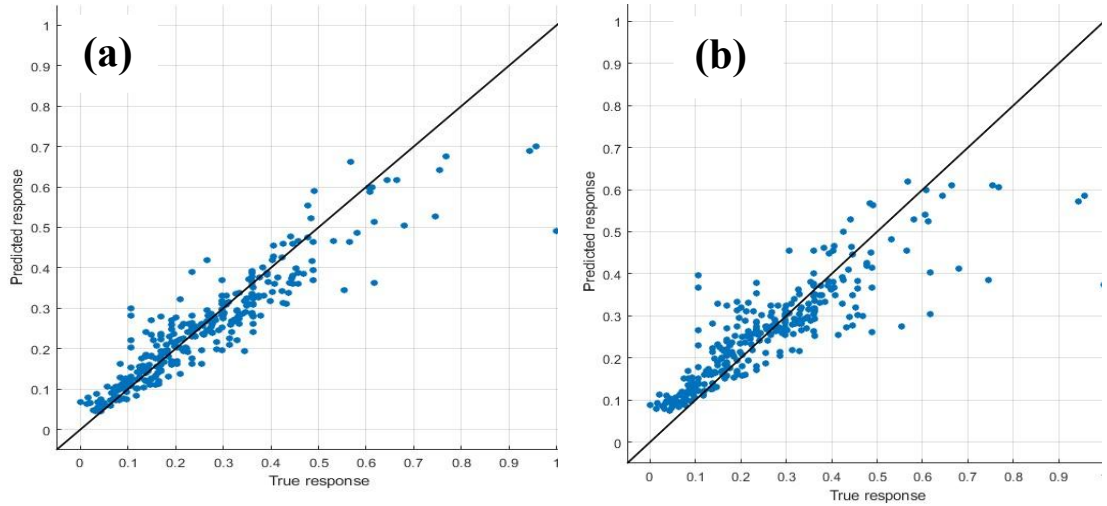
Figure 6.6: Predicted vs. True response curves of output flux for Ensemble of Trees models of the training and validation (a) Boosted Trees (b) Bagged Trees

The Predicted vs. True response curves of output flux for Neural Network models are shown in Figure 6.7
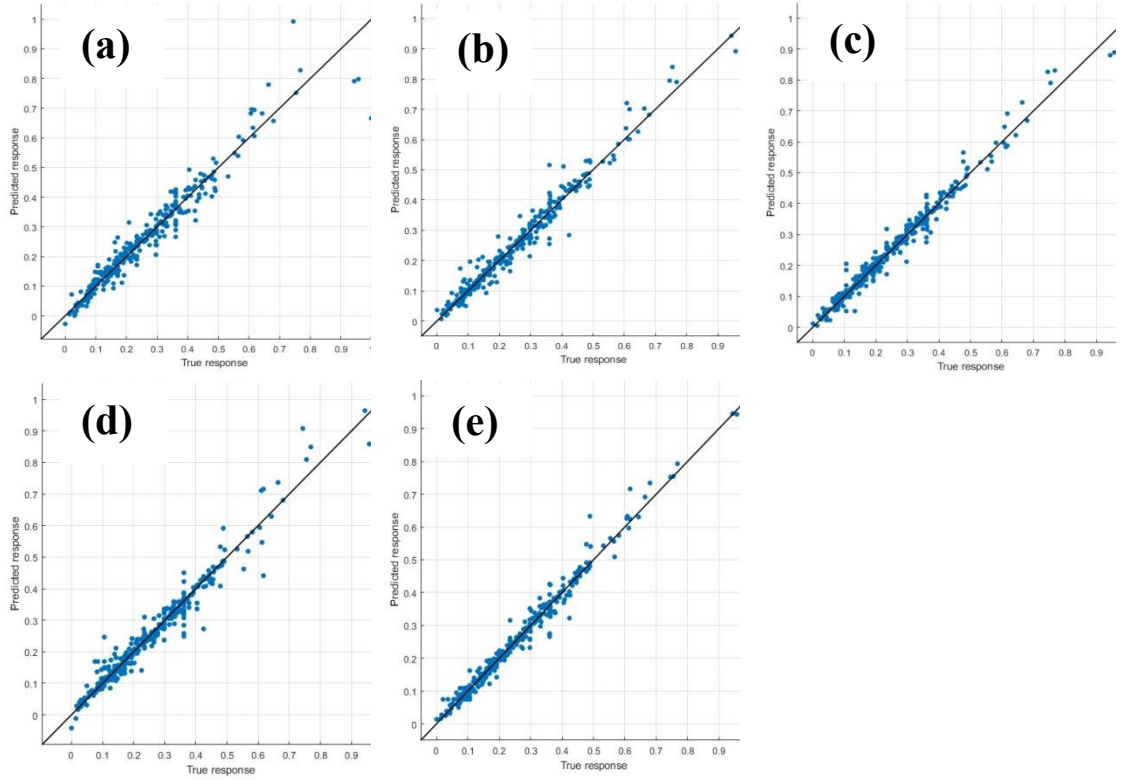
Figure 6.7: Predicted vs. True response curves of output flux for Neural Networks models of the training and validation (a) Narrow Neural Networks (b) Medium Neural Networks (c) Wide Neural Networks (d) Bilayered Neural Networks (e) Trilayered Neural Networks

The comprehensive analysis of the predictive models revealed a clear hierarchy in performance based on the coefficient of determination (R^2). Gaussian Process Regression (GPR) models demonstrated exceptional predictive capability at $R^2 = 0.98$ across Rational Quadratic, Squared Exponential and Matern 5/2 variants. This indicates their superior ability to explain 98% of the data variance. Following closely behind were the Neural Network architectures, with Wide and Trilayered Neural Networks achieving $R^2 = 0.97$, while Medium Neural Networks and Exponential GPR reached $R^2 = 0.96$, and Cubic SVM attained $R^2 = 0.95$. The high-performing category included Narrow and Bilayered Neural Networks ($R^2 = 0.94$), SVM Kernel ($R^2 = 0.92$) and linear variants such as Interactions Linear ($R^2 = 0.91$) and Stepwise Linear ($R^2 = 0.90$). Good performance was demonstrated by Quadratic SVM ($R^2 = 0.88$), Fine Gaussian SVM ($R^2 = 0.85$) and several models clustered around $R^2 = 0.83$ - 0.84, including Linear, Medium Gaussian SVM, Linear SVM, Robust Linear and

Boosted Trees. Moderate performance was observed in Least Squares Regression Kernel (R^2 = 0.74), Fine Tree and Bagged Trees (both R^2 = 0.72), while lower performance was seen in Coarse Gaussian SVM (R^2 = 0.63), Medium Tree (R^2 = 0.60) and notably poor performance in Coarse Tree (R^2 = 0.39). The analysis revealed that complex models, particularly GPR and Neural Networks, consistently outperformed simpler approaches by achieving better R^2 values. This pattern was further supported by the RMSE values, where models with higher R^2 values consistently showed lower RMSE values, with GPR models achieving the lowest RMSE values around 0.024. The poor performance of simpler tree-based models suggests that the underlying data structure likely contains complex, non-linear relationships that require more sophisticated modeling approaches for effective capture and prediction.

6.2.2 Optimization of Hidden layers (HL) and neurons (N)

6.2.2.1 Data split ratio of 70:15:15

Table 6.2 presents the evaluated configurations of hidden layers and neurons for the 70:15:15 data split ratio. Using two hidden layers as the default configuration, the optimal architectures are highlighted in bold italics within the table.

Table 6.2: Model performance metrics across phases using two hidden layers with varying neuron configurations (70:15:15 data split)

HL	N	Training (218 observations)		Validation (47 observations)		Testing (47 observations)	
		MSE	R^2	MSE	R^2	MSE	R^2
2	1	0.0033	0.9300	0.0022	0.9391	0.0106	0.8831
2	5	0.0041	0.9223	0.0024	0.9485	0.0042	0.9327
2	10	0.0001	0.9974	0.0021	0.9686	0.0008	0.9839
2	15	0.00005418	0.9989	0.00098079	0.9905	0.00014646	0.9958
2	20	0.00003187	0.9993	0.00073758	0.9912	0.00043781	0.9942
2	25	0.0011	0.9793	0.0018	0.9671	0.0026	0.9534
2	30	0.00012108	0.9980	0.0003113	0.9921	0.00022256	0.9950
2	35	0.000031507	0.9994	0.00048129	0.9915	0.00048392	0.9935
2	40	0.000036308	0.9992	0.00044939	0.9929	0.00088486	0.9905
2	45	0.0007	0.9877	0.0013	0.9803	0.0020	0.9598
2	50	0.00004904	0.9992	0.00020482	0.9931	0.00082641	0.9863

2	55	0.000074443	0.9987	0.00029566	0.9934	0.00052964	0.9893
2	60	0.000020852	0.9996	0.0004216	0.9897	0.00076632	0.9848
2	65	0.00023066	0.9959	0.0005279	0.9889	0.00081041	0.9875
2	70	0.00026109	0.9954	0.00049688	0.9911	0.00093686	0.9770
2	75	0.0001533	0.9972	0.00098177	0.9792	0.00095502	0.9894
2	80	0.0000	0.9996	0.0004	0.9947	0.0033	0.9668
2	85	0.0001	0.9986	0.0006	0.9869	0.0012	0.9817
2	90	0.000020045	0.9997	0.00032944	0.9944	0.00030521	0.9902
2	95	0.000016439	0.9997	0.00060198	0.9935	0.00089194	0.9754
2	*100*	*0.000036522*	*0.9994*	*0.00022592*	*0.9935*	*0.00044681*	*0.9896*
HL - Hidden layers N - Number of neurons							

The influence of the varying number of neurons is depicted in Figure 6.8. Based on the neural network training results in Table 6.2, the optimum configuration was found to be 2 hidden layers with 100 neurons, which demonstrated exceptional performance metrics across all evaluation sets. This configuration achieved a remarkably low training MSE of 0.000036522 with a corresponding R^2 value of 0.9994, indicating excellent model fit during the training phase. The validation performance maintained strong consistency with an MSE of 0.00022592 and R^2 of 0.9935, while the test set performance showed robust generalization with an MSE of 0.00044681 and R^2 of 0.9896. When compared to other configurations, particularly those with fewer neurons (N < 50) which showed higher MSE values and less consistent performance, this configuration represented an optimal balance between model complexity and predictive accuracy. The relatively small gap between training and test performance metrics suggests effective generalization without overfitting, which is crucial for practical applications. Notably, while some configurations with fewer neurons (such as N=90 with training MSE of 0.000020045 and R^2 of 0.9997) showed slightly better individual metrics, they demonstrated less consistency across the validation and test sets. The selected configuration's balanced performance across all three datasets (training, validation and test) provides strong evidence for its selection as the optimal architecture. It offers sufficient network capacity to capture complex patterns while maintaining computational efficiency and avoiding the diminishing returns observed in larger configurations.
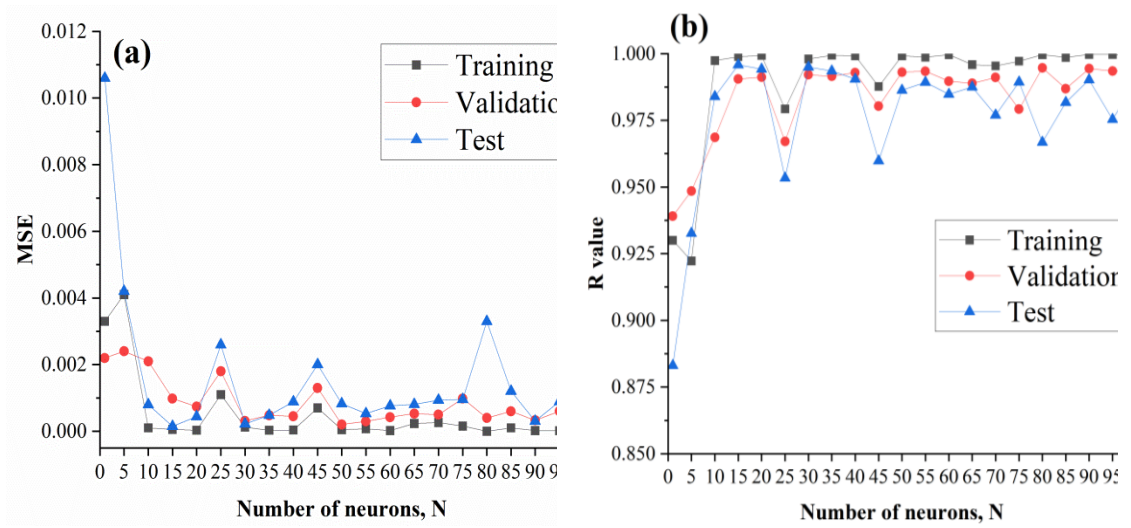
Figure 6.8: Influence of varying number of neurons (70:15:15 data split) (a) MSE
(b) R-squared

The consistent R^2 values above 0.989 across all evaluation sets further validate this
architecture's robust predictive capabilities and stability.

6.2.2.2 Data split ratio of 80:10:10

Table 6.3 presents the evaluated configurations of hidden layers and neurons for the
80:10:10 data split ratio. Using two hidden layers as the default configuration, the
optimal architectures are highlighted in bold italics within the table.

Table 6.3: Model performance metrics across phases using two hidden layers with
varying neuron configurations (80:10:10 data split)

HL	N	Training (250 observations)		Validation (31 observations)		Test (31 observations)	
		MSE	R^2	MSE	R^2	MSE	R^2
2	1	0.0038	0.9295	0.0049	0.8535	0.0055	0.9084
2	5	0.0024	0.9560	0.0011	0.9534	0.0021	0.9753
2	10	0.0001	0.9979	0.0023	0.9767	0.0005	0.9819
2	15	0.000089201	0.9985	0.00068519	0.9796	0.0007122	0.9864
2	20	0.000067825	0.9986	0.00060991	0.9923	0.00059379	0.9949
2	25	0.000039561	0.9993	0.00046567	0.9783	0.00076685	0.9915
2	30	0.0000	0.9991	0.0009	0.9777	0.0055	0.9461
2	35	0.00038875	0.9931	0.00038377	0.9936	0.00040321	0.9876
2	40	0.00012655	0.9977	0.00031432	0.9940	0.00065144	0.9881
2	45	0.0002	0.9951	0.0001	0.9976	0.0017	0.9839

HL	N						
2	50	0.000061611	0.9989	0.00056667	0.9873	0.00017158	0.9953
2	55	0.00016125	0.9972	0.00035239	0.9897	0.00027492	0.9955
2	60	0.0001	0.9986	0.0003	0.9949	0.0058	0.9439
2	*65*	*0.000016488*	*0.9997*	*0.00092097*	*0.9899*	*0.00035835*	*0.9928*
2	70	0.0000	0.9992	0.0005	0.9913	0.0016	0.9806
2	75	0.0000	0.9992	0.0001	0.9973	0.0011	0.9875
2	80	0.00010109	0.9983	0.00016087	0.9943	0.00071315	0.9846
2	85	0.00027877	0.9995	0.00044373	0.9884	0.00043259	0.9913
2	90	0.000021065	0.9996	0.00038238	0.9946	0.00025404	0.9926
2	95	0.0000	0.9998	0.0002	0.9936	0.0011	0.9817
2	100	0.0001	0.9981	0.0011	0.9877	0.0010	0.9559
HL - Hidden Layers			*N - Number of neurons*				

The influence of the varying number of neurons is depicted in Figure 6.9. Based on comprehensive analysis of the neural network performance data in Table 6.3, the optimal configuration with 2 hidden layers and 65 neurons demonstrated exceptional predictive capabilities and generalization performance. This is evidenced by the outstanding training performance (MSE = 0.000016488, R^2 = 0.9997), robust validation metrics (MSE = 0.00092097, R^2 = 0.9899) and strong test set performance (MSE = 0.00035835, R^2 = 0.9928). This configuration was selected as optimal because it achieves the best balance between model complexity and performance, exhibiting the lowest training MSE among all tested configurations while maintaining excellent generalization ability across validation and test sets. The architecture with 65 neurons' superior performance is further supported by its consistently high R^2 values across all three datasets. This indicates excellent explanatory power and robust generalization, with the test set R^2 of 0.9928 suggesting that the model captures the underlying patterns in the data without memorizing noise, which is crucial for real-world applications.
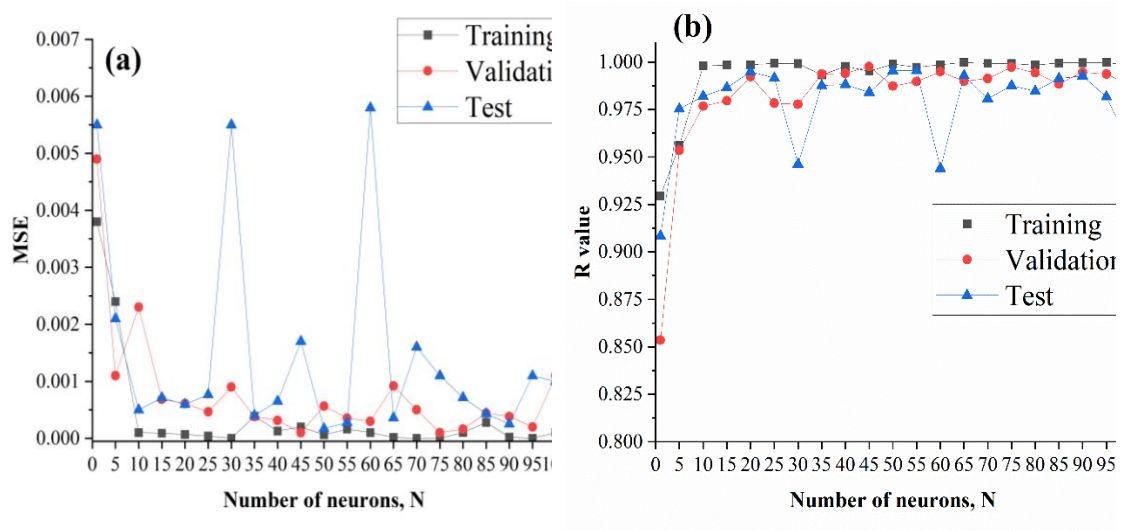
Figure 6.9: Influence of varying number of neurons (80:10:10 data split) (a) MSE
(b) R-squared

6.2.2.3 Data split ratio of 90:5:5

Table 6.4 presents the evaluated configurations of hidden layers and neurons for the 90:5:5 data split ratio. Using two hidden layers as the default configuration, the optimal architectures are highlighted in bold italics within the table.

Table 6.4: Model performance metrics across phases using two hidden layers with varying neuron configurations (90:5:5 data split)

HL	N	Training (280 observations)		Validation (16 observations)		Test (16 observations)	
		MSE	R^2	MSE	R^2	MSE	R^2
2	1	0.0041	0.9212	0.0028	0.9315	0.0036	0.9413
2	5	0.0013	0.9759	0.0004	0.9965	0.0010	0.9807
2	10	0.0001	0.9989	0.0030	0.9896	0.0004	0.9909
2	15	0.0005	0.9908	0.0003	0.9925	0.0058	0.8564
2	20	0.0021	0.9626	0.0007	0.9789	0.0009	0.9684
2	25	0.0002	0.9970	0.0005	0.9939	0.0018	0.9921
2	30	0.00043828	0.9929	0.00031464	0.9884	0.00094974	0.9799
2	35	0.0006	0.9885	0.0005	0.9909	0.0023	0.9680
2	40	0.00014318	0.9973	0.00024682	0.9941	0.00072432	0.9977
2	45	0.00013343	0.9975	0.00024705	0.9953	0.0003033	0.9956
2	50	0.0001	0.9978	0.0001	0.9976	0.0010	0.9913
2	55	0.00020579	0.9962	0.00019831	0.9970	0.00051261	0.9904
2	60	0.000034296	0.9994	0.00039189	0.9804	0.00015195	0.9980
2	*65*	*0.000013184*	*0.9998*	*0.000054543*	*0.9990*	*0.000050275*	*0.9984*

2	70	0.000062910	0.9989	0.00025718	0.9877	0.00040564	0.9905
2	75	0.0000	0.9994	0.0011	0.9952	0.0002	0.9939
2	80	0.000046563	0.9992	0.00017597	0.9961	0.00017966	0.9983
2	85	0.000055164	0.9990	0.00027855	0.9951	0.00060678	0.9780
2	90	0.00013017	0.9977	0.00033628	0.9930	0.00040557	0.9902
2	95	0.000045532	0.9992	0.000033418	0.9991	0.000096146	0.9980
2	100	0.00013561	0.9974	0.00015810	0.9973	0.00034860	0.9954
HL - Hidden Layers N - Number of neurons						

The influence of the varying number of neurons is depicted in Figure 6.10. The extensive parametric study of a two-hidden-layer neural network architecture from Table 6.4 revealed that the optimal configuration was achieved with 65 neurons, demonstrating superior performance metrics across all three data partitions. This configuration yielded remarkably low MSE values of 0.000013184, 0.000054543 and 0.000050275 for training, validation and testing sets respectively, accompanied by exceptionally high R^2 values of 0.9998, 0.9990 and 0.9984. The selection of 65 neurons as the optimal architecture is justified by several key observations.
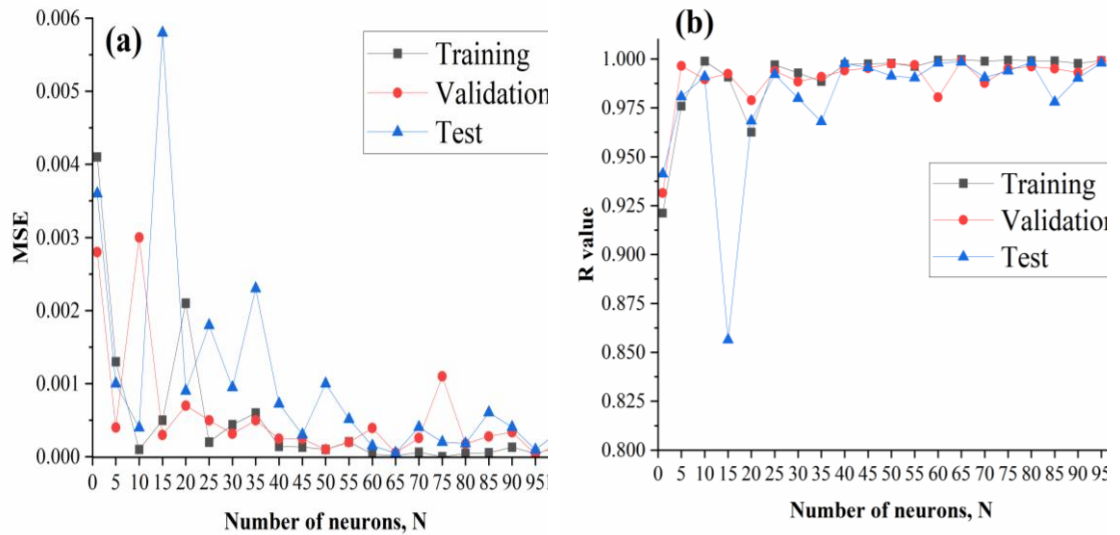
Figure 6.10: Influence of varying number of neurons (90:5:5 data split) (a) MSE (b) R-squared

Firstly, it achieved the most balanced performance across all three datasets, indicating robust generalization capability without overfitting. Secondly, it demonstrated a three-fold improvement in MSE compared to the next best

configuration (60 neurons) during training, while maintaining superior performance in both validation and testing phases. Thirdly, while some configurations (such as 75 and 80 neurons) showed comparable performance in individual metrics, they failed to maintain consistent excellence across all evaluation criteria. The progressive improvement in network performance from 1 to 65 neurons, followed by a slight degradation or inconsistent performance beyond 65 neurons, suggests that this configuration strikes an optimal balance between network complexity and generalization ability. This is further supported by the negligible difference between training and testing performance metrics, indicating that the network successfully captured the underlying patterns in the data without memorizing the training set, a crucial consideration for practical applications.

6.2.3 Optimal Trained ANN FO model results

6.2.3.1 70:15:15 data split

The performance evaluation of the ANN model for the data split ratio of 70:15:15 is shown in Figure 6.11
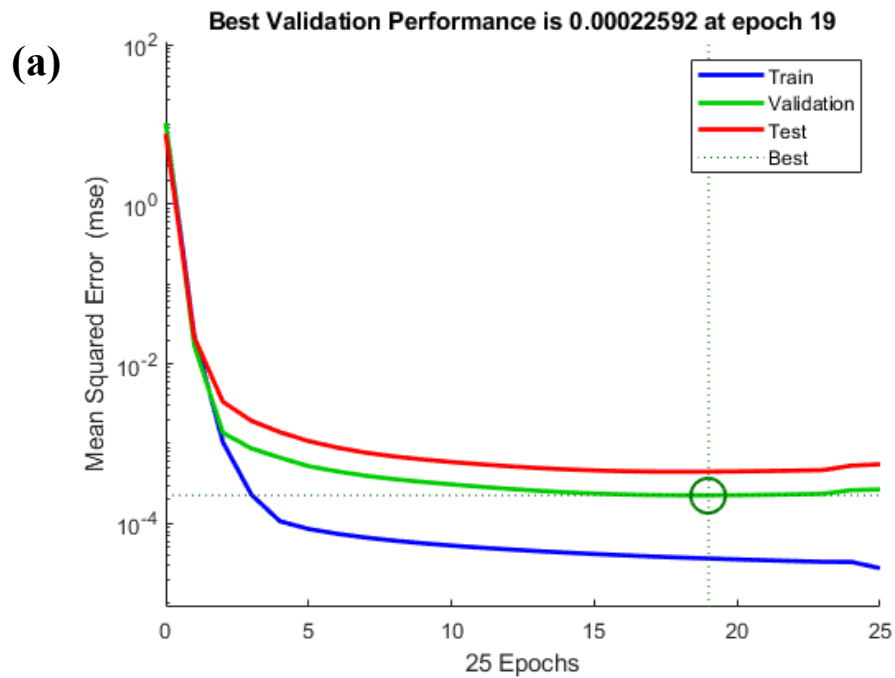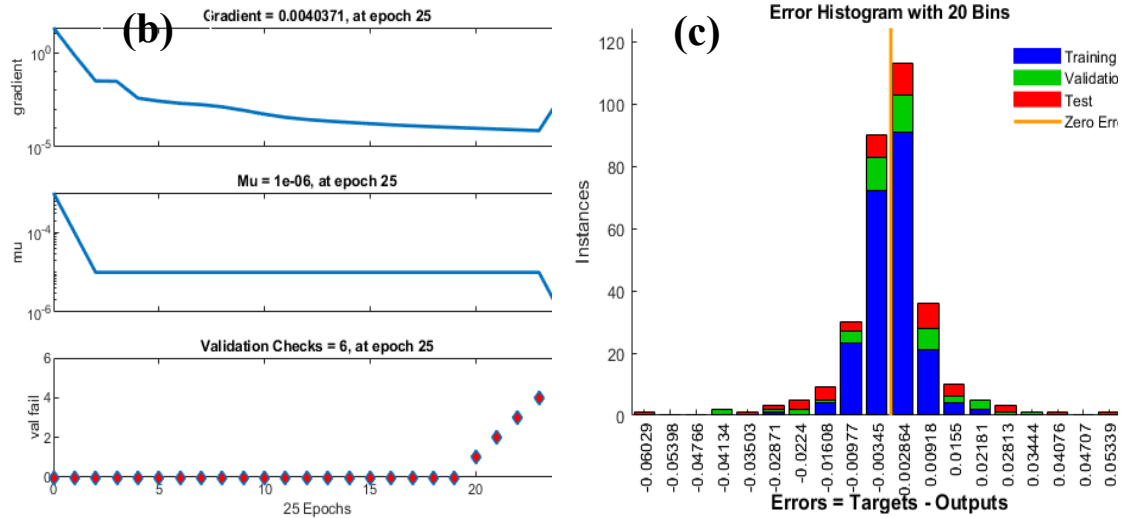
Figure 6.11: Performance evaluation for 70:15:15 data split (a) Best validation performance (b) Training state plot (c) Error Histogram plot

The ANN modeling results from Figure 6.11 demonstrate several key characteristics indicative of successful neural network training and performance. The training performance plot shows the MSE progression over 25 epochs, with the best validation performance achieved at epoch 19 with MSE of 0.00022592. The training curve exhibits consistent error reduction, while validation and test curves follow similar trajectories. This indicates good generalization without significant overfitting since the validation error does not increase after the best epoch. The error histogram, divided into 20 bins, displays a roughly normal distribution of network errors concentrated near zero, with similar error patterns across training, validation, and test sets, and minimal outliers in the tail regions. The observed convergence pattern, early stopping implementation at epoch 19, well-balanced error distribution across datasets, and appropriately tuned training parameters collectively indicate a robust and well-performing neural network model suitable for the intended application. The close alignment between training, validation and test performance metrics suggests good generalization capabilities and reliable model predictions across different data subsets.

Figure 6.12 presents the regression analysis for the ANN model's training, validation and testing stages, illustrating the relationship between targeted and predicted outputs for the 70:15:15 data split.
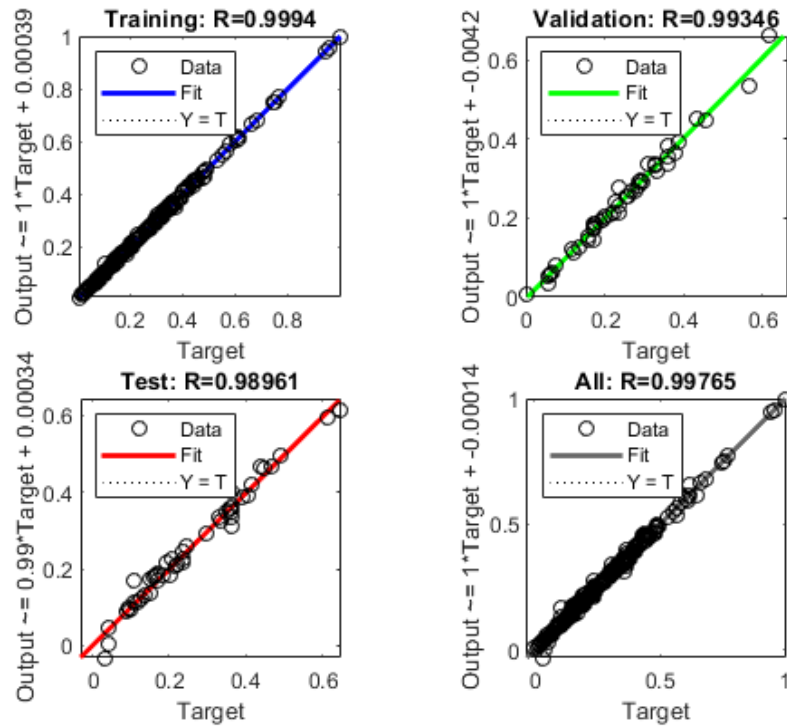
Figure 6.12: Trained ANN FO model results for regression analysis for 70:15:15 data split

The regression analysis plots from Figure 6.12 demonstrate comprehensive model performance through multiple correlation metrics. The training dataset shows exceptional correlation ($R^2 = 0.9994$), indicating nearly perfect prediction accuracy for the training data. The validation set maintains strong performance ($R^2 = 0.99346$) with minimal scatter, confirming robust generalization to unseen data. The test set exhibits continued high correlation ($R^2 = 0.98961$) with slightly increased but still acceptable scatter, validating the model's predictive capabilities on independent data. This all culminates in an impressive aggregate performance ($R^2 = 0.99765$). The outputs consistently match targets across the full value range, with evenly distributed data points along the regression line and minimal outliers. The high R-values across all subsets, combined with the consistent distribution patterns, demonstrate excellent model generalization, absence of overfitting (as evidenced by strong test performance), reliable prediction capability across the entire data range, balanced performance between training, validation, and test sets, and minimal bias in the model's predictions. This provides robust statistical evidence of a well-trained neural

network model suitable for accurate predictions within its trained domain. The regression plots clearly illustrate the model's strong predictive capabilities and successful training outcomes.

6.2.3.2 80:10:10 data split

The performance evaluation of the ANN model for the data split ratio of 80:10:10 is shown in Figure 6.13
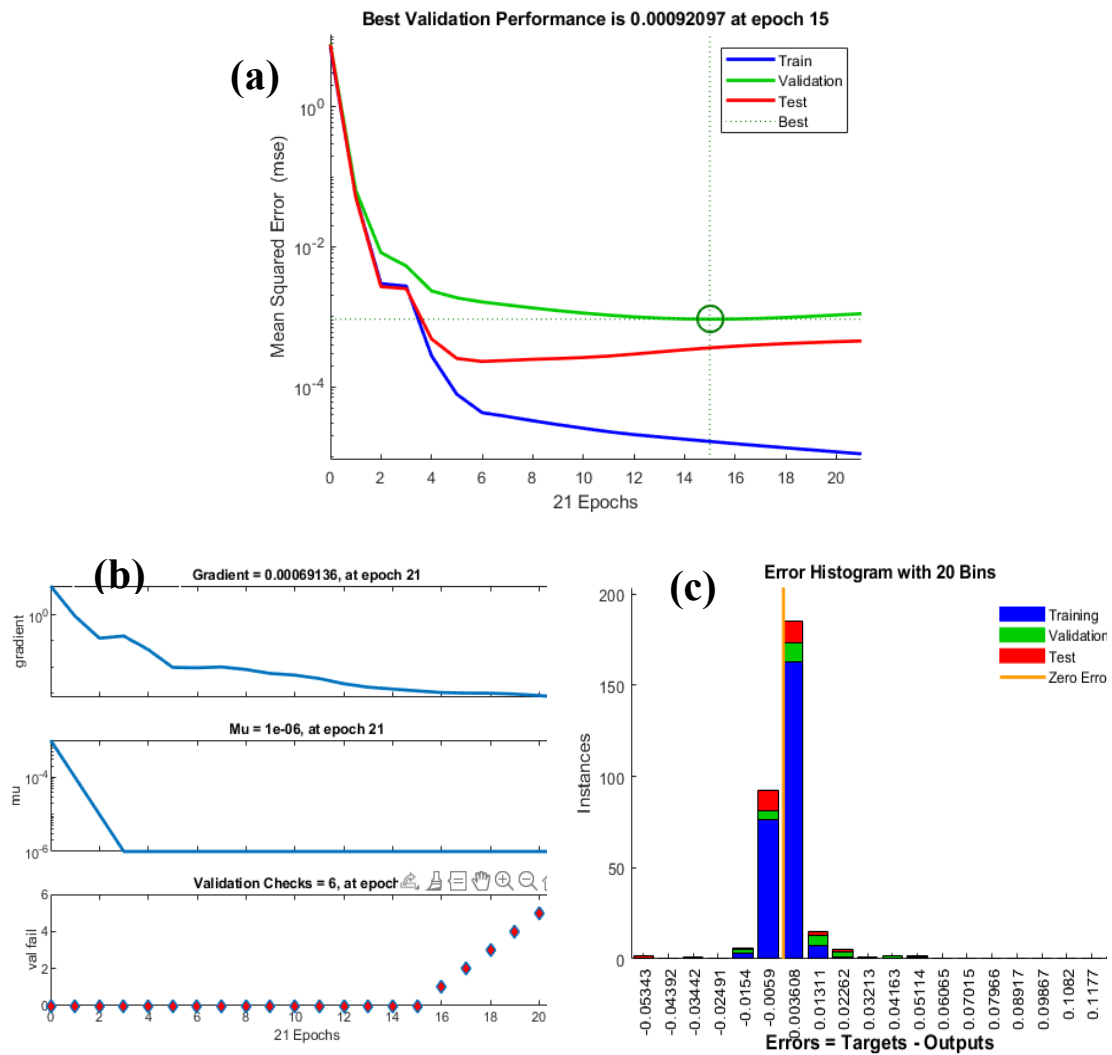
Figure 6.13: Performance evaluation for 80:10:10 data split (a) Best validation performance (b) Training state plot (c) Error Histogram plot

The modeling results from Figure 6.13 show optimized network performance with best validation at epoch 15 (MSE = 0.00092097). The training curve demonstrates

consistent error reduction, while validation and test curves follow similar patterns, indicating good generalization without severe overfitting. Training state plots reveal stable gradient values; appropriate Mu parameter adaptation and steady validation checks until final epochs. The error histogram shows a concentrated normal distribution near zero across all datasets, with minimal outliers. The parallel performance of training, validation and test sets, combined with early stopping at epoch 15, suggests a well-tuned model with robust prediction capabilities.

Figure 6.14 presents the regression analysis for the ANN model's training, validation and testing stages, illustrating the relationship between targeted and predicted outputs for the 80:10:10 data split.
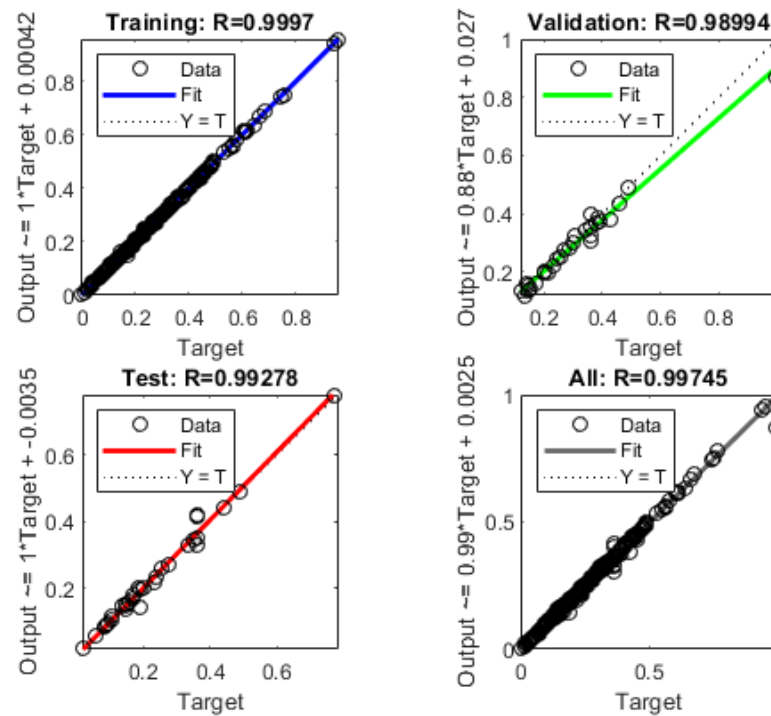
Figure 6.14: Trained ANN FO model results for regression analysis for 80:10:10 data split

The regression analysis results from Figure 6.14 shows exceptional performance across all datasets, with R^2 approaching unity: training ($R^2 = 0.9997$), validation ($R^2 = 0.98994$), test ($R^2 = 0.99278$) and overall ($R^2 = 0.99745$). The training phase exhibits remarkable accuracy, indicating optimal model convergence and learning of

underlying patterns. The validation phase maintains high performance with only minor deviations, particularly at higher values, suggesting robust model generalization. The test phase demonstrates consistent predictive capability despite fewer data points, reinforcing the model's reliability on unseen data. The aggregate performance shows exceptional consistency across all datasets with minimal deviation from the ideal Y=T line. The uniformly high R^2 values across all phases, coupled with the consistent clustering patterns around regression lines, definitively indicate successful model training, absence of overfitting, strong generalization capabilities and high prediction reliability, making this implementation particularly noteworthy for its consistency and accuracy across all evaluation metrics.

6.2.3.3 90:5:5 data split

The performance evaluation of the ANN model for the data split ratio of 90:5:5 is shown in Figure 6.15
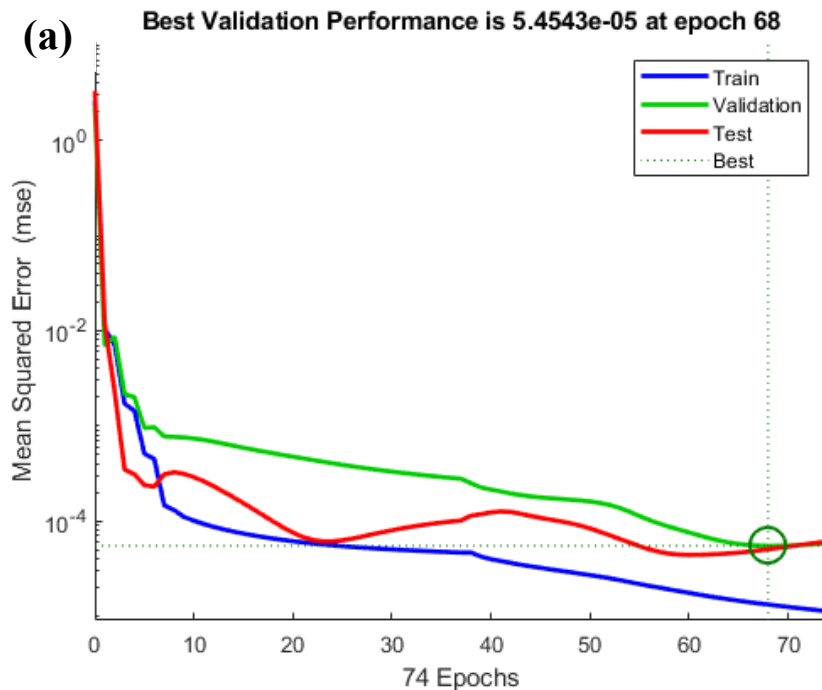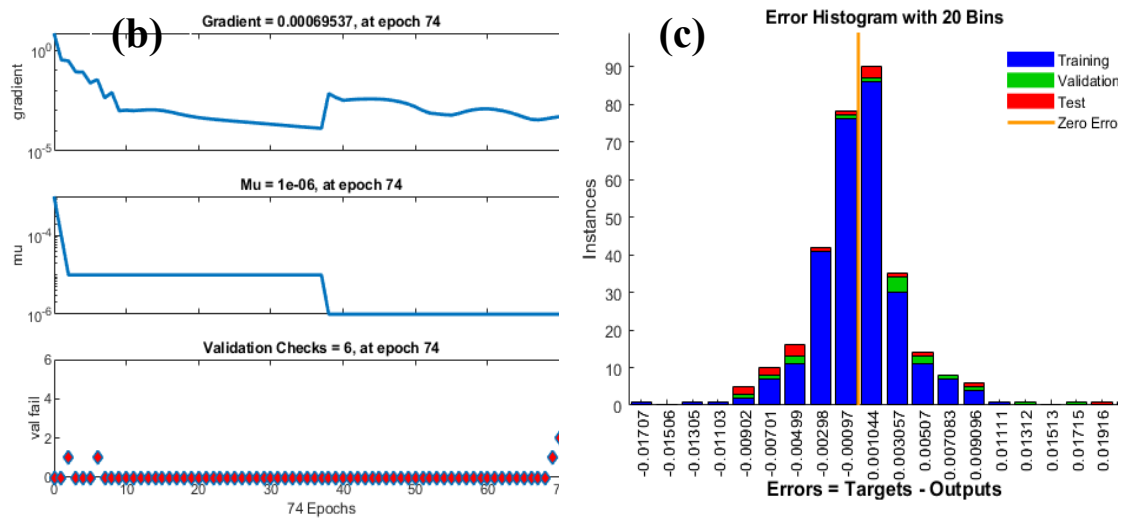
Figure 6.15: Performance evaluation for 90:5:5 data split (a) Best validation performance (b) Training state plot (c) Error Histogram plot

The results from Figure 6.15 demonstrate excellent network performance with best validation achieved at epoch 68 (MSE of 0.000054543). The training curve exhibits steady error reduction MSE over 74 epochs, while validation and test curves follow comparable trajectories, indicating robust generalization. Training state metrics show gradient stability with minor fluctuations; appropriate Mu parameter adaptation and consistent validation checks until later epochs. The error histogram presents a well-defined normal distribution centred near zero across all datasets, with balanced distribution between training, validation, and test sets. The extended training period of 74 epochs, combined with the gradual convergence and low final MSE, suggests a well-optimized model with strong predictive capabilities and minimal overfitting risk.

Figure 6.16 presents the regression analysis for the ANN model's training, validation and testing stages, illustrating the relationship between targeted and predicted outputs for the 90:5:5 data split
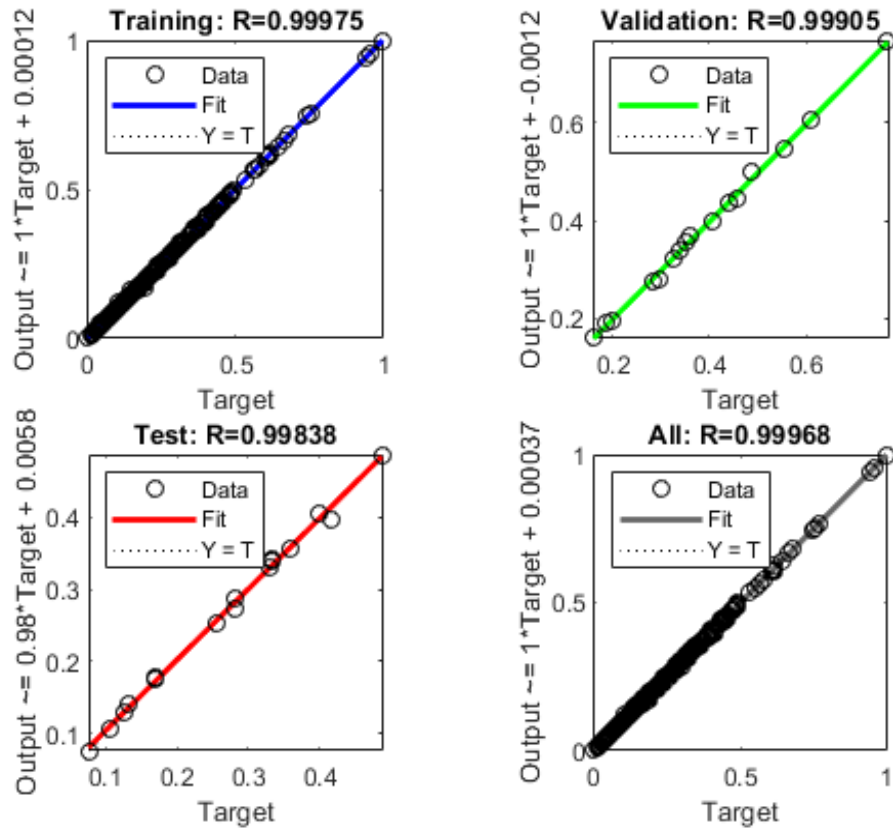
Figure 6.16: Trained ANN FO model results for regression analysis for 90:5:5 data split

The ANN regression analysis from Figure 6.16 demonstrates exceptional performance with remarkably high correlation coefficients: training ($R^2 = 0.99975$), validation ($R^2 = 0.99905$), test ($R^2 = 0.99838$) and overall ($R^2 = 0.99968$). The training phase shows optimal convergence with dense data points along the Y=T line. The validation maintains superior performance with minimal scatter whilst the test results confirm strong generalization despite a smaller sample size. The aggregate performance displays exceptional consistency. The uniformly high R^2 values and tight clustering around regression lines indicate successful training, absence of overfitting, robust generalization capabilities and high prediction reliability. The training plot shows near-perfect alignment, validation and test plots maintain high accuracy with minimal scatter and the overall plot confirms consistent performance across the entire dataset. This suggests optimal ANN architecture and training parameters for the given problem domain.

6.2.3.4 Comparison of the performances of the three data split ratios

When comparing the overall R^2 values, the 90:5:5 split achieved marginally better performance (0.99968) compared to 70:15:15 (0.99765) and 80:10:10 (0.99745), though all splits showed excellent results above 0.997. Training performance improved with larger training sets, as evidenced by R^2 values of 0.9994 (70:15:15), 0.9997 (80:10:10), and 0.99975 (90:5:5), suggesting more training data enhanced model learning. Examining the validation/test set trade-offs reveals that 70:15:15 maintained strong validation (0.99346) and test (0.98961) performance with larger evaluation sets. The 80:10:10 showed balanced validation (0.98994) and test (0.99278) results, while 90:5:5 achieved highest validation (0.99905) and test (0.99838) scores but with smallest evaluation sets. Critical analysis shows that while the 90:5:5 split demonstrates highest overall accuracy, it may have less reliable generalization assessment due to smaller validation/test sets. The 70:15:15 split provides most robust validation with larger evaluation sets despite slightly lower metrics. The 80:10:10 split offers good balance between training data and evaluation set sizes. While 90:5:5 shows best metrics, the 80:10:10 split likely offers optimal balance between model training and reliable performance assessment, as the larger validation/test sets in 70:15:15 provide more confidence in generalization capabilities despite marginally lower metrics.

The mean absolute percentage errors (MAPE) of the various novel organic draw solutions for the various FO runs and different data split ratios are shown in Table 6.5

Table 6.5: Mean absolute percentage errors for the various organic draw solutions at different data spilt ratios

Draw solution	FO Run	Feed solution (NaCl)	D.F.R (LPM)	F.F.R (LPM)	Exp. flux (LMH)	DSR of 70:15:15		DSR of 80:10:10		DSR of 90:5:5	
						J_v (LMH)	MAPE	J_v (LMH)	MAPE	J_v (LMH)	MAPE
0.5NaCMC-3.75PGPE	1	5000 ppm	0.20	0.20	14.303	14.299	0.0280	14.278	0.1748	14.314	0.0769
0.5NaCMC-3.75PGPE	2	5000 ppm	0.20	0.20	12.514	12.510	0.0320	12.508	0.0479	12.525	0.0879
0.5NaCMC-3.75PGPE	3	5000 ppm	0.20	0.20	11.927	11.923	0.0335	11.926	0.0084	11.938	0.0922
0.5NaCMC-3.75PGPE	1	5000 ppm	0.15	0.20	9.006	9.002	0.0444	9.035	0.3220	9.017	0.1221
0.5NaCMC-3.75PGPE	2	5000 ppm	0.15	0.20	7.769	7.765	0.0515	7.810	0.5277	7.780	0.1416
0.5NaCMC-3.75PGPE	3	5000 ppm	0.15	0.20	8.534	8.530	0.0469	8.568	0.3984	8.545	0.1289
0.5NaCMC-3.75PGPE	1	5000 ppm	0.25	0.20	15.361	15.357	0.0260	15.326	0.2278	15.372	0.0716
0.5NaCMC-3.75PGPE	2	5000 ppm	0.25	0.20	14.221	14.217	0.0281	14.197	0.1688	14.232	0.0774
0.5NaCMC-3.75PGPE	3	5000 ppm	0.25	0.20	14.727	14.723	0.0272	14.698	0.1969	14.738	0.0747
0.5NaCMC-3.75PGPE	1	5000 ppm	0.20	0.15	7.629	7.625	0.0524	7.671	0.5505	7.640	0.1442
0.5NaCMC-3.75PGPE	2	5000 ppm	0.20	0.15	7.760	7.756	0.0515	7.801	0.5284	7.771	0.1418
40PGPE	1	35 000 ppm	0.20	0.15	22.436	22.432	0.0178	22.330	0.4725	22.447	0.0490
40PGPE	2	35 000 ppm	0.20	0.15	19.738	19.734	0.0203	19.659	0.4002	19.749	0.0557
0.5HPC-3.75PGPE	1	1000 ppm	0.40	0.40	19.793	19.789	0.0202	19.713	0.4042	19.804	0.0556
0.5HPC-3.75PGPE	2	1000 ppm	0.40	0.40	13.618	13.614	0.0294	13.600	0.1322	13.629	0.0808
0.75HPC-3.75PGPE	1	1000 ppm	0.40	0.40	8.612	8.608	0.0464	8.645	0.3832	8.623	0.1277
0.75HPC-3.75PGPE	2	1000 ppm	0.40	0.40	8.093	8.089	0.0494	8.131	0.4695	8.104	0.1359
0.5NaCMC-3.75PGPE	1	1000 ppm	0.20	0.15	12.173	12.169	0.0329	12.169	0.0329	12.184	0.0904
0.5NaCMC-3.75PGPE	2	1000 ppm	0.20	0.15	11.899	11.895	0.0336	11.899	0.0000	11.910	0.0924
0.5NaCMC-3.75PGPE	3	1000 ppm	0.20	0.15	10.140	10.136	0.0394	10.157	0.1677	10.151	0.1085

0.5NaCMC-3.75PGPE	4	1000 ppm	0.20	0.15	8.772	8.768	0.0456	8.803	0.3534	8.783	0.1254
0.5NaCMC-20PGPE	1	35 000 ppm	0.20	0.15	13.975	13.972	0.0215	13.954	0.1503	13.987	0.0859
0.5NaCMC-20PGPE	2	35 000 ppm	0.20	0.15	14.284	14.280	0.0280	14.260	0.1680	14.295	0.0770
0.25HPC-3.75PGPE	1	1000 ppm	0.20	0.40	11.062	11.058	0.0362	11.070	0.0723	11.073	0.0994
0.25HPC-3.75PGPE	2	1000 ppm	0.20	0.40	9.852	9.848	0.0406	9.873	0.2132	9.863	0.1117
0.25HPC-3.75PGPE	3	1000 ppm	0.20	0.40	9.242	9.238	0.0433	9.268	0.2813	9.253	0.1190
DFR – draw flow rate FFR – feed flow rate DSR – data split ratio MAPE – mean absolute percentage error											

The examination of MAPE across various data split ratios (DSR) revealed that the 70:15:15 partition consistently demonstrates superior predictive accuracy, exhibiting remarkably low MAPE values ranging from 0.0178% to 0.0524% with a mean of 0.036% across all draw solutions. In contrast, the 80:10:10 partition exhibits the highest variability and magnitude of errors, with MAPE values spanning from 0.0% to 0.5505% and a mean of 0.264%. The 90:5:5 partition presents intermediate performance, with MAPE values ranging from 0.049% to 0.1442% and a mean of 0.1%. These findings strongly indicate that the 70:15:15 partition ratio provides optimal predictive accuracy across the spectrum of draw solutions and experimental conditions within this dataset.

6.2.4   Techno-economic assessment

The cost distribution analysis for the stand-alone FO system is presented in Figure 6.17a, delineating both OPEX and CAPEX components. The most significant contributors to the total costs were ancillary operational parameters (labour, maintenance and cleaning chemicals), accounting for 31.86% of the total expenditure. Power consumption-related operating costs followed at 24.73%, while the capital costs for the feed solution pump represented 19.15% of the total costs. Other notable cost factors included capital costs for the draw solution pump (6.38%), FO membrane (1.99%) and site development (5.51%). Indirect capital and membrane replacement operating costs contributed 9.91% and 0.47%, respectively. The annual operating costs were $ 23 273.92, with annual capital costs amounting to $ 17 487.60. The yearly cost per unit volume of produced water for the stand-alone FO system was determined to be 0.47 $ m^{-3}, based on a plant capacity of 160 m^3 d^{-1}. This water production cost is relatively high compared to other FO processes, primarily due to the slightly elevated costs associated with the organic draw solutions. However, it is essential to note that these draw solutions' high regeneration and reuse efficiency is expected to yield long-term cost savings for the overall process.
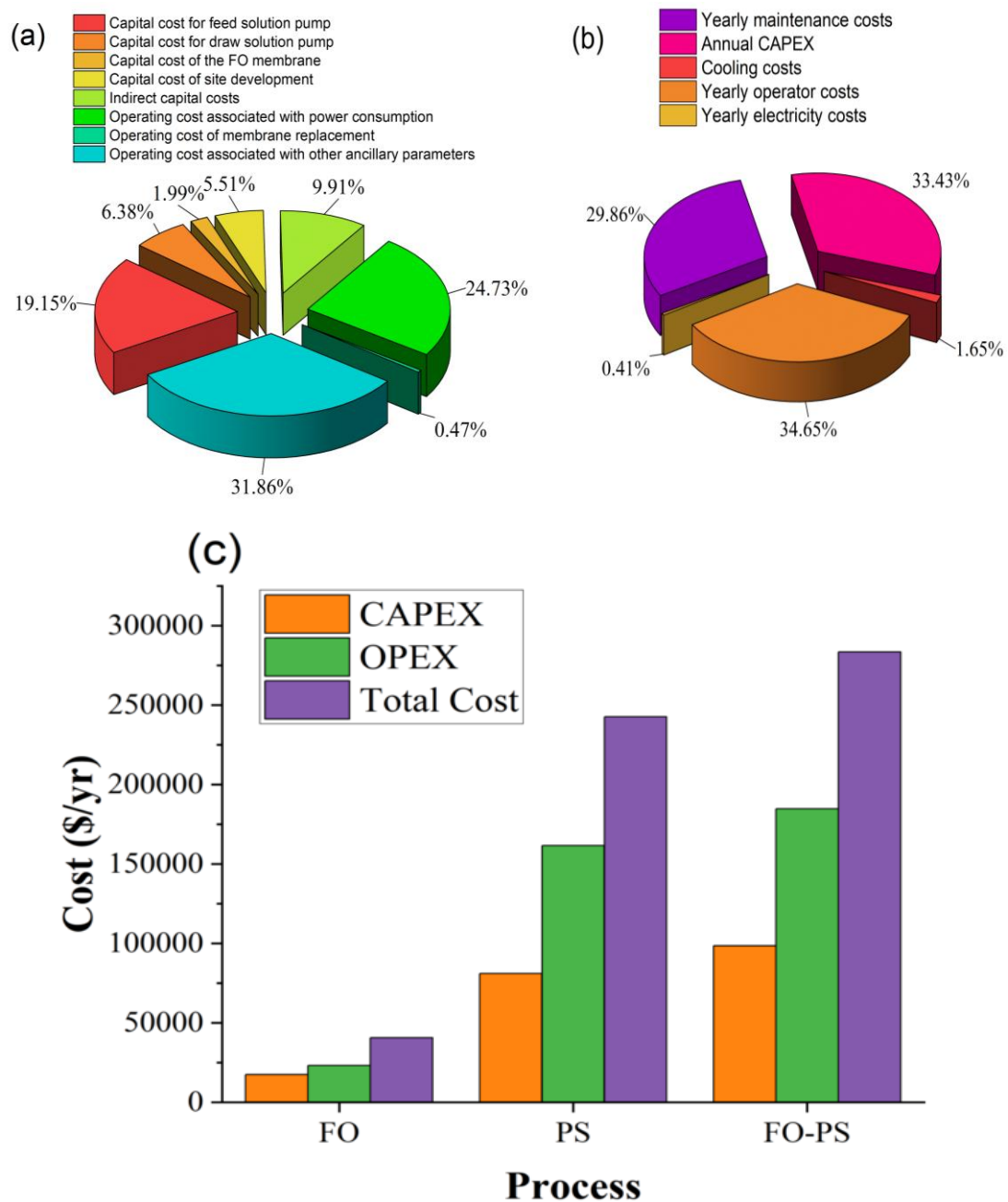
Figure 6.17: Total OPEX and CAPEX for (a) stand-alone FO, (b) PS and (c) annual costs for FO, PS, and combined FO-PS processes

Figure 6.17b illustrates the annual cost distribution for the PS regeneration process, delineating both CAPEX and OPEX components. The three primary cost contributors for the process were operator costs (34.65%), CAPEX (33.43%) and maintenance costs (29.86%). Yearly electricity and cooling costs contributed 0.41% and 1.65% to the total costs, respectively. The total installed equipment costs, based on Figure 2.4, were calculated to be $ 1 811 789.21. The total yearly costs for the PS

regeneration process were estimated at $ 242 691.18. The cost of steam was determined to be 1.60 $ ton^{-1}. This relatively low steam cost indicates potential for cost-effective operation, mainly if waste heat can be used. The economic feasibility of the FO-PS hybrid desalination system is contingent upon two critical factors, i.e., high efficiency in draw solution regeneration and reuse and utilization of industrial waste heat in the phase separation process. These findings emphasize optimizing regeneration and pursuing industrial symbiosis opportunities to leverage waste heat streams. Such integration could significantly enhance the system's economic viability by reducing energy costs and improving overall process efficiency. Furthermore, the substantial contribution of operator and maintenance costs to the total expenditure suggests that automation and predictive maintenance strategies could play a crucial role in enhancing the system's economic performance. Future research directions should focus on developing more efficient draw solutions, optimizing membrane performance and exploring innovative heat integration techniques to reduce operational costs further. The OPEX, CAPEX and total costs for the FO, PS and combined FO-PS processes are shown in Figure 6.17c.

6.3 References

1. Zubair, M. M., Saleem, H., & Zaidi, S. J. (2023). Recent progress in reverse osmosis modeling: An overview. Desalination, 564, 116705. https://doi.org/10.1016/j.desal.2023.116705

2. Tiwari, A. K., & Jain, M. (2024). A novel process for rutin recovery from model solutions using nanofiltration: Experimental study, mathematical modeling, and scale-up design. Journal of Food Process Engineering, 47(3), e14592. https://doi.org/10.1111/jfpe.14592

3. Ahmad, A., Chong, M., & Bhatia, S. (2006). Ultrafiltration modeling of multiple solutes system for continuous cross-flow process. Chemical Engineering Science, 61(15), 5057–5069. https://doi.org/10.1016/j.ces.2006.03.017

4. Kegl, T., Korenak, J., Bukšek, H., & Petrinić, I. (2024). Modeling and multi-objective optimization of forward osmosis process. Desalination, 580, 117550. https://doi.org/10.1016/j.desal.2024.117550

5. Ali, M. T., Le-Clech, P., & Taylor, R. A. (2024). Flux performance modeling of forward osmosis draw solutions in the absence of mass diffusivity data. Industrial & Engineering Chemistry Research, 63(9), 4093–4100. https://doi.org/10.1021/acs.iecr.4c00193

6. Boubakri, A., Elgharbi, S., Bouguecha, S., Bechambi, O., Bilel, H., Alanazy, H. D., & Hafiane, A. (2024). Accurate prediction of reverse solute flux in forward osmosis systems using comparative machine learning models. Arabian Journal for Science and Engineering, 50, 3909–3923. https://doi.org/10.1007/s13369-024-09267-0

7. Ruzicka, M., Helgeland, I., & Paulen, R. (2024). Modelling and simulation of a forward osmosis process. Computer-aided chemical engineering, 53, 319-324. https://doi.org/10.1016/b978-0-443-28824-1.50054-5

8. Soukane, S., Nawaz, M. S., Obaid, M., Gudideni, V., Al-Qahtani, A., & Ghaffour, N. (2023). Advanced 3D multiscale modeling of forward osmosis-membrane distillation integrated designs. Desalination, 571, 117089. https://doi.org/10.1016/j.desal.2023.117089

9. Mahawer, K., Mutto, A., & Gupta, S. K. (2023). A modeling-based comparison study of data-driven and transport models for forward osmosis-nanofiltration hybrid system. Desalination, 574, 117251. https://doi.org/10.1016/j.desal.2023.117251

10. Wijmans, J., & Baker, R. (1995). The solution-diffusion model: A review. Journal of Membrane Science, 107(1–2), 1–21. https://doi.org/10.1016/0376-7388(95)00102-i

11. Heiranian, M., Fan, H., Wang, L., Lu, X., & Elimelech, M. (2023). Mechanisms and models for water transport in reverse osmosis membranes: History, critical assessment, and recent developments. Chemical Society Reviews, 52(24), 8455–8480. https://doi.org/10.1039/d3cs00395g

12. Foo, Z. H., Rehman, D., Coombs, O. Z., Deshmukh, A., & Lienhard, J. H. (2021). Multicomponent Fickian solution-diffusion model for osmotic transport through membranes. Journal of Membrane Science, 640, 119819. https://doi.org/10.1016/j.memsci.2021.119819

13. Ibrar, I., Yadav, S., Altaee, A., Hawari, A., Nguyen, V., & Zhou, J. (2020). A novel empirical method for predicting concentration polarization in forward osmosis for

single and multicomponent draw solutions. Desalination, 494, 114668. https://doi.org/10.1016/j.desal.2020.114668

14. Yong, J. S., Phillip, W. A., & Elimelech, M. (2011). Coupled reverse draw solute permeation and water flux in forward osmosis with neutral draw solutes. Journal of Membrane Science, 392–393, 9–17. https://doi.org/10.1016/j.memsci.2011.11.020

15. Ruzvidzo, K. H., Kaur, R., & Jain, M. (2024). Novel polyelectrolyte-glycol ether ternary phase-separating draw solutions for desalination using forward osmosis. Desalination, 586, 117897. https://doi.org/10.1016/j.desal.2024.117897

16. Ruzvidzo, K. H., Kaur, R., & Jain, M. (2024). Enhanced forward osmosis desalination of brackish water using phase-separating ternary organic draw solutions of hydroxypropyl cellulose and propylene glycol propyl ether. Water Environment Research, 96(8), e11110. https://doi.org/10.1002/wer.11110

CHAPTER 7

CONCLUSION, FUTURE SCOPE AND SOCIAL IMPACT

7.1 Conclusion

The world's ever-growing population, coupled with the impacts of climate change and pollution, is projected to lead to widespread water scarcity by the year 2040, especially in Africa and Asia. This impending crisis underscores the urgent need for more research focused on averting this catastrophic scenario. While reverse osmosis (RO) remains the more common desalination technology, forward osmosis (FO) presents a viable and promising alternative. FO offers a probable efficient, cleaner and less energy-intensive means of desalination, as it does not require external hydraulic pressure and exhibits lower fouling propensities compared to RO. However, the full commercialization of FO has been hindered by several challenges, primarily the lack of an optimal draw solution and energy-intensive draw solution regeneration processes. This research work has addressed these limitations by developing novel organic draw solutions that leverage their lower critical solution temperatures for efficient phase separation and regeneration. The aim was to leverage waste heat to improve the overall efficiency of the FO desalination process. The significant findings of this research work contribute towards overcoming the barriers to the widespread adoption of FO technology as a sustainable solution to impending global water scarcity.

Major scientific contributions

Novel draw solution development and characterization: This work successfully developed novel PGPE-based draw solutions that fundamentally advance FO technology. The binary 40PGPE and ternary 0.5NaCMC-20PGPE draw solutions produced significantly higher osmotic pressures of 130.297 and 59.455 bars, respectively. Adding NaCMC to PGPE solutions significantly increases the viscosity, but the solutions maintain high osmotic pressures suitable for use as FO draw solutions. For draw solution applications, these draw solutions can be considered as Newtonian fluids only.

Critical phase behaviour studies revealed that the binary 3.75PGPE solution showed successful regeneration, but the more concentrated 40PGPE solution did not exhibit visible phase separation at 70 °C, highlighting the critical influence of concentration on phase behaviour. However, dilution of the 40PGPE draw solution during FO may facilitate phase separation. The 3.75PGPE, 0.5NaCMC-3.75PGPE and 0.5NaCMC-20PGPE draw solutions can be regenerated by heating the solutions at a temperature of 70 °C. The novel 0.25HPC-3.75PGPE ternary draw solution demonstrated successful regeneration upon heating above the cloud point temperatures, resulting in the formation of three distinct phases: insoluble white HPC precipitates and separated PGPE and water liquid phases.

Forward osmosis performance and membrane characterization: Comprehensive testing established the membrane hydraulic permeability constant, A, at 0.78274 L m^{-2} h^{-1} bar^{-1}. The 0.5NaCMC-3.75PGPE draw solution against a 5 000 ppm NaCl feed had average experimental water fluxes of 7.629 LMH and 7.760 LMH with corresponding solute fluxes of 2.255 gMH and 2.479 gMH. The water fluxes declined over time suggesting potential membrane fouling or concentration polarization.

For higher salinity applications, the 40PGPE draw solution had average experimental water fluxes of 22.436 LMH and 19.738 LMH when desalinating a 35 000 ppm NaCl feed, while the 0.5NaCMC-20PGPE ternary draw had average experimental water fluxes of 13.975 LMH and 14.284 LMH. The solute fluxes of the binary 40PGPE draw solution surpassed those of the ternary 0.5NaCMC-20PGPE for both FO runs. The novel 0.25HPC-3.75PGPE ternary draw solution achieved experimental water fluxes of 11.062 and 9.852 LMH against 1000 ppm NaCl brackish feed solution.

Membrane compatibility analysis showed that minor morphological variations were observed, particularly for the membrane immersed in the binary 3.75PGPE solution, compared to the original membrane. Importantly, the FO membrane's overall shape and integrity were preserved after immersion in the draw solutions. Based on the Spiegler-Kedem model, the solute permeability coefficient and the reflection

coefficient of the HPC-PGPE draw solutions were determined to be 4.05×10^{-8} m/s and 0.999, respectively.

Machine learning optimization and predictive modeling: Advanced computational approaches were successfully implemented to optimize FO performance prediction. Among the predictive machine learning approaches evaluated, Gaussian Process Regression achieved superior performance ($R^2 = 0.98$), closely followed by Wide and Trilayered Neural Networks ($R^2 = 0.97$). Through systematic optimization, this work identified an optimal ANN architecture comprising two hidden layers with 65 neurons.

Analysis of data split ratios revealed the 70:15:15 partition demonstrated superior predictive accuracy with remarkably low MAPE (0.0178 - 0.0524%, mean 0.036%), outperforming both 80:10:10 (0 - 0.5505%, mean 0.264%) and 90:5:5 (0.049 - 0.1442%, mean 0.1%) splits. This configuration achieved exceptional accuracy with R^2 values exceeding 0.99 across all datasets, peaking at $R^2 = 0.99968$ with a 90:5:5 split.

Economic analysis and commercial viability: Comprehensive techno-economic evaluation demonstrated the commercial potential of the developed FO system. The annual operating costs were \$23 273.92, with annual capital costs amounting to \$17 487.60. The yearly cost per unit volume of produced water for the stand-alone FO system was determined to be 0.47 \$ m^{-3}, based on a plant capacity of 160 m^3 d^{-1}. The total yearly costs for the PS regeneration process were estimated at \$242 691.18, with the cost of steam determined to be 1.60 \$ ton^{-1}.

Significance and impact

The developed novel draw solutes exhibited competitive FO performances with those from literature, while offering the critical advantage of efficient thermal regeneration. This research provides a comprehensive pathway toward overcoming the primary barriers to FO commercialization by delivering draw solutions that combine high osmotic driving force with low-temperature regeneration capabilities.

The ability to utilize waste heat at 70 ^{o}C positions this technology as particularly attractive for industrial integration and sustainable desalination applications.

The demonstrated performance of these novel draw solutions, coupled with their thermal regeneration capabilities and economic viability, positions FO as a credible alternative to conventional desalination technologies. This work contributes essential building blocks toward addressing the impending global water crisis through sustainable, energy-efficient desalination solutions that can leverage industrial waste heat and renewable energy sources, ultimately supporting global efforts toward water security in an increasingly water-stressed world.

7.2 Future Scope

FO desalination, whilst demonstrating promising laboratory-scale performance, faces critical limitations that constrain practical implementation. Most studies rely on synthetic feed solutions with controlled ionic compositions that poorly represent real seawater or wastewater complexity, where organic matter and biological contaminants create substantially different fouling behaviours. Furthermore, investigations typically focus on short-term performance metrics rather than the long-term operational stability required for commercial viability. The majority of studies have omitted the determination of specific energy consumption and techno-economic assessments of their FO processes. The limited studies that report high specific energy consumption values universally recommend utilising waste heat or renewable energy sources for draw agent recovery processes. However, these recommendations lack empirical validation in subsequent research.

This research work has laid the foundation for significant advancements in FO desalination technologies. Building upon the insights and findings of this thesis, a three-phase strategy is suggested for the future prospects of FO. Economic viability fundamentally hinges on draw agent recovery costs. The transition to commercial implementation requires addressing specific technical milestones across three phases. FO research suffers from critical fragmentation preventing commercial implementation. Researchers developing innovative draw agents with stimulus-responsive cost-effective recovery publish their work and move on. Membrane

specialists creating materials that reduce concentration polarisation whilst increasing water flux similarly fail to collaborate beyond publication. Researchers utilising machine learning algorithms for optimisation operate in isolation. The first step requires collaborative integration of these three domains to develop optimised membrane–draw agent–machine learning systems that function together rather than as isolated components. Key research questions focus on how machine learning algorithms can predict optimal membrane-draw agent pairings for specific feed water compositions. Research should investigate fundamental compatibility requirements between different membrane materials and draw agents. Studies must determine how real-time monitoring systems can optimise FO performance through adaptive control strategies. Methodologies should develop multi-objective optimisation algorithms using experimental databases of membrane performance and draw agent properties. Research requires standardised testing protocols for membrane-draw agent compatibility assessment. Implementation needs pilot systems with real-time monitoring of key performance indicators. Collaborative research networks must link membrane developers, draw solution researchers, and artificial intelligence specialists. Once these integrated systems demonstrate superior performance in laboratory settings, scale-up should focus on real feed waters in remote areas where FO's low-pressure operation provides clear competitive advantages. Mercury-contaminated mining wastewaters in African artisanal and small-scale gold mines represent an ideal initial application. This requires membranes that prevent mercury adhesion and minimise reverse solute flux. FO's ability to function at low pressure suits treating complex contaminated streams in energy-limited remote locations. Research questions must identify critical design parameters for FO systems treating real industrial wastewaters with complex contaminant matrices. Studies should investigate how long-term fouling mechanisms differ between synthetic and real feed waters. Research must determine optimal system configurations for achieving low energy consumption using renewable energy sources. Methodologies require extended pilot-scale studies with actual contaminated waters from mining operations, municipal wastewater, and agricultural runoff. Research needs comprehensive fouling analysis protocols including the use of spectroscopy. Techno-economic models must be developed incorporating real-world operational costs and

maintenance requirements. Field testing stations in water-stressed regions should validate performance under variable environmental conditions. Future development should expand successful remote applications into autonomous, AI-powered networks that integrate multiple treatment sites. These systems would use real-time environmental data and distributed learning algorithms for adaptive responses to climate variability and demand fluctuations. Research questions focus on how distributed FO networks can adapt autonomously to changing environmental conditions whilst maintaining optimal performance. Methodologies require federated learning algorithms that enable individual FO systems to learn from collective network experience. Development needs predictive maintenance protocols using learning diagnostics. Implementation must create edge computing solutions for real-time decision making in remote locations with limited connectivity. Design should focus on modular, standardised FO units that can be easily replaced without disrupting network operations. Immediate focus should prioritise integration activities due to their high impact and feasibility. Medium-term development should begin pilot-scale validation with real waters once laboratory success is demonstrated. Long-term vision represents the ultimate goal but requires successful completion of earlier phases. FO desalination will likely succeed in niche applications where its unique advantages justify current economic limitations. Currently, FO plays a complementary rather than transformative role in global water security. Yet FO has the potential to capture a substantial portion of the desalination market in the coming decades if draw solution recovery processes can achieve energy consumption below 3.75 kWh/m^3. Success depends on systematic advancement across technical and economic fronts, enabling FO to establish a sustainable position in specific applications whilst complementing rather than replacing conventional desalination technologies in the global water treatment landscape. This work has laid the foundation for significant advancements in FO desalination technologies. Building upon these insights, several promising avenues for future research and development have been identified. These research directions position FO as a transformative technology that can reshape how societies approach water security, resource management, and environmental sustainability in an era of increasing global challenges. Whilst key technical hurdles such as energy-intensive draw solution

recovery requirements still need resolution, the unique advantages of FO systems make them well-positioned to address diverse water treatment applications across multiple scales and contexts.

7.3 Environmental and Social Impact

The social implications of this research on osmotic pressure-driven desalination processes extend across multiple dimensions of sustainable development and public welfare. By developing more efficient draw solutions, this work contributes to addressing global water security challenges, particularly in developing regions where conventional desalination technologies remain cost-prohibitive. The FO approach demonstrates enhanced environmental sustainability through reduced energy requirements compared to traditional desalination methods, with the added potential for utilizing waste heat or solar energy given the 70 °C regeneration temperature of draw solutions. This improved environmental profile, coupled with increased accessibility to clean water sources, has direct positive implications for public health outcomes, especially in areas currently relying on contaminated water supplies. Furthermore, the research aligns with and advances the United Nations Sustainable Development Goals, specifically SDG 6 regarding clean water access and sanitation, while supporting sustainable urban development through more effective water management strategies.

The creation of organic draw solutions made from cellulose for forward osmosis is a sustainable step forward in water treatment technology. Such an innovation carries significant environmental and socioeconomic implications. The inherently biodegradable nature of these organic compounds eliminates environmental accumulation concerns associated with inorganic draw solutions. FO eliminates energy-intensive high-pressure pumps required in RO, substantially reducing the operational energy demands. The regeneration process operates at moderate temperatures of 70 °C using industrial waste heat. This creates a synergistic relationship that transforms discarded thermal energy into productive water treatment capacity while simultaneously reducing the overall carbon footprint. FO membranes demonstrate exceptional durability through multiple operational cycles with minimal

requirements for cleaning using chemicals. The extended lifespan of membranes reduces replacement frequency and minimizes solid waste generation. The reduced chemical cleaning requirements eliminate hazardous waste streams and environmental toxicity risks. FO systems effectively treat highly saline feeds and severely contaminated water sources, expanding treatment applications to previously unusable water resources. Such capability proves particularly valuable in water-stressed regions where conventional treatment approaches demonstrate limited effectiveness. From a socio-economic perspective, these processes address critical water security challenges in developing nations where millions lack access to safely managed drinking water services. This process demonstrates economic viability in resource-constrained regions through the elimination of huge pumping costs and the utilization of waste heat for draw solution recovery. Clean water becomes accessible to communities where conventional treatment remains economically unfeasible. The integration with industries creates mutually beneficial relationships that improve both water treatment economics and industrial energy efficiency while facilitating knowledge transfer to developing nations. Employment opportunities emerge across manufacturing, installation, and maintenance sectors. Climate change has intensified global water scarcity, making cellulose-derived phase-separating FO processes both an environmental solution and an economic opportunity. This solution addresses fundamental human development challenges through sustainable approaches, transforming industrial waste heat into productive water treatment resources.

Table AP-1: FO raw experimental dataset used in ANN modeling

Data points	Data Type	INPUT FO Run	INPUT Time (mins)	INPUT Feed side temp. (°C)	INPUT Feed side conc. (M)	INPUT Feed side flowrate (L/h)	INPUT Draw side temp. (°C)	INPUT Draw side conc. (M)	INPUT Draw side solute Mol. Weight (g/mol)	INPUT Draw side flowrate (L/h)	OUTPUT FO flux (L/h/m²)
1	Exp	1	10	30	0.093778	12	30	2.39818	119.50	12	15.163
2	Exp	1	20	30	0.095781	12	30	2.37720	119.50	12	15.163
3	Exp	1	30	30	0.097785	12	30	2.35621	119.50	12	15.163
4	Exp	1	40	30	0.099538	12	30	2.33785	119.50	12	14.689
5	Exp	1	50	30	0.101541	12	30	2.31687	119.50	12	14.784
6	Exp	1	60	30	0.103294	12	30	2.29851	119.50	12	14.532
7	Exp	1	70	30	0.105047	12	30	2.28014	119.50	12	14.351
8	Exp	1	80	30	0.106800	12	30	2.26178	119.50	12	14.216
9	Exp	1	90	30	0.108803	12	30	2.24080	119.50	12	14.321
10	Exp	1	100	30	0.110055	12	30	2.22768	119.50	12	13.837
11	Exp	1	110	30	0.110806	12	30	2.21981	119.50	12	13.096
12	Exp	1	120	30	0.111307	12	30	2.21456	119.50	12	12.320
13	Exp	2	10	30	0.093778	12	30	2.39818	119.50	12	15.163
14	Exp	2	20	30	0.095531	12	30	2.37982	119.50	12	14.216
15	Exp	2	30	30	0.097284	12	30	2.36146	119.50	12	13.900

16	Exp	2	40	30	0.099037	12	30	2.34310	119.50	12	13.742
17	Exp	2	50	30	0.100539	12	30	2.32736	119.50	12	13.268
18	Exp	2	60	30	0.101791	12	30	2.31424	119.50	12	12.636
19	Exp	2	70	30	0.103294	12	30	2.29851	119.50	12	12.456
20	Exp	2	80	30	0.104546	12	30	2.28539	119.50	12	12.083
21	Exp	2	90	30	0.105548	12	30	2.27490	119.50	12	11.583
22	Exp	2	100	30	0.106299	12	30	2.26703	119.50	12	10.993
23	Exp	2	110	30	0.106800	12	30	2.26178	119.50	12	10.339
24	Exp	2	120	30	0.107301	12	30	2.25653	119.50	12	9.793
25	Exp	3	10	30	0.093778	12	30	2.25721	119.50	12	15.163
26	Exp	3	20	30	0.095781	12	30	2.23623	119.50	12	15.163
27	Exp	3	30	30	0.097284	12	30	2.22049	119.50	12	13.890
28	Exp	3	40	30	0.098786	12	30	2.20475	119.50	12	13.268
29	Exp	3	50	30	0.100289	12	30	2.18901	119.50	12	12.889
30	Exp	3	60	30	0.101541	12	30	2.17589	119.50	12	12.320
31	Exp	3	70	30	0.102543	12	30	2.16540	119.50	12	11.643
32	Exp	3	80	30	0.103544	12	30	2.15491	119.50	12	11.136
33	Exp	3	90	30	0.104045	12	30	2.14966	119.50	12	10.320
34	Exp	3	100	30	0.104546	12	30	2.14442	119.50	12	9.667
35	Exp	3	110	30	0.105047	12	30	2.13917	119.50	12	9.132
36	Exp	3	120	30	0.105297	12	30	2.13655	119.50	12	8.529
37	Exp	1	10	30	0.093164	12	30	2.37476	119.50	9	17.059
38	Exp	1	20	30	0.094091	12	30	2.35009	119.50	9	13.268
39	Exp	1	30	30	0.094709	12	30	2.33035	119.50	9	11.373
40	Exp	1	40	30	0.095018	12	30	2.32049	119.50	9	9.477

41	Exp	1	50	30	0.095326	12	30	2.31062	119.50	9	8.340
42	Exp	1	60	30	0.095790	12	30	2.29581	119.50	9	7.898
43	Exp	1	70	30	0.096099	12	30	2.28595	119.50	9	7.311
44	Exp	1	80	30	0.096716	12	30	2.27114	119.50	9	7.108
45	Exp	1	90	30	0.097025	12	30	2.26127	119.50	9	6.739
46	Exp	1	100	30	0.097488	12	30	2.24647	119.50	9	6.634
47	Exp	1	110	30	0.097952	12	30	2.23167	119.50	9	6.548
48	Exp	1	120	30	0.098260	12	30	2.22180	119.50	9	6.318
49	Exp	2	10	30	0.093072	12	30	2.37970	119.50	9	15.163
50	Exp	2	20	30	0.093720	12	30	2.35996	119.50	9	11.373
51	Exp	2	30	30	0.094207	12	30	2.34516	119.50	9	9.477
52	Exp	2	40	30	0.094693	12	30	2.33035	119.50	9	8.529
53	Exp	2	50	30	0.095018	12	30	2.32049	119.50	9	7.582
54	Exp	2	60	30	0.095342	12	30	2.31062	119.50	9	6.950
55	Exp	2	70	30	0.095666	12	30	2.30075	119.50	9	6.499
56	Exp	2	80	30	0.095828	12	30	2.29581	119.50	9	5.923
57	Exp	2	90	30	0.096153	12	30	2.28595	119.50	9	5.686
58	Exp	2	100	30	0.096477	12	30	2.27608	119.50	9	5.497
59	Exp	2	110	30	0.096801	12	30	2.26621	119.50	9	5.342
60	Exp	2	120	30	0.097125	12	30	2.25634	119.50	9	5.212
61	Exp	3	10	30	0.093072	12	30	2.28572	119.50	9	15.163
62	Exp	3	20	30	0.093883	12	30	2.26104	119.50	9	12.320
63	Exp	3	30	30	0.094531	12	30	2.24131	119.50	9	10.741
64	Exp	3	40	30	0.095180	12	30	2.22157	119.50	9	9.951
65	Exp	3	50	30	0.095504	12	30	2.21170	119.50	9	8.719

66	Exp	3	60	30	0.095828	12	30	2.20183	119.50	9	7.898
67	Exp	3	70	30	0.096153	12	30	2.19197	119.50	9	7.311
68	Exp	3	80	30	0.096477	12	30	2.18210	119.50	9	6.871
69	Exp	3	90	30	0.096639	12	30	2.17716	119.50	9	6.318
70	Exp	3	100	30	0.096963	12	30	2.16729	119.50	9	6.065
71	Exp	3	110	30	0.097125	12	30	2.16236	119.50	9	5.686
72	Exp	3	120	30	0.097288	12	30	2.15743	119.50	9	5.370
73	Exp	1	10	30	0.094279	12	30	2.39294	119.50	15	18.954
74	Exp	1	20	30	0.096533	12	30	2.36933	119.50	15	18.006
75	Exp	1	30	30	0.098286	12	30	2.35097	119.50	15	16.427
76	Exp	1	40	30	0.100289	12	30	2.32998	119.50	15	16.111
77	Exp	1	50	30	0.102042	12	30	2.31162	119.50	15	15.542
78	Exp	1	60	30	0.103544	12	30	2.29588	119.50	15	14.847
79	Exp	1	70	30	0.105047	12	30	2.28014	119.50	15	14.351
80	Exp	1	80	30	0.107301	12	30	2.25653	119.50	15	14.689
81	Exp	1	90	30	0.109554	12	30	2.23293	119.50	15	14.953
82	Exp	1	100	30	0.110556	12	30	2.22243	119.50	15	14.216
83	Exp	1	110	30	0.111307	12	30	2.21456	119.50	15	13.440
84	Exp	1	120	30	0.112058	12	30	2.20669	119.50	15	12.794
85	Exp	2	10	30	0.094028	12	30	2.39556	119.50	15	17.059
86	Exp	2	20	30	0.096032	12	30	2.37458	119.50	15	16.111
87	Exp	2	30	30	0.097785	12	30	2.35621	119.50	15	15.163
88	Exp	2	40	30	0.100038	12	30	2.33261	119.50	15	15.637
89	Exp	2	50	30	0.102042	12	30	2.31162	119.50	15	15.542
90	Exp	2	60	30	0.103043	12	30	2.30113	119.50	15	14.216

91	Exp	2	70	30	0.104296	12	30	2.28801	119.50	15	13.539
92	Exp	2	80	30	0.106549	12	30	2.26440	119.50	15	13.979
93	Exp	2	90	30	0.107551	12	30	2.25391	119.50	15	13.268
94	Exp	2	100	30	0.108553	12	30	2.24342	119.50	15	12.699
95	Exp	2	110	30	0.109304	12	30	2.23555	119.50	15	12.062
96	Exp	2	120	30	0.109805	12	30	2.23030	119.50	15	11.373
97	Exp	3	10	30	0.094279	12	30	2.30836	119.50	15	18.954
98	Exp	3	20	30	0.096533	12	30	2.28475	119.50	15	18.006
99	Exp	3	30	30	0.098786	12	30	2.26114	119.50	15	17.691
100	Exp	3	40	30	0.100539	12	30	2.24278	119.50	15	16.585
101	Exp	3	50	30	0.102292	12	30	2.22442	119.50	15	15.922
102	Exp	3	60	30	0.103544	12	30	2.21130	119.50	15	14.847
103	Exp	3	70	30	0.104796	12	30	2.19819	119.50	15	14.080
104	Exp	3	80	30	0.105798	12	30	2.18769	119.50	15	13.268
105	Exp	3	90	30	0.106800	12	30	2.17720	119.50	15	12.636
106	Exp	3	100	30	0.107801	12	30	2.16671	119.50	15	12.131
107	Exp	3	110	30	0.108553	12	30	2.15884	119.50	15	11.545
108	Exp	3	120	30	0.109304	12	30	2.15097	119.50	15	11.057
109	Exp	1	10	25	0.093778	9	25	2.39818	119.50	12	15.163
110	Exp	1	20	25	0.094780	9	25	2.38769	119.50	12	11.373
111	Exp	1	30	25	0.095781	9	25	2.37720	119.50	12	10.109
112	Exp	1	40	25	0.096282	9	25	2.37195	119.50	12	8.529
113	Exp	1	50	25	0.096783	9	25	2.36671	119.50	12	7.582
114	Exp	1	60	25	0.097284	9	25	2.36146	119.50	12	6.950
115	Exp	1	70	25	0.097785	9	25	2.35621	119.50	12	6.499

116	Exp	1	80	25	0.097785	9	25	2.35621	119.50	12	5.686
117	Exp	1	90	25	0.098286	9	25	2.35097	119.50	12	5.476
118	Exp	1	100	25	0.098286	9	25	2.35097	119.50	12	4.928
119	Exp	1	110	25	0.098786	9	25	2.34572	119.50	12	4.825
120	Exp	1	120	25	0.098786	9	25	2.34572	119.50	12	4.423
121	Exp	2	10	25	0.093528	9	25	2.40081	119.50	12	13.268
122	Exp	2	20	25	0.094529	9	25	2.39032	119.50	12	10.425
123	Exp	2	30	25	0.095531	9	25	2.37982	119.50	12	9.477
124	Exp	2	40	25	0.096533	9	25	2.36933	119.50	12	9.003
125	Exp	2	50	25	0.097033	9	25	2.36408	119.50	12	7.961
126	Exp	2	60	25	0.097534	9	25	2.35884	119.50	12	7.266
127	Exp	2	70	25	0.098035	9	25	2.35359	119.50	12	6.769
128	Exp	2	80	25	0.098536	9	25	2.34834	119.50	12	6.397
129	Exp	2	90	25	0.099037	9	25	2.34310	119.50	12	6.107
130	Exp	2	100	25	0.099538	9	25	2.33785	119.50	12	5.876
131	Exp	2	110	25	0.099788	9	25	2.33523	119.50	12	5.514
132	Exp	2	120	25	0.099788	9	25	2.33523	119.50	12	5.054
133	Exp	1	10	30	0.584093	9	30	38.46614	118.17	12	32.897
134	Exp	1	20	30	0.591042	9	30	37.32877	118.17	12	27.302
135	Exp	1	30	30	0.597174	9	30	36.32522	118.17	12	24.193
136	Exp	1	40	30	0.604123	9	30	35.18786	118.17	12	23.572
137	Exp	1	50	30	0.610255	9	30	34.18430	118.17	12	22.453
138	Exp	1	60	30	0.617613	9	30	32.98004	118.17	12	22.639
139	Exp	1	70	30	0.623335	9	30	32.04339	118.17	12	21.707
140	Exp	1	80	30	0.629467	9	30	31.03983	118.17	12	21.240

141	Exp	1	90	30	0.634372	9	30	30.23699	118.17	12	20.256
142	Exp	1	100	30	0.638051	9	30	29.63486	118.17	12	18.908
143	Exp	1	110	30	0.641321	9	30	29.09963	118.17	12	17.637
144	Exp	1	120	30	0.644183	9	30	28.63130	118.17	12	16.422
145	Exp	2	10	30	0.586431	9	30	38.26543	118.17	12	32.492
146	Exp	2	20	30	0.595462	9	30	36.92735	118.17	12	26.897
147	Exp	2	30	30	0.602687	9	30	35.85690	118.17	12	22.545
148	Exp	2	40	30	0.610814	9	30	34.65263	118.17	12	21.302
149	Exp	2	50	30	0.617136	9	30	33.71598	118.17	12	19.064
150	Exp	2	60	30	0.625263	9	30	32.51171	118.17	12	18.815
151	Exp	2	70	30	0.631585	9	30	31.57506	118.17	12	17.572
152	Exp	2	80	30	0.63881	9	30	30.50461	118.17	12	17.105
153	Exp	2	90	30	0.643325	9	30	29.83557	118.17	12	16.499
154	Exp	2	100	30	0.646937	9	30	29.30034	118.17	12	15.841
155	Exp	2	110	30	0.649646	9	30	28.89892	118.17	12	15.146
156	Exp	2	120	30	0.651904	9	30	28.56440	118.17	12	13.578
157	Exp	1	10	25	0.018581	24	25	2.44361	119.50	24	26.590
158	Exp	1	20	25	0.019207	24	25	2.41499	119.50	24	24.691
159	Exp	1	30	25	0.019729	24	25	2.39113	119.50	24	22.791
160	Exp	1	40	25	0.020147	24	25	2.37205	119.50	24	20.892
161	Exp	1	50	25	0.020460	24	25	2.35773	119.50	24	18.993
162	Exp	1	60	25	0.020878	24	25	2.33865	119.50	24	18.360
163	Exp	1	70	25	0.021295	24	25	2.31956	119.50	24	17.907
164	Exp	1	80	25	0.021817	24	25	2.29571	119.50	24	18.043
165	Exp	1	90	25	0.022235	24	25	2.27662	119.50	24	17.727

166	Exp	1	100	25	0.022652	24	25	2.25754	119.50	24	17.473
167	Exp	1	110	25	0.023070	24	25	2.23845	119.50	24	17.266
168	Exp	1	120	25	0.023383	24	25	2.22414	119.50	24	16.777
169	Exp	2	10	25	0.018790	24	25	2.43407	119.50	24	34.187
170	Exp	2	20	25	0.019103	24	25	2.41976	119.50	24	22.791
171	Exp	2	30	25	0.019207	24	25	2.41499	119.50	24	16.460
172	Exp	2	40	25	0.019207	24	25	2.41499	119.50	24	12.345
173	Exp	2	50	25	0.019312	24	25	2.41021	119.50	24	10.636
174	Exp	2	60	25	0.019520	24	25	2.40067	119.50	24	10.129
175	Exp	2	70	25	0.019729	24	25	2.39113	119.50	24	9.768
176	Exp	2	80	25	0.019938	24	25	2.38159	119.50	24	9.496
177	Exp	2	90	25	0.020147	24	25	2.37205	119.50	24	9.285
178	Exp	2	100	25	0.020460	24	25	2.35773	119.50	24	9.496
179	Exp	2	110	25	0.020669	24	25	2.34819	119.50	24	9.324
180	Exp	2	120	25	0.020982	24	25	2.33388	119.50	24	9.496
181	Exp	1	10	25	0.018059	24	25	2.46110	120.17	24	7.597
182	Exp	1	20	25	0.018268	24	25	2.43369	120.17	24	7.597
183	Exp	1	30	25	0.018685	24	25	2.37887	120.17	24	10.129
184	Exp	1	40	25	0.018894	24	25	2.35146	120.17	24	9.496
185	Exp	1	50	25	0.019103	24	25	2.32405	120.17	24	9.117
186	Exp	1	60	25	0.019312	24	25	2.29664	120.17	24	8.863
187	Exp	1	70	25	0.019520	24	25	2.26923	120.17	24	8.682
188	Exp	1	80	25	0.019729	24	25	2.24182	120.17	24	8.547
189	Exp	1	90	25	0.019938	24	25	2.21441	120.17	24	8.441
190	Exp	1	100	25	0.020147	24	25	2.18700	120.17	24	8.357

191	Exp	1	110	25	0.020356	24	25	2.15959	120.17	24	8.288
192	Exp	1	120	25	0.020564	24	25	2.13218	120.17	24	8.230
193	Exp	2	10	25	0.018059	24	25	2.46110	120.17	24	7.597
194	Exp	2	20	25	0.018372	24	25	2.41999	120.17	24	9.496
195	Exp	2	30	25	0.018581	24	25	2.39258	120.17	24	8.863
196	Exp	2	40	25	0.018894	24	25	2.35146	120.17	24	9.496
197	Exp	2	50	25	0.019103	24	25	2.32405	120.17	24	9.117
198	Exp	2	60	25	0.019312	24	25	2.29664	120.17	24	8.863
199	Exp	2	70	25	0.019416	24	25	2.28294	120.17	24	8.140
200	Exp	2	80	25	0.019520	24	25	2.26923	120.17	24	7.597
201	Exp	2	90	25	0.019625	24	25	2.25553	120.17	24	7.175
202	Exp	2	100	25	0.019834	24	25	2.22812	120.17	24	7.217
203	Exp	2	110	25	0.019938	24	25	2.21441	120.17	24	6.906
204	Exp	2	120	25	0.020042	24	25	2.20071	120.17	24	6.647
205	Exp	1	10	25	0.01832	9	25	2.43780	119.50	12	17.094
206	Exp	1	20	25	0.01869	9	25	2.40843	119.50	12	15.194
207	Exp	1	30	25	0.01911	9	25	2.37486	119.50	12	15.194
208	Exp	1	40	25	0.01942	9	25	2.34969	119.50	12	14.245
209	Exp	1	50	25	0.01963	9	25	2.33291	119.50	12	12.915
210	Exp	1	60	25	0.01984	9	25	2.31612	119.50	12	12.029
211	Exp	1	70	25	0.02000	9	25	2.30354	119.50	12	11.124
212	Exp	1	80	25	0.02015	9	25	2.29095	119.50	12	10.446
213	Exp	1	90	25	0.02036	9	25	2.27417	119.50	12	10.129
214	Exp	1	100	25	0.02052	9	25	2.26158	119.50	12	9.686
215	Exp	1	110	25	0.02062	9	25	2.25319	119.50	12	9.151

216	Exp	1	120	25	0.02078	9	25	2.24060	119.50	12	8.863
217	Exp	2	10	25	0.01827	9	25	2.44199	119.50	12	15.194
218	Exp	2	20	25	0.01869	9	25	2.40843	119.50	12	15.194
219	Exp	2	30	25	0.01911	9	25	2.37486	119.50	12	15.194
220	Exp	2	40	25	0.01937	9	25	2.35388	119.50	12	13.770
221	Exp	2	50	25	0.01963	9	25	2.33291	119.50	12	12.915
222	Exp	2	60	25	0.01984	9	25	2.31612	119.50	12	12.029
223	Exp	2	70	25	0.02005	9	25	2.29934	119.50	12	11.396
224	Exp	2	80	25	0.02020	9	25	2.28675	119.50	12	10.683
225	Exp	2	90	25	0.02031	9	25	2.27836	119.50	12	9.918
226	Exp	2	100	25	0.02041	9	25	2.26997	119.50	12	9.306
227	Exp	2	110	25	0.02052	9	25	2.26158	119.50	12	8.806
228	Exp	2	120	25	0.02062	9	25	2.25319	119.50	12	8.388
229	Exp	3	10	25	0.01827	9	25	2.44199	119.50	12	15.194
230	Exp	3	20	25	0.01858	9	25	2.41682	119.50	12	13.295
231	Exp	3	30	25	0.01890	9	25	2.39165	119.50	12	12.662
232	Exp	3	40	25	0.01911	9	25	2.37486	119.50	12	11.396
233	Exp	3	50	25	0.01942	9	25	2.34969	119.50	12	11.396
234	Exp	3	60	25	0.01952	9	25	2.34130	119.50	12	10.129
235	Exp	3	70	25	0.01963	9	25	2.33291	119.50	12	9.225
236	Exp	3	80	25	0.01973	9	25	2.32451	119.50	12	8.547
237	Exp	3	90	25	0.01984	9	25	2.31612	119.50	12	8.019
238	Exp	3	100	25	0.01994	9	25	2.30773	119.50	12	7.597
239	Exp	3	110	25	0.02005	9	25	2.29934	119.50	12	7.252
240	Exp	3	120	25	0.02015	9	25	2.29095	119.50	12	6.964

241	Exp	4	10	25	0.01816	9	25	2.45039	119.50	12	11.396
242	Exp	4	20	25	0.01848	9	25	2.42521	119.50	12	11.396
243	Exp	4	30	25	0.01874	9	25	2.40423	119.50	12	10.763
244	Exp	4	40	25	0.01895	9	25	2.38745	119.50	12	9.971
245	Exp	4	50	25	0.01916	9	25	2.37067	119.50	12	9.496
246	Exp	4	60	25	0.01931	9	25	2.35808	119.50	12	8.863
247	Exp	4	70	25	0.01942	9	25	2.34969	119.50	12	8.140
248	Exp	4	80	25	0.01952	9	25	2.34130	119.50	12	7.597
249	Exp	4	90	25	0.01968	9	25	2.32871	119.50	12	7.386
250	Exp	4	100	25	0.01979	9	25	2.32032	119.50	12	7.027
251	Exp	4	110	25	0.01989	9	25	2.31193	119.50	12	6.734
252	Exp	4	120	25	0.02000	9	25	2.30354	119.50	12	6.489
253	Exp	1	10	30	0.580228	9	30	4.94420	118.42	12	18.651
254	Exp	1	20	30	0.581816	9	30	4.80832	118.42	12	17.718
255	Exp	1	30	30	0.583052	9	30	4.70261	118.42	12	16.164
256	Exp	1	40	30	0.584111	9	30	4.61200	118.42	12	14.921
257	Exp	1	50	30	0.585170	9	30	4.52140	118.42	12	14.175
258	Exp	1	60	30	0.586229	9	30	4.43079	118.42	12	13.677
259	Exp	1	70	30	0.587287	9	30	4.34018	118.42	12	13.322
260	Exp	1	80	30	0.588170	9	30	4.26468	118.42	12	12.823
261	Exp	1	90	30	0.589052	9	30	4.18917	118.42	12	12.434
262	Exp	1	100	30	0.589582	9	30	4.14387	118.42	12	11.750
263	Exp	1	110	30	0.590111	9	30	4.09856	118.42	12	11.191
264	Exp	1	120	30	0.590817	9	30	4.03816	118.42	12	10.880
265	Exp	2	10	30	0.576445	9	30	4.94423	118.42	12	18.651
266	Exp	2	20	30	0.578198	9	30	4.79322	118.42	12	18.651

267	Exp	2	30	30	0.579601	9	30	4.67241	118.42	12	17.408
268	Exp	2	40	30	0.580828	9	30	4.56670	118.42	12	16.320
269	Exp	2	50	30	0.582056	9	30	4.46099	118.42	12	15.667
270	Exp	2	60	30	0.582757	9	30	4.40059	118.42	12	14.299
271	Exp	2	70	30	0.583458	9	30	4.34018	118.42	12	13.322
272	Exp	2	80	30	0.584160	9	30	4.27978	118.42	12	12.589
273	Exp	2	90	30	0.584861	9	30	4.21937	118.42	12	12.019
274	Exp	2	100	30	0.585387	9	30	4.17407	118.42	12	11.377
275	Exp	2	110	30	0.585913	9	30	4.12877	118.42	12	10.851
276	Exp	2	120	30	0.586264	9	30	4.09856	118.42	12	10.258
277	Exp	1	10	25	0.018268	24	25	2.22730	118.84	12	15.194
278	Exp	1	20	25	0.018581	24	25	2.19520	118.84	12	13.295
279	Exp	1	30	25	0.018894	24	25	2.16310	118.84	12	12.662
280	Exp	1	40	25	0.019103	24	25	2.14169	118.84	12	11.396
281	Exp	1	50	25	0.019312	24	25	2.12029	118.84	12	10.636
282	Exp	1	60	25	0.019520	24	25	2.09889	118.84	12	10.129
283	Exp	1	70	25	0.019938	24	25	2.05608	118.84	12	10.853
284	Exp	1	80	25	0.020147	24	25	2.03468	118.84	12	10.446
285	Exp	1	90	25	0.020356	24	25	2.01328	118.84	12	10.129
286	Exp	1	100	25	0.020460	24	25	2.00258	118.84	12	9.496
287	Exp	1	110	25	0.020669	24	25	1.98117	118.84	12	9.324
288	Exp	1	120	25	0.020878	24	25	1.95977	118.84	12	9.180
289	Exp	2	10	25	0.018268	24	25	2.22730	118.84	12	15.194
290	Exp	2	20	25	0.018581	24	25	2.19520	118.84	12	13.295
291	Exp	2	30	25	0.018790	24	25	2.17380	118.84	12	11.396

292	Exp	2	40	25	0.018998	24	25	2.15239	118.84	12	10.446
293	Exp	2	50	25	0.019207	24	25	2.13099	118.84	12	9.876
294	Exp	2	60	25	0.019416	24	25	2.10959	118.84	12	9.496
295	Exp	2	70	25	0.019520	24	25	2.09889	118.84	12	8.682
296	Exp	2	80	25	0.019729	24	25	2.07749	118.84	12	8.547
297	Exp	2	90	25	0.019938	24	25	2.05608	118.84	12	8.441
298	Exp	2	100	25	0.020042	24	25	2.04538	118.84	12	7.977
299	Exp	2	110	25	0.020147	24	25	2.03468	118.84	12	7.597
300	Exp	2	120	25	0.020251	24	25	2.02398	118.84	12	7.281
301	Exp	3	10	25	0.018268	24	25	2.22730	118.84	12	15.194
302	Exp	3	20	25	0.018529	24	25	2.20055	118.84	12	12.345
303	Exp	3	30	25	0.018790	24	25	2.17380	118.84	12	11.396
304	Exp	3	40	25	0.018998	24	25	2.15239	118.84	12	10.446
305	Exp	3	50	25	0.019155	24	25	2.13634	118.84	12	9.496
306	Exp	3	60	25	0.019312	24	25	2.12029	118.84	12	8.863
307	Exp	3	70	25	0.019416	24	25	2.10959	118.84	12	8.140
308	Exp	3	80	25	0.019520	24	25	2.09889	118.84	12	7.597
309	Exp	3	90	25	0.019625	24	25	2.08819	118.84	12	7.175
310	Exp	3	100	25	0.019781	24	25	2.07213	118.84	12	7.027
311	Exp	3	110	25	0.019886	24	25	2.06143	118.84	12	6.734
312	Exp	3	120	25	0.019938	24	25	2.05073	118.84	12	6.489

<h1 style="text-align: center">LIST OF PUBLICATIONS</h1>

Research publications

1. **Kudzai Hamish Ruzvidzo**, Raminder Kaur and Manish Jain (2024), "Novel polyelectrolyte-glycol ether ternary phase-separating draw solutions for desalination using forward osmosis", *Desalination*, Volume 586, 117897, DOI: https://doi.org/10.1016/j.desal.2024.117897 **(SCIE) (Impact Factor – 8.3)**

2. **Kudzai Hamish Ruzvidzo**, Raminder Kaur and Manish Jain (2024), "Enhanced forward osmosis desalination of brackish water using phase-separating ternary organic draw solutions of hydroxypropyl cellulose and propylene glycol propyl ether", *Water Environment Research*, 96(8), e11110, DOI: https://doi.org/10.1002/wer.11110 **(SCIE) (Impact Factor – 2.5)**

3. **Kudzai Hamish Ruzvidzo**, Ashwani Kumar Tiwari, Raminder Kaur and Manish Jain, "A critical review on the progress, challenges and future outlook of forward osmosis desalination in the 21st century" – **UNDER REVIEW**

4. **Kudzai Hamish Ruzvidzo**, Ashwani Kumar Tiwari, Raminder Kaur and Manish Jain, "Artificial neural network-based modeling of forward osmosis-phase separation desalination processes with novel ternary organic draw solutions" – **SUBMITTTED**

Conferences

1. **Kudzai Hamish Ruzvidzo**, Raminder Kaur and Manish Jain (2023), **poster presentation** on title: "Overview of osmotic pressure-driven water desalination processes in the Indian context", Conference on Desalination, Brine management and Water recycling (DeSaltM 23), organized by Environmental Science and Engineering Department, Indian Institute of Technology Bombay (IIT-B), Mumbai, India, July 21 – 22, 2023.

2. **Kudzai Hamish Ruzvidzo**, Raminder Kaur and Manish Jain (2023), **oral presentation** on title: "Exploring novel organic draw solutions for forward osmosis desalination of brackish water: A comprehensive study", International Conference on Basic, Analytical and Allied Sciences at the Interface of
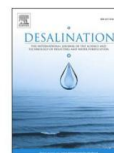
Carbohydrates and Biomass Valorisation (CARBO XXXVII), jointly organized by Department of Applied Chemistry, Delhi Technological University (DTU), Delhi, India, and the Association of Carbohydrate Chemists and Technologists (India), Delhi, India, November 30 – December 2, 2023.

3. **Kudzai Hamish Ruzvidzo**, Raminder Kaur and Manish Jain (2023), **oral presentation** on title: "Rheological, Physical, Thermal, Spectroscopical, Chemical and Electrical properties of novel organic draw solutes for forward osmosis desalination of brackish and seawater feed solutions", 2nd International Conference on Recent Trends in Materials Science & Devices 2023 (ICRTMD 2023), jointly organized by Research Plateau Publishers (An academic publisher of scientific and technical journals) & Sat Kabir Institute of Technology & Management Bahadurgarh, Haryana, India (Affiliated to M.D. University, Rohtak, Haryana, India), December 29 – 31, 2023. **Awarded best paper presentation award**

4. **Kudzai Hamish Ruzvidzo**, Raminder Kaur and Manish Jain (2024), **oral presentation** on title: "Exploring novel organic draw solutions for forward osmosis desalination: Performance, regeneration, modeling, and cost analysis", Emerging Techno-Economic Development for Sustainable Environment (ETDSE – 2024), organized by Department of Chemical Engineering Institute of Engineering & Science Indore, Indore, Madhya Pradesh, India, 12 – 13 January, 2024.

Novel polyelectrolyte-glycol ether ternary phase-separating draw solutions for desalination using forward osmosis

Kudzai Hamish Ruzvidzo, Raminder Kaur, Manish Jain[*]

Department of Applied Chemistry, Delhi Technological University, New Delhi 110042, India

HIGHLIGHTS

- The polyelectrolyte, NaCMC (MW ~ 90,000) was mixed with propylene glycol propyl ether (PGPE) as draw solutes for FO processes.
- The binary 40PGPE draw solution produced an osmotic pressure of 130.297 bars.
- The binary 40PGPE solution had higher reverse solute fluxes compared to the ternary 0.5NaCMC-20PGPE solution.
- Morphological evaluations confirmed the compatibility of the FO membrane with the newly developed organic draw solutions.

GRAPHICAL ABSTRACT
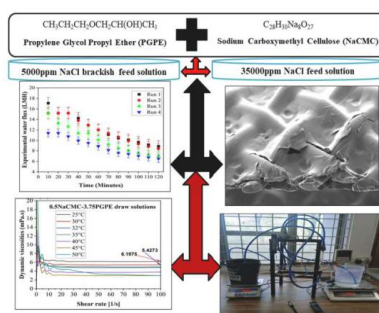
ARTICLE INFO

ABSTRACT

This study systematically evaluated the potential of novel organic draw solutions for forward osmosis (FO) desalination. The formulations included 4 binary and 6 ternary systems incorporating sodium carboxymethyl cellulose (NaCMC) and propylene glycol propyl ether (PGPE). Using a custom-built FO laboratory setup, the experimental water and solute fluxes of the new draw solutions were investigated. The ternary 0.5NaCMC-3.75PGPE draw solution demonstrated an osmotic pressure of 33.9942 bars. When tested at 30 °C, this draw solution yielded average experimental water fluxes of 17.487, 15.654, and 12.482 LMH while desalinating 5000 ppm NaCl brackish feed solutions. Furthermore, scaling up to 0.5NaCMC-20PGPE was effective for seawater desalination, with experimental water fluxes averaging 13.975 and 14.284 LMH against a 35,000 ppm NaCl feed solution. A comprehensive morphological analysis was conducted to evaluate the compatibility of the FO membrane with the organic draw solutions following a 21-day immersion period.

1. Introduction

The access to clean drinking water has been acknowledged as a fundamental human right enshrined in the constitutions of numerous nations across the globe [1]. The continual growth in the global population has necessitated the development of efficient and sustainable

---

RESEARCH ARTICLE

water
ENVIRONMENT RESEARCH

Enhanced forward osmosis desalination of brackish water using phase-separating ternary organic draw solutions of hydroxypropyl cellulose and propylene glycol propyl ether

Kudzai Hamish Ruzvidzo | Raminder Kaur [ORCID] | Manish Jain [ORCID]

Department of Applied Chemistry, Delhi Technological University, New Delhi, India

Correspondence

Manish Jain, Department of Applied Chemistry, Delhi Technological University, New Delhi 110042, India.
Email: manishjain@dtu.ac.in

Abstract

This study introduces draw solutions for application in forward osmosis (FO) processes, combining mono propylene glycol propyl ether (PGPE) with the cellulose derivative hydroxypropyl cellulose (HPC). A total of 16 unique single-solute and ternary organic draw solutions were prepared and evaluated, leading to the selection of three promising solutions for further investigation. Notably, eight of the initial organic draw solutions demonstrated osmotic pressures exceeding 2.4 MPa. The dynamic viscosities of all draw solutions exhibited a significant reduction with increasing temperature. Among the investigated solutions, the 0.25HPC-3.75PGPE demonstrated the most favorable FO performance, achieving average experimental water fluxes of 11.062 and 9.852 $Lm^{-2}h^{-1}$ (LMH) against a 1 g/L NaCl brackish feed solution across two FO runs.

Practitioner Points

- Hydroxypropyl cellulose (HPC, MW ~100,000) was mixed with propylene glycol propyl ether (PGPE) as draw solutes for FO processes.
- Seven combinations of HPC and PGPE produced osmolalities greater than 1000 mOsm/kg.
- 0.5HPC-7.5PGPE ternary draw solution achieved experimental water fluxes of 11.062 and 9.852 LMH against 1 g/L NaCl brackish feed solution.
- Leveraging the LCSTs of these ternary organic solutions holds promise for improved separation and regeneration processes.

KEYWORDS

desalination, forward osmosis, hydroxypropyl cellulose, mono propylene glycol propyl ether, ternary organic draw solutions

INTRODUCTION

In areas with freshwater scarcity, the desalination of brackish water plays a critical role in providing a sustainable freshwater supply (Meerganz von Medeazza, 2004).

Forward osmosis (FO) is a promising membrane separation system based on the osmotic pressure gradient, thus requiring lesser energy requirements than reverse osmosis (RO) (Ndiaye et al., 2019). Cath et al. (2006) have reported the advantages of FO over pressure-driven

DELHI TECHNOLOGICAL UNIVERSITY
(Formerly Delhi College of Engineering)
Shahbad Daulatpur, Main Bawana Road, Delhi-42

PLAGIARISM VERIFICATION

Title of the Thesis **"Studies on water desalination using osmotic pressure-driven processes"**

Total Pages **221,** Name of the Scholar **Kudzai Hamish Ruzvidzo**

Supervisor (s)

(1) Dr. Manish Jain

(2) Dr. Raminder Kaur

Department **Applied Chemistry**

This is to report that the above thesis was scanned for similarity detection. Process and outcome are given below:

Software used: **Turnitin,** Similarity Index: **6 %,** Total Word Count: **48,477**

Date**: 9-1-2025**

Candidate's Signature   **Signature of Supervisor(s)**

Kudzai Hamish Ruzvidzo FINAL PhD THESIS 2025.docx

🎓 Delhi Technological University

Document Details

Submission ID

trn:oid:::27535:78625128

Submission Date

Jan 9, 2025, 4:04 PM GMT+5:30

Download Date

Jan 9, 2025, 4:15 PM GMT+5:30

File Name

Kudzai Hamish Ruzvidzo FINAL PhD THESIS 2025.docx

File Size

26.6 MB

221 Pages

48,477 Words

280,103 Characters

6% Overall Similarity

The combined total of all matches, including overlapping sources, for each database.

Filtered from the Report

- Bibliography
- Quoted Text
- Cited Text
- Small Matches (less than 10 words)

Exclusions

- 1 Excluded Source
- 13 Excluded Matches

Match Groups

🟥 **129** Not Cited or Quoted 6%
Matches with neither in-text citation nor quotation marks

🟧 **0** Missing Quotations 0%
Matches that are still very similar to source material

🟨 **0** Missing Citation 0%
Matches that have quotation marks, but no in-text citation

🟩 **0** Cited and Quoted 0%
Matches with in-text citation present, but no quotation marks

Top Sources

3% 🌐 Internet sources

5% 📖 Publications

3% 👤 Submitted works (Student Papers)

CURRICULUM VITAE

KUDZAI HAMISH RUZVIDZO

Lecturer
Department of Polymer Technology and
Engineering
Harare Institute of Technology
Zimbabwe
kruzvidzo@hit.ac.zw
vakudzaihamish@gmail.com
+263 775 021 469

Professional Experiences & Qualifications

August 2018 – Contd.	Lecturer in Department of Polymer Technology and Engineering
	Harare Institute of Technology, Zimbabwe
August 2021 – Contd.	Ph.D in Chemical Engineering (Pursuing)
	Delhi Technological University, Delhi, India
August 2016 – July 2018	Staff Development Fellow
	Harare Institute of Technology, Zimbabwe

Academic Qualifications

Examination	Institution/Board	Year	Results
M.Tech	Amity University Gurgaon, Haryana, India	2018	Overall CGPA 10.00 on a 10 point scale
B.Tech	Harare Institute of Technology, Zimbabwe	2015	2.1
Advanced level	ZIMSEC	2009	3 A level passes
Ordinary level	ZIMSEC	2007	12 O level passes (9As and 3Bs)

Awards

❖ Date: Feb 2019
  Award name: Gold medal for standing first in academic performance

Institution: Amity University Gurgaon, Haryana, India

❖ Date: Feb 2019
Award name: Trophy for academic excellence
Institution: Amity University Gurgaon, Haryana, India

❖ Date: Dec 2023
Award: Best paper presentation
Conference: 2nd International Conference on Recent Trends in Materials Science & Devices 2023 (ICRTMD 2023)
Organizers: Research Plateau Publishers (An academic publisher of scientific and technical journals) & Sat Kabir Institute of Technology & Management Bahadurgarh, Haryana, India (Affiliated to M.D. University, Rohtak, Haryana, India)

Personal Dossier

Discipline	Chemical Engineering
Positive Traits	Confidence, Teamwork, Hardwork, Leadership
Areas of Research Interest	Water Desalination, Membrane Separation, Polymer Chemistry
Personal Details	Date of Birth : 20 March 1991
	Sex : Male
	Marital Status : Married
	Nationality : Zimbabwean
	Religion : Christianity
	Languages : Shona and English